

Library Declaration and Deposit Agreement

1. STUDENT DETAILS

Please complete the following:

Full name:

University ID number:

2. THESIS DEPOSIT

2.1 Under your registration at the University, you are required to deposit your thesis with the University in BOTH hard copy and in digital format. The digital copy should normally be saved as a single pdf file.

2.2 The hard copy will be housed in the University Library. The digital copy will be deposited in the University's Institutional Repository (WRAP). Unless otherwise indicated (see 2.6 below), this will be made immediately openly accessible on the Internet and will be supplied to the British Library to be made available online via its Electronic Theses Online Service (EThOS) service.
[At present, theses submitted for a Master's degree by Research (MA, MSc, LL.M, MS or MMedSci) are not being deposited in WRAP and not being made available via EthOS. This may change in future.]

2.3 In exceptional circumstances, the Chair of the Board of Graduate Studies may grant permission for an embargo to be placed on public access to the thesis **in excess of two years**. This must be applied for when submitting the thesis for examination (further information is available in the *Guide to Examinations for Higher Degrees by Research*.)

2.4 If you are depositing a thesis for a Master's degree by Research, the options below only relate to the hard copy thesis.

2.5 If your thesis contains material protected by third party copyright, you should consult with your department, and if appropriate, deposit an abridged hard and/or digital copy thesis.

2.6 Please tick one of the following options for the availability of your thesis (guidance is available in the *Guide to Examinations for Higher Degrees by Research*):

- Both the hard and digital copy thesis can be made publicly available immediately
- The hard copy thesis can be made publicly available immediately and the digital copy thesis can be made publicly available after a period of two years (*should you subsequently wish to reduce the embargo period please inform the Library*)
- Both the hard and digital copy thesis can be made publicly available after a period of two years (*should you subsequently wish to reduce the embargo period please inform the Library*)
- Both the hard copy and digital copy thesis can be made publicly available after _____ (insert time period in excess of two years). **This option requires the prior approval of the Chair of the Board of Graduate Studies (see 2.3 above)**

The University encourages users of the Library to utilise theses as much as possible, and unless indicated below users will be able to photocopy your thesis.

I **do not** wish for my thesis to be photocopied

3. GRANTING OF NON-EXCLUSIVE RIGHTS

Whether I deposit my Work personally or through an assistant or other agent, I agree to the following:

- Rights granted to the University of Warwick and the British Library and the user of the thesis through this agreement are non-exclusive. I retain all rights in the thesis in its present version or future versions. I agree that the institutional repository administrators and the British Library or their agents may, without changing content, digitise and migrate the thesis to any medium or format for the purpose of future preservation and accessibility.

4. **DECLARATIONS**

I DECLARE THAT:

- I am the author and owner of the copyright in the thesis and/or I have the authority of the authors and owners of the copyright in the thesis to make this agreement. Reproduction of any part of this thesis for teaching or in academic or other forms of publication is subject to the normal limitations on the use of copyrighted materials and to the proper and full acknowledgement of its source.
- The digital version of the thesis I am supplying is either the same version as the final, hard-bound copy submitted in completion of my degree once any minor corrections have been completed, or is an abridged version (see 2.5 above).
- I have exercised reasonable care to ensure that the thesis is original, and does not to the best of my knowledge break any UK law or other Intellectual Property Right, or contain any confidential material.
- I understand that, through the medium of the Internet, files will be available to automated agents, and may be searched and copied by, for example, text mining and plagiarism detection software.
- At such time that my thesis will be made publically available digitally (see 2.6 above), I grant the University of Warwick and the British Library a licence to make available on the Internet the thesis in digitised format through the Institutional Repository and through the British Library via the EThOS service.
- If my thesis does include any substantial subsidiary material owned by third-party copyright holders, I have sought and obtained permission to include it in any version of my thesis available in digital format and that this permission encompasses the rights that I have granted to the University of Warwick and to the British Library.

5. **LEGAL INFRINGEMENTS**

I understand that neither the University of Warwick nor the British Library have any obligation to take legal action on behalf of myself, or other rights holders, in the event of infringement of intellectual property rights, breach of contract or of any other right, in the thesis.

Please sign this agreement and ensure it is bound into the final hard bound copy of your thesis, which should be submitted to Student Reception, Senate House.

Student's signature: Date:

**Biochemically Adaptive
Materials based on
(Iso)Thermally-
Responsive Polymers**

Daniel James Phillips

A thesis submitted in partial fulfilment of the requirements for
the degree of Doctor of Philosophy in Chemistry



University of Warwick, Department of Chemistry

September 2014

Table of Contents

List of Figures	viii
List of Schemes	xiv
List of Tables	xvi
Acknowledgements	xviii
Declaration	xx
Abstract	xxii
Abbreviations and Symbols	xxiii

1. Introduction

1.1	The Importance of Drug Delivery in Modern Medicine	1
1.2	Enhancing Drug Delivery with Polymers	2
1.3	Towards Well-Defined Polymers: Controlled Radical Polymerisation Techniques	5
1.4	Stimuli-Responsive Materials: Looking to Nature for Inspiration	10
1.5	Thermally-Responsive Materials	11
1.6	Modulating Thermal Transitions through Polymer Structure Manipulation: The "Isothermal" Response	18
1.6.1	Triggering an "Isothermal" Response <i>via</i> Backbone Modification	21
1.6.2	Triggering an "Isothermal" Response <i>via</i> End-Group Modification	22
1.6.3	Triggering an "Isothermal" Response <i>via</i> Side-Chain Modification	24
1.6.4	Triggering an "Isothermal" Response <i>via</i> the Surrounding Environment	31
1.7	Aims and Thesis Summary	34
1.8	References	36

2. Isothermally-Responsive, Biodegradable Poly(disulfide)s

2.1	Chapter Summary	52
2.2	Introduction	53
2.3	Results and Discussion	57
2.4	Conclusions	76
2.5	Experimental	77
2.5.1	Materials	77
2.5.2	Analytical Methods	78
2.5.3	Procedures	80
2.5.3.1	Synthesis of hydroxyethyl pyridyldisulfide	80
2.5.3.2	Synthesis of 2-(dodecylthiocarbonothioylthio)-2-methylpropanoic acid	82
2.5.3.3	Synthesis of 2-(pyridyldisulfanyl) ethyl 2-(dodecylthiocarbonothioylthio)-2-methylpropanoate	84
2.5.3.4	Synthesis of 2-(pyridyldisulfanyl) ethyl 4-cyano-4-(phenylcarbonothioylthio)pentanoate	85
2.5.3.5	Polymerisation of <i>N</i> -isopropylacrylamide	87
2.5.3.6	Polymerisation of oligo(ethylene glycol) methyl ether methacrylate	87
2.5.3.7	Polymerisation of oligo(ethylene glycol) methyl ether acrylate	88
2.5.3.8	Polymerisation of diethyleneglycol methyl ether methacrylate	89
2.5.3.9	Polymerisation of methyl methacrylate	89
2.5.3.10	Polymerisation of <i>tert</i> -butyl acrylate	90
2.5.3.11	Polymerisation of <i>N,N</i> -dimethylacrylamide with 2-(pyridyldisulfanyl) ethyl 2-(dodecylthiocarbonothioylthio)-2-methylpropanoate	90
2.5.3.12	Polymerisation of <i>N,N</i> -dimethylacrylamide with 2-(pyridyldisulfanyl) ethyl 4-cyano-4-(phenylcarbonothioylthio)pentanoate	91
2.5.3.13	General polycondensation procedure	92
2.5.4	Assay Conditions	92

2.5.4.1	General procedure for turbidimetry-monitored, glutathione-mediated degradation of disulfide-containing polymers	92
2.5.4.2	General procedure for SEC evaluation of glutathione-mediated degradation	93
2.6	References	94

3. Glutathione-Triggered Disassembly of Isothermally Responsive Polymer Nanoparticles Obtained by Nanoprecipitation of Hydrophilic Polymers

3.1	Chapter Summary	100
3.2	Introduction	101
3.3	Results and Discussion	105
3.4	Conclusions	121
3.5	Experimental	122
3.5.1	Materials	122
3.5.2	Analytical Methods	123
3.5.3	Procedures	125
3.5.3.1	Synthesis of benzyl 2-[(<i>tert</i> -butoxycarbonyl)amino]ethyl trithiocarbonate	125
3.5.3.2	Polymerisation of <i>N</i> -isopropylacrylamide using 2-(pyridyldisulfanyl) ethyl 2-(dodecylthiocarbonothioylthio)-2-methylpropanoate	127
3.5.3.3	Polymerisation of <i>N</i> -isopropylacrylamide using benzyl 2-[(<i>tert</i> -butoxycarbonyl)amino]ethyl trithiocarbonate	127
3.5.3.4	Co-polymerisation of <i>N</i> -isopropylacrylamide and <i>N</i> -hydroxyethylacrylamide	128
3.5.3.5	General procedure for nanoparticle preparation	129
3.5.4	Assay Conditions	129
3.5.4.1	DLS assay	129
3.5.4.2	Nanoparticle fluorescence assay	130
3.5.4.3	UV-visible spectrophotometric experiments	130
3.6	References	131

4. Isothermally-Responsive Polymers Triggered by Selective Binding of Fe³⁺ to Siderophoric Catechol End-Groups

4.1	Chapter Summary	137
4.2	Introduction	138
4.3	Results and Discussion	142
4.4	Conclusions	153
4.5	Experimental	154
4.5.1	Materials	154
4.5.2	Analytical Methods	154
4.5.3	Procedures	156
4.5.3.1	Synthesis of 2,5-dioxopyrrolidin-1-yl 2-(((dodecylthio)carbonothioyl)thio)-2-methylpropanoate	156
4.5.3.2	Synthesis of 1-((3,4-dihydroxyphenethyl)amino)2-methyl-1-oxopropan-2-yl dodecyl carbonotrithioate	158
4.5.3.3	Example polymerisation of <i>N</i> -isopropylacrylamide using 1-((3,4-dihydroxyphenethyl)amino)2-methyl-1-oxopropan-2-yl dodecyl carbonotrithioate	159
4.5.3.4	Polymerisation of <i>N</i> -isopropylacrylamide using 2-[(<i>tert</i> -butoxycarbonyl)amino]ethyl trithiocarbonate	159
4.5.4	Assay Conditions	160
4.5.4.1	General procedure for the turbidimetry-monitored, Fe ³⁺ mediated isothermal precipitation of pNIPAM-2	160
4.6	References	161

5. Siderophore-Inspired Nanoparticle-based Biosensor for the Selective Detection of Fe³⁺

5.1	Chapter Summary	166
5.2	Introduction	167
5.3	Results and Discussion	171
5.4	Conclusions	186
5.5	Experimental	188

5.5.1	Materials	188
5.5.2	Analytical Methods	188
5.5.3	Procedures	190
5.5.3.1	Example polymerisation of <i>N</i> -hydroxyethylacrylamide using 1-((3,4-dihydroxyphenethyl)amino)2-methyl-1-oxopropan-2-yl dodecyl carbonotrithioate	190
5.5.3.2	Polymerisation of <i>N</i> -hydroxyethylacrylamide using benzyl 2-[(<i>tert</i> -butoxycarbonyl)amino]ethyl trithiocarbonate	191
5.5.3.3	Functionalisation of gold nanoparticles with polymer	191
5.5.4	Assay Conditions	192
5.5.4.1	General procedure for UV/visible spectrophotometry assay of gold nanoparticles	192
5.6	References	193

6. Using an Enzymatic Trigger to Stimulate Isothermal Cell Uptake

6.1	Chapter Summary	199
6.2	Introduction	200
6.3	Results and Discussion	205
6.3.1	Synthesis of Phosphorylated Polymers	205
6.3.2	Phosphate-Containing, Thermally-Responsive Systems	217
6.3.3	Cell Studies	222
6.4	Conclusions	237
6.5	Experimental	239
6.5.1	Materials	239
6.5.2	Analytical Methods	240
6.5.3	Synthetic Methods	242
6.5.3.1	Synthesis of 2-(methacryloyloxy)ethyl phosphate	242
6.5.3.2	Synthesis of benzyl 2-hydroxyethyl carbonotrithioate	243
6.5.3.3	Example polymerisation of 2-(methacryloyloxy)ethyl phosphate using 4-cyano-4-(phenylcarbonothioylthio)pentanoic acid	245

6.5.3.4	Example polymerisation of 2-(methacryloyloxy)ethyl phosphate using 2-(dodecylthiocarbonothioylthio)-2-methylpropanoic acid	245
6.5.3.5	Polymerisation of oligo(ethylene glycol) methyl ether methacrylate using 4-cyano-4-(phenylcarbonothioylthio) pentanoic acid	246
6.5.3.6	Example co-polymerisation of 2-(methacryloyloxy)ethyl phosphate and diethylene glycol methyl ether methacrylate using 4-cyano-4-(phenylcarbonothioylthio) pentanoic acid	247
6.5.3.7	Co-polymerisation of <i>N</i> -isopropylacrylamide and hostasol methacrylate using benzyl 2-hydroxyethyl carbonotrithioate	247
6.5.3.8	Polymerisation of <i>N</i> -isopropylacrylamide using benzyl 2-hydroxyethyl carbonotrithioate	248
6.5.3.9	Example co-polymerisation of 2-(methacryloyloxy)ethyl phosphate, diethylene glycol methyl ether methacrylate and hostasol methacrylate using 4-cyano-4-(phenylcarbonothioylthio) pentanoic acid	249
6.5.4	Assay Conditions	249
6.5.4.1	General assay conditions for colorimetric determination of phosphate release	249
6.5.4.2	Assay determining the effect of phosphatase on polymer cloud point	250
6.5.4.3	Turbidimetric assay for phosphatase-mediated isothermal polymer response	250
6.5.5	Cell Culture	250
6.5.5.1	General cell culture	250
6.5.5.2	Cytotoxicity testing of polymers: MTT assay	251
6.5.5.3	Cell uptake at fixed temperature	252
6.5.5.4	Calf intestinal alkaline phosphatase-driven cell uptake	253
6.6	References	254

7. Conclusions 261

**Appendix. Redox-Sensitive Materials for Drug Delivery:
Targeting the Correct Intracellular Environment; Tuning
Release Rates and Appropriate Predictive Systems**

264

List of Figures

Chapter 1: Introduction

Figure 1.1	Blood circulating life of catalase and PEG-5000-catalase in acatalasemic mice.	3
Figure 1.2	General mechanism for C(L)RP processes.	6
Figure 1.3	Chemical structures of the main classes of RAFT CTA.	7
Figure 1.4	Generally accepted mechanism of the RAFT process.	8
Figure 1.5	"Switchable" RAFT CTA developed by Benaglia <i>et al.</i>	9
Figure 1.6	Schematic demonstrating the change in polymer conformation (coil - globule) observed when a polymer solution is heated through its LCST.	13
Figure 1.7	Representation of the phase transition associated with the LCST and UCST.	13
Figure 1.8	Formulation of thermoresponsive nanoparticles and the enhancement in cellular uptake due to change in surface corona with thermal response, as proposed by Alexander and co-workers.	16
Figure 1.9	Representation of the phase diagrams associated with a polymer exhibiting an isothermal LCST transition.	19
Figure 1.10	Sections of a polymer structure/solution which may be modified to tune the macroscopic behaviour.	20
Figure 1.11	Light-triggered isothermal transition: The application of different wavelengths of light to alter the conformation of α - and ω -terminal azobenzene units and hence the LCST, as described by Theato and co-workers.	23
Figure 1.12	Metal ion isothermochromic sensor: Observed changes in the solubility and colour in the absence and presence of metal ions.	26
Figure 1.13	Acid-catalysed isothermal transition: Synthesis and self-assembly of thermoresponsive and self-catalysed degradable polymers described by Monteiro and co-workers.	29

Figure 1.14 Summary of the multi-responsive copolymers prepared by Sharma and Srivistava. 33

Chapter 2: Isothermally-Responsive, Biodegradable Poly(disulfide)s

Figure 2.1	Preparation of disulfide-linked polymers using a polycondensation-type methodology.	55
Figure 2.2	Chapter 2 study concept.	56
Figure 2.3	NMR characterisation of PADE.	59
Figure 2.4	SEC data showing the polycondensation of pNIPAM-1 .	61
Figure 2.5	Polycondensation of pDMA with PADE and CTA 1 .	64
Figure 2.6	Attempted polycondensation of pOEGMA₃₀₀ .	65
Figure 2.7	Representation of possible thiolactone-forming side-reaction following aminolysis of a thiocarbonylthio-terminated methacrylate.	66
Figure 2.8	Attempted polycondensation of pDEGMA .	67
Figure 2.9	Attempted polycondensation of pOEGA₄₈₀ .	68
Figure 2.10	Attempted polycondensation of pMMA .	68
Figure 2.11	Polycondensation of pt-BuA .	69
Figure 2.12	SEC data showing polycondensation and subsequent reduction from pNIPAM-2/3 precursors.	70
Figure 2.13	ESI (+ve) mass spectrometry analysis of ss-pNIPAM-2 following degradation by tributyl phosphine.	71
Figure 2.14	Cloud point data for pNIPAM-2/3 and ss-pNIPAM-2/3 .	72
Figure 2.15	SEC data showing degradation of ss-pNIPAM-2/3 at different GSH concentrations.	73
Figure 2.16	Isothermal turbidimetry data for ss-pNIPAM-2/3 .	75
Figure 2.17	NMR characterisation of hydroxyethyl pyridyl disulfide.	81
Figure 2.18	NMR characterisation of 2-(dodecylthiocarbonothioylthio)-2-methylpropanoic acid.	83
Figure 2.19	NMR characterisation of 2-(pyridyldisulfanyl) ethyl 4-cyano-4-(phenylcarbonothioylthio)pentanoate.	86

Chapter 3: Glutathione-Triggered Disassembly of Isothermally Responsive Polymer Nanoparticles Obtained by Nanoprecipitation of Hydrophilic Polymers

Figure 3.1	Nanoprecipitation as a route towards nanoparticle preparation.	103
Figure 3.2	Chapter 3 isothermal disassembly concept.	105
Figure 3.3	Characterisation of pNIPAM-1 .	107
Figure 3.4	Characterisation of nanoparticles prepared from pNIPAM-1 .	108
Figure 3.5	Cryo-TEM images (and particle size analysis) of nanoparticles prepared from pNIPAM-1 .	110
Figure 3.6	Thermal disassembly of nanoparticles (DLS) and turbidimetric data of linear pNIPAM-1 .	111
Figure 3.7	GSH-triggered disassembly of nanoparticles prepared from pNIPAM-1 (DLS).	112
Figure 3.8	GSH-triggered disassembly of cargo-loaded nanoparticles prepared from pNIPAM-1 (fluorescence assay).	114
Figure 3.9	SEC characterisation of pNIPAM-2/3 .	116
Figure 3.10	UV/visible spectra of pNIPAM-2/3 as a function of GSH concentration.	117
Figure 3.11	SEC characterisation of pNIPAM-co-HEA .	118
Figure 3.12	Characterisation of nanoparticles prepared from pNIPAM₉₅-co-HEA₅ .	119
Figure 3.13	Turbidimetric response of linear pNIPAM₉₅-co-HEA₅ and change in fluorescence of nanoparticles in response to 1 mM GSH.	120
Figure 3.14	NMR characterisation of benzyl 2-[(<i>tert</i> -butoxycarbonyl)amino]ethyl trithicarbonate.	126

Chapter 4: Isothermally-Responsive Polymers Triggered by Selective Binding of Fe³⁺ to Siderophoric Catechol End-Groups

Figure 4.1	Chapter 4 isothermal concept.	141
Figure 4.2	NMR characterisation of 1-((3,4-dihydroxyphenethyl)amino)2-methyl-1-oxopropan-2-yl dodecyl carbonotrithioate.	143
Figure 4.3	Infrared spectra showing the sequential modification of the carboxylic acid terminus of CTA 1 to the activated ester 2 and catechol 3 .	144
Figure 4.4	SEC characterisation and polymer structure of pNIPAM-1/2 .	145
Figure 4.5	Results from RAFT polymerisation of NIPAM-1 .	146
Figure 4.6	MALDI-ToF spectrum of pNIPAM-2 .	147
Figure 4.7	¹ H NMR spectrum of pNIPAM-2 .	147
Figure 4.8	Polymer structures and cloud points of pNIPAM-1/2 with Fe ³⁺ .	149
Figure 4.9	Cloud point data and polymer structure of pNIPAM-2 with Fe ²⁺ .	150
Figure 4.10	SEC characterisation and polymer structure of pNIPAM-3 .	151
Figure 4.11	Cloud point data of pNIPAM-3 with Fe ³⁺ .	151
Figure 4.12	Isothermal turbidimetry data for pNIPAM-2 .	152
Figure 4.13	NMR characterisation of 2,5-dioxopyrrolidin-1-yl 2-(((dodecylthio)carbonothioyl)thio)-2-methylpropanoate.	157

Chapter 5: Siderophore-Inspired Nanoparticle-based Biosensor for the Selective Detection of Fe³⁺

Figure 5.1	Chemical structures (and classification) of example siderophores.	168
Figure 5.2	SEC characterisation of pHEA-1/2/3/4 .	172
Figure 5.3	Characterisation of pHEA-1/2/3/4@AuNP₄₀ .	174
Figure 5.4	UV/visible spectra showing response of pHEA-2@AuNP₄₀ in presence of Fe ³⁺ and 0 or 50 mM NaCl.	178
Figure 5.5	Response of pHEA-2@AuNP₄₀ in the presence of 10 μM Fe ³⁺ and various NaCl concentrations.	179

Figure 5.6	Response of pHEA-2@AuNP₄₀ in 150 mM NaCl to various concentrations of Fe ³⁺ .	180
Figure 5.7	UV/visible spectra showing response of pHEA-4@AuNP₄₀ and pHEA-2@AuNP₄₀ to various concentrations of Fe ³⁺ and Fe ²⁺ respectively.	182
Figure 5.8	UV/visible spectra showing response of pHEA-1@AuNP₄₀ to NaCl and pHEA-3@AuNP₄₀ to Fe ³⁺ .	183
Figure 5.9	Response of pHEA-2@AuNP₄₀ , doped with 150 mM NaCl, to a variety of metal ions.	184
Figure 5.10	Response of pHEA-2@AuNP₄₀ , suspended in bovine plasma, to various concentrations of Fe ³⁺ .	185

Chapter 6: Using an Enzymatic Trigger to Stimulate Isothermal Cell Uptake

Figure 6.1	Enzyme and temperature induced self-assembly behaviour of polymer bioconjugate demonstrated by Ulijn and co-workers.	203
Figure 6.2	³¹ P NMR spectrum of commercially available ethylene glycol methacrylate phosphate.	206
Figure 6.3	NMR characterisation of Phos-HEMA.	207
Figure 6.4	Kinetic results from the RAFT polymerisation of Phos-HEMA with dithiobenzoate and trithiocarboante chain transfer agents.	208
Figure 6.5	SEC characterisation of pPhos-HEMA-1/2/3 and ³¹ P NMR spectrum of pPhos-HEMA-1 .	210
Figure 6.6	Colour observed and calibration plot for colorimetric phosphate release assay.	211
Figure 6.7	Effect of temperature and time on absorbance profile of phosphate colorimetric assay.	212
Figure 6.8	Percentage phosphate release from pPhos-HEMA-3 upon incubation with CIALP.	213
Figure 6.9	Effect of polymer molecular weight and side-chain functionality on phosphate release.	215
Figure 6.10	SEC characterisation of pOEGMA₃₀₀ .	216

Figure 6.11	Characterisation of pDEGMA- <i>co</i> -PhosHEMA.	218
Figure 6.12	Anticipated change in chemical structure of poly(DEGMA- <i>co</i> -PhosHEMA) and effect on P_{co}5% cloud point upon incubation with CIALP.	219
Figure 6.13	Cloud point of P_{co}5% in 1x NEBuffer 3 over time and pOEGMA₃₀₀ with and without CIALP.	220
Figure 6.14	Isothermal turbidimetry data for P_{co}5% .	221
Figure 6.15	Synthesis and SEC characterisation of pNIPAM-<i>co</i>-HMA .	223
Figure 6.16	Turbidimetric analysis of pNIPAM-<i>co</i>-HMA in various media at various polymer concentrations.	225
Figure 6.17	Cloud points of pNIPAM-<i>co</i>-HMA as a function of polymer concentration in a variety of media.	226
Figure 6.18	Synthesis and characterisation of pNIPAM .	227
Figure 6.19	Turbidimetric analysis of pNIPAM in various media at various polymer concentrations.	229
Figure 6.20	Cloud points of pNIPAM as a function of polymer concentration in a variety of media.	230
Figure 6.21	MTT assay results of pNIPAM and fluorescence intensity following cell uptake experiments in MCF7 cells of pNIPAM-<i>co</i>-HMA .	231
Figure 6.22	MTT assay results of pOEGMA₃₀₀ and P_{co}5% with MCF7 cells.	232
Figure 6.23	SEC characterisation and turbidimetric analysis of pNIPAM-<i>co</i>-Phos-HEMA-<i>co</i>-HMA .	233
Figure 6.24	Fluorescence intensity following cell uptake experiments of pDEGMA-<i>co</i>-Phos-HEMA-<i>co</i>-HMA in MCF7 cells.	234
Figure 6.25	Cell uptake results of pDEGMA-<i>co</i>-Phos-HEMA-<i>co</i>-HMA in MCF7 cells with varying concentrations of CIALP.	236
Figure 6.26	NMR characterisation of benzyl 2-hydroxyethyl carbonotrithioate.	244

List of Schemes

Chapter 2: Isothermally-Responsive, Biodegradable Poly(disulfide)s

- Scheme 2.1** Synthetic strategy for the preparation of a disulfide-linked polymer from a trithiocarbonate and pyridyl disulfide containing starting material. 58
- Scheme 2.2** RAFT agents used in this study. 58

Chapter 3: Glutathione-Triggered Disassembly of Isothermally Responsive Polymer Nanoparticles Obtained by Nanoprecipitation of Hydrophilic Polymers

- Scheme 3.1** Synthesis of **pNIPAM-1**. 106
- Scheme 3.2** Potential reactions of glutathione with RAFT-derived pNIPAM. 115
- Scheme 3.3** Thiol-disulfide exchange reaction between a thiol and pyridyl disulfide to yield a mixed disulfide and pyridine thione. 116

Chapter 4: Isothermally-Responsive Polymers Triggered by Selective Binding of Fe³⁺ to Siderophoric Catechol End-Groups

- Scheme 4.1** Synthetic scheme for synthesis of catechol-functional chain transfer agent **3**. 142

Chapter 5: Siderophore-Inspired Nanoparticle-based Biosensor for the Selective Detection of Fe³⁺

- Scheme 5.1** Synthetic scheme for the preparation of catechol-functional gold nanoparticles. 173
- Scheme 5.2** Gold nanoparticles functionalised with catechol of phenyl end-groups and their response to Fe²⁺ and Fe³⁺. 182

Chapter 6: Using an Enzymatic Trigger to Stimulate Isothermal Cell Uptake

Scheme 6.1 Synthetic scheme for the preparation of Phos-HEMA. 206

Scheme 6.2 Synthetic scheme for the preparation of a fluorescent, phosphate-labelled thermo-responsive polymer. 232

List of Tables

Chapter 2: Isothermally-Responsive, Biodegradable Poly(disulfide)s

Table 2.1 Characterisation of polymers prepared in Chapter 2 using PADE. 62

Table 2.2 SEC characterisation of poly(disulfide)s. 63

Chapter 3: Glutathione-Triggered Disassembly of Isothermally Responsive Polymer Nanoparticles Obtained by Nanoprecipitation of Hydrophilic Polymers

Table 3.1 Characterisation of pNIPAM-1. 106

Table 3.2 Characterisation of polymers used for UV/visible spectrophotometry experiments. 115

Table 3.3 Characterisation of pNIPAM-*co*-HEA samples prepared in Chapter 3. 118

Chapter 4: Isothermally-Responsive Polymers Triggered by Selective Binding of Fe³⁺ to Siderophoric Catechol End-Groups

Table 4.1 Characterisation of catechol-terminated pNIPAM samples prepared in Chapter 4. 145

Table 4.2 Characterisation of benzyl-terminated pNIPAM. 151

Chapter 5: Siderophore-Inspired Nanoparticle-based Biosensor for the Selective Detection of Fe³⁺

Table 5.1 Characterisation of pHEA samples prepared in Chapter 5. 171

Table 5.2 Characterisation of gold nanoparticles used in Chapter 5. 174

Chapter 6: Using an Enzymatic Trigger to Stimulate Isothermal Cell Uptake

Table 6.1	Characterisation of pPhos-HEMA samples prepared using 4-cyano-4-(phenylcarbonothioylthio) pentanoic acid in Chapter 6.	209
Table 6.2	Characterisation of pOEGMA₃₀₀ prepared using 4-cyano-4-(phenylcarbonothioylthio) pentanoic acid.	216
Table 6.3	Characterisation of poly(DEGMA- <i>co</i> -Phos-HEMA) samples prepared using 4-cyano-4-(phenylcarbonothioylthio) pentanoic acid used in Chapter 6.	217
Table 6.4	Characterisation of pNIPAM-<i>co</i>-HMA prepared using benzyl 2-hydroxyethyl carbonotrithioate.	223
Table 6.5	Cloud points of pNIPAM-<i>co</i>-HMA at various concentrations in different media.	226
Table 6.6	Characterisation of pNIPAM prepared using benzyl 2-hydroxyethyl carbonotrithioate.	228
Table 6.7	Cloud points of pNIPAM at various concentrations in different media.	229
Table 6.8	Characterisation of pDEGMA-<i>co</i>-Phos-HEMA-<i>co</i>-HMA prepared using benzyl 2-hydroxyethyl carbonotrithioate.	233

Acknowledgements

First and foremost, I would like to thank Dr Matthew Gibson for not only introducing me to the field of practical polymer science but for providing time, enthusiasm and, above all, endless patience and optimism which somehow managed to put a positive spin on even the bleakest of moments! Grateful thanks also go the University of Warwick for the provision of funding throughout my studies.

Secondly to those who have contributed to practical aspects of this work including Dr Ivan Prokes, Dr Lijiang Song and Mr Philip Aston, for their endless knowledge of NMR Spectroscopy and Mass Spectrometry, Dr Joe Patterson for his incredible ability with all things microscopy, and Dr Francesca Greco and Ms Marleen Wilde at the University of Reading for both hosting and providing me with valuable insight into the challenging world of cell culture!

The true art of scientific discovery lies in the discussions held with others. There are too many people to thank in this regard but special mention goes to my advisory board of Professors Stefan Bon and Richard Walton, Dr Gemma-Louise Davies for providing fresh ideas and impetus late in my studies, as well as Drs Mat Jones, Anthony Grice, James Burns, Kayleigh McEwan, Paul Wilson, Tom Skelhon, Rob Deller, Tom Wilks, Mr Rajan Randev and the many listed below.

I thank Mr Nick Barker for his inspirational commitment to an Outreach programme which has allowed me to develop my scientific communication and teaching skills.

To Caroline Biggs, Tom Congdon, Sarah-Jane Richards and Lucienne Otten for putting up with my regular rants, for helping put bad days in perspective and for your general support and kind natures, I cannot thank-you all enough.

Moreover, to the rest of the Gibson group as well as Matthew Summers, Laura Wilkins, Charlene Wilmet, Julia Polt and all the other UG/PG students I have had the (in general!) pleasure of teaching.

The Chemistry department at Warwick is vast and there are too many faces to mention but thanks to Jamie Godfrey, Alex Simula, Helen Thomas, Andy Sellars, Andy Ross, Danielle Lloyd, Jenny Collins, Vasiliki Nikolaou, Athina Anastasaki, Chris Waldron, Mike Perryman, Matt Blackmore, Katie Farrance, Ed Malins, Gokhan Yilmaz and Barak Aaronsen for your friendly conversation throughout. Also to the Chemistry Department Cricket Club, particularly Rob Channon (who organised like a trooper and finally lifted the Staff-Student trophy!), Craig Bell, Andy Davidson, Jai Gupta and Tanvir Hasan.

Thank-you to Steve, Sophia, Jack, Chris, Robin, Verity, Rachel, Yvonne, Lynn, Matthew, Louise, Kirsty, Pete, Matt, Heather, Rich, the many at KWCC and anyone I may have missed (!) – I will be forever thankful for your friendship.

Furthermore, to Cath, Geoff, Susannah, Michael, Pam, Tom and Kathie for your support, good wishes and for always providing a warm welcome.

Heartfelt thanks go to Mum, Dad, Ben, Lucy, Momma, Grandpa, Grandma, Grandpa and Uncle Jonathan for providing such a wonderful home and for the constant love, support and unwavering faith without which this Thesis would not have happened.

And finally to Laura who has lived this entire “adventure” with me, tolerated far more ups and downs than could reasonably be expected of anyone, and yet who has always been there with a smile at the end of every day ☺

Declaration

This thesis is submitted to the University of Warwick in support of my application for the degree of Doctor of Philosophy. It has been composed by myself and has not been submitted in any previous form for any degree at any other University.

The work presented was carried out by the author except in the case of collaborative research, as outlined below:

- Cryo-TEM analysis of polymer nanoparticles prepared in **Chapter 3** was performed by Dr Joseph Patterson at the University of Warwick;
- TEM analysis of the gold nanoparticles prepared in **Chapter 5** was performed by Dr Gemma-Louise Davies at the University of Warwick;
- The cell culture work discussed in **Chapter 6** was performed by Ms. Marleen Wilde, under the supervision of Dr Francesca Greco at the University of Reading.

Sections of this thesis have been accepted for publication as follows:

- **Chapter 1:** Phillips, D. J.; Gibson, M. I. Towards Next-Generation Materials: Using (Iso)thermally-Sensitive Polymers as Scaffolds for the Preparation of Multiply-Responsive Structures. *Polym. Chem.* **2015**, DOI: 10.1039/C4PY01539H;
- **Chapter 2:** Phillips, D. J.; Gibson, M. I. Biodegradable poly(disulfide)s derived from RAFT polymerization: Monomer scope, Glutathione Degradation and Tunable Thermal Responses. *Biomacromolecules* **2012**, *13*, 3200-2308;
- **Chapter 3:** Phillips, D. J.; Patterson, J.; O'Reilly, R. K.; Gibson, M. I. Glutathione-Triggered Disassembly of Isothermally Responsive Polymer Nanoparticles obtained by Nanoprecipitation of Hydrophilic Polymers. *Polym. Chem.* **2014**, *21*, 126-131;
- **Chapter 4:** Phillips, D. J.; Davies, G.-L.; Gibson, M. I. Isothermally-Responsive Polymers Triggered by Selective Binding of Fe³⁺ to Siderophoric Catechol End-Groups. *ACS Macro Lett.* **2015**, *3*, 270-275;
- **Chapter 5:** Phillips, D. J.; Davies, G.-L.; Gibson, M. I. Siderophore-Inspired Nanoparticle-based Biosensor for the Selective Detection of Fe³⁺. *J. Mater. Chem. B* **2014**, *3*, 1225-1229.

Abstract

The ability to programme and manipulate small changes at the molecular level to elicit a dramatically enhanced macroscopic response makes “stimuli-responsive” materials a fascinating topic of study. This work seeks to manipulate the solubility switch associated with polymers exhibiting a Lower Critical Solution Temperature without a temperature change (*isothermally*). This concept, as overviewed in **Chapter 1**, has attractive applications in biological settings where variations in *in vivo* microenvironments may be used to produce increasingly targeted delivery vehicles, and to mediate cell membrane interactions.

Using controlled radical polymerisation, pre-designed backbones, end-group(s) or side-chains can be targeted to control the hydrophilic-hydrophobic balance of a thermo-responsive system. **Chapters 2 and 3** investigate this concept, using the chemical reduction of a functional polymer backbone or end-group to trigger isothermal polymer precipitation or solubilisation in linear and nanoparticle systems respectively. **Chapter 4** applies a metal-ligand binding motif, prevalent in bacteria, to end-functional polymers as an alternative means of promoting isothermal polymer precipitation. This binding motif is then transferred to a nanoparticle system in **Chapter 5**, and used for the first time to prepare an optical, particle-based biosensor for the detection of physiologically relevant iron concentrations. Finally, **Chapter 6** describes the enzymatic degradation of a polymer side-chain as a means of triggering isothermal precipitation and considers its potential to mediate cellular uptake.

In summary, a series of functionalised polymers and nanoparticles have been synthesised and their (isothermal) responses characterised. These materials may have exciting potential in the emerging field of nanomedicine.

Abbreviations

ACVA	4,4'-Azobis(4-cyanovaleric acid)
ALP	Alkaline phosphatase
ATP	Adenosine 5'-triphosphate
ATRP	Atom transfer radical polymerisation
AuNP	Gold nanoparticle
BA	Butyl acrylate
BSA	Bovine serum albumin
C(L)RP	Controlled living radical polymerisation
CDCl₃	Deuterated chloroform
CIALP	Calf intestinal alkaline phosphatase
CP	Cloud point
CTA	Chain transfer agent
(Cryo)-TEM	(Cryogenic)-Transmission Electron Microscopy
DCTB	<i>Trans</i> -2-[3-(4- <i>tert</i> -butylphenyl)-2-methyl-2-propenylidene]malonitrile
DEGMA	Diethylene glycol methyl ether methacrylate
DIC	<i>N,N'</i> -Diisopropylacrylamide
DLS	Dynamic light scattering
DMA	<i>N,N</i> -Dimethylacrylamide
DMAEA	<i>N,N</i> -Dimethylaminoethyl acrylate
DMAEMA	<i>N,N</i> -Dimethylaminoethyl methacrylate
DMF	<i>N,N</i> -Dimethylformamide
DMSO	Dimethyl sulfoxide
Dop.HCl	Dopamine hydrochloride
DPH	Diphenylhexatriene
DRI	Differential refractive index
EO	Ethylene oxide
EPR	Enhanced permeability and retention
ESI	Electrospray ionisation
EtOx	2-Ethyl-2-oxazoline
FBS	Foetal bovine serum

Fmoc-pY	Fluorenylmethoxycarbonyl-tyrosine
FTIR	Fourier Transform Infrared Spectroscopy
GSH	Glutathione
HEA	<i>N</i> -Hydroxyethylacrylamide
HEMA	2-Hydroxyethyl methacrylate
HIFU	High-Intensity Focused Ultrasound
HMA	Hostasol methacrylate
iPrOx	2-Isopropyl-2-oxazoline
LCST	Lower Critical Solution Temperature
MALDI-ToF	Matrix-Assisted Laser Desorption Ionisation Time-of-Flight Mass Spectrometry
MEMA	<i>N</i> -(Morpholino)ethyl methacrylate
MMA	Methyl methacrylate
M_n	Number-average molecular weight
M_p	Peak maximum molecular weight
MTT	3-(4,5-Dimethylthiazol-2-yl)2,5-diphenyl-tetrazolium bromide
M_w	Weight-average molecular weight
NH₄BF₄	Ammonium tetrafluoroborate
NHS	<i>N</i> -Hydroxysuccinimide
NIPAM	<i>N</i> -Isopropylacrylamide
NMP	Nitroxide-Mediated Polymerisation
OEGA	Oligo(ethylene glycol) methyl ether acrylate
OEGMA	Oligo(ethylene glycol) methyl ether methacrylate
PADE	Propanoic acid 2-{[(dodecylthio)thioxomethyl]thio}-2-methyl-2-(2-pyridinyldithio)ethyl ester
PBS	Phosphate buffered saline
Pc	Polycondensed product
PDS	Pyridyl disulfide
PEG	Poly(ethylene glycol)
Phos-HEMA	Ethylene glycol methacrylate phosphate
PLGA	Poly(lactic- <i>co</i> -glycolic acid)
RAFT	Reversible Addition-Fragmentation Chain Transfer
r.t.	Room temperature

SEC	Size exclusion chromatography
SET-LRP	Single-Electron Transfer Living Radical Polymerisation
SM	Starting material
SPR	Surface plasmon resonance
SVBP	4-(2-Sulfoethyl)-1-(4-vinylbenzyl)pyridinium betaine
<i>t</i>BuA	<i>Tert</i> -butyl acrylate
TCEP	Tris(2-carboxyethyl)phosphine
TEA	Triethylamine
TEMPO	4- <i>N</i> -Amino-2,2,6,6-tetramethylpiperidin-1-oxyl-4-yl
THF	Tetrahydrofuran
THPMA	2-Tetrahydropyranyl methacrylate
TMS	Tetramethylsilane
UCST	Upper Critical Solution Temperature
UV	Ultraviolet
β-CD	β -Cyclodextrin
ΔF_{mix}	Helmholtz free energy of mixing
χ	Flory interaction parameter

Chapter 1

1. Introduction

1.1 The Importance of Drug Delivery in Modern Medicine

One cannot underestimate the immense progress that has been made in medical fields over the past 100 years. Some spectacularly successful statistics have arisen from advances within the scientific community. For example, vaccine development saw the worldwide eradication of smallpox in 1977¹ and today, only three countries remain polio endemic.² The development of new chemotherapies and screening techniques has seen the 5-year survival rates for testicular cancer increase from 63 % to over 90% in the last 3 decades³ and, in those diagnosed with breast cancer, by over 50% since 1971.⁴ However, as the average life expectancy continues to rise, the mortality associated with a multitude of diseases remains an ever-increasing problem. Cancer, for example, is responsible for over 8 million deaths worldwide, with the number of new diagnoses expected to exceed 22 million in the next two decades.⁵ It is therefore imperative that developments in the field of “Drug Delivery”, a phrase which describes the approaches/technologies used to safely transport a pharmaceutical compound in order to achieve a therapeutic effect,^{6, 7} continue if current limitations are to be overcome.

1.2 Enhancing Drug Delivery with Polymers

In 1908, Paul Ehrlich proposed his revolutionary *magische Kugel* (magic bullet) theory. This idea reasoned that the ideal therapeutic agent should be a compound able to selectively target a disease-causing organism.⁸ Practically, this involves the delivery of a therapeutic agent, regardless of its composition and physical form, accurately, precisely and specifically to maximise efficacy whilst minimising undesirable side-effects.⁹ To achieve this, several fundamental physicochemical and processing properties require consideration. These include compound availability (or ease of synthesis), stability, solubility, therapeutic index, circulatory half-life and the ability to cross multiple biological barriers.¹⁰⁻¹³ Some of these challenges are well exemplified by the antimicrotubule agent Paclitaxel (Taxol®), a popular treatment for ovarian, breast and non-small cell lung cancers. This compound is notoriously difficult to synthesise¹⁴ and is hence obtained from the Pacific Yew tree, where the bark of four trees is required to produce the 2 g necessary for one patient's chemotherapy. It possesses a low therapeutic index, is highly lipophilic and thus poorly soluble in aqueous media. Moreover, a lack of ionisable functional groups within a pharmaceutically useful range removes pH manipulation as a route towards improving solubility.¹⁵ Consequently, administration using an adjuvant containing the neuro- and cardio-toxic compound Cremophor EL is currently employed.¹⁶ Novel ways of formulating Paclitaxel to circumvent some of these issues would clearly be highly desirable.

In 1975, Ringsdorf introduced the concept of a polymer-anticancer drug.¹⁷ This prompted the study and development of a wide field of research, now broadly termed "polymer therapeutics" which, alongside polymeric drugs, includes the likes of

polymer-protein conjugates, multi-component micelles and polyplexes.¹⁸ The addition of a polymer to a drug delivery system has been shown to provide multiple therapeutic advantages such as increasing the plasma half-life, suppressing non-specific drug-protein interactions, improving drug solubility and allowing the combination of multiple active components in a single system.¹⁹ The first example of this involved the addition of poly(ethylene glycol), PEG, to a protein in a process called PEGylation, as demonstrated by Abuchowski *et al.* This was shown to significantly enhance the properties of bovine serum albumin and bovine liver catalase in mice (Figure 1.1).^{20, 21}

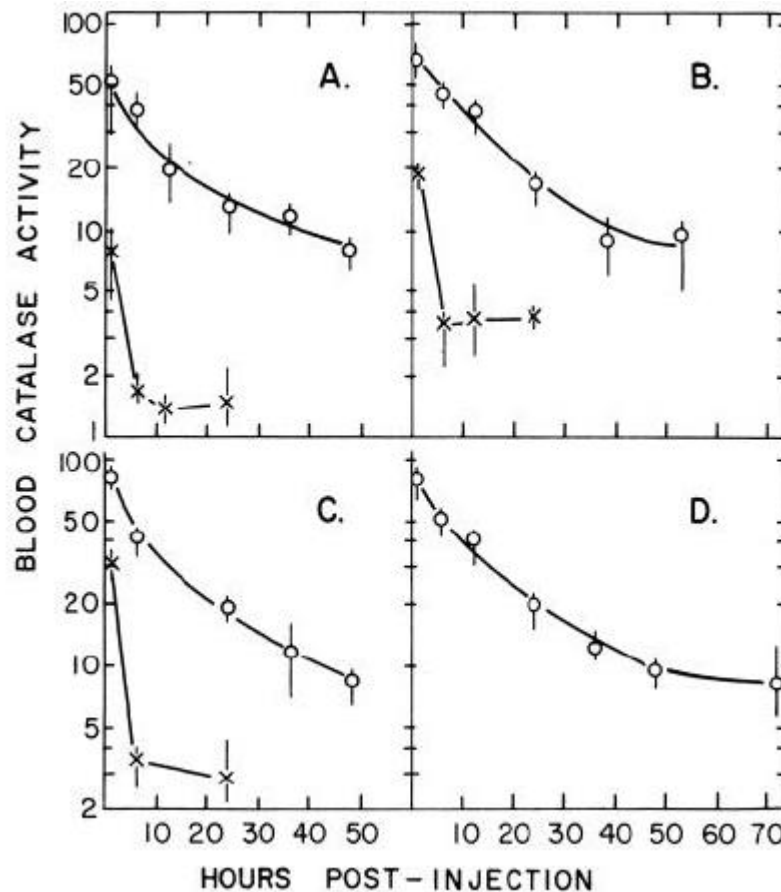


Figure 1.1 Blood circulating life of catalase (x) and PEG-5000-catalase (o) in acatalasemic mice. Circulation time determined following injections three times per week after 1 (A), 30 (B), 60 (C) and 90 (D) days. Individual points represent mean and range of 4 animals. Taken from work by Abuchowski *et al.*²¹

Cancer remains a common target for polymer therapeutics, largely due to the Enhanced Permeability and Retention (EPR) Effect which describes the preferential accumulation of macromolecular species in tumours. This effect occurs due to rapid angiogenesis which results in the formation of a “leaky” vasculature.^{22, 23} A classic clinical demonstration of this phenomenon is in gallium scintigraphy where the radioactive ⁶⁷Ga is injected intravenously; complexation of the gallium ion with the plasma protein transferrin produces a 90 kDa macromolecule complex which accumulates inside tumours to produce a distinct image.^{24, 25} In the early 1990’s, this concept inspired the preparation of SMANCS, the first polymer-protein therapeutic to reach the clinic comprising the anti-tumour protein neocarzinostatin (NCS) covalently linked to two styrene maleic anhydride (SMA) polymer chains. This development prompted a cascade of further research into polymer therapeutics.¹⁹

Although the size of macromolecular species does offer an intrinsic advantage over small molecule analogues in some cases, these compounds can also be applied in a more sophisticated fashion. For instance, the body is an incredibly complex organism possessing a plethora of biochemical microenvironments varying in, amongst others, temperature, pH, osmotic pressure, enzymes, metal ion concentration and redox conditions. Furthermore, these environments are known to vary between disease states. For example, Alzheimer’s and cardiovascular disease have been characterised by elevated levels of oxidative stress;^{26, 27} Huntingdon’s disease has been shown to illicit an elevated cerebral pH²⁸ whilst metal ions have emerged as a factor in epilepsy²⁹ and neurodegenerative states such as Parkinson’s disease.³⁰ It follows that such environments could be utilised to further improve the nature of drug delivery systems and hence target a range of disease states including and beyond cancer.³¹

1.3 Towards Well-Defined Polymers: Controlled Radical Polymerisation Techniques

The preparation of polymers for biological applications is often hindered by the inherent dispersity associated with such systems. Fortunately, modern developments in polymer chemistry have provided several innovative ways of producing materials with high levels of definition, *i.e.* compounds in which high levels of control over the molecular weight, dispersity and architecture are observed. These techniques are generally referred to as controlled (living) radical polymerisation (C(L)RP) processes.³²

The concept of a “living” polymer was first highlighted by Szwarc *et al.* in 1956 who noted the existence of “living” ends in the polymerisation of styrene by a sodium-naphthalene complex.^{33, 34} Following this ground-breaking report, the search for synthetic routes enabling high levels of control over the preparation of polymeric structures has progressed with ever-increasing speed. In the 1980's, Otsu and co-workers first suggested the concept of living radical polymerisation following the development of "iniferters" – initiators which can induce radical polymerisation *via* initiation, propagation, primary radical termination and transfer to another initiator molecule. These polymerisations functioned by the insertion of the monomer into the iniferter bond, leading to two iniferter fragments at both chain ends which can continue to propagate. The so-called "living radical process" was coined given the negligible presence of bimolecular termination.^{35, 36} More recent developments have seen the growth of additional C(L)RP processes providing the modern chemist with a toolbox from which increasingly well-defined polymers of a pre-designed molecular weight and low dispersity can be accessed easily. Today, materials

possessing a wide-range of architectures and topologies are routinely available, with one's own imagination arguably becoming the main limiting factor in the search for novel materials.

A variety of C(L)RP methodologies are now commonly used, a universal trait of which is the ability to cycle propagating chains between active and dormant states. The concentration of active radicals in a polymerisation mixture, and hence termination events, is therefore reduced. In Nitroxide-Mediated Polymerisation (NMP), this is achieved through the addition of an alkoxyamine initiator which results in the reversible end-capping of growing polymer chains with a nitroxide species.^{37, 38} Likewise, copper-mediated polymerisation techniques, of which an ongoing debate exists in the literature as to the true mechanism of this process, either single-electron transfer living radical polymerisation (SET-LRP)^{39, 40} or atom transfer radical polymerisation (ATRP),^{41, 42} cycles through the redox state of the metal (typically copper) catalyst used (Figure 1.2).

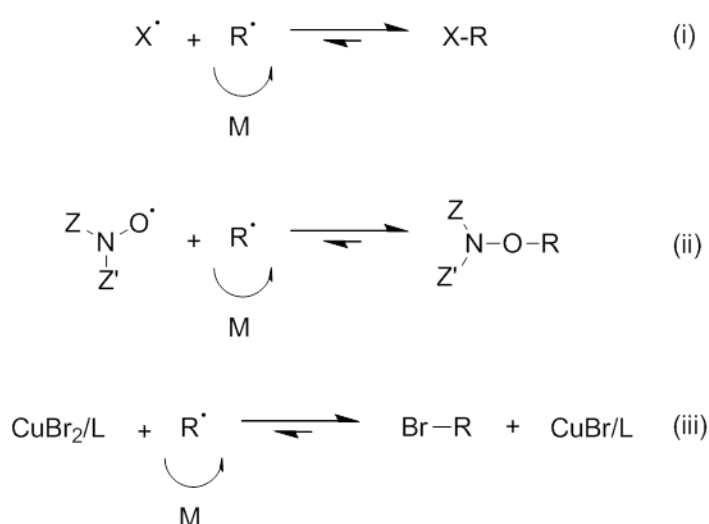


Figure 1.2 (i) General mechanism for C(L)RP processes and how this is achieved in (ii) Nitroxide-Mediated and (iii) copper-mediated polymerisation processes.

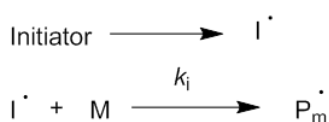
The other major C(L)RP method, Reversible Addition-Fragmentation Chain Transfer (RAFT) polymerisation, was first reported by the CSIRO group in 1998.⁴³ In this seminal work, a variety of (meth)acrylates, styrenic and acid(salt) monomers were polymerised by adding a small amount of a thiocarbonylthio-containing compound as a chain transfer agent (CTA, Figure 1.3) in an otherwise free radical process. This enabled the production of polymers with dispersities typically < 1.2.



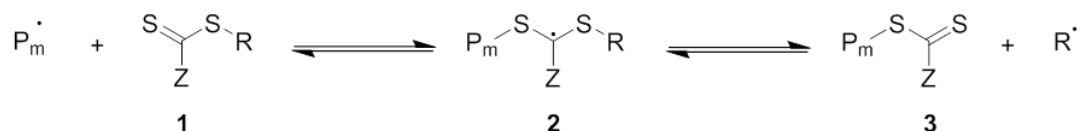
Figure 1.3 Chemical structures of the main classes of RAFT CTA.

Although an in-depth discussion of the mechanistic principles of RAFT is beyond the scope of this work, an overview of the generally accepted mechanism is shown below (Figure 1.4). Firstly, initiation is achieved in a conventional free-radical manner - the most common method of which is through the thermal decomposition of radical initiators such as 4,4'-azobis(4-cyanovaleric acid), ACVA, in which the initial radicals react with the CTA **1** to form species **2**. Then, an initial equilibrium develops in which the radical intermediate **2** can fragment to yield the original CTA or, an oligomeric RAFT agent **3** with a reinitiating radical. Following re-initiation, the main propagating equilibrium ensues in which exchange between growing radicals and thiocarbonylthio-capped species occurs *via* intermediate **4**. Finally, a small amount of termination will occur given its initiation based on free radical principles. It is for this reason that RAFT is sometimes referred to as a *pseudo*-living technique.⁴⁴

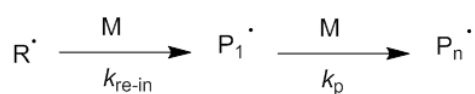
(i) Initiation



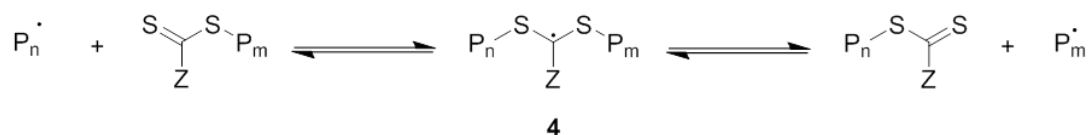
(ii) Initial Equilibrium



(iii) Re-initiation



(iv) Main Equilibrium



(v) Termination

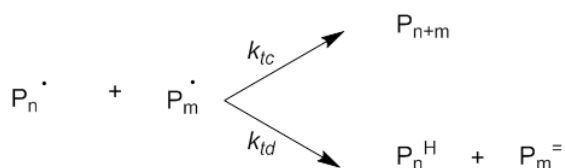


Figure 1.4 Generally accepted mechanism of the RAFT process.⁴⁴

RAFT is arguably one of the most versatile C(L)RP techniques. A wide range of monomer species are accessible through simple modifications to the CTA structure which, broadly speaking, contains two key components. Firstly, the "R" group, which initiates polymer chain growth, should be a better leaving group than the propagating radical and must also be sufficiently reactive to re-initiate polymerisation. Secondly, the "Z" group should activate the C=S bond towards radical addition before providing enough, but not too much stability, to the resultant adduct.⁴⁵ A number of factors have been shown to be important when optimising the

CTA structure for a given monomer and guidelines for effective Z and R groups have been provided by Moad *et al.*⁴⁶ In the case of the "R" group, factors such as steric bulk and polarity should be considered whilst the rate of addition to the C=S bond is generally high when Z=aryl, alkyl (dithioesters) or S-alkyl (trithiocarbonates), and lower when Z=O-alkyl (xanthates) or N,N-dialkyl (dithiocarbamates). Typically, dithioesters and trithiocarbonates are better for "more-activated" monomers such as vinyl aromatics, (meth)acrylates and (meth)acrylamides, whilst xanthates and dithiocarbamates are better for "less-activated" monomers such as vinyl esters and vinyl amides.⁴⁷ It should be recognised that tailoring CTA structure for each monomer is not ideal - the development of a "universal" CTA, which can be applied to all monomer classes, would help make the RAFT process even more accessible. Benaglia *et al.* have proposed a solution to this problem by preparing a pyridine-containing CTA which can polymerise different classes depending on the compounds electronics (Figure 1.5). When the CTA exists in its protonated and deprotonated states, controlled polymerisation of more and less activated monomers is achieved respectively.⁴⁸

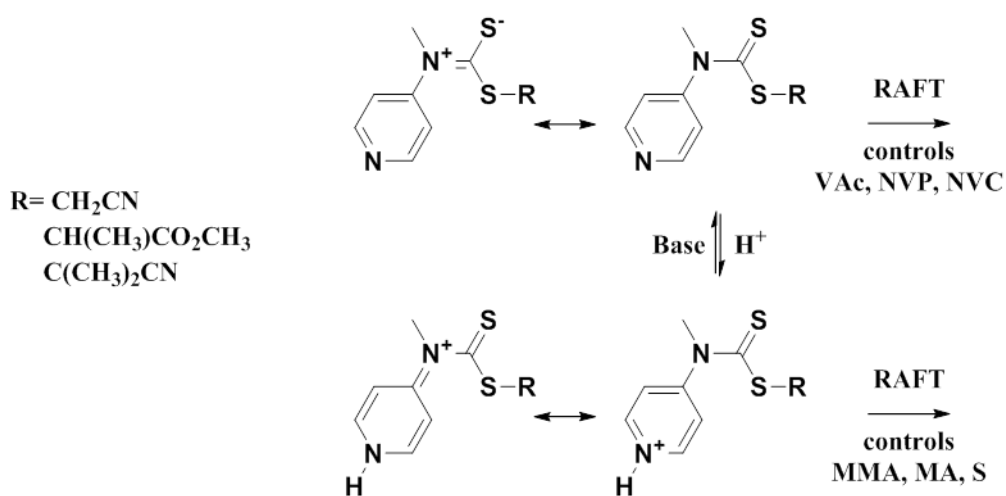


Figure 1.5 "Switchable" RAFT CTA developed by Benaglia *et al.*⁴⁸

An additional advantage of the RAFT methodology is its inherent ability to provide chemical functionality at both ends of the polymer chain. The α -terminus can be selected based on the R group of the CTA used, akin to the initiators employed in both NMP and copper-mediated polymerisations. Moreover, a particular advantage of RAFT is the presence of the thiocarbonylthio moiety at the ω -chain-end given its propensity for a variety of further chemistries.^{49, 50} For example, the addition of a nucleophile such as a primary amine (aminolysis) can produce a thiol terminus⁵¹ which can be used for a variety of reactions such as Michael addition,⁵² thiol-disulfide exchange⁵³ and for the functionalisation of gold nanoparticles.⁵⁴ Other reported reactions of the RAFT end-group include thermal elimination,^{55, 56} radical-induced removal^{57, 58} and hetero Diels-Alder addition.^{59, 60}

1.4 Stimuli-Responsive Materials: Looking to Nature for Inspiration

Much scientific research seeks to replicate what Mother Nature does so well. For one, She has mastered the concept of triggered responses providing us with endless examples of systems designed to react to changes in local environment. The human body is an excellent example of a carefully monitored and regulated system: The pancreas reacts to modulate our blood sugar levels,⁶¹ we intrinsically respond to repair wounds⁶² and muscular reflex reactions react to pain to help protect the body from further damage.⁶³ Responses can also be seen on a far broader scale, such as in the animal kingdom where camouflage is crucial for survival.⁶⁴ Inspired by Nature, the ability to prepare and apply synthetic materials capable of responding

specifically to one or multiple stimuli, either externally-applied or naturally occurring, has increasingly found itself at the fore-front of scientific and technological innovation.

As described above, the variety of biochemical environments present *in vivo* provide attractive targets for chemists looking to develop suitably amenable materials. The concept of “responsive polymers”, whereby materials undergo significant structural changes in response to an external stimulus, is not new and such materials, also often termed as “stimuli-responsive” or “smart”, have received increasing attention.⁶⁵ This has been further enhanced by the advances in C(L)RP given the high levels of definition afforded to polymer structures by these methods. Example stimuli can include temperature, pH, redox triggers, light, ultrasonication, ionic strength, magnetic and electric fields, whilst typical responses may include changes in shape, surface characteristics and solubility.⁶⁶⁻⁶⁹

1.5 Thermally-Responsive Materials

Of all stimuli-responsive materials, temperature is arguably the most commonly used trigger. These materials are characterised by a change in aqueous solubility, either the precipitation of a polymer solution at a lower critical solution temperature (LCST) or the solubilisation of a polymer precipitate at an upper critical solution temperature (UCST).⁷⁰ Generally for therapeutic applications, the LCST is of greater utility given the human body temperature of approximately 37 °C. This phenomenon is understood by considering how the “favourability” of mixing changes with variations in temperature, as derived from the Helmholtz equation of Free Energy

(eqn. 1). Binary mixing of two species A and B (ΔF_{mix}) is dependent on both entropic and enthalpic phenomena, where φ is the volume fraction of A, N_x is the number of lattice sites occupied by species A or B and χ is the Flory interaction parameter.

$$\Delta F_{mix} = kT \left[\frac{\varphi}{N_A} \ln(\varphi) + \frac{(1-\varphi)}{N_B} \ln(1-\varphi) + \varphi\chi(1-\varphi) \right] \quad (1)$$

The enthalpics of mixing depend heavily on the Flory interaction parameter, itself comprised of an entropic term (A) and a temperature-dependent enthalpic term (B) (eqn. 2). When $\chi < 0$, mixing is favoured and B is negative; when $\chi > 0$, mixing is disfavoured and B is positive.

$$\chi \cong A + \frac{B}{T} \quad (2)$$

The LCST can be appreciated by considering equation 2. X can be rendered more positive by increasing the temperature and hence negating the ‘B’ term. Likewise, for a UCST, where B is positive, χ can be decreased by increasing the temperature. In practice, polymers exhibiting LCST-type behaviour exist in flexible, extended coils when dissolved in aqueous solution due to extensive hydrogen bonding with the surrounding water molecules. As the temperature is increased, this bonding is disrupted allowing intra- and inter-molecular hydrogen bonding between polymer molecules, together with hydrophobic interactions to become significant. Consequently, the polymer chains hydrophobically collapse and aggregate in a globule conformation (Figure 1.6).⁷¹

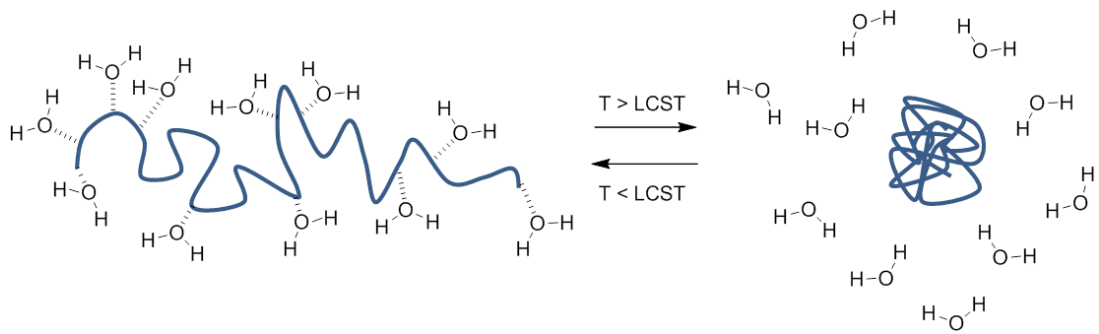


Figure 1.6 Schematic demonstrating the change in polymer conformation (coil - globule) observed when a polymer solution is heated through its LCST.

It should also be highlighted at this point that transition temperatures quoted in the literature are not always the absolute LCST. This single temperature is represented as the lowest point on a temperature vs. volume fraction phase diagram (Figure 1.7). In the absence of such a diagram, the term “cloud point” is a more suitable term, describing the temperature at which a solution transitions from transparent to opaque at a given solution composition (or concentration).⁷²

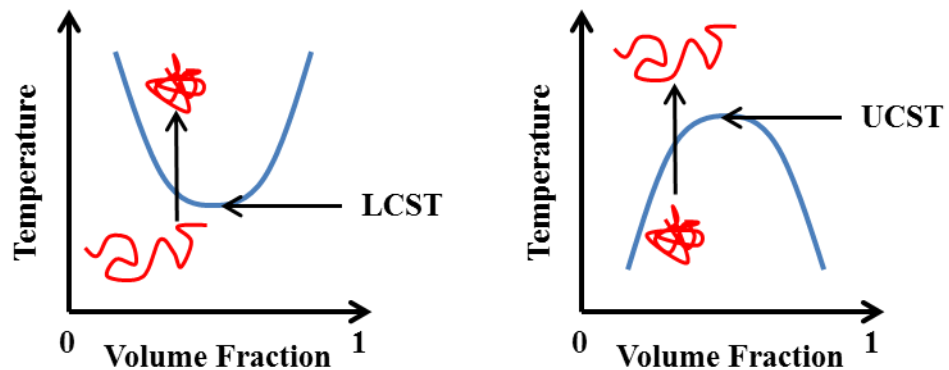


Figure 1.7 Representation of the phase transition associated with the LCST (left) and UCST (right). Blue line represents the phase separation boundary at which a cloud point is observed. Red line represents the conformational change of a polymer from coil (open chain) to globule (compact chain).

The earliest study reporting a thermal transition was discussed by Klotz and co-workers on a poly(*N*-isopropylacrylamide), pNIPAM, system.⁷³ They measured the kinetics of hydrogen-deuterium exchange in D₂O solutions and observed precipitation when the temperature of a 2 % aqueous polymer solution (molecular weight $\approx 200,000 \text{ g}\cdot\text{mol}^{-1}$) reached 31 °C. Although the most commonly used thermally responsive polymer is arguably still pNIPAM,⁷⁴ a wide range of other polymers have been introduced including poly(*N*-substituted (meth)acrylamide)s, poly(*N*-vinylalkylamide)s, poly(lactam)s, poly(pyrrolidone)s, poly(alkoxide)s and poly(2-alkyl-2-oxazoline)s.⁷⁵ The LCST response can also be translated into increasingly complex structures. For instance, thermo-responsive polymers have been used to instil the likes of polymer and inorganic nanoparticles with a responsive corona.⁷⁶⁻⁷⁸ Flat substrates have been functionalised such that the resulting polymer brushes can exist in extended or collapsed state depending on the temperature of the system^{79, 80} and desired properties have also been conveyed on polymer-protein conjugates.⁸¹⁻⁸⁴

The concept of an LCST transition holds a myriad of attractive applications such as to control cell culture and adhesion,^{85, 86} to influence catalytic activity,⁸⁷ and as a purification tool.⁸⁸ In a biological context, the hydrophilic-hydrophobic switch can be used to enhance a polymer's interaction with biological membranes. In this manner, the cell uptake of thermo-responsive architectures can be enhanced by employing polymers in their hydrophobic, collapsed state.⁸⁹ For instance, Saaka *et al.* have demonstrated that above their LCST poly[oligo (ethylene glycol) methyl ether methacrylates], pOEGMAs, are sufficiently lipophilic to insert into, or adhere to, lipid bilayers.⁹⁰ Edwards *et al.* have demonstrated that gold nanoparticles capped

with thermo responsive pOEGMAs can cross reversibly between a water/oil interface which was used as a basic mimic of a biological surface.⁹¹

Gold nanoparticles functionalised with a pNIPAM-*co*-acrylamide co-polymer possessing an LCST at 37 °C have also been used by Alexander and co-workers to drive uptake into human breast adenocarcinoma MCF7 cells. When heated at 40 °C (above LCST), an 80-fold greater uptake was observed compared to when the same cells were heated at 34 °C (below LCST).⁹² This group has also prepared polymer particles comprising a biodegradable lactide-*co*-glycolide core, in which was internalised the anticancer drug paclitaxel and the dye rhodamine 6G, and a thermo-responsive, PEG-based shell. A significantly enhanced uptake into MCF7 cells and paclitaxel-based cytotoxicity was observed when incubated above the particle thermal transition temperature (Figure 1.8).⁹³

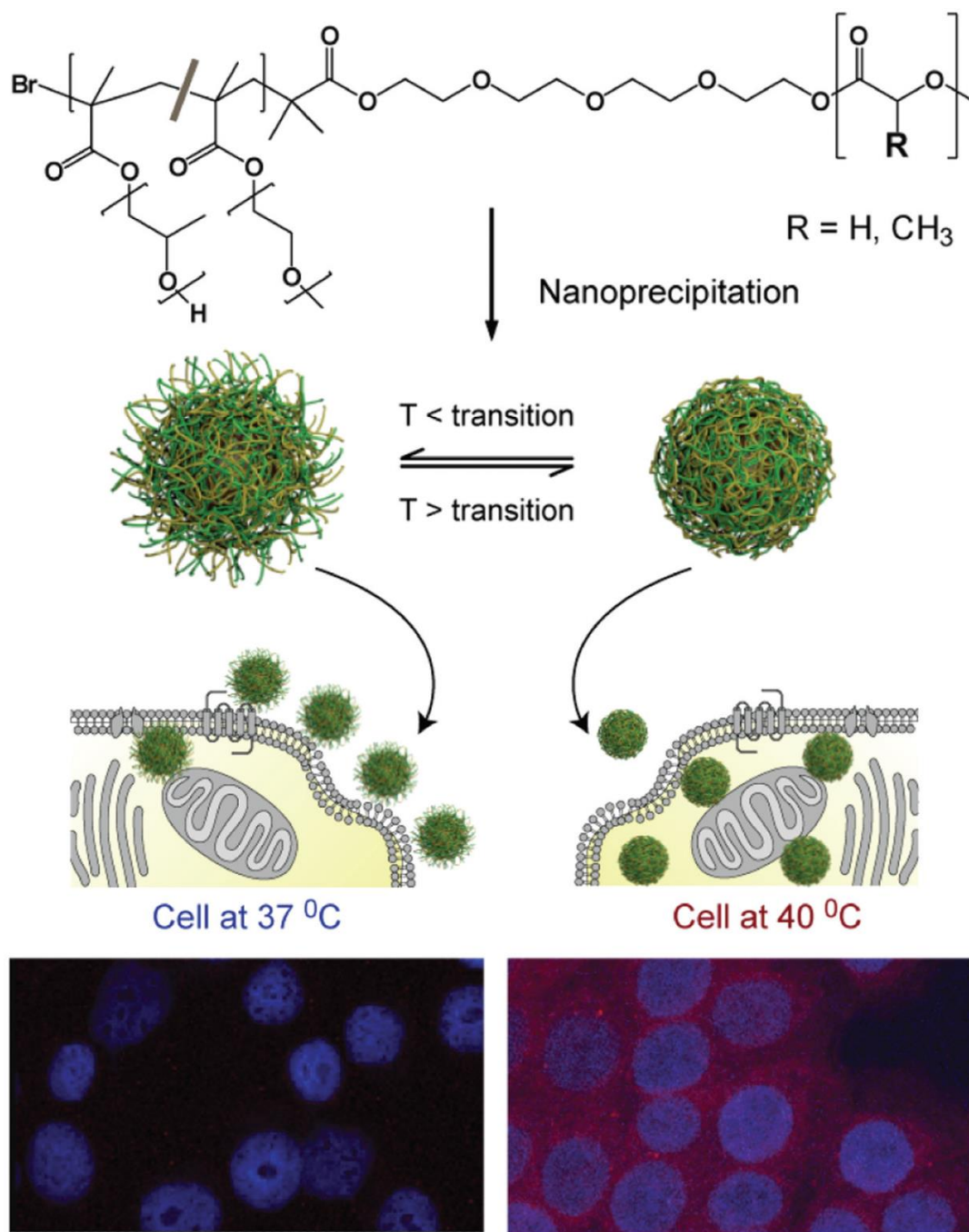


Figure 1.8 Formulation of thermoresponsive nanoparticles and the enhancement in cellular uptake due to change in surface corona with thermal response, as proposed by Alexander and co-workers: An increased signal from nanoparticle-encapsulated fluorescent dye is indicative of increased particle uptake above their thermal transition temperature in cells at 40 °C (bottom right) compared to 37 °C (bottom left).⁹³

Okano and co-workers have loaded polymeric micelles comprising pNIPAM and the hydrophobic poly(butylmethacrylate) with the anti-cancer drug andriamycin. Higher cytotoxicity towards bovine aortic endothelial cells was observed above the micelle LCST with the temperature-induced hydrophobicity triggering drug release and/or enhanced adsorption to cells mediated by hydrophobic interactions.⁸⁹ The same group has further explored the potential for thermo-responsive micelles prepared from fluorescently tagged p(NIPAM-*co*-dimethylacrylamide)-*b*-p(D,L-lactide) as drug delivery vehicles. These polymers were shown to form large aggregates and enhanced intracellular uptake into bovine carotid endothelial cells when held above the LCST. This uptake was proposed to be either the result of unique hydrophobic interactions between the cell membranes and hydrophobic micelle cores, promoted by a collapse of the thermo-responsive corona, or, due to the pNIPAM corona which can regulate micelle adhesion to cell surfaces and sustain intracellular uptake. Interestingly, the linear polymers devoid of a p(D,L-lactide) block (and hence unable to form micelles) exhibited no additional uptake when held above the LCST.^{94, 95} Alternatively, Chilkoti and co-workers have demonstrated the accumulation of pNIPAM-*co*-acrylamide inside solid tumours to be greater when heated above its cloud point, though not to the extent of a thermally responsive elastin-like polypeptide where a higher, two-fold increase was observed.⁹⁶

1.6 Modulating Thermal Transitions through Polymer Structure Manipulation: The “Isothermal” Response

A further extension of thermally-driven cell uptake lies in the treatment of disease. Many cancers, for instance, are characterised by mild hyperthermia (1-2 °C above healthy tissues) which can be used by materials to enhance targeted tumour delivery.⁹⁶⁻⁹⁸ Induced hyperthermia or thermotherapy using an external heat generator has therefore been applied previously as cancer treatment.⁹⁹ Alternatively, the ability to trigger the benefits of thermo-responsive polymer systems (*i.e.* a solubility switch), without the need for external energy sources may be beneficial. Indeed, as our material understanding improves, an obvious extension is to prepare substances capable of responding to multiple stimuli, either in a parallel nature, or by serial interplay whereby the impact of one response affects another.¹⁰⁰ It follows that for thermally-responsive systems, the hydrophilic-hydrophobic balance could be manipulated *isothermally*, through changes in the local environment. This can be understood by considering a simplified phase diagram of a typical LCST process where, at a fixed temperature (T_1), the phase separation boundary of a system can be increased such that a hydrophobic polymer globule can solubilise (Figure 1.9A) or a hydrophilic coil can precipitate (Figure 1.9B). This provides an attractive approach where *in vivo* applications are to be considered. For example, the ability to trigger a solubility switch based on disease biomarkers, of which there are several including changes in pH or redox environment, would help increase specificity and minimise side-effects.¹⁰¹ Such a programmed response also offers a route towards specific,

controlled therapeutic release.^{102, 103} Removing the need for an external heat source may benefit patient compliance, such as in some hyperthermic cancer treatments for instance, and would remove the sometimes challenging need for an energy source that can penetrate sufficiently through the skin.¹⁰⁴

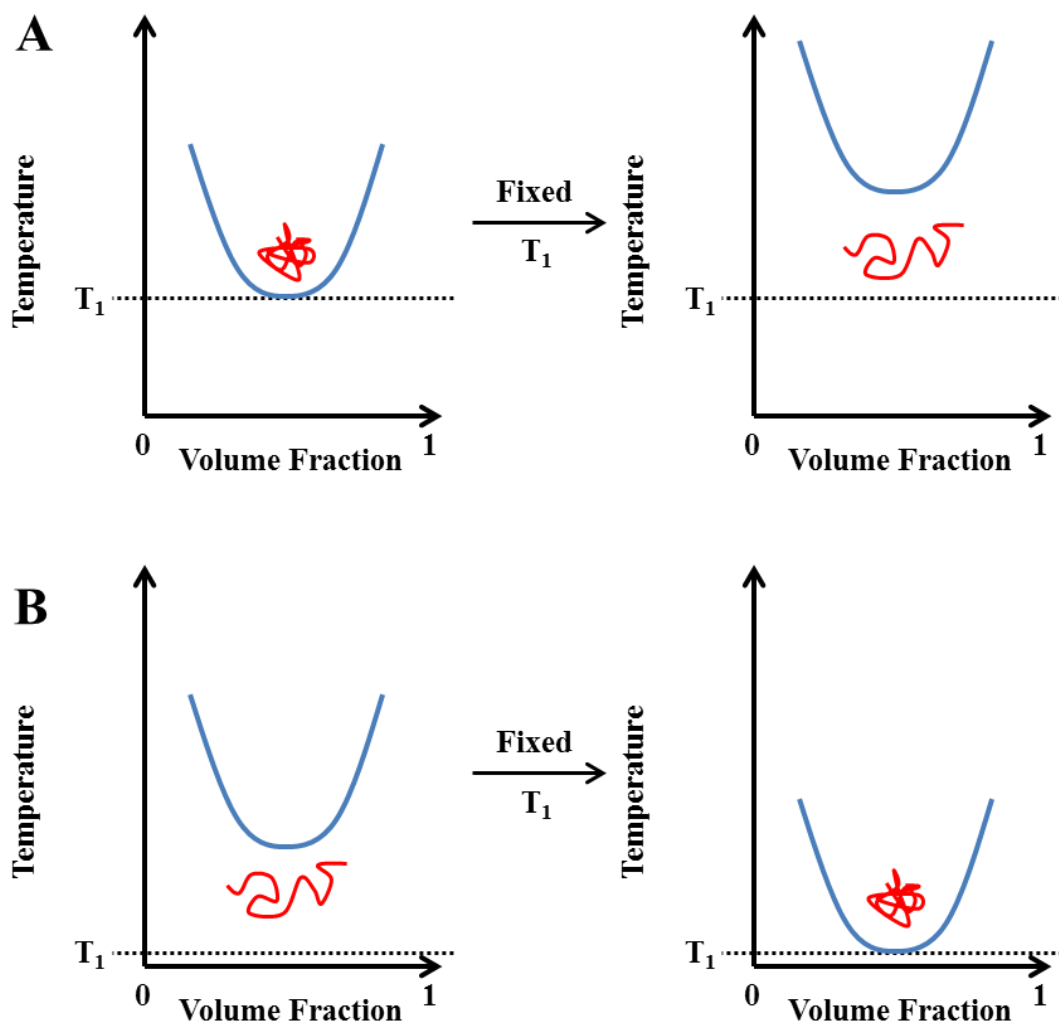


Figure 1.9 Representation of the phase diagrams associated with a polymer exhibiting an isothermal LCST transition at a fixed temperature, T_1 . Blue line represents the phase separation boundary at which a cloud point is observed. Red line represents a polymer coil (open chain) or globule (compact chain).

To respond to such environments, a carefully designed synthetic structure is required. Analysis of a typical polymer suggests four main areas which could be manipulated to alter the overall hydrophilic-hydrophobic balance of the compound and hence the transition temperature of an aqueous polymer solution. These are the (i) backbone; (ii) end-group(s); (iii) side-chain or (iv) local aqueous environment (*i.e.* presence of additives, Figure 1.10).

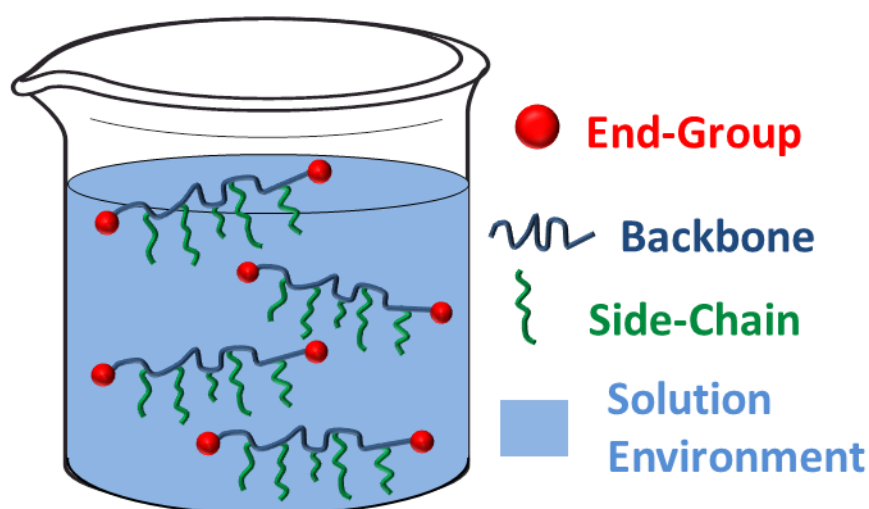


Figure 1.10 Areas of a polymer structure/solution which may be modified to tune the macroscopic behaviour.

The following sections therefore seek to highlight some of the published reports describing the use of multiple stimuli to achieve changes in polymer LCST by influencing these areas of a polymer chain. It should be noted that some cases merely demonstrate the ability to shift the system LCST; not all utilise the change to trigger an isothermal property change.

1.6.1 Triggering an “Isothermal” Response *via* Backbone Modification

To introduce a responsive element to polymer backbones, functionality beyond the carbon-carbon chains intrinsic to many polymerisation processes is required. Poly(esters) or poly(amides), prepared by ring-opening or NCA polymerisation respectively, offer a route towards this where degradation by hydrolytic and/or enzymatic means is possible. Moreover, the development of further functionalised backbones upon which further chemistry can be performed remains an important area of study.¹⁰⁵⁻¹¹⁰ Poly(sulfides) provide an option for situations in which an oxidative response, such as those found in wound sites, is required^{111, 112} and poly(disulfides) have potential application given the highly reducing environment found within cells compared to the systemic circulation.^{113, 114} However, there are minimal reports using backbone degradation or alteration to further manipulate the material's thermal response. One report which has utilised a functional polymer chain, namely PEG, has been described by Choi *et al.* who showed the polymer LCST to be sensitive to the gases dissolved in the solution. A reversible LCST was observed between the temperatures of 24.5 °C to 26.0 °C when dissolved carbon dioxide was replaced by oxygen. This observation was accounted for by considering differing degrees of PEG dehydration and also minute differences in the intermolecular interactions in the presence of the two gases.¹¹⁵ Given the lack of additional reports, methods of combining main-chain degradation with thermal responses would be a profitable investigation.

1.6.2 Triggering an “Isothermal” Response *via* End-Group Modification

The development of C(L)RP has increasingly afforded polymers with high levels of structural control. Importantly, the functionality of both chain-ends is now routinely accessible following careful selection of the chain transfer agents/initiators that are employed, and/or through the use of post-polymerisation modification methodologies.¹¹⁶⁻¹¹⁸ Thermo-responsive polymer function can therefore be elegantly modified using single, simple alterations to the chain-end in a controlled manner to manipulate the hydrophilic-hydrophobic balance. The functionality of any end-groups is known to have a pronounced effect on the thermal transition temperature with hydrophilic/hydrophobic moieties generally increasing/decreasing the overall LCST respectively.¹¹⁹⁻¹²¹ Moreover, the effect of the end-group is more pronounced with decreasing molecular weight on account of it contributing to a higher percentage of the total structure.^{122, 123}

Theato and co-workers prepared thermally responsive systems based on pOEGMA in which the hydrophilic-hydrophobic balance could be modulated by irradiation with light. Samples were prepared by the RAFT methodology and azobenzene units installed at either the α -terminus alone, or at both chain-ends using a combination of functional CTAs and aminolysis-based post polymerisation processing. The LCST of the polymers decreased with increasing azobenzene incorporation and with decreasing polymer chain length. Moreover, azobenzene units undergo a *trans-cis* conformational change upon application of UV light, which was shown to increase the LCST due to a change in dipole moment. This transition could also be reversed

by irradiating with visible light, providing a region in which a light-triggered isothermal transition could be realised (Figure 1.11).¹²⁴

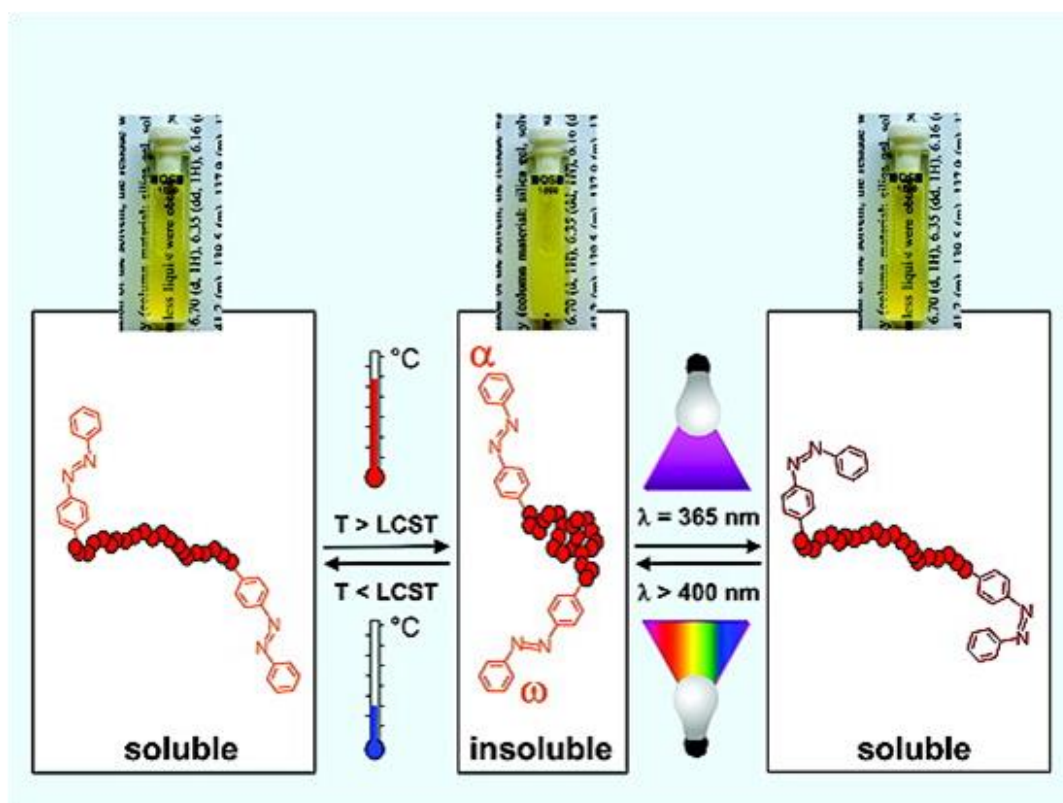


Figure 1.11 Light-triggered isothermal transition: The application of different wavelengths of light to alter the conformation of α - and ω -terminal azobenzene units and hence the LCST, as described by Theato and co-workers.¹²⁴

Hyperbranched polymers provide an attractive option for end-group modulations given the inherently large number associated with their structure. The Rimmer group has exploited this to prepare imidazole-terminated hyperbranched pNIPAM which exhibit higher LCSTs in the presence of Cu(II) due to an increased hydrophilicity of the polymer chains.¹²⁵ Similarly, when functionalised with vancomycin or polymyxin end-groups, a selective ligand for Gram-positive/negative bacteria respectively, incubation with *Staphylococcus aureus* or *Pseudomonas aeruginosa* induced a coil-

to-globule phase transition. Subsequent cooling of the aggregated bacterium/polymer mixture below its LCST released the bacterium.^{126, 127}

pH remains an intriguing stimulus given the range found throughout the body and in diseased tissues. For instance, *in vivo* pH ranges from 1 – 8.2, whilst chronic wounds and cancer tumours have different pH to healthy tissues.⁷² Typical monomers which are pH responsive are those containing carboxylic acid or tertiary amine functional groups which can be deprotonated or protonated respectively to generate polyelectrolytes from neutral starting materials.¹²⁸ Work by Stayton and co-workers using carboxylic acid-terminated pNIPAM-*co*-propylacrylic acid exemplifies this, where alkaline conditions prompted an increase in LCST due to ionisation of the chain-end.¹²⁹

1.6.3 Triggering an “Isothermal” Response *via* Side-Chain Modification

The side-chain remains the most commonly accessed way of influencing the macromolecular properties of a polymer given the wide-range of monomers applicable to C(L)RP and easy modification of the resulting structure. For example, the ability to tailor the polymer response by co-polymerising with hydrophilic or hydrophobic monomers is well known.¹³⁰⁻¹³⁴ Jochum and Theato have prepared thermo-responsive acrylamides containing salicylideneaniline groups *via* postpolymerisation modification of a poly(pentafluorophenyl acrylate) precursor. Salicylideneaniline is known to isomerise upon UV irradiation from the *enol* form to the *keto* form, with the accompanying difference in dipole moment capable of influencing the polymer LCST.¹³⁵ Light has also been used by Shimoboji *et al.* to regulate substrate access and enzyme activity of endoglucanase 12A. This was

achieved by varying the wavelength of light irradiated on copolymers of *N,N*-dimethylacrylamide (DMA) and azophenyl-containing monomers held at a fixed temperature. Changes in size and hydration of the polymer chain were photo-induced to regulate enzyme activity.¹³⁶ Light-triggered solution self-assembly of amphiphilic co-polymers comprising NIPAM, ethylene oxide and azobenzene-functional acrylamide blocks has been described by Liu *et al.* The LCST of the co-polymers decreased with increasing hydrophobic azobenzene units up to 11 mol% before unexpectedly increasing above this. Moreover, a surprising decrease in LCST upon irradiation with UV light was observed, implying the azobenzene units in their more polar (*cis*) form exhibit poorer aqueous solubility, in contrast to that typically expected. This was shown to correlate with the formation of inter-chain assemblies in solution, highlighting the potential of hydrophobic clustering as a tool for tailoring the thermal properties of these polymer systems.¹³⁷ In addition to azobenzene and salicylideneaniline,¹³⁵ studies utilising fulgimides¹³⁸ and spiropyran¹³⁹ as light-responsive units have also been reported.

Another popular motif for influencing a systems' solubility is based on compound binding/sequestration. Yin and co-workers have developed an isothermal, thermochromic sensor based on an ABC triblock copolymer consisting of pNIPAM, poly(methacrylic acid) and poly(2-hydroxyethyl methacrylate) which was modified to contain tetra(4-carboxylatophenyl)porphyrin. In water at 32 °C, the polymer has a transparent, red-brown colour which becomes turbid and orange when heated above its LCST due to porphyrin aggregation. When held below its cloud point, a variety of colours are produced depending on the metal cation added to the system. The sensor also displayed thermochromic characteristics in the temperature range of 35 – 61 °C depending on the metal ion used (Figure 1.12).¹⁴⁰

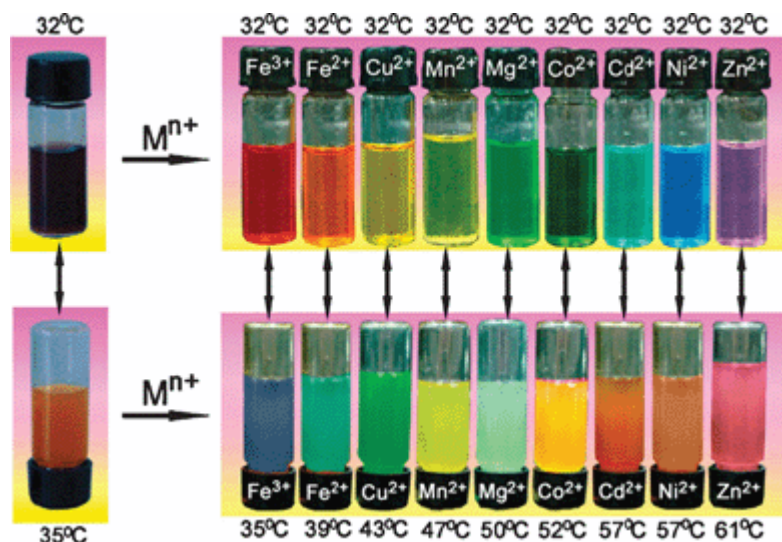


Figure 1.12 Metal ion-driven isothermochromic sensor: Observed changes in the solubility and colour in the absence (left) and upon introduction (right) of various metal ions.¹⁴⁰

Wischerhoff and co-workers have used protein binding to influence the thermoresponsive behaviour of biotin-containing pOEGMA samples prepared by free-radical polymerisation. The high affinity of this unit for avidin was used to manipulate the LCST with the cloud point increasing proportionally with avidin concentration up to a maximum of 9 °C at 60 $\mu\text{mol.L}^{-1}$. This observation suggested the polymer-biotin complex was more hydrophilic than the polymer alone. The specificity of this binding process was demonstrated by a reduction in LCST upon the addition of free biotin due to competition with the polymer-bound avidin.¹⁴¹

Redox cycling motifs have been applied by a variety of groups to modulate the LCST of thermo-responsive systems. For example, Fu *et al.* have synthesised acrylamide co-polymers containing *N*-isopropyl and redox-sensitive 4-*N*-amino-2,2,6,6-tetramethylpiperidin-1-oxyl-4-yl (TEMPO) groups. The incorporation of 5 – 10 % TEMPO groups in the copolymer structure was sufficient to afford the material redox-responsive LCST behaviour: At a polymer concentration of 10 mg.mL^{-1} ,

reduction with 19.2 mM ascorbic acid increased the LCST by 14 °C whilst re-oxidation with 48 mM $K_3[Fe(CN)_6]$ largely reversed the change.¹⁴² Simple redox activity of the ferrocene/ferrocenium ion pair has been used by Kuramoto and Shishido to shift the cloud point of a variety of thermo-responsive polymers isothermally.^{143, 144} Likewise, Peng and co-workers have used host-guest complexation between ferrocene and β -cyclodextrin as a means of modulating the LCST of a thermo-responsive co-polymer comprising *N,N*-dimethylacrylamide and ferrocene. When in its reduced form, ferrocene could interact with β -cyclodextrin (β -CD), increasing the LCST due to disruptions in hydrophobic associations between ferrocene side groups. However, minimal change in LCST was observed when the ferrocene was oxidised to the ferrocenium ion due to a weaker interaction with β -CD.¹⁴⁵ The same group has developed an approach to self-tuneable thermosensitive behaviour using the Belousov-Zhabotinsky reaction. Redox-triggered dynamic complex formation between NIPAM-containing co-polymers and a terpyridine-ruthenium complex was sufficient to cycle the system between soluble and insoluble states.¹⁴⁶

The application of pH to trigger hydrophilic-hydrophobic changes in the side-chain has been explored by several groups. Xiao *et al.* demonstrated a significant effect of pH on the LCST of tertiary amine-functionalised poly(L-glutamates). As the *N*-substituted groups became more hydrophobic, the LCST was observed to increase in acidic conditions due to the increased hydrophilicity imparted by the protonated amino group.¹⁴⁷ Müller and co-workers have employed a similar strategy to change the cloud point of star and linear polymers of poly(*N,N*-dimethylaminoethyl methacrylate), pDMAEMA.¹⁴⁸ Several other examples describing the protonation of

tertiary-amine functionalised side-chains as a way of altering LCST have also been reported.^{149, 150}

The incorporation of acid-labile groups has proven attractive where a response at low pH is required. For example, Huang *et al.* have prepared polymers from *N*-(2-ethoxy-1,3-dioxan-5-yl) methacrylamide where hydrolysis of the cyclic orthoester to hydroxyl groups allowed complete re-solubilisation of previously hydrophobic polymers at 37 °C - an acid-catalysed isothermal transition.¹⁵¹ Similarly, Heath *et al.* have used trimethoxy benzene-linked acetal-functional polymers to influence the solution self-assembly of NIPAM-based materials isothermally. This was achieved due to increased system hydrophilicity upon acid-catalysed cleavage of an acetal to diol.¹⁵² Acetals have also been employed by Zhang *et al.* to raise the cloud point of tri(ethylene glycol) acrylate-based co-polymers upon cleavage. In this case, acid-catalysed hydrolysis was used to promote micelle disassembly at pH 4, release the encapsulated Nile Red within 200 hrs and re-solubilise the polymer materials. The co-polymers were also shown to be well tolerated by the mouse macrophage (RAW264.7) cell line and a primary dermal fibroblast cell line (HCA2-hTERT).¹⁵³ Monteiro and co-workers have devised a clever hydrolysis-based degradation strategy to disassemble nanoparticles within a pre-determined timeframe (Figure 1.13). Micelles were prepared by heating a solution of diblock copolymers comprising a hydrophilic pDMA block and a random copolymer block comprising *N,N*-dimethylaminoethyl acrylate, DMAEA, butyl acrylate, BA, and NIPAM at 37 °C (above NIPAM LCST). As DMAEA hydrolysed to acrylic acid, the LCST of the diblock increased above 37 °C resulting in micelle disassembly. The time taken for disassembly to start was controlled by the number of BA units whilst the time taken

for complete disassembly was controlled by the number of DMAEA units in the polymer structure.¹⁵⁴

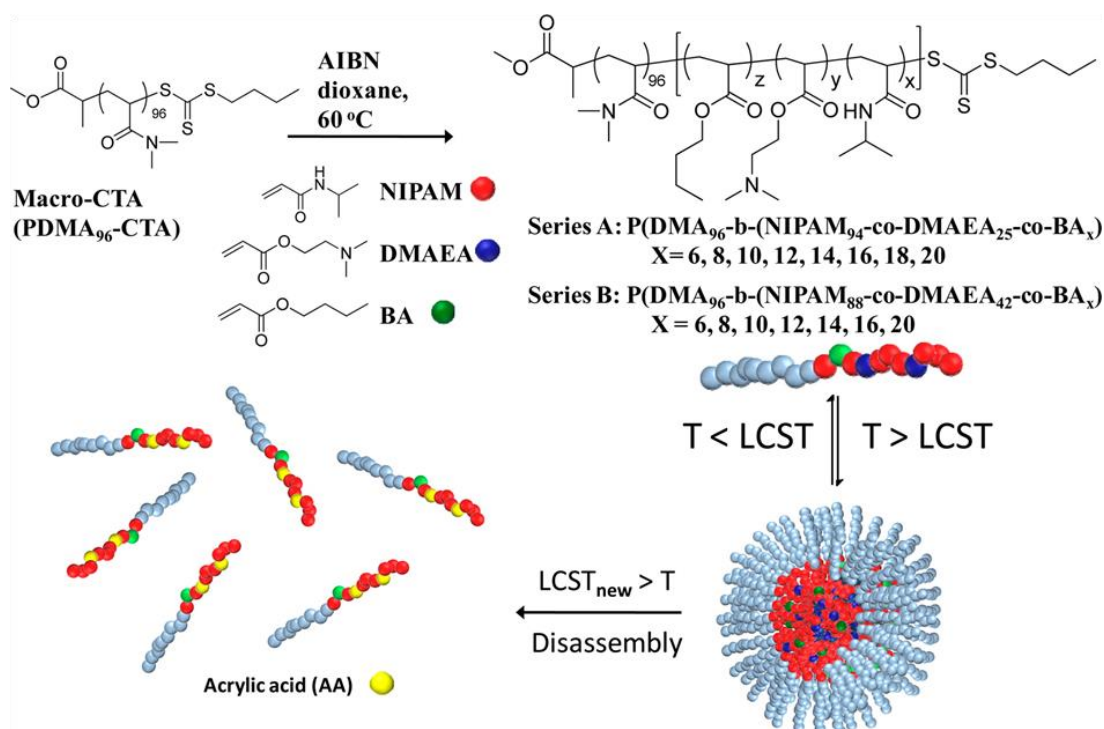


Figure 1.13 Acid-catalysed isothermal transition: Synthesis and self-assembly of thermoresponsive and self-catalysed degradable polymers described by Monteiro and co-workers. Degradation of DMAEA to acrylic acid shifts the polymer LCST and triggers micelle disassembly.¹⁵⁴

Other stimuli that have also been applied to trigger an “isothermal”-type transition include ultrasound, dynamic covalent bond formation, dissolved gases and enzymes. Ultrasound, a longitudinal pressure wave with frequency above 20 kHz, has been used for a variety of medical applications including tissue ablation and release of drugs from a polymer matrix. This is largely due to the heat generated following absorbance of energy by tissues and delivery systems.^{155, 156} Using this trigger, Xuan *et al.* prepared micelles from a diblock copolymer comprising the water soluble poly(ethylene oxide), pEO, and the thermoresponsive poly(2-(2-

methoxyethoxy)ethyl methacrylate). The latter block was modified to contain a small amount of high-intensity focused ultrasound (HIFU)-labile 2-tetrahydropyranyl methacrylate (THPMA). Hence, ultrasound irradiation-triggered hydrolysis of the THPMA groups to the more hydrophilic methacrylic acid increased the LCST resulting in isothermal micelle disassembly.¹⁵⁷

Bon and co-workers have exploited hydrazide-aldehyde chemistry to control the solubility of pNIPAM-based microgels. Here, the addition of aldehydes to a methacryloyl hydrazide containing co-polymer chain furnished dynamic hydrazone bonds. Importantly the microgel solubility, and hence volume phase transition, could be modulated by careful selection of aldehydes with varying hydrophilicities.¹⁵⁸

Guo *et al.* prepared an amidine-based polymer which underwent a hydrophobic-hydrophilic transition using CO₂ as a stimulus. When added to a biphasic water-chloroform system, the polymer initially resided within the organic layer. However, upon bubbling with CO₂, the amidine groups converted into amidinium bicarbonates producing a charged, hydrophilic polyelectrolyte which transferred into the aqueous phase. Moreover, the reversible hydrophilic-hydrophobic transition was observed to be reversible at 60 °C upon the bubbling of CO₂ or N₂ respectively.¹⁵⁹

Finally, the ability to alter solubility isothermally through enzymatic activity has obvious application *in vivo*, yet there are few examples in the literature. Thayumanvan and co-workers tethered varying numbers of pOEGMA chains to oligoamine scaffolds also containing a hydrophobic, methyl ester-terminated alkyl chain. Upon increasing the number of pOEGMA chains involved from one (monomer) to six (hexamer), a systematic decrease in the LCST was observed. Moreover, incubation with porcine liver esterase converted the methyl esters to a

more hydrophilic carboxylic acid. Thus, a significant increase in the onset temperature was observed following enzyme treatment at pH 7.4, whilst no change was seen in the absence of enzyme. To verify the propensity for ester hydrolysis, the authors measured the cloud point without enzyme at various pH. Whilst the cloud point gradually increased at pH 10.8 due to hydrolysis and subsequent deprotonation of the carboxylic acid group, no change was observed between pH 5.0 and pH 8.5, confirming the change in LCST was due to esterase-mediated degradation.¹⁶⁰

1.6.4 Triggering an “Isothermal” Response *via* the Surrounding Environment

The phase separation properties of an aqueous polymer solution are well-known to be influenced by the presence of a variety of additives. Salts, for instance, are able to act as water "structure-makers" or "structure-breakers", thus affecting the polymer hydration shell and the resulting transition temperature.¹⁶¹⁻¹⁶³ This is largely dictated by the Hofmeister series which originates from the ability of ions to precipitate egg white proteins.¹⁶⁴ Surfactants have been shown to improve the solubility of polymer chains and hence increase the transition temperature as they adsorb onto the polymer by means of their hydrophobic tails, either individually or as micelles.^{165, 166} Ionic liquids have been shown to have an impact depending on their hydrophilicity; the LCST of poly(*N*-vinylcaprolactam), for example, increases in the presence of hydrophobic ionic liquids, but remains largely unaffected in the presence of hydrophilic alternatives.¹⁶⁷ Other additives such as saccharides¹⁶⁸ and alcohols¹⁶⁹ have also been reported to have an effect. It therefore stands to reason that alterations in the solution in which the polymer is dissolved can be used to isothermally change its solubility.

To date, most reports have used salts to achieve this. Alexander and co-workers prepared thermally responsive co-polymers of different OEGMAs containing 3 and 8 PEG units. A linear increase in LCST was observed with increasing proportions of the more hydrophilic, larger PEG-containing OEGMA. Incubation of these polymers with NaSCN (a strong chaotrope), NaCl and Na₂SO₄ (a strong kosmotrope) greatly affected the cloud point with NaSCN and Na₂SO₄ prompting an increase and decrease respectively. "Hybrid" co-polymers were then prepared by adding an additional 8-PEG containing OEGMA homoblock to the pre-existing statistical co-polymer. As the two blocks had different LCSTs, heating at a temperature above the LCST of the statistical block, but below that of the homoblock generated micelles, in which the dye carboxyfluorescein was encapsulated. When these micelles were held at 37 °C, minimal dye release was observed. The addition of NaCl however lowered the cloud point of the statistical block so that it returned to a hydrophilic state, resulting in micelle disassembly and dye release. Sharper release was observed when Na₂SO₄ was added due to a salting-out effect.¹⁷⁰ Wang *et al.* have used the influence of salts to affect the self-assembly behaviour of double hydrophilic block co-polymers comprising the weak polybase poly(*N*-(morpholino)ethyl methacrylate), pMEMA and the zwitterionic poly 4-(2-sulfoethyl)-1-(4-vinylbenzyl)pyridinium betaine, pSVBP. In aqueous solution, pMEMA becomes insoluble in the presence of Na₂SO₄ (> 0.6 M), whereas pSVBP dissolves in the presence of NaBr (> 0.2 M). Hence, "schizophrenic" micellisation behaviour was observed depending on the concentrations and types of salts added.¹⁷¹

Bloksma *et al.* have also demonstrated the Hofmeister effect on poly(2-oxazoline)s observing an ionic response that was strongly dependent on the hydrophilicity of the polymer. Here, the LCST of the most hydrophilic polymer, poly(2-ethyl-2-

oxazoline), could be tuned over almost the whole temperature range of water under atmospheric pressure whilst the LCST of the more hydrophobic poly(2-isopropyl-2-oxazoline) and poly(2-*n*-propyl-2-oxazoline) varied to a lesser extent. Comparisons between linear and comb polymers highlighted the architecture did not significantly influence the effect of the Hofmeister ions.¹⁷² Finally, Sharma and Srivastava have prepared amphiphilic random copolymers based on biodegradable polyaspartamides that respond to temperature, pH and metal-ions. Reversible thermosensitivity was achieved by the attachment of the hydrophobic 1-propylimidazole or hydrophilic, dimethylpropylammonium pendants. The anions of the Hofmeister series were found to affect the thermosensitivity. Modulation of the LCST was also achieved by varying the pH or by including metal ions in the solution (Figure 1.14).¹⁷³

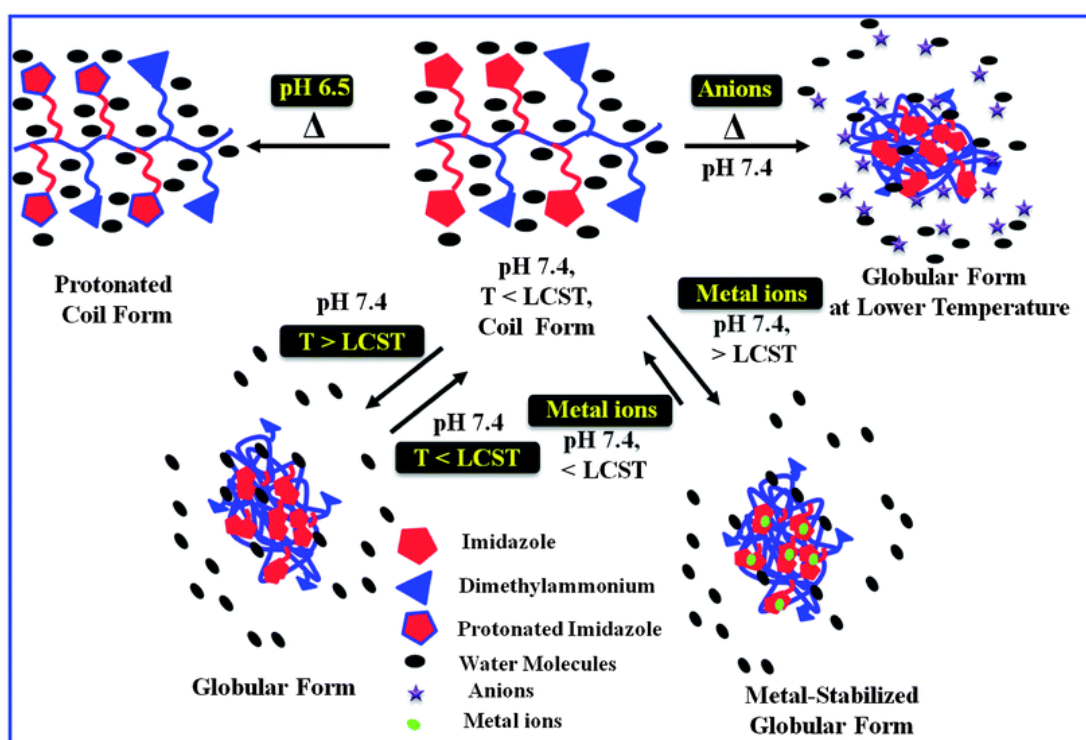


Figure 1.14 Summary of the multi-responsive co-polymers prepared by Sharma and Srivastava. Response to temperature, pH, anions and transition metals was observed.¹⁷³

1.7 Aims and Thesis Summary

Considering the above, this project aimed to develop several ways of introducing polymer solubility switches under physiologically-relevant conditions utilising the diverse sections of a polymer chain. Analysis of the literature suggests the number of examples using backbone modifications is sparse. **Chapter 2** describes a novel method with which to introduce redox-susceptible disulfide linkages into a thermo-responsive backbone. A post-polymerisation modification strategy is used to introduce these linkages into pNIPAM chains which exhibit an inversely proportional relationship between cloud point and molecular weight. Selective degradation by a crucial *in vivo* anti-oxidant (glutathione) at intracellular concentrations, rather than those found in the extracellular environment, is demonstrated. The associated change in molecular weight is sufficient to trigger a change in cloud point, allowing for an isothermal solubility switch.

Literature examples using end-group modifications to alter a polymer's solubility are also limited. This is perhaps surprising given the elegant and simple nature of a single functional-group modification as a way of altering a system's macroscopic properties. In **Chapter 3**, the LCST is first used to prepare polymer nanoparticles following a "nanoprecipitation"-type approach using hot water as the "bad solvent". These polymers contain a disulfide end-group which is easily installed by judicious application of a functional RAFT chain transfer agent. Glutathione-mediated cleavage of this disulfide end-group is shown to be sufficient to disassemble these polymer nanoparticles and release encapsulated cargo. Moreover, this degradation increases the hydrophilicity and hence cloud point of the polymers used, meaning the resulting polymer matrix can be re-solubilised, isothermally.

Chapter 4 describes another simple end-group modification using a metal-ion binding phenomenon to cause isothermal precipitation of an aqueous polymer solution. The 1,2-dihydroxybenzene (catechol)-Fe³⁺ binding motif, which is of critical importance in the competitive sequestration of iron by bacteria inside mammalian hosts, is applied and shown to decrease the cloud point of a catechol-terminated thermo-responsive polymer.

Chapter 5 describes the first example of a gold nanoparticle-based biosensor based on the catechol-Fe³⁺ binding motif for the detection of physiologically relevant iron concentrations. Gold nanoparticles were coated with water-soluble polymer chains containing a catechol moiety protruding from the nanoparticle surface. The introduction of Fe³⁺ at concentrations found in serum (between 8 and 25 μM) was sufficient to cause gold nanoparticle aggregation due to catechol-unit cross-linking and hence introduce an optical, colorimetric response.

Finally, **Chapter 6** describes an alternative method of triggering polymer precipitation isothermally using side-chain modifications. Specifically, given the minimal examples describing enzymes as LCST-modifiers, a polymer with a phosphorylated side-chain is prepared and shown to be degraded by calf intestinal alkaline phosphatase. Thermally responsive co-polymers containing partially phosphorylated side-chains are then prepared. The enzyme-mediated functional group interconversion of phosphate to less hydrophilic hydroxyl group promotes a reduction in cloud point, causing isothermal polymer precipitation. Initial investigations into the biocompatibility of these polymers with MCF7 cells, together with the ability to enhance polymer uptake by heating the polymer through its LCST are described. Finally, attempts to trigger this uptake isothermally, using phosphatase-mediated dephosphorylation as a trigger, are discussed.

1.8 References

- 1 Riedel, S. Edward Jenner and the history of smallpox and vaccination. *Proc. (Bayl. Univ. Med. Cent.)* **2005**, *18*, 21-25.
- 2 Centers for Disease Control and Prevention. Poliomyelitis. In *Epidemiology and Prevention of Vaccine-Preventable Diseases*, Atkinson, W.; Wolfe, C.; Hamborsky, J., Eds. Public Health Foundation: Washington DC, **2012**; pp 249-261.
- 3 Shanmugalingam, T.; Soultati, A.; Chowdhury, S.; Rudman, S.; Van Hemelrijck, M. Global incidence and outcome of testicular cancer. *Clin. Epidemiol.* **2013**, *5*, 417-427.
- 4 Office for National Statistics. Cancer Statistics Registrations, England (Series MB1), No. 42. <http://www.ons.gov.uk/ons/rel/vsob1/cancer-statistics-registrations--england--series-mb1-/no--42--2011/sty-breast-cancer-survival.html> (accessed 18/6/2014).
- 5 World Health Organisation. GLOBOCAN 2012: Estimated Cancer Incidence, Mortality and Prevalence Worldwide in 2012. http://globocan.iarc.fr/Pages/fact_sheets_cancer.aspx (accessed 18/06/2014).
- 6 Langer, R. Drug delivery and targeting. *Nature* **1998**, *392(6679 Suppl)*, 5-10.
- 7 Allen, T. M.; Cullis, P. R. Drug Delivery Systems: Entering the Mainstream. *Science* **2004**, *303*, 1818-1822.
- 8 Strebhardt, K.; Ullrich, A. Paul Ehrlich's magic bullet concept: 100 years of progress. *Nat. Rev. Cancer* **2008**, *8*, 473-480.
- 9 Moses, M. A.; Brem, H.; Langer, R. Advancing the field of drug delivery: Taking aim at cancer. *Cancer Cell* **2003**, *4*, 337-341.
- 10 Chauhan, V. P.; Stylianopoulos, T.; Boucher, Y.; Jain, R. K. Delivery of Molecular and Nanoscale Medicine to Tumors: Transport Barriers and Strategies. *Ann. Rev. Chem. Biomol. Eng.* **2011**, *2*, 281-298.
- 11 Garnett, M. C.; Kallinteri, P. Nanomedicines and nanotoxicology: some physiological principles. *Occ. Med.* **2006**, *56*, 307-311.
- 12 Vasir, J. K.; Reddy, M. K.; Labhasetwar, V. D. Nanosystems in Drug Targeting: Opportunities and Challenges. *Curr. Nanosci.* **2005**, *1*, 47-64.

- 13 Schroeder, A.; Heller, D. A.; Winslow, M. M.; Dahlman, J. E.; Pratt, G. W.; Langer, R.; Jacks, T.; Anderson, D. G. Treating metastatic cancer with nanotechnology. *Nat. Rev. Cancer* **2012**, *12*, 39-50.
- 14 Nicolaou, K. C.; Yang, Z.; Liu, J. J.; Ueno, H.; Nantermet, P. G.; Guy, R. K.; Claiborne, C. F.; Renaud, J.; Couladouros, E. A.; Paulvannan, K.; Sorensen, E. J. Total synthesis of taxol. *Nature* **1994**, *367*, 630-634.
- 15 Panchagnula, R. Pharmaceutical aspects of paclitaxel. *Int. J. Pharm.* **1998**, *172*, 1-15.
- 16 Singla, A. K.; Garg, A.; Aggarwal, D. Paclitaxel and its formulations. *Int. J. Pharm.* **2002**, *235*, 179-192.
- 17 Ringsdorf, H. Structure and properties of pharmacologically active polymers. *J. Polym. Sci.: Polym. Symp.* **1975**, *51*, 135-153.
- 18 Duncan, R. The dawning era of polymer therapeutics. *Nat. Rev. Drug Discov.* **2003**, *2*, 347-360.
- 19 Duncan, R. Polymer conjugates as anticancer nanomedicines. *Nat. Rev. Cancer* **2006**, *6*, 688-701.
- 20 Abuchowski, A.; van Es, T.; Palczuk, N. C.; Davis, F. F. Alteration of immunological properties of bovine serum albumin by covalent attachment of polyethylene glycol. *J. Biol. Chem.* **1977**, *252*, 3578-3581.
- 21 Abuchowski, A.; McCoy, J. R.; Palczuk, N. C.; van Es, T.; Davis, F. F. Effect of covalent attachment of polyethylene glycol on immunogenicity and circulating life of bovine liver catalase. *J. Biol. Chem.* **1977**, *252*, 3582-3586.
- 22 Matsumura, Y.; Maeda, H. A New Concept for Macromolecular Therapeutics in Cancer Chemotherapy: Mechanism of Tumoritropic Accumulation of Proteins and the Antitumor Agent Smancs. *Cancer Res.* **1986**, *46*, 6387-6392.
- 23 Iyer, A. K.; Khaled, G.; Fang, J.; Maeda, H. Exploiting the enhanced permeability and retention effect for tumor targeting. *Drug Discov. Today* **2006**, *11*, 812-818.
- 24 Winchell, H. S.; Sanchez, P. D.; Watanabe, C. K.; Hollander, L.; Anger, H. O.; McRae, J.; Hayes, R. L.; Edwards, C. L. Visualization of Tumors in Humans Using ⁶⁷Ga-Citrate and the Anger Whole-Body Scanner, Scintillation Camera and Tomographic Scanner. *J. Nucl. Med.* **1970**, *11*, 459-466.

- 25 Maeda, H. The link between infection and cancer: Tumor vasculature, free radicals, and drug delivery to tumors via the EPR effect. *Cancer Sci.* **2013**, *104*, 779-789.
- 26 Perry, G.; Castellani, R. J.; Hirai, K.; Smith, M. A. Reactive Oxygen Species Mediate Cellular Damage in Alzheimer Disease. *J. Alzheimers Dis.* **1998**, *1*, 45-55.
- 27 Sugamura, K.; Keaney, J. J. F. Reactive oxygen species in cardiovascular disease. *Free Radic. Biol. Med.* **2011**, *51*, 978-992.
- 28 Chaumeil, M. M.; Valette, J.; Baligand, C.; Brouillet, E.; Hantraye, P.; Bloch, G.; Gaura, V.; Riolland, A.; Krystkowiak, P.; Verny, C.; Damier, P.; Remy, P.; Bachoud-Levi, A.-C.; Carlier, P.; Lebon, V. pH as a biomarker of neurodegeneration in Huntington's disease: a translational rodent-human MRS study. *J. Cereb. Blood Flow Metab.* **2012**, *32*, 771-779.
- 29 Janigro, D. Are you in or out? Leukocyte, ion, and neurotransmitter permeability across the epileptic blood–brain barrier. *Epilepsia* **2012**, *53*, 26-34.
- 30 Gaeta, A.; Hider, R. C. The crucial role of metal ions in neurodegeneration: the basis for a promising therapeutic strategy. *Br. J. Pharmacol.* **2005**, *146*, 1041-1059.
- 31 Bajpai, A. K.; Shukla, S. K.; Bhanu, S.; Kankane, S. Responsive polymers in controlled drug delivery. *Prog. Polym. Sci.* **2008**, *33*, 1088-1118.
- 32 Matyjaszewski, K.; Spanswick, J. Controlled/living radical polymerization. *Mater. Today* **2005**, *8*, 26-33.
- 33 Szwarc, M.; Levy, M.; Milkovich, R. Polymerization Initiated by Electron Transfer to Monomer. A New Method of Formation of Block Copolymers. . *J. Am. Chem. Soc.* **1956**, *78*, 2656-2657.
- 34 Szwarc, M. ^Living^ Polymers. *Nature* **1956**, *178*, 1168-1169.
- 35 Otsu, T.; Yoshida, M. Role of initiator-transfer agent-terminator (iniferter) in radical polymerizations: Polymer design by organic disulfides as iniferters. *Makromol. Chem.* **1982**, *3*, 127-132.
- 36 Otsu, T. Iniferter concept and living radical polymerization. *J. Polym. Sci. Part A: Polym. Chem.* **2000**, *38*, 2121-2136.

- 37 Hawker, C. J.; Bosman, A. W.; Harth, E. New Polymer Synthesis by Nitroxide Mediated Living Radical Polymerizations. *Chem. Rev.* **2001**, *101*, 3661-3688.
- 38 Nicolas, J.; Guillaneuf, Y.; Lefay, C.; Bertin, D.; Gigmes, D.; Charleux, B. Nitroxide-mediated polymerization. *Prog. Polym. Sci.* **2013**, *38*, 63-235.
- 39 Percec, V.; Guliashvili, T.; Ladislaw, J. S.; Wistrand, A.; Stjern Dahl, A.; Sienkowska, M. J.; Monteiro, M. J.; Sahoo, S. Ultrafast Synthesis of Ultrahigh Molar Mass Polymers by Metal-Catalyzed Living Radical Polymerization of Acrylates, Methacrylates, and Vinyl Chloride Mediated by SET at 25 °C. *J. Am. Chem. Soc.* **2006**, *128*, 14156-14165.
- 40 Zhang, Q.; Wilson, P.; Li, Z.; McHale, R.; Godfrey, J.; Anastasaki, A.; Waldron, C.; Haddleton, D. M. Aqueous Copper-Mediated Living Polymerization: Exploiting Rapid Disproportionation of CuBr with Me6TREN. *J. Am. Chem. Soc.* **2013**, *135*, 7355-7363.
- 41 Matyjaszewski, K.; Xia, J. Atom Transfer Radical Polymerization. *Chem. Rev.* **2001**, *101*, 2921-2990.
- 42 Matyjaszewski, K.; Tsarevsky, N. V. Macromolecular Engineering by Atom Transfer Radical Polymerization. *J. Am. Chem. Soc.* **2014**, *136*, 6513-6533.
- 43 Chiefari, J.; Chong, Y. K.; Ercole, F.; Krstina, J.; Jeffery, J.; Le, T. P. T.; Mayadunne, R. T. A.; Meijs, G. F.; Moad, C. L.; Moad, G.; Rizzardo, E.; Thang, S. H. Living Free-Radical Polymerization by Reversible Addition–Fragmentation Chain Transfer: The RAFT Process. *Macromolecules* **1998**, *31*, 5559-5562.
- 44 Perrier, S.; Takolpuckdee, P. Macromolecular design via reversible addition–fragmentation chain transfer (RAFT)/xanthates (MADIX) polymerization. *J. Polym. Sci. Part A: Polym. Chem.* **2005**, *43*, 5347-5393.
- 45 Boyer, C.; Bulmus, V.; Davis, T. P.; Ladmiral, V.; Liu, J.; Perrier, S. Bioapplications of RAFT Polymerization. *Chem. Rev.* **2009**, *109*, 5402-5436.
- 46 Moad, G.; Rizzardo, E.; Thang, S. H. Living Radical Polymerization by the RAFT Process. *Aust. J. Chem.* **2005**, *58*, 379-410.
- 47 Moad, G.; Rizzardo, E.; Thang, S. H. Toward Living Radical Polymerization. *Acc. Chem. Res.* **2008**, *41*, 1133-1142.

- 48 Benaglia, M.; Chiefari, J.; Chong, Y. K.; Moad, G.; Rizzardo, E.; Thang, S. H. Universal (Switchable) RAFT Agents. *J. Am. Chem. Soc.* **2009**, *131*, 6914-6915.
- 49 Willcock, H.; O'Reilly, R. K. End group removal and modification of RAFT polymers. *Polym. Chem.* **2010**, *1*, 149-157.
- 50 Roth, P. J.; Boyer, C.; Lowe, A. B.; Davis, T. P. RAFT Polymerization and Thiol Chemistry: A Complementary Pairing for Implementing Modern Macromolecular Design. *Macromol. Rapid Commun.* **2011**, *32*, 1123-1143.
- 51 Xu, J.; He, J.; Fan, D.; Wang, X.; Yang, Y. Aminolysis of Polymers with Thiocarbonylthio Termini Prepared by RAFT Polymerization: The Difference between Polystyrene and Polymethacrylates. *Macromolecules* **2006**, *39*, 8616-8624.
- 52 Boyer, C.; Granville, A.; Davis, T. P.; Bulmus, V. Modification of RAFT-polymers via thiol-ene reactions: A general route to functional polymers and new architectures. *J. Polym. Sci. Part A: Polym. Chem.* **2009**, *47*, 3773-3794.
- 53 Boyer, C.; Bulmus, V.; Davis, T. P. Efficient Usage of Thiocarbonates for Both the Production and the Biofunctionalization of Polymers. *Macromol. Rapid Commun.* **2009**, *30*, 493-497.
- 54 Takara, M.; Toyoshima, M.; Seto, H.; Hoshino, Y.; Miura, Y. Polymer-modified gold nanoparticles via RAFT polymerization: a detailed study for a biosensing application. *Polym. Chem.* **2014**, *5*, 931-939.
- 55 Legge, T. M.; Slark, A. T.; Perrier, S. Thermal stability of reversible addition-fragmentation chain transfer/macromolecular architecture design by interchange of xanthates chain-transfer agents. *J. Polym. Sci. Part A: Polym. Chem.* **2006**, *44*, 6980-6987.
- 56 Chong, B.; Moad, G.; Rizzardo, E.; Skidmore, M.; Thang, S. H. Thermolysis of RAFT-Synthesized Poly(Methyl Methacrylate). *Aust. J. Chem.* **2006**, *59*, 755-762.
- 57 Perrier, S.; Takolpuckdee, P.; Mars, C. A. Reversible Addition-Fragmentation Chain Transfer Polymerization: End Group Modification for Functionalized Polymers and Chain Transfer Agent Recovery. *Macromolecules* **2005**, *38*, 2033-2036.

- 58 Chen, M.; Moad, G.; Rizzardo, E. Thiocarbonylthio end group removal from RAFT-synthesized polymers by a radical-induced process. *J. Polym. Sci. Part A: Polym. Chem.* **2009**, *47*, 6704-6714.
- 59 Inglis, A. J.; Sinnwell, S.; Davis, T. P.; Barner-Kowollik, C.; Stenzel, M. H. Reversible Addition Fragmentation Chain Transfer (RAFT) and Hetero-Diels–Alder Chemistry as a Convenient Conjugation Tool for Access to Complex Macromolecular Designs. *Macromolecules* **2008**, *41*, 4120-4126.
- 60 Sinnwell, S.; Inglis, A. J.; Davis, T. P.; Stenzel, M. H.; Barner-Kowollik, C. An atom-efficient conjugation approach to well-defined block copolymers using RAFT chemistry and hetero Diels-Alder cycloaddition. *Chem. Commun.* **2008**, 2052-2054.
- 61 Russell, S. J.; El-Khatib, F. H.; Sinha, M.; Magyar, K. L.; McKeon, K.; Goergen, L. G.; Balliro, C.; Hillard, M. A.; Nathan, D. M.; Damiano, E. R. Outpatient Glycemic Control with a Bionic Pancreas in Type 1 Diabetes. *N. Engl. J. Med.* **2014**, *371*, 313-325.
- 62 Gurtner, G. C.; Werner, S.; Barrandon, Y.; Longaker, M. T. Wound repair and regeneration. *Nature* **2008**, *453*, 314-321.
- 63 Craig, A. D. Interoception: the sense of the physiological condition of the body. *Curr. Opin. Neurobiol.* **2003**, *13*, 500-505.
- 64 Stuart-Fox, D.; Moussalli, A. Camouflage, communication and thermoregulation: lessons from colour changing organisms. *Phil. Trans. R. Soc. B: Biol. Sci.* **2009**, *364*, 463-470.
- 65 Stuart, M. A. C.; Huck, W. T. S.; Genzer, J.; Muller, M.; Ober, C.; Stamm, M.; Sukhorukov, G. B.; Szleifer, I.; Tsukruk, V. V.; Urban, M.; Winnik, F.; Zauscher, S.; Luzinov, I.; Minko, S. Emerging applications of stimuli-responsive polymer materials. *Nat. Mater.* **2010**, *9*, 101-113.
- 66 Tong, R.; Tang, L.; Ma, L.; Tu, C.; Baumgartner, R.; Cheng, J. Smart chemistry in polymeric nanomedicine. *Chem. Soc. Rev.* **2014**, DOI: 10.1039/C4CS00133H.
- 67 Liu, F.; Urban, M. W. Recent advances and challenges in designing stimuli-responsive polymers. *Prog. Polym. Sci.* **2010**, *35*, 3-23.
- 68 Mano, J. F. Stimuli-Responsive Polymeric Systems for Biomedical Applications. *Adv. Eng. Mater.* **2008**, *10*, 515-527.

- 69 Yan, X.; Wang, F.; Zheng, B.; Huang, F. Stimuli-responsive supramolecular polymeric materials. *Chem. Soc. Rev.* **2012**, *41*, 6042-6065.
- 70 Seuring, J.; Agarwal, S. Polymers with Upper Critical Solution Temperature in Aqueous Solution. *Macromol. Rapid Commun.* **2012**, *33*, 1898-1920.
- 71 Ruel-Gariépy, E.; Leroux, J.-C. In situ-forming hydrogels—review of temperature-sensitive systems. *Eur. J. Pharm. Biopharm.* **2004**, *58*, 409-426.
- 72 Schmaljohann, D. Thermo- and pH-responsive polymers in drug delivery. *Adv. Drug Deliv. Rev.* **2006**, *58*, 1655-1670.
- 73 Scarpa, J. S.; Mueller, D. D.; Klotz, I. M. Slow hydrogen-deuterium exchange in a non- α -helical polyamide. *J. Am. Chem. Soc.* **1967**, *89*, 6024-6030.
- 74 Schild, H. G. Poly(N-isopropylacrylamide): experiment, theory and application. *Prog. Polym. Sci.* **1992**, *17*, 163-249.
- 75 Roy, D.; Brooks, W. L. A.; Sumerlin, B. S. New directions in thermoresponsive polymers. *Chem. Soc. Rev.* **2013**, *42*, 7214-7243.
- 76 Gibson, M. I.; Paripovic, D.; Klok, H.-A. Size-Dependent LCST Transitions of Polymer-Coated Gold Nanoparticles: Cooperative Aggregation and Surface Assembly. *Adv. Mater.* **2010**, *22*, 4721-4725.
- 77 Jeong, N. S.; Bebis, K.; Daniel, L. E.; O'Reilly, R. K.; Gibson, M. I. The critical importance of size on thermoresponsive nanoparticle transition temperatures: gold and micelle-based polymer nanoparticles. *Chem. Commun.* **2011**, *47*, 11627-11629.
- 78 Jones, M.-C.; Leroux, J.-C. Polymeric micelles – a new generation of colloidal drug carriers. *Eur. J. Pharm. Biopharm.* **1999**, *48*, 101-111.
- 79 Wang, J.; Gibson, M. I.; Barbey, R.; Xiao, S.-J.; Klok, H.-A. Nonfouling Polypeptide Brushes via Surface-initiated Polymerization of N ϵ -oligo(ethylene glycol)succinate-L-lysine N-carboxyanhydride. *Macromol. Rapid Commun.* **2009**, *30*, 845-850.
- 80 Barbey, R.; Lavanant, L.; Paripovic, D.; Schüwer, N.; Sugnaux, C.; Tugulu, S.; Klok, H.-A. Polymer Brushes via Surface-Initiated Controlled Radical Polymerization: Synthesis, Characterization, Properties, and Applications. *Chem. Rev.* **2009**, *109*, 5437-5527.

- 81 Jones, M. W.; Gibson, M. I.; Mantovani, G.; Haddleton, D. M. Tunable thermo-responsive polymer-protein conjugates via a combination of nucleophilic thiol-ene "click" and SET-LRP. *Polym. Chem.* **2011**, *2*, 572-574.
- 82 Jones, M. W.; Strickland, R. A.; Schumacher, F. F.; Caddick, S.; Baker, J. R.; Gibson, M. I.; Haddleton, D. M. Polymeric Dibromomaleimides As Extremely Efficient Disulfide Bridging Bioconjugation and Pegylation Agents. *J. Am. Chem. Soc.* **2011**, *134*, 1847-1852.
- 83 Bebis, K.; Jones, M. W.; Haddleton, D. M.; Gibson, M. I. Thermoresponsive behaviour of poly[(oligo(ethyleneglycol methacrylate)]s and their protein conjugates: importance of concentration and solvent system. *Polym. Chem.* **2011**, *2*, 975-982.
- 84 Stayton, P. S.; Shimoboji, T.; Long, C.; Chilkoti, A.; Ghen, G.; Harris, J. M.; Hoffman, A. S. Control of protein-ligand recognition using a stimuli-responsive polymer. *Nature* **1995**, *378*, 472-474.
- 85 Tsai, H.-Y.; Vats, K.; Yates, M. Z.; Benoit, D. S. W. Two-Dimensional Patterns of Poly(N-isopropylacrylamide) Microgels to Spatially Control Fibroblast Adhesion and Temperature-Responsive Detachment. *Langmuir* **2013**, *29*, 12183-12193.
- 86 Dey, S.; Kellam, B.; Alexander, M. R.; Alexander, C.; Rose, F. R. A. J. Enzyme-passage free culture of mouse embryonic stem cells on thermo-responsive polymer surfaces. *J. Mater. Chem.* **2011**, *21*, 6883-6890.
- 87 Chen, G.; Hoffman, A. S. Preparation and properties of thermoreversible, phase-separating enzyme-oligo(N-isopropylacrylamide) conjugates. *Bioconj. Chem.* **1993**, *4*, 509-514.
- 88 Chang, C.-W.; Nguyen, T. H.; Maynard, H. D. Thermoprecipitation of Glutathione S-Transferase by Glutathione-Poly(N-isopropylacrylamide) Prepared by RAFT Polymerization. *Macromol. Rapid Commun.* **2010**, *31*, 1691-1695.
- 89 Chung, J. E.; Yokoyama, M.; Yamato, M.; Aoyagi, T.; Sakurai, Y.; Okano, T. Thermo-responsive drug delivery from polymeric micelles constructed using block copolymers of poly(N-isopropylacrylamide) and poly(butylmethacrylate). *J. Contr. Rel.* **1999**, *62*, 115-127.

- 90 Saaka, Y.; Deller, R. C.; Rodger, A.; Gibson, M. I. Exploiting Thermoresponsive Polymers to Modulate Lipophilicity: Interactions With Model Membranes. *Macromol. Rapid Commun.* **2012**, *33*, 779-784.
- 91 Edwards, E. W.; Chanana, M.; Wang, D.; Möhwald, H. Stimuli-Responsive Reversible Transport of Nanoparticles Across Water/Oil Interfaces. *Angew. Chem. Int. Ed.* **2008**, *47*, 320-323.
- 92 Salmaso, S.; Caliceti, P.; Amendola, V.; Meneghetti, M.; Magnusson, J. P.; Pasparakis, G.; Alexander, C. Cell up-take control of gold nanoparticles functionalized with a thermoresponsive polymer. *J. Mater. Chem.* **2009**, *19*, 1608-1615.
- 93 Abulateefeh, S. R.; Spain, S. G.; Thurecht, K. J.; Aylott, J. W.; Chan, W. C.; Garnett, M. C.; Alexander, C. Enhanced uptake of nanoparticle drug carriers via a thermoresponsive shell enhances cytotoxicity in a cancer cell line. *Biomater. Sci.* **2013**, *1*, 434-442.
- 94 Akimoto, J.; Nakayama, M.; Sakai, K.; Okano, T. Temperature-Induced Intracellular Uptake of Thermoresponsive Polymeric Micelles. *Biomacromolecules* **2009**, *10*, 1331-1336.
- 95 Akimoto, J.; Nakayama, M.; Sakai, K.; Okano, T. Thermally Controlled Intracellular Uptake System of Polymeric Micelles Possessing Poly(N-isopropylacrylamide)-Based Outer Coronas. *Mol. Pharm.* **2010**, *7*, 926-935.
- 96 Meyer, D. E.; Shin, B. C.; Kong, G. A.; Dewhirst, M. W.; Chilkoti, A. Drug targeting using thermally responsive polymers and local hyperthermia. *J. Contr. Rel.* **2001**, *74*, 213-224.
- 97 Abulateefeh, S. R.; Spain, S. G.; Aylott, J. W.; Chan, W. C.; Garnett, M. C.; Alexander, C. Thermoresponsive Polymer Colloids for Drug Delivery and Cancer Therapy. *Macromol. Biosci.* **2011**, *11*, 1722-1734.
- 98 Dreher, M. R.; Liu, W.; Michelich, C. R.; Dewhirst, M. W.; Chilkoti, A. Thermal Cycling Enhances the Accumulation of a Temperature-Sensitive Biopolymer in Solid Tumors. *Cancer Res.* **2007**, *67*, 4418-4424.
- 99 Tirelli, N. (Bio)Responsive nanoparticles. *Current Opinion in Colloid & Interface Science* **2006**, *11*, 210-216.
- 100 Schattling, P.; Jochum, F. D.; Theato, P. Multi-stimuli responsive polymers - the all-in-one talents. *Polym. Chem.* **2014**, *5*, 25-36.

- 101 Alarcon, C. d. I. H.; Pennadam, S.; Alexander, C. Stimuli responsive polymers for biomedical applications. *Chem. Soc. Rev.* **2005**, *34*, 276-285.
- 102 Timko, B. P.; Dvir, T.; Kohane, D. S. Remotely Triggerable Drug Delivery Systems. *Adv. Mater.* **2010**, *22*, 4925-4943.
- 103 Priya James, H.; John, R.; Alex, A.; Anoop, K. R. Smart polymers for the controlled delivery of drugs – a concise overview. *Act. Pharm. Sin. B* **2014**, *4*, 120-127.
- 104 Mura, S.; Nicolas, J.; Couvreur, P. Stimuli-responsive nanocarriers for drug delivery. *Nat. Mater.* **2013**, *12*, 991-1003.
- 105 Hillmyer, M. A.; Tolman, W. B. Aliphatic Polyester Block Polymers: Renewable, Degradable, and Sustainable. *Acc. Chem. Res.* **2014**, *47*, 2390-2396.
- 106 Undin, J.; Finne-Wistrand, A.; Albertsson, A.-C. Adjustable Degradation Properties and Biocompatibility of Amorphous and Functional Poly(ester-acrylate)-Based Materials. *Biomacromolecules* **2014**, *15*, 2800-2807.
- 107 Sanders, D. P.; Coady, D. J.; Yasumoto, M.; Fujiwara, M.; Sardon, H.; Hedrick, J. L. Synthesis of functionalized cyclic carbonate monomers using a versatile pentafluorophenyl carbonate intermediate. *Polym. Chem.* **2014**, *5*, 327-329.
- 108 Hedir, G. G.; Bell, C. A.; Jeong, N. S.; Chapman, E.; Collins, I. R.; O'Reilly, R. K.; Dove, A. P. Functional Degradable Polymers by Xanthate-Mediated Polymerization. *Macromolecules* **2014**, *47*, 2847-2852.
- 109 Lenz, R. W.; Marchessault, R. H. Bacterial Polyesters: Biosynthesis, Biodegradable Plastics and Biotechnology. *Biomacromolecules* **2004**, *6*, 1-8.
- 110 Gibson, M. I.; Cameron, N. R. Experimentally facile controlled polymerization of N-carboxyanhydrides (NCAs), including O-benzyl-L-threonine NCA. *J. Polym. Sci. Part A: Polym. Chem.* **2009**, *47*, 2882-2891.
- 111 Carampin, P.; Lallana, E.; Laliturai, J.; Carroccio, S. C.; Puglisi, C.; Tirelli, N. Oxidant-Dependent REDOX Responsiveness of Polysulfides. *Macromol. Chem. Phys.* **2012**, *213*, 2052-2061.
- 112 Reddy, S. T.; Rehor, A.; Schmoekel, H. G.; Hubbell, J. A.; Swartz, M. A. In vivo targeting of dendritic cells in lymph nodes with poly(propylene sulfide) nanoparticles. *J. Contr. Rel.* **2006**, *112*, 26-34.

- 113 Chang, C.-C.; Emrick, T. Functional Polyolefins Containing Disulfide and Phosphoester Groups: Synthesis and Orthogonal Degradation. *Macromolecules* **2014**, *47*, 1344-1350.
- 114 Lee, Y.; Mo, H.; Koo, H.; Park, J.-Y.; Cho, M. Y.; Jin, G.-w.; Park, J.-S. Visualization of the Degradation of a Disulfide Polymer, Linear Poly(ethylenimine sulfide), for Gene Delivery. *Bioconj. Chem.* **2006**, *18*, 13-18.
- 115 Choi, J. Y.; Kim, J. Y.; Moon, H. J.; Park, M. H.; Jeong, B. CO₂- and O₂-Sensitive Fluorophenyl End-Capped Poly(ethylene glycol). *Macromol. Rapid Commun.* **2014**, *35*, 66-70.
- 116 Coessens, V.; Pintauer, T.; Matyjaszewski, K. Functional polymers by atom transfer radical polymerization. *Prog. Polym. Sci.* **2001**, *26*, 337-377.
- 117 Tasdelen, M. A.; Kahveci, M. U.; Yagci, Y. Telechelic polymers by living and controlled/living polymerization methods. *Prog. Polym. Sci.* **2011**, *36*, 455-567.
- 118 Boyer, C.; Stenzel, M. H.; Davis, T. P. Building nanostructures using RAFT polymerization. *J. Polym. Sci. Part A: Polym. Chem.* **2011**, *49*, 551-595.
- 119 Xia, Y.; Burke, N. A. D.; Stöver, H. D. H. End Group Effect on the Thermal Response of Narrow-Disperse Poly(N-isopropylacrylamide) Prepared by Atom Transfer Radical Polymerization. *Macromolecules* **2006**, *39*, 2275-2283.
- 120 Jiang, X.; Zhao, B. End group effect on the thermo-sensitive properties of well-defined water-soluble polystyrenics with short pendant oligo(ethylene glycol) groups synthesized by nitroxide-mediated radical polymerization. *J. Polym. Sci. Part A: Polym. Chem.* **2007**, *45*, 3707-3721.
- 121 Chung, J. E.; Yokoyama, M.; Aoyagi, T.; Sakurai, Y.; Okano, T. Effect of molecular architecture of hydrophobically modified poly(N-isopropylacrylamide) on the formation of thermoresponsive core-shell micellar drug carriers. *J. Contr. Rel.* **1998**, *53*, 119-130.
- 122 Steinhauer, W.; Hoogenboom, R.; Keul, H.; Moeller, M. Copolymerization of 2-Hydroxyethyl Acrylate and 2-Methoxyethyl Acrylate via RAFT: Kinetics and Thermoresponsive Properties. *Macromolecules* **2010**, *43*, 7041-7047.

- 123 Duan, Q.; Miura, Y.; Narumi, A.; Shen, X.; Sato, S.-I.; Satoh, T.; Kakuchi, T. Synthesis and thermoresponsive property of end-functionalized poly(N-isopropylacrylamide) with pyrenyl group. *J. Polym. Sci. Part A: Polym. Chem.* **2006**, *44*, 1117-1124.
- 124 Jochum, F. D.; zur Borg, L.; Roth, P. J.; Theato, P. Thermo- and Light-Responsive Polymers Containing Photoswitchable Azobenzene End Groups. *Macromolecules* **2009**, *42*, 7854-7862.
- 125 Carter, S.; Hunt, B.; Rimmer, S. Highly Branched Poly(N-isopropylacrylamide)s with Imidazole End Groups Prepared by Radical Polymerization in the Presence of a Styryl Monomer Containing a Dithioester Group. *Macromolecules* **2005**, *38*, 4595-4603.
- 126 Shepherd, J.; Sarker, P.; Swindells, K.; Douglas, I.; MacNeil, S.; Swanson, L.; Rimmer, S. Binding Bacteria to Highly Branched Poly(N-isopropylacrylamide) Modified with Vancomycin Induces the Coil-to-Globule Transition. *J. Am. Chem. Soc.* **2010**, *132*, 1736-1737.
- 127 Sarker, P.; Shepherd, J.; Swindells, K.; Douglas, I.; MacNeil, S.; Swanson, L.; Rimmer, S. Highly Branched Polymers with Polymyxin End Groups Responsive to *Pseudomonas aeruginosa*. *Biomacromolecules* **2010**, *12*, 1-5.
- 128 Dai, S.; Ravi, P.; Tam, K. C. pH-Responsive polymers: synthesis, properties and applications. *Soft Matter* **2008**, *4*, 435-449.
- 129 Yin, X.; Hoffman, A. S.; Stayton, P. S. Poly(N-isopropylacrylamide-co-propylacrylic acid) Copolymers That Respond Sharply to Temperature and pH. *Biomacromolecules* **2006**, *7*, 1381-1385.
- 130 Feil, H.; Bae, Y. H.; Feijen, J.; Kim, S. W. Effect of comonomer hydrophilicity and ionization on the lower critical solution temperature of N-isopropylacrylamide copolymers. *Macromolecules* **1993**, *26*, 2496-2500.
- 131 Diehl, C.; Schlaad, H. Thermo-Responsive Polyoxazolines with Widely Tuneable LCST. *Macromol. Biosci.* **2009**, *9*, 157-161.
- 132 Ali, M. M.; Stöver, H. D. H. Well-Defined Amphiphilic Thermosensitive Copolymers Based on Poly(ethylene glycol monomethacrylate) and Methyl Methacrylate Prepared by Atom Transfer Radical Polymerization. *Macromolecules* **2004**, *37*, 5219-5227.
- 133 Eggenhuisen, T. M.; Becer, C. R.; Fijten, M. W. M.; Eckardt, R.; Hoogenboom, R.; Schubert, U. S. Libraries of Statistical Hydroxypropyl

- Acrylate Containing Copolymers with LCST Properties Prepared by NMP. *Macromolecules* **2008**, *41*, 5132-5140.
- 134 Becer, C. R.; Kokado, K.; Weber, C.; Can, A.; Chujo, Y.; Schubert, U. S. Metal-free synthesis of responsive polymers: Cloud point tuning by controlled “click” reaction. *J. Polym. Sci. Part A: Polym. Chem.* **2010**, *48*, 1278-1286.
- 135 Jochum, F. D.; Theato, P. Temperature- and Light-Responsive Polyacrylamides Prepared by a Double Polymer Analogous Reaction of Activated Ester Polymers. *Macromolecules* **2009**, *42*, 5941-5945.
- 136 Shimoboji, T.; Larenas, E.; Fowler, T.; Kulkarni, S.; Hoffman, A. S.; Stayton, P. S. Photoresponsive polymer–enzyme switches. *Proc. Natl. Acad. Sci. U.S.A.* **2002**, *99*, 16592-16596.
- 137 Liu, Y.-J.; Pallier, A.; Sun, J.; Rudiuk, S.; Baigl, D.; Piel, M.; Marie, E.; Tribet, C. Non-monotonous variation of the LCST of light-responsive, amphiphilic poly(NIPAM) derivatives. *Soft Matter* **2012**, *8*, 8446-8455.
- 138 Jochum, F. D.; Forst, F. R.; Theato, P. PNIPAM Copolymers Containing Light-Responsive Chromophores: A Method Toward Molecular Logic Gates. *Macromol. Rapid Commun.* **2010**, *31*, 1456-1461.
- 139 Ivanov, A. E.; Ereemeev, N. L.; Wahlund, P. O.; Galaev, I. Y.; Mattiasson, B. Photosensitive copolymer of N-isopropylacrylamide and methacryloyl derivative of spirobenzopyran. *Polymer* **2002**, *43*, 3819-3823.
- 140 Yan, Q.; Yuan, J.; Kang, Y.; Cai, Z.; Zhou, L.; Yin, Y. Dual-sensing porphyrin-containing copolymer nanosensor as full-spectrum colorimeter and ultra-sensitive thermometer. *Chem. Commun.* **2010**, *46*, 2781-2783.
- 141 Buller, J.; Laschewsky, A.; Lutz, J.-F.; Wischerhoff, E. Tuning the lower critical solution temperature of thermoresponsive polymers by biospecific recognition. *Polym. Chem.* **2011**, *2*, 1486-1489.
- 142 Fu, H.; Policarpio, D. M.; Batteas, J. D.; Bergbreiter, D. E. Redox-controlled 'smart' polyacrylamide solubility. *Polym. Chem.* **2010**, *1*, 631-633.
- 143 Kuramoto, N.; Shishido, Y. Property of thermo-sensitive and redox-active poly(N-cyclopropylacrylamide-co-vinylferrocene) and poly(N-isopropylacrylamide-co-vinylferrocene). *Polymer* **1998**, *39*, 669-673.
- 144 Kuramoto, N.; Shishido, Y.; Nagai, K. Thermosensitive and redox-active polymers: Preparation and properties of poly(N-ethylacrylamide-co-

- vinylferrocene) and poly(N,N-diethylacrylamide-co-vinylferrocene). *J. Polym. Sci. Part A: Polym. Chem.* **1997**, *35*, 1967-1972.
- 145 Zuo, F.; Luo, C.; Ding, X.; Zheng, Z.; Cheng, X.; Peng, Y. Redox-responsive Inclusion Complexation between β -Cyclodextrin and Ferrocene-functionalized Poly(N-isopropylacrylamide) and its Effect on the Solution Properties of this Polymer. *Supramol. Chem.* **2008**, *20*, 559-564.
- 146 Zhou, H.; Liang, E.; Pan, Y.; Ding, X.; Zheng, Z.; Peng, Y. Self-tunable thermosensitive behavior by reorganizable architecture variation in the Belousov-Zhabotinsky reaction. *RSC Adv.* **2013**, *3*, 2182-2185.
- 147 Xiao, C.; Cheng, Y.; Zhang, Y.; Ding, J.; He, C.; Zhuang, X.; Chen, X. Side chain impacts on pH- and thermo-responsiveness of tertiary amine functionalized polypeptides. *J. Polym. Sci. Part A: Polym. Chem.* **2014**, *52*, 671-679.
- 148 Plamper, F. A.; Ruppel, M.; Schmalz, A.; Borisov, O.; Ballauff, M.; Müller, A. H. E. Tuning the Thermoresponsive Properties of Weak Polyelectrolytes: Aqueous Solutions of Star-Shaped and Linear Poly(N,N-dimethylaminoethyl Methacrylate). *Macromolecules* **2007**, *40*, 8361-8366.
- 149 Fournier, D.; Hoogenboom, R.; Thijs, H. M. L.; Paulus, R. M.; Schubert, U. S. Tunable pH- and Temperature-Sensitive Copolymer Libraries by Reversible Addition-Fragmentation Chain Transfer Copolymerizations of Methacrylates. *Macromolecules* **2007**, *40*, 915-920.
- 150 Mertoglu, M.; Garnier, S.; Laschewsky, A.; Skrabania, K.; Storsberg, J. Stimuli responsive amphiphilic block copolymers for aqueous media synthesised via reversible addition fragmentation chain transfer polymerisation (RAFT). *Polymer* **2005**, *46*, 7726-7740.
- 151 Huang, X.; Du, F.; Liang, D.; Lin, S.-S.; Li, Z. Stereochemical Effect of Trans/Cis Isomers on the Aqueous Solution Properties of Acid-Labile Thermoresponsive Polymers. *Macromolecules* **2008**, *41*, 5433-5440.
- 152 Heath, F.; Saeed, A. O.; Pennadam, S. S.; Thurecht, K. J.; Alexander, C. 'Isothermal' phase transitions and supramolecular architecture changes in thermoresponsive polymers via acid-labile side-chains. *Polym. Chem.* **2010**, *1*, 1252-1262.
- 153 Zhang, Q.; Vanparijs, N.; Louage, B.; De Geest, B. G.; Hoogenboom, R. Dual pH- and temperature-responsive RAFT-based block co-polymer

- micelles and polymer-protein conjugates with transient solubility. *Polym. Chem.* **2014**, *5*, 1140-1144.
- 154 Tran, N. T. D.; Jia, Z.; Truong, N. P.; Cooper, M. A.; Monteiro, M. J. Fine Tuning the Disassembly Time of Thermoresponsive Polymer Nanoparticles. *Biomacromolecules* **2013**, *14*, 3463-3471.
- 155 Lentacker, I.; De Smedt, S. C.; Sanders, N. N. Drug loaded microbubble design for ultrasound triggered delivery. *Soft Matter* **2009**, *5*, 2161-2170.
- 156 Ferrara, K. W. Driving delivery vehicles with ultrasound. *Adv. Drug Deliv. Rev.* **2008**, *60*, 1097-1102.
- 157 Xuan, J.; Boissière, O.; Zhao, Y.; Yan, B.; Tremblay, L.; Lacelle, S.; Xia, H.; Zhao, Y. Ultrasound-Responsive Block Copolymer Micelles Based on a New Amplification Mechanism. *Langmuir* **2012**, *28*, 16463-16468.
- 158 Chen, Y.; Ballard, N.; Coleman, O. D.; Hands-Portman, I. J.; Bon, S. A. F. Dynamic control of volume phase transitions of poly(N-isopropylacrylamide) based microgels in water using hydrazide-aldehyde chemistry. *J. Polym. Sci. Part A: Polym. Chem.* **2014**, *52*, 1745-1754.
- 159 Guo, Z.; Feng, Y.; Wang, Y.; Wang, J.; Wu, Y.; Zhang, Y. A novel smart polymer responsive to CO₂. *Chem. Commun.* **2011**, *47*, 9348-9350.
- 160 Wang, F.; Klaiherd, A.; Thayumanavan, S. Temperature Sensitivity Trends and Multi-Stimuli Sensitive Behavior in Amphiphilic Oligomers. *J. Am. Chem. Soc.* **2011**, *133*, 13496-13503.
- 161 Nwankwo, I.; Xia, D. W.; Smid, J. Salt effects on cloud points and viscosities of polymethacrylates with pendant oligo-oxyethylene chains. *J. Polym. Sci. Part B: Polym. Phys.* **1988**, *26*, 581-594.
- 162 Baltes, T.; Garret-Flaudy, F.; Freitag, R. Investigation of the LCST of polyacrylamides as a function of molecular parameters and the solvent composition. *J. Polym. Sci. Part A: Polym. Chem.* **1999**, *37*, 2977-2989.
- 163 Yang, Y.; Zeng, F.; Tong, Z.; Liu, X.; Wu, S. Phase separation in poly(N-isopropyl acrylamide)/water solutions. II. Salt effects on cloud-point curves and gelation. *J. Polym. Sci. Part B: Polym. Phys.* **2001**, *39*, 901-907.
- 164 Hofmeister, F. Zur Lehre von der Wirkung der Salze. *Arch. Exp. Pathol. Pharmacol.* **1888**, *24*, 247-260.

- 165 Van Durme, K.; Rahier, H.; Van Mele, B. Influence of Additives on the Thermoresponsive Behavior of Polymers in Aqueous Solution. *Macromolecules* **2005**, *38*, 10155-10163.
- 166 Lee, L.-T.; Cabane, B. Effects of Surfactants on Thermally Collapsed Poly(N-isopropylacrylamide) Macromolecules. *Macromolecules* **1997**, *30*, 6559-6566.
- 167 Li, W.; Wu, P. On the thermodynamic phase behavior of poly(N-vinylcaprolactam) solution in the presence of different ionic liquids. *Polym. Chem.* **2014**, *5*, 761-770.
- 168 Belbekhouche, S.; Dulong, V.; Picton, L.; Le Cerf, D. Saccharide effect on the LCST property of a polyether: Influence of structure and length. *Colloids Surf. A* **2013**, *428*, 25-31.
- 169 Hoogenboom, R.; Thijs, H. M. L.; Wouters, D.; Hoepfener, S.; Schubert, U. S. Tuning solution polymer properties by binary water-ethanol solvent mixtures. *Soft Matter* **2008**, *4*, 103-107.
- 170 Magnusson, J. P.; Khan, A.; Pasparakis, G.; Saeed, A. O.; Wang, W.; Alexander, C. Ion-Sensitive “Isothermal” Responsive Polymers Prepared in Water. *J. Am. Chem. Soc.* **2008**, *130*, 10852-10853.
- 171 Wang, D.; Wu, T.; Wan, X.; Wang, X.; Liu, S. Purely Salt-Responsive Micelle Formation and Inversion Based on a Novel Schizophrenic Sulfobetaine Block Copolymer: Structure and Kinetics of Micellization. *Langmuir* **2007**, *23*, 11866-11874.
- 172 Bloksma, M. M.; Bakker, D. J.; Weber, C.; Hoogenboom, R.; Schubert, U. S. The Effect of Hofmeister Salts on the LCST Transition of Poly(2-oxazoline)s with Varying Hydrophilicity. *Macromol. Rapid Commun.* **2010**, *31*, 724-728.
- 173 Sharma, A.; Srivastava, A. Pronounced influence of pH, metal-ion and solvent isotope on the thermoresponse of synthetic amphiphilic polypeptides. *Polym. Chem.* **2013**, *4*, 5119-5128.

Chapter 2

2. Isothermally-Responsive, Biodegradable Poly(disulfide)s

2.1 Chapter Summary

Telechelic, Reversible Addition-Fragmentation Chain Transfer (RAFT)-derived macromonomers with a pyridyl disulfide end-group were converted into high molecular weight, disulfide-linked polymers using a polycondensation, step-growth procedure. The applicability of this method to polycondense a library of macromonomers with different functionalities including (meth)acrylates and acrylamides was investigated. Side-chain sterics were found to be important as non-linear poly(ethylene glycol) analogues proved incompatible with this synthetic methodology, as did methacrylates due to their pendant methyl group. This method was used to incorporate disulfide bonds into poly(*N*-isopropylacrylamide), pNIPAM, precursors to give dual-responsive (thermo- and redox) materials. These polymers were shown to selectively degrade in the presence of intracellular concentrations of glutathione, but be stable at low, extracellular concentrations. Due to the molecular weight-dependent cloud point of pNIPAM, the lower critical solution temperature behaviour could be switched off by a glutathione gradient without a temperature change; an isothermal transition.

2.2 Introduction

Responsive or ‘smart’ materials are capable of undergoing a physical response upon the application of an external stimulus. These materials are finding application in a diverse range of fields including switching surfaces and adhesives, artificial muscles, sensors,¹ and biomedical fields such as drug delivery,² gene delivery³ and tissue engineering.⁴ Synthetic polymers exhibiting a lower critical solution temperature (LCST) have been extensively investigated as smart, thermo-responsive materials. Upon increasing the solution temperature above the cloud point (the measurable property of an LCST) an aqueous polymer solution becomes insoluble and aggregates/precipitates. This property can be exploited for either drug release⁵ or hyperthermia-triggered cellular uptake due to increased lipophilicity above the LCST.⁵⁻⁷ Examples of polymers displaying this behaviour include poly[(oligoethyleneglycol)methyl ether methacrylate] (pOEGMA),^{8, 9} poly(*N*-isopropylacrylamide) (pNIPAM)¹⁰ and poly(*N*-vinylpiperidone).¹¹ While temperature changes are useful, some applications may require a change in polymer solubility (*i.e.* to switch between “active” and “inactive” states) without applying a thermal gradient. “*Isothermal*” transitions have previously been demonstrated by Alexander and co-workers based on salt concentration gradients,^{12, 13} Steinhauer *et al.* following aminolysis of RAFT-derived polymer chains¹⁴ and by Rimmer and co-workers due to bacterial binding.¹⁵ Other examples include the use of light,^{16, 17} protein binding¹⁸ and the application of dissolved gases.¹⁹ We have demonstrated that selective cleavage of a single polymer end-group results in a shift in pNIPAM cloud point allowing an isothermal transition based on bioreduction.²⁰

Polymer degradation is a critical consideration for *in vivo* applications such as drug or gene delivery. This is typically achieved by the incorporation of one or more cleavable linkers into either the polymer backbone, side-chain or as a cross-linker.^{21,}
²² Common degradation triggers include hydrolysis, thermolysis or enzymatic action.²³⁻²⁶ A major challenge associated with the development of biodegradable polymers is the introduction of functional groups onto the polymer backbone. For example ring opening polymerisation of *N*-carboxyanhydrides or cyclic esters, which give degradable poly(amides) or poly(esters) respectively, are incompatible with most functional groups.²⁷⁻²⁹ Conversely, controlled radical polymerisation processes enable a vast range of functional groups to be incorporated into a polymer structure, but give rise to an all-carbon backbone which cannot degrade.³⁰ To address the above paradox, we have previously reported a synthetic route towards degradable, main-chain disulfide bond-containing pNIPAM. This was achieved by polymerising NIPAM using a RAFT chain transfer agent containing a pyridyl disulfide moiety at the α -terminus. Following aminolysis of the ω -terminal dithioester, a polycondensation-type, step-growth polymerisation with release of pyridine thione occurred (Figure 2.1). The degradability of this material was demonstrated by the addition of a reducing agent which produced polymer chains with a higher LCST than the disulfide-linked counterpart. Hence, a novel method to ‘switch off’ LCST behaviour using a secondary chemical stimulus was illustrated.³¹ A similar procedure combining aminolysis and thiol-disulfide exchange has also been recently applied to alkyl disulfides.³²

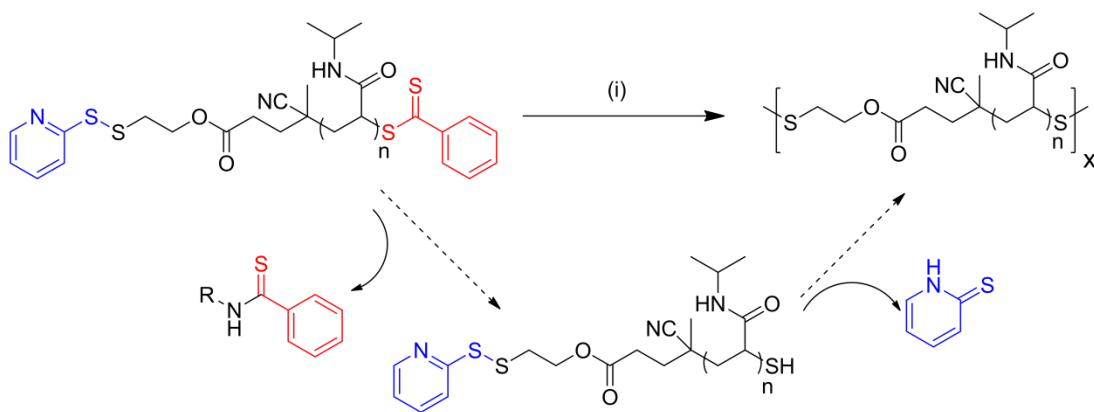


Figure 2.1 Preparation of disulfide-linked polymers using a polycondensation-type methodology: (i) Ethanolamine (1 eq.); triethylamine (2 eq.); THF; N₂; 25 °C; 24h.³¹

The redox-sensitive nature of disulfide-containing polymers is of particular interest for triggered cellular delivery applications. The main reducing agent (anti-oxidant) inside cells is glutathione (GSH) where it is present at mM concentrations. Conversely, the extracellular GSH concentration is only μM hence this differential provides a unique and selective trigger to promote intracellular degradation, whilst ensuring stability in the circulation.^{33, 34} The use of disulfide-containing polymers has seen a particular focus on gene delivery therapies to date³⁵⁻⁴⁰ though there are also reports utilising redox-sensitive materials for targeted, drug delivery applications.⁴¹⁻⁴⁷

This chapter explores the scope of our synthetic methodology as a means of preparing controlled radical polymerisation-derived, highly functionalised disulfide-linked polymers. The biodegradability of these materials using biorelevant glutathione concentrations is investigated to ensure selectivity for intracellular conditions. Finally, thermally responsive, degradable polymers are tested for their

isothermal response to glutathione gradients to enable their LCST behaviour to be ‘switched off’ once inside a cell (Figure 2.2).

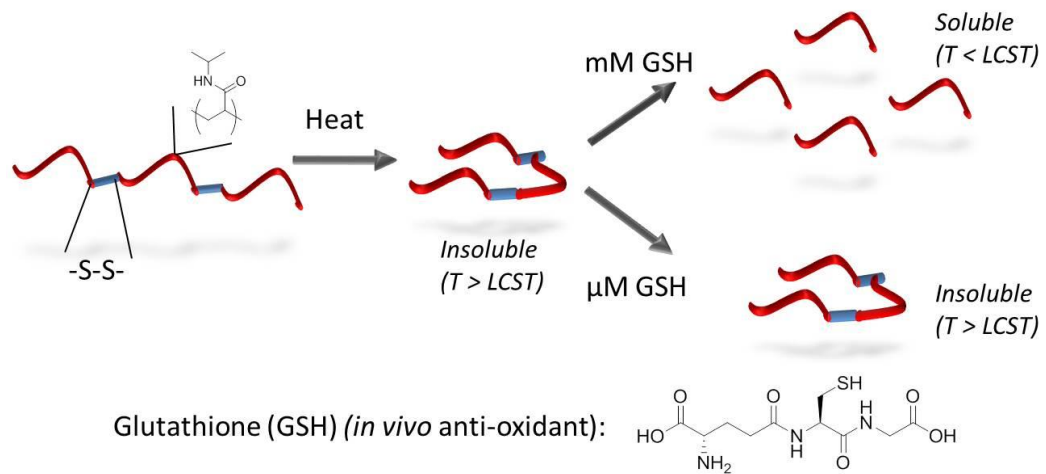


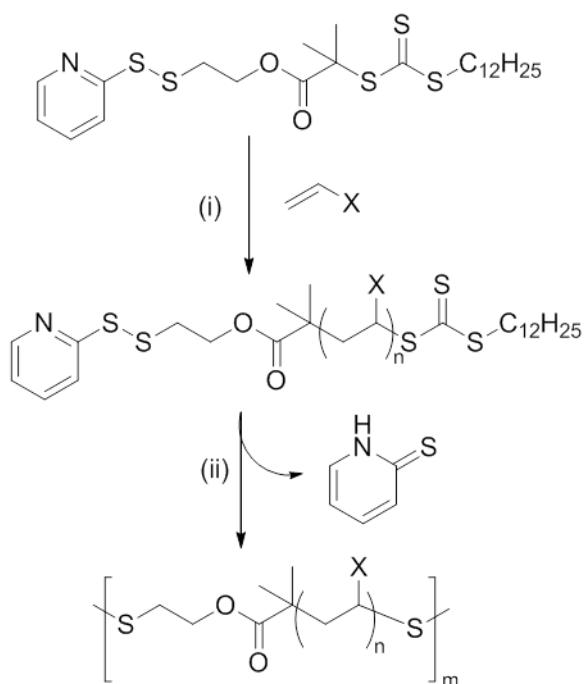
Figure 2.2 Study concept: Disulfide-linked, biodegradable pNIPAM will be prepared and the *in vivo* GSH concentration gradient used to trigger selective degradation and isothermal LCST behaviour.

2.3 Results and Discussion

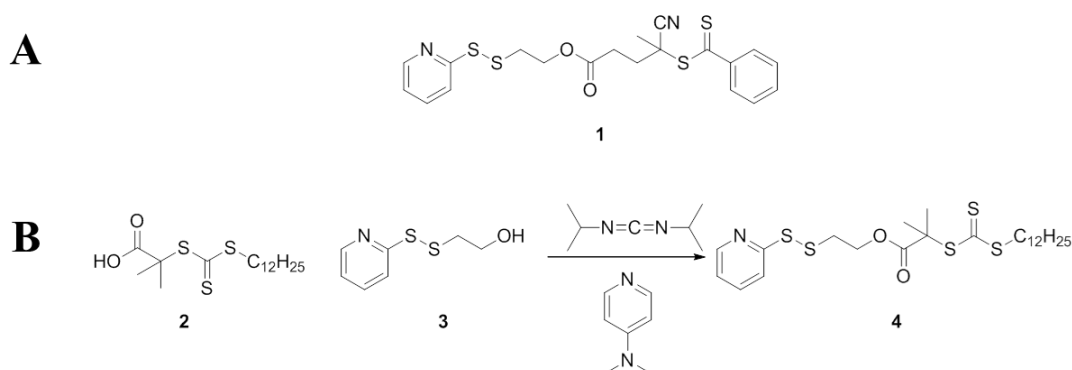
The aim of this work was to exemplify our previous report on the synthesis of disulfide-linked pNIPAM, obtained by a polycondensation-type reaction of pyridyl disulfide-terminated, RAFT-derived polymers, Scheme 2.1.³¹ Previously we used a dithioester chain transfer agent (Scheme 2.2, compound **1**) which, although an excellent mediator for the polymerisation of a wide range of monomers, is less synthetically accessible than trithiocarbonate RAFT agents. We therefore prepared the trithiocarbonate propanoic acid 2-[[[(dodecylthio)thioxomethyl]thio]-2-methyl-2-(2-pyridinyldithio)ethyl ester (PADE, **4**) using a method modified from that described by Skey and O'Reilly.⁴⁸ First, 2-(dodecylthiocarbonothioylthio)-2-methylpropanoic acid, **2**, was prepared by the reaction of dodecane thiol with carbon disulfide and 2-bromo methyl propionic acid in the presence of potassium phosphate. This compound was then coupled to pyridyl disulfide-containing alcohol **3** in the presence of *N,N*-diisopropylcarbodiimide and 4-dimethylaminopyridine to give PADE (Scheme 2.2, compound **4**), which was isolated using column chromatography on silica to give a yellow oil in good yield (78 %).

Structure and purity was confirmed by ¹H NMR, ¹³C NMR spectroscopies and high resolution mass spectrometry. As shown in Figure 2.3, analysis by ¹H NMR spectroscopy revealed 4 peaks between 7.10 and 8.47 ppm and two triplets at 4.36 and 3.03 ppm corresponding to the pyridyl protons and two CH₂ groups on the starting alcohol. Signature peaks from the carboxylic acid fragment include a triplet and doublet at 0.88 and 3.27 ppm corresponding to the CH₃ and terminal CH₂ group in the dodecyl chain. Key signature peaks in the ¹³C NMR spectrum include the C=S

carbon at 221.5 ppm and the CH₃ carbon at 25.3 ppm from the carboxylic acid fragment together with the pyridyl carbons between 119.8 and 159.9 ppm.



Scheme 2.1 Synthetic strategy for the preparation of a disulfide-linked polymer from trithiocarbonate starting material: (i) Polymerisation of monomer; (ii) Polycondensation-type reaction, employing nucleophile and base, with liberation of pyridine thione.



Scheme 2.2 RAFT agents used in this study: (A) Chemical structure of pyridyl disulfide-containing dithiobenzoate (1); (B) Synthetic strategy for the preparation of pyridyl disulfide-containing trithiocarbonate (PADE, 4).

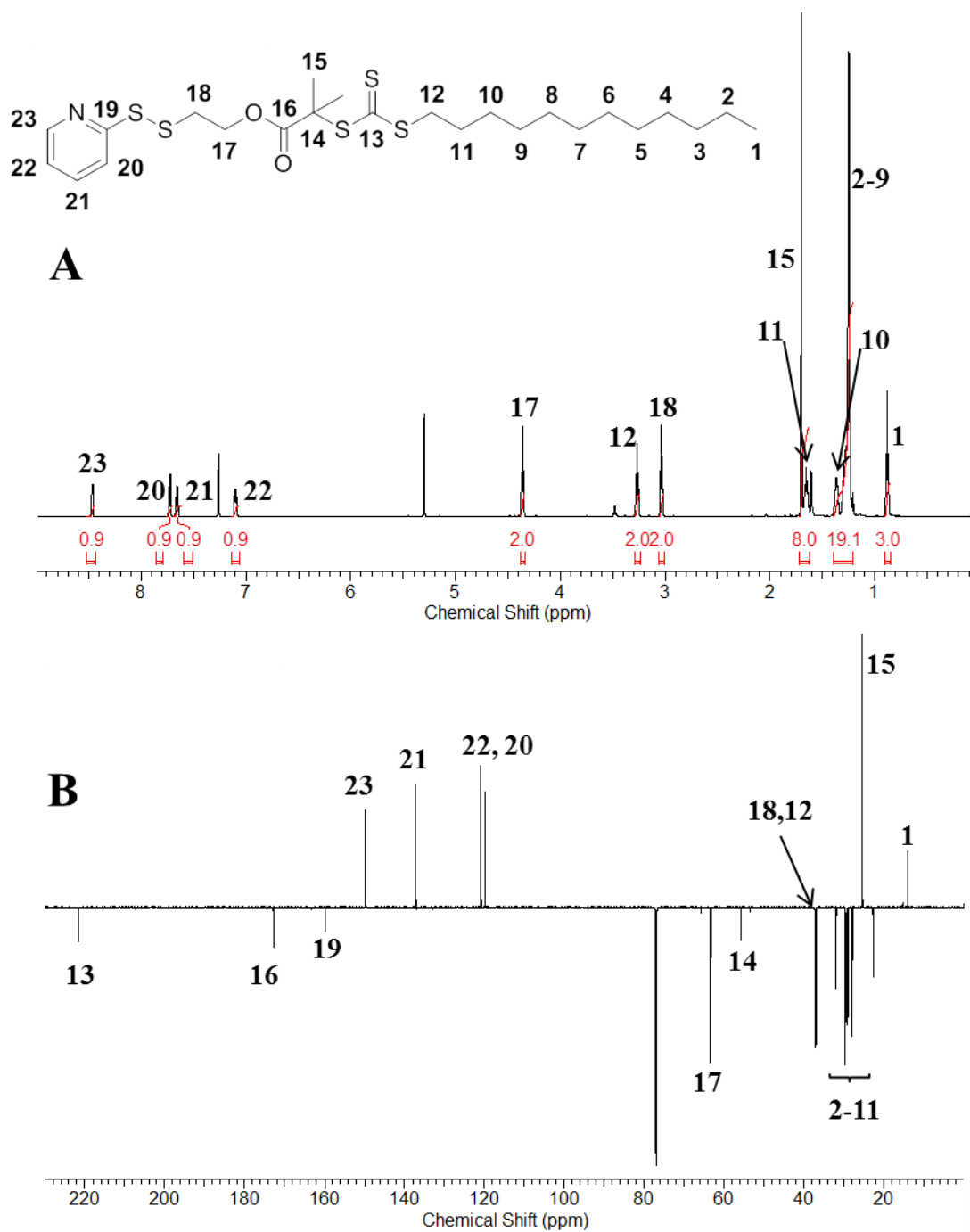


Figure 2.3 NMR spectroscopic characterisation of PADE in CDCl_3 : (A) ^1H and (B) ^{13}C spectra.

Our strategy for the preparation of disulfide-linked polymers from RAFT-derived macromonomers requires aminolysis of the RAFT agent to yield a thiol-terminated polymer. This can then react *in situ* with pyridyl disulfide groups on neighbouring chains (Scheme 2.1) giving a polycondensation type, step-growth polymerisation, with elimination of pyridine thione. To verify that our method could be extended to a trithiocarbonate CTA, **pNIPAM-1** was prepared using PADE (Table 2.1, entry 1). Attempts to polycondense in the presence of oxygen failed to produce a substantially higher molecular weight polymer due to oxidative side-reactions giving macromonomer- and dimer-derived species only (Figure 2.4A). When degassed (Figure 2.4A), the same bimodal trace was observed, albeit with a small high molecular weight tail indicating either a slow rate of reaction or the presence of residual oxygen. To circumvent the former issue, triethylamine (TEA) was added to the degassed solution. In this case, a higher molecular weight polymer was formed with only small amounts of residual macromonomer observed. Inclusion of base was therefore crucial, presumably by increasing thiol nucleophilicity by deprotonation.

To verify that the resulting polycondensed product contained the desired disulfide linkages, it was incubated with the strong reducing agent tributylphosphine and analysed by Size Exclusion Chromatography (SEC) (Figure 2.4B). A trace with a molecular weight slightly lower than the starting material was observed, concurrent with disulfide bond cleavage. The loss of end-groups and the potentially different elution behaviour of thiol-terminated chains could explain the difference in observed molecular weight between starting and cleaved materials. These results confirm that trithiocarbonates provide suitable end-groups for our new polycondensation-type polymerisation.

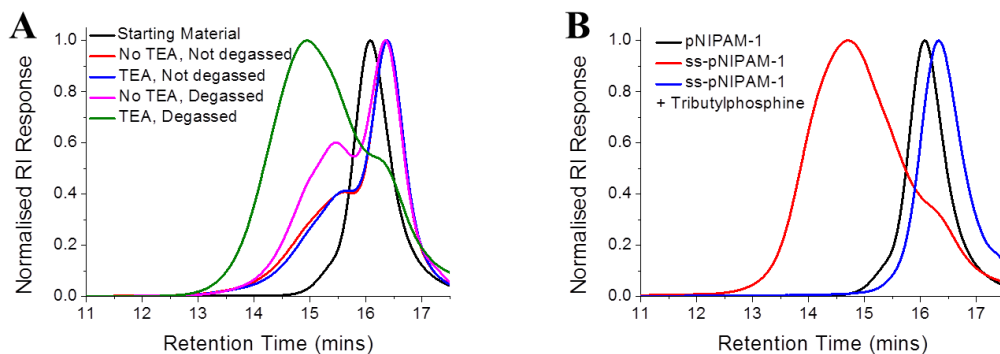


Figure 2.4 SEC data showing the polycondensation of **pNIPAM-1**: (A) Optimisation of the polycondensation conditions using an inert atmosphere, and a base; (B) Verifying the redox-responsive nature of the polycondensed species.

Our study subsequently focused on extending the polycondensation methodology to a wider range of polymeric precursors. A representative library of polymers was synthesised using 4,4'-azobis(4-cyanovaleric acid), ACVA, as radical initiator and PADE covering methacrylate, acrylate and acrylamide functionalities. Targeted molecular weights were determined by the ratio of Monomer:PADE used in the polymerisation and all polymers were characterised by SEC and ^1H NMR spectroscopy. All polymers were found to be well-defined with narrow dispersities and most molecular weights, as determined by SEC, were in decent agreement with the theoretical values (Table 2.1). Any differences can be accounted for by the different solvation and elution behaviour of the polymers relative to the poly(methyl methacrylate) standards used. These polymers were subjected to the optimised polycondensation conditions (*vide supra*) and the results are summarised in Table 2.2.

Table 2.1 Characterisation of polymers prepared in this study using PADE.

Entry	Polymer	[M]:[CTA]	Conversion (%) ^a	$M_{n(th)}$ (g.mol ⁻¹) ^a	$M_{n(SEC)}$ (g.mol ⁻¹) ^b	M_w/M_n ^b
1	pNIPAM-1	20	91.7	2100	2000	1.18
2	pNIPAM-2	40	91.4	4100	3100	1.16
3	pNIPAM-3	488	73.3	40500	25400 ^c	1.24 ^c
4	pOEGMA ₃₀₀	15	89.9	5400	18300	1.12
5	pOEGA ₄₈₀	22	85.1	10600	9600	1.10
6	pDEGMA	20	80.4	3000	23000	1.24
7	pMMA	30	58.1	1700	6400	1.38
8	p <i>t</i> BuA	20	91.0	2300	2500	1.16
9	pDMA ^d	34	93.1	3000	2800	1.10
10	pDMA ^e	100	56.7	5700	3700	1.18

pNIPAM = poly(*N*-isopropylacrylamide); pOEGMA₃₀₀ = poly[oligo(ethylene glycol, average $M_n = 300$ g.mol⁻¹) methyl ether methacrylate]; pOEGA₄₈₀ = poly[oligo(ethylene glycol, average $M_n = 480$ g.mol⁻¹) methyl ether acrylate]; pDEGMA = poly(diethylene glycol methyl ether methacrylate); pMMA = poly(methyl methacrylate); p*t*BuA = poly(*tert*-butyl acrylate); pDMA = poly(*N,N*-dimethylacrylamide); ^aDetermined by ¹H NMR spectroscopy relative to an internal standard (mesitylene); ^bDetermined by SEC (THF inc. 2 % TEA) relative to PMMA standards unless otherwise stated; ^cDetermined by SEC (DMF inc. 5 mM NH₄BF₄) relative to PMMA standards; ^dPrepared with trithiocarbonate CTA (PADE, **4**); ^ePrepared with dithiobenzoate CTA **1**.

Table 2.2 SEC Characterisation of poly(disulfide)s.

Entry	Poly (disulfide)	M_w (SM) ^a	M_w (Pc) ^a	M_p (SM) ^a	M_p (Pc) ^a	-S-S- links/chain ^b	M_w/M_n (Pc) ^a
1	ss-pNIPAM-1	2400	8900	2400	7600	2.2	1.81
2	ss-pNIPAM-2	3600	20300	3700	15300	3.1	1.78
3	ss-pNIPAM-3	31200 ^c	128900 ^c	35900 ^c	140700 ^c	2.9	2.01 ^c
4	ss-pOEGMA ₃₀₀	22100	59600	20000	38500	0.9	1.38
5	ss-pOEGA ₄₈₀	28500	44200	26600	32600	0.2	1.5
6	ss-pDEGMA	10500	15700	10400	10900	0.0	1.27
7	ss-pMMA	8900	8800	9000	8900	0.0	1.61
8	ss-ptBuA	2900	12200	3100	11700	2.8	2.35
9	ss-pDMA ^d	2800	8300	3100	11100	2.6	1.45
10	ss-pDMA ^e	4400	7600	4800	10100	1.1	1.49

ss-pNIPAM = disulfide-linked poly(*N*-isopropylacrylamide); ss-pOEGMA₃₀₀ = disulfide-linked poly[oligo(ethylene glycol, average $M_n = 300 \text{ g.mol}^{-1}$) methyl ether methacrylate]; ss-pOEGA₄₈₀ = disulfide-linked poly[oligo(ethylene glycol, average $M_n = 480 \text{ g.mol}^{-1}$) methyl ether acrylate]; ss-pDEGMA = disulfide-linked poly(diethylene glycol methyl ether methacrylate); ss-pMMA = disulfide-linked poly(methyl methacrylate); ss-ptBuA = disulfide-linked poly(*tert*-butyl acrylate); ss-pDMA = disulfide-linked poly(*N,N*-dimethylacrylamide); ^aWeight-average molecular weight (M_w), peak maximum molecular weight (M_p) or dispersity (M_w/M_n) of starting material (SM) or polycondensed product (Pc) determined by SEC (THF inc. 2 % TEA) relative to PMMA standards unless otherwise stated; ^bAverage number of disulfide links per chain following polycondensation $\{[M_p(\text{Pc})/M_p(\text{SM})]-1\}$; ^cDetermined by SEC (DMF inc. 5 mM NH_4BF_4) relative to PMMA standards; ^dHomopolymer prepared with trithiocarbonate CTA (PADE, **4**); ^eHomopolymer prepared with dithiobenzoate CTA **1**.

Polycondensation of poly(*N,N*-dimethylacrylamide) (**pDMA**) proceeded to give a noticeable increase in both M_w (weight-average molecular weight) and M_p (peak maximum molecular weight) (Table 2.2, entry 9; Figure 2.5A/B). Identical results were observed for **pDMA** obtained from the precursor prepared with dithioester **1** as a control experiment (Table 2.2, entry 10; Figure 2.5C/D), indicating that this strategy can be applied to monomer types other than NIPAM; a key aim of this study. The average number of ‘macro’ repeat units per chain was estimated from SEC and shown in Table 2.2. All successful polymerisations gave 2 – 3 disulfides (3-4 repeat units) whereas the unsuccessful (*vide infra*) gave numbers close to 0.

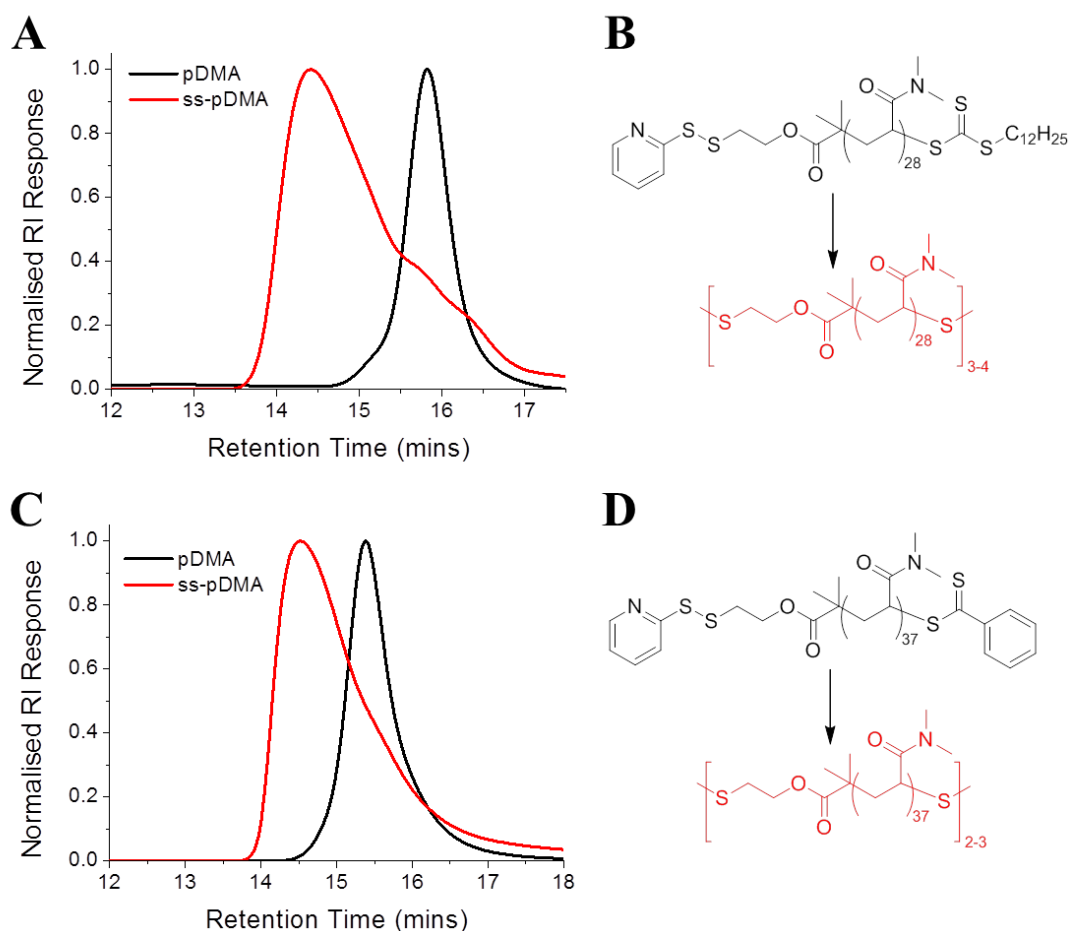


Figure 2.5 Polycondensation of **pDMA** with PADE and CTA **1**: (A/C) SEC data; (B/D) Chemical structure of polymer precursor/product.

A particularly interesting class of polymers is those based on oligo(ethylene glycol) methacrylates (OEGMAs). These polymers are indicated to be biocompatible, similar to their parent linear PEG,⁴⁹ but are synthetically accessible by controlled radical polymerisation. Furthermore, they also display tuneable LCST behaviour which can be exploited for a range of biotechnological applications.^{8, 50} It is important to note that the pOEG(M)As prepared in Table 2.1 have notably higher molecular weights than the other polymers due to their relatively long side chains. They were designed to have similar degrees of polymerisation to allow direct comparison with other polymers used in this study. Initial attempts to polycondense **pOEGMA₃₀₀** proved unsuccessful indicating dimers and no higher order polymers could be formed (Table 2.2, entry 4; Figure 2.6).

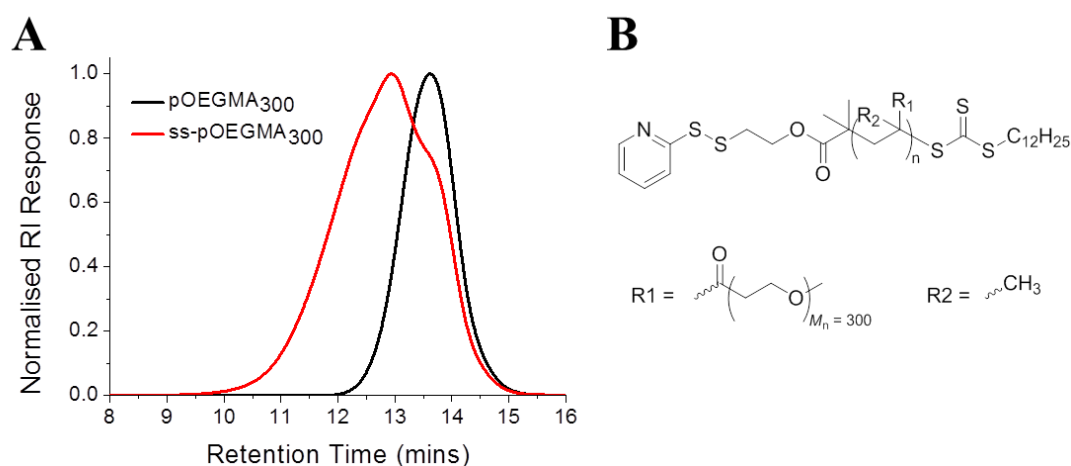


Figure 2.6 (A) SEC data showing the attempted polycondensation reaction of **pOEGMA₃₀₀** and (B) chemical structure of polymer precursor.

Xu *et al.* observed that thiolactones can form between a terminal thiol, generated by aminolysis of a RAFT end-group, and the penultimate repeat unit of a methyl methacrylate backbone (Figure 2.7).⁵¹ While this explanation for thiol deactivation fits our observations, there are other reports of the successful reaction of RAFT-

derived thiols with pyridyl disulfide groups in acrylate and methacrylate polymers.⁵² An alternative explanation therefore may be steric hindrance of the terminal thiol by the oligo(ethylene glycol) side chains. This theory is supported by visual examination of the reaction mixture: when pyridyl disulfide is successfully displaced by a thiol, the released pyridine thione has a strong yellow colouration. In the case of pOEGMAs however, no colour change was observed suggesting no thiol-pyridyl disulfide reaction had occurred.

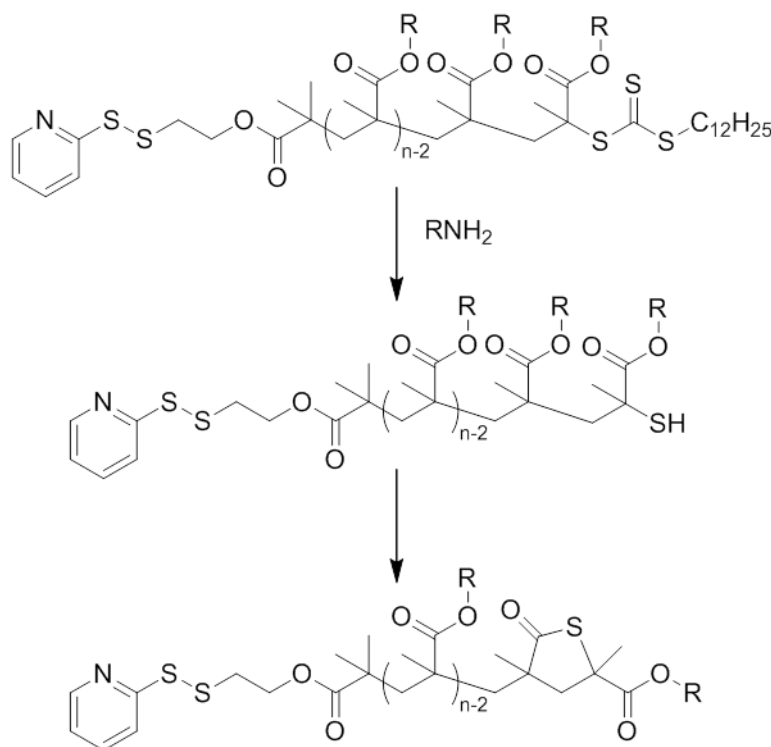


Figure 2.7 Representation of possible thiolactone-forming side-reaction following aminolysis of a thiocarbonylthio-terminated methacrylate. Adapted from work by Xu *et al.*⁵¹

To further probe this, poly(diethylene glycol methacrylate), **pDEGMA**, which has a shorter PEG chain (2 units as opposed to 7) was tested, but yielded only a minor increase in M_p (Table 2.2, entry 6; Figure 2.8). The increase in M_w of approximately 50 % suggested some dimer-formation was occurring, whilst the solution remained

colourless, indicating limited or no pyridine thione elimination. To confirm that the reaction was not kinetically limited, it was left for an extended time period (7 days). Analysis after this time showed no additional change to that seen after 48 hrs suggesting that pOEGMAs cannot be polycondensed in this fashion.

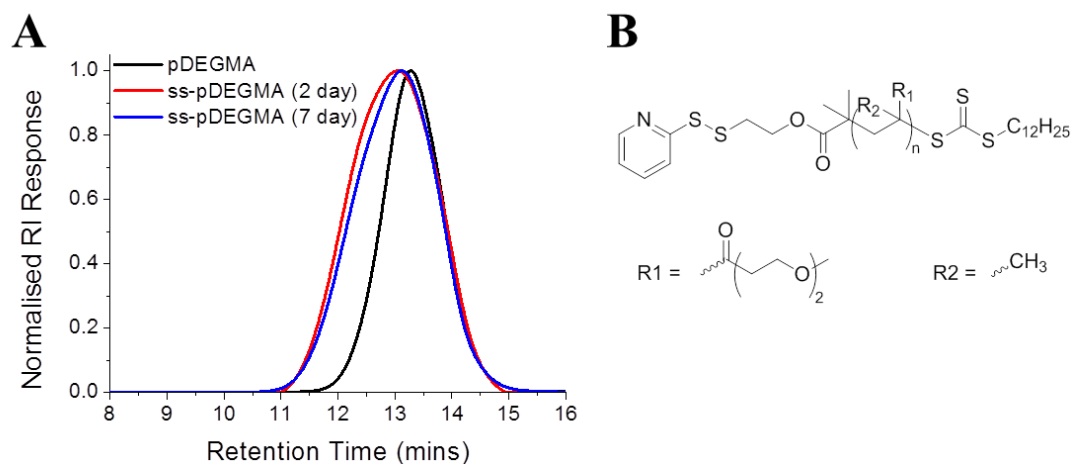


Figure 2.8 (A) SEC data showing the attempted polycondensation reaction of **pDEGMA** and (B) chemical structure of polymer precursor.

Another reason for the successful polycondensation of pDMA and pNIPAM compared to the pOEGMAs could be the lack of a backbone methyl group. The resulting secondary thiol would be expected to be more nucleophilic than a tertiary thiol. To address this, poly[oligo(ethylene glycol) methyl ether acrylate] (**pOEGA₄₈₀**) was also synthesised using PADE. However, subsequent polycondensation gave only a higher molecular weight shoulder of approximately double the starting material molecular weight (Table 2.2, entry 5; Figure 2.9), confirming that that the PEG side chain can limit the polycondensation process.

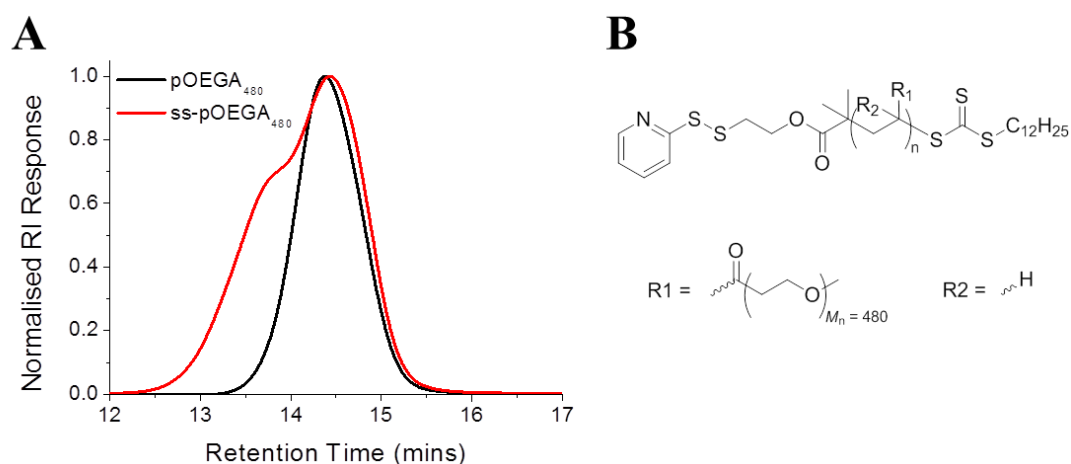


Figure 2.9 (A) SEC data showing the attempted polycondensation reaction of **pOEGA₄₈₀** and (B) chemical structure of polymer precursor.

To elucidate the role of the pendant methyl group, polycondensation of a poly(methyl methacrylate) macromonomer, **pMMA**, which should have no steric hindrance was attempted (Table 2.2, entry 7). SEC analysis showed no evidence for multi disulfide-linked polymers even with extended reaction times (4 days, Figure 2.10). We propose the tertiary thiol present at the chain end of poly(methacrylate)s is not sufficiently nucleophilic to react with the pyridyl disulfide moiety meaning methacrylates are not compatible with this methodology.

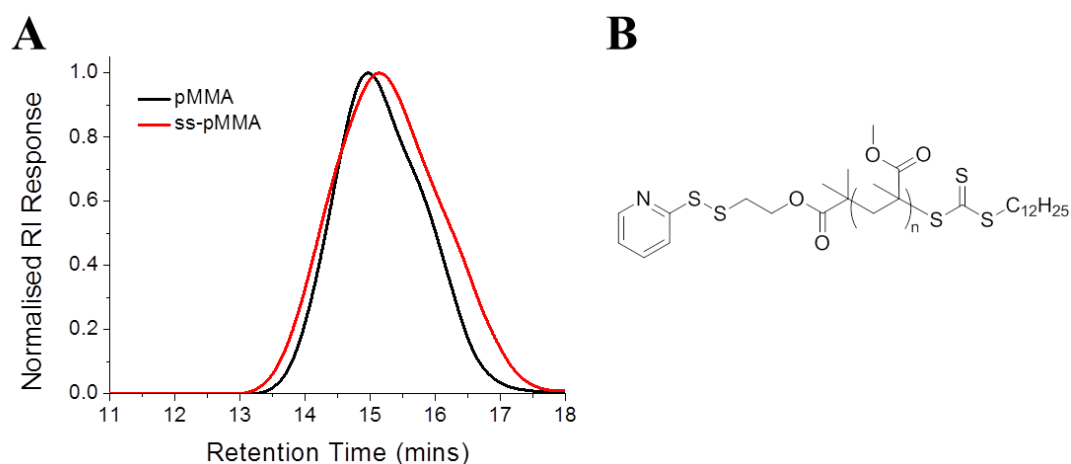


Figure 2.10 (A) SEC data showing the attempted polycondensation of **pMMA** and (B) chemical structure of the polymer precursor.

To further investigate steric effects of the thiol terminus, *tert*-butyl acrylate was utilised given its branched structure is similar to NIPAM and DMA. It also lacks the long side-chain present in OEGMA, DEGMA and OEGA and has no pendant methyl group. Polycondensation of **ptBuA** saw a 4-fold increase in M_w and M_p indicative of a disulfide-linked polymer (Table 2.2, entry 8; Figure 2.11). This demonstrates that acrylates are compatible with our technique to generate disulfide-linked polymers, but that sterics must be considered. Post-polymerisation modification may offer an approach to overcome this.

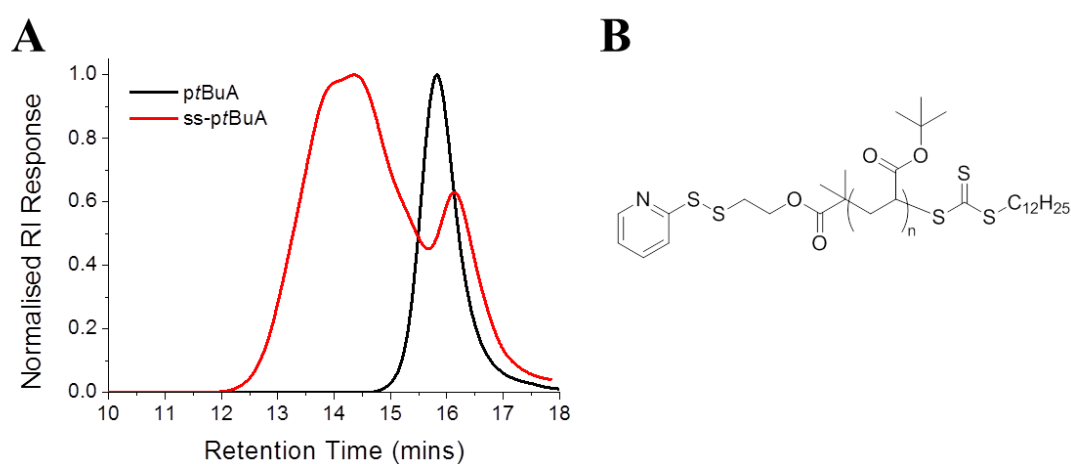


Figure 2.11 (A) SEC data showing the polycondensation of **ptBuA** and (B) chemical structure of the polymer precursor.

The work described above utilised relatively low molecular weight polymers as it was anticipated that these would show faster rates of polycondensation. It was therefore prudent to attempt to apply this methodology to larger precursors, which in turn may give rise to higher molecular weight, disulfide-linked polymers. This is particularly important for drug delivery applications where the polymeric delivery device should ideally be larger than the renal filtration limit (~ 40 kDa), but have degradation products below this.²¹ In the case of pNIPAM, tuning the molecular

weight of the polymeric precursors also allows control over their lower critical solution temperatures.³¹ Two further pNIPAM homopolymers were therefore prepared with PADE to give molecular weights (by SEC) of 3100 (**pNIPAM-2**) and 25400 (**pNIPAM-3**) g.mol⁻¹ respectively (Table 2.1, entries 2 and 3). Both polymers were successfully polycondensed into disulfide-linked materials (Table 2.2, entries 2 and 3; Figure 2.12). It should be noted that these reactions were performed on a larger scale (~ 100 mg) than those shown in the above section (5-10 mg) and therefore required longer reaction times to achieve high conversions (5-7 days). **ss-pNIPAM-3** gave an M_w above the renal filtration limit ($M_w = 128900$ g.mol⁻¹), whilst the precursor M_w of 31200 g.mol⁻¹ was below this. The redox-sensitivity of these disulfide-linked pNIPAMs was again demonstrated by the addition of tributylphosphine (Figure 2.12), resulting in a reduction in molecular weight back to the original polymer.

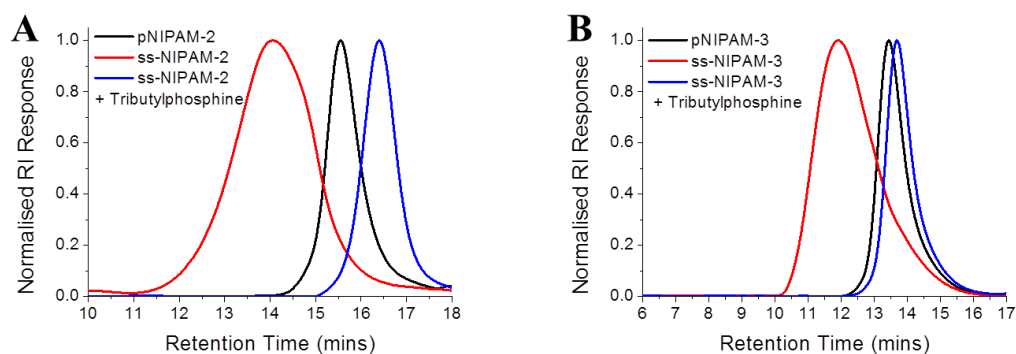


Figure 2.12 SEC data showing polycondensation and subsequent reduction from (A) **pNIPAM-2** and (B) **pNIPAM-3** precursors.

Analysis of **ss-pNIPAM-2** by electrospray ionisation (ESI) mass spectrometry following the addition of tributylphosphine confirmed that degradation was *via* disulfide bond reduction (Figure 2.13). Lower molecular weight, thiol-terminated

polymers were observed, thus ruling out alternative modes of degradation such as hydrolysis or reduction of the ester units.

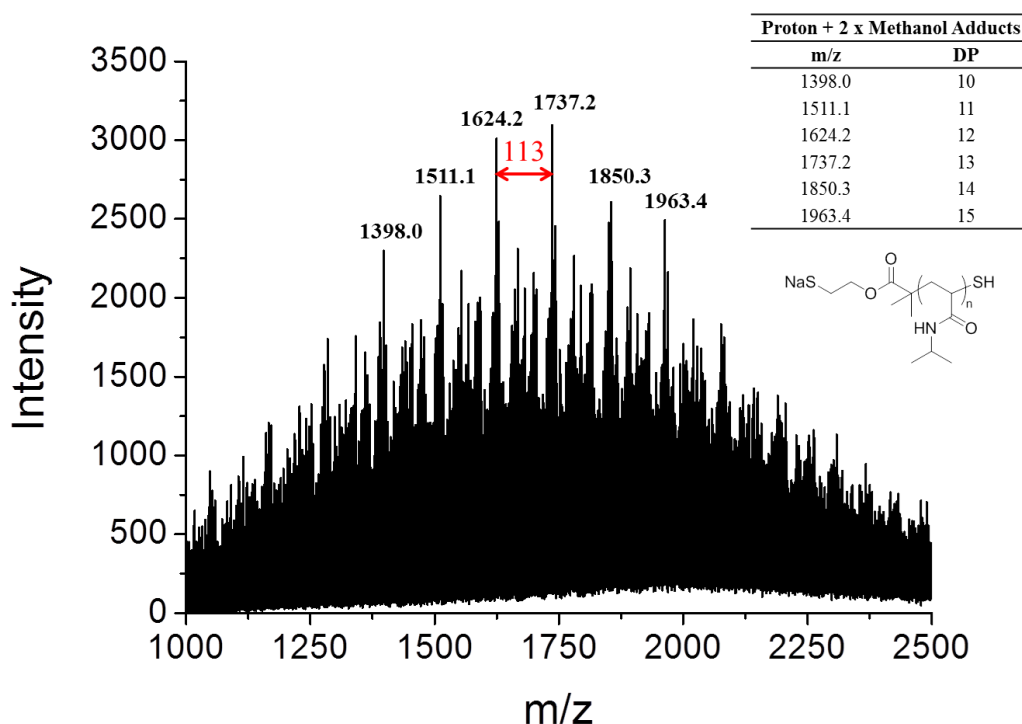


Figure 2.13 ESI (+ve) mass spectrometry analysis of **ss-pNIPAM-2** following degradation by tributyl phosphine.

The molecular weight dependent cloud point (CP) of these materials was measured with the small and large precursors giving CPs of 22 °C and 31 °C respectively (Figure 2.14). Turbidity measurements indicated a higher CP for both disulfide-linked polymers relative to their precursors. **ss-pNIPAM-2** had a CP of 30 °C (Fig. 2.14A), whilst **ss-pNIPAM-3** had a CP of 32 °C (Figure 2.14B), an increase of 8 °C and 1 °C respectively. Although pNIPAM generally exhibits an inversely proportional relationship between cloud point and molecular weight, the increase observed here can be attributed to a change in end-group functionality, namely loss

of the highly hydrophobic dodecane thiol and pyridyl disulfide moieties. We have recently reported the importance of end-groups on the cloud point of pNIPAMs.²⁰

To assess the effect of disulfide degradation on the CP, the samples were treated with tris(2-carboxyethyl)phosphine, TCEP, a water soluble phosphine, and analysed by turbidimetry (Figure 2.14). The CP of **ss-pNIPAM-2** following TCEP reduction increased compared to the disulfide-linked starting material, as expected given the inversely proportional relationship between CP and pNIPAM molecular weight. The CP of **ss-pNIPAM-3** following TCEP reduction did not change as pNIPAMs CP is relatively constant above 10000 g.mol⁻¹.³¹

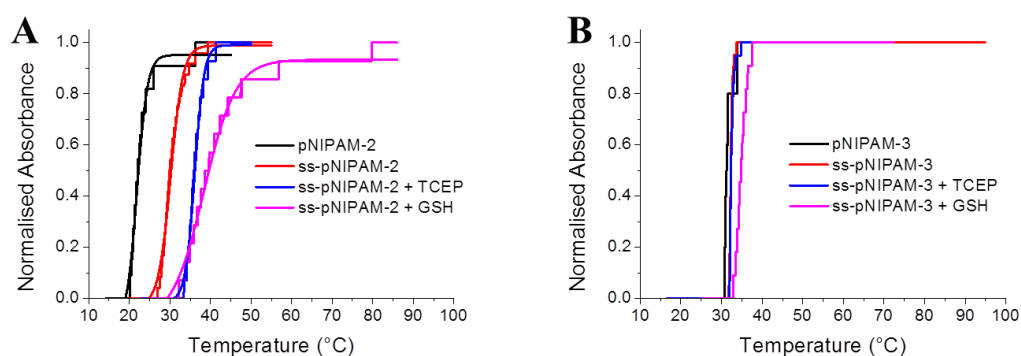


Figure 2.14 Cloud point data (polymer concentration = 5 mg.mL⁻¹) for (A) pNIPAM-2/ss-pNIPAM-2 (solid curves added to guide the eye) and (B) pNIPAM-3/ss-pNIPAM-3. Note: GSH concentration = 1 mM.

To test degradation under more biorelevant conditions, glutathione (GSH) was used as the reducing agent. This *in vivo* reducing agent is present at μ M concentrations in the extracellular environment but mM concentrations in the intracellular environment. Previous work has shown that poly(disulfide)s are preferentially cleaved at higher GSH concentrations, providing a selective, intracellular trigger for polymer degradation.^{38, 39, 41} Both **ss-pNIPAM-2** and **ss-pNIPAM-3** were stirred in

aqueous glutathione solutions at 1 μ M and 1 mM concentrations for 24 hrs. The samples were then analysed by turbidimetry (Figure 2.14). An increase in CP was again observed, with the change larger than that obtained with TCEP for both samples. This is possibly due to a difference in the mechanism of degradation: TCEP works by simple disulfide bond cleavage whilst GSH, a tripeptide containing a cysteine residue, is more likely to degrade by thiol-disulfide exchange. There is hence a difference in hydrophilicity of the generated end-groups. After stirring in aqueous GSH solution the polymers were freeze-dried and analysed by SEC. After 72 hrs at mM GSH concentrations, both polymers had undergone significantly more degradation than those incubated at μ M GSH concentration (Figure 2.15) indicating the specific response to intracellular-GSH.

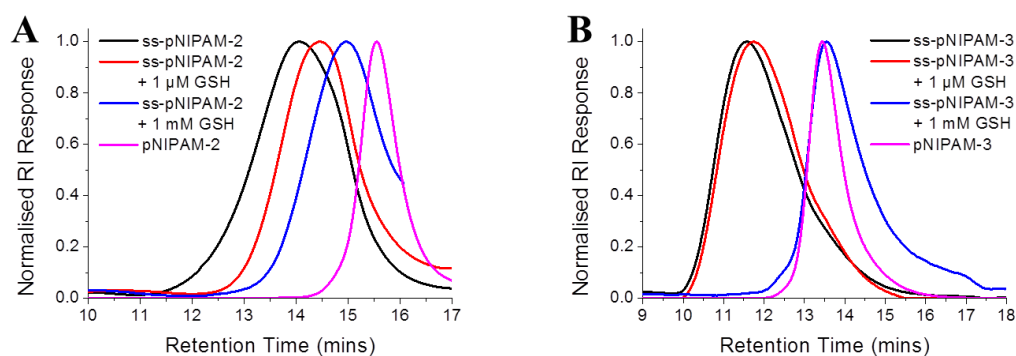


Figure 2.15 SEC data showing degradation of (A) **ss-pNIPAM-2** and (B) **ss-pNIPAM-3** at different GSH concentrations.

Given the large change in CP following incubation of **ss-pNIPAM-2** with GSH (shift of 9 $^{\circ}$ C), we investigated whether this could be used as a switch to trigger isothermal polymer re-solubilisation. This would be useful, for example, following thermally triggered uptake into hyperthermic cells⁷ where the increased GSH concentration should lead to degradation and an increase in cloud point. This will prompt polymer resolubilisation, which is preferable for eventual excretion, and

removes the issue of insoluble polymer aggregates inside cells. Three aqueous polymer solutions of **ss-pNIPAM-2** were incubated at 37 °C and their absorbance at 650 nm was observed. Each sample aggregated in solution as expected given the CP of the polymer was 30 °C. Glutathione was then added to give total GSH concentrations of 0 (control), 1 μM and 1 mM. Whilst the polymer solutions with 0 and 1 μM GSH concentrations remained turbid, re-solubilisation of the polymer held at 1 mM GSH concentration occurred rapidly (within mins) as the CP exceeded that of the temperature at which it was being held (Figure 2.16A). This was confirmed by the rapid decrease in absorbance and was also observed visually (Figure 2.16A, inset). The same experiment using **ss-pNIPAM-3** yielded the same results (Figure 2.16B). It was not possible to estimate the kinetics of degradation from this experiment due to the cooperative behaviour of pNIPAM. We have demonstrated that mixtures of pNIPAMs with different chain lengths (and hence CPs) show a single transition, controlled by the mass fraction of each chain length.⁵³ Therefore, complete resolubilisation will occur when sufficient numbers of short chains are present to increase the CP above the local temperature. This is a desirable feature allowing for more rapid responses without being limited by chain degradation kinetics.

These experiments demonstrate that disulfide-linked polymers obtained by RAFT polymerisation can be used as doubly responsive polymeric carriers with potential application in drug delivery or biosensing fields.

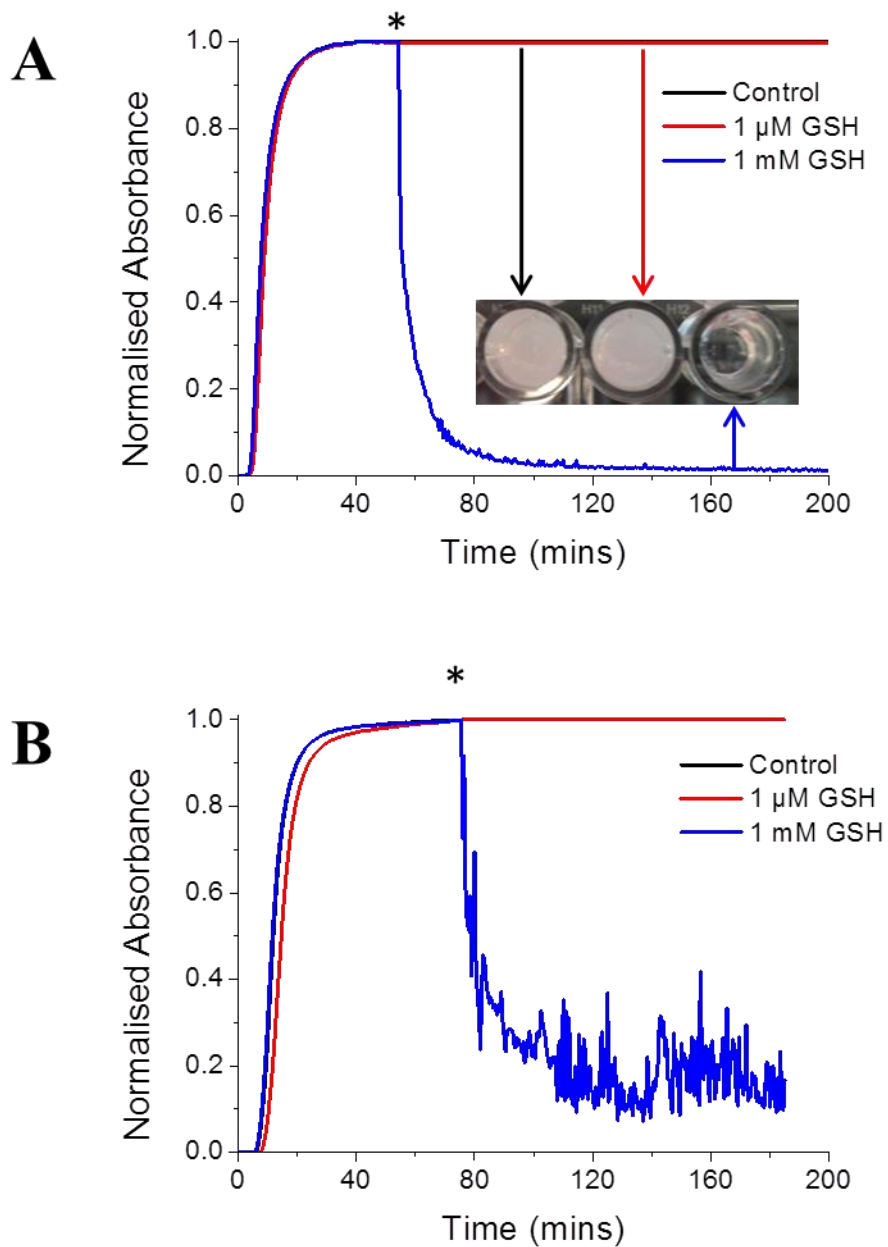


Figure 2.16 Isothermal turbidimetry data for (A) **ss-pNIPAM-2** and (B) **ss-pNIPAM-3** (polymer concentration = 5 mg.mL⁻¹). Temperature = 37 °C (A) and 34 °C (B), GSH added at time indicated by asterisk. Black = control (polymer and water); red = 1 μ M GSH; blue = 1 mM GSH. Inset (A) = photo at end of experiment (left = control; centre = 1 μ M GSH; right = 1 mM GSH).

2.4 Conclusions

This chapter demonstrates the polycondensation of pyridyl disulfide-terminated, RAFT derived polymers to obtain a library of disulfide-linked polymers. The use of trithiocarbonate RAFT agents widens the scope of this versatile method. Investigations into the polycondensation process indicated that macromonomer side-chain length limits the reactivity of the thiol-end groups and hence prevents the polymerisation of non-linear PEG analogues. Moreover methacrylates, on account of their pendant methyl group, were found to be incompatible. A range of acrylamides and acrylates were shown to be applicable to this methodology. Dual-responsive materials were created by introducing disulfides into the main chain of the thermo-responsive pNIPAM. The disulfide unit showed a strong selectivity for glutathione degradation at concentrations expected in an intracellular environment. This, coupled with the molecular-weight dependent cloud point behaviour of pNIPAM enabled a change in solubility to be triggered without the need for a change in applied temperature, an isothermal transition. This may be important in some biological situations where, for example, an LCST-type transition is desired whilst avoiding protein denaturation. Ultimately this method provides a valuable way of incorporating redox-responsive linkages into polymer structures *en route* to preparing increasingly complex materials with multiple responses.

2.5 Experimental

2.5.1 Materials

All chemicals were used as supplied unless stated. Methanol, hexane, ethyl acetate, dichloromethane, toluene, acetone, 40-60 °C petroleum ether, tetrahydrofuran, diethyl ether, glacial acetic acid (analytical reagent grade) and 1,4-dioxane (analytical reagent grade) were all purchased from Fisher Scientific at laboratory reagent grade unless otherwise stated. Deuterated chloroform (99.9 atom % D), aldrithiol-2 (98.0 %), 2-mercaptoethanol (≥ 99.0 %), 4-cyano-4-(phenylcarbonothioylthio)pentanoic acid (≥ 98.0 %), dodecane thiol (≥ 98.0 %), tribasic potassium phosphate (reagent grade, ≥ 98.0 %), 2-bromo-2-methylpropionic acid (98.0 %), 4-dimethylaminopyridine (≥ 99.0 %), *N,N'*-diisopropylcarbodiimide (99.0 %), *N*-isopropylacrylamide (97.0 %), 4,4'-azobis(4-cyanovaleric acid) (≥ 98.0 %), ethanolamine (≥ 99.0 %), tributylphosphine (97.0 %), triethylamine (≥ 99.0 %), tris(2-carboxyethyl)phosphine hydrochloride (≥ 98.0 %), glutathione (99.0 % reduced) and mesitylene (analytical standard) were all purchased from Sigma-Aldrich. Oligo(ethylene glycol, average $M_n = 300 \text{ g.mol}^{-1}$) methyl ether methacrylate, di(ethylene glycol) methyl ether methacrylate (95.0 %), oligo(ethylene glycol, average $M_n = 480 \text{ g.mol}^{-1}$) methyl ether acrylate, *tert*-butyl acrylate (98.0 %), methyl methacrylate (99.0 %) and *N,N*-dimethylacrylamide (99.0 %) were also purchased from Sigma-Aldrich but inhibitors were removed by passing through a column of basic alumina before polymerisation.

2.5.2 Analytical Methods

NMR spectroscopy (^1H , ^{13}C) was conducted on a Bruker DPX-300, Bruker DRX-500 or a Bruker AV III 600 spectrometer. Deuterated chloroform was used with all chemical shifts reported in ppm (δ) relative to that solvent.

High resolution mass spectra were recorded on a Bruker Electrospray Ultra-High Resolution tandem TOF mass spectrometer using electrospray ionization (ESI) in positive mode on samples prepared in methanol. Degraded sample mass spectral analysis was carried using a Bruker MaXis UHR-Q-TOF mass spectrometer using ESI in positive mode over a scan range of 500 – 7000 m/z. Samples were prepared in methanol, diluted 20-fold in 50:50 methanol: water and introduced by direct infusion at $90 \mu\text{L}\cdot\text{hr}^{-1}$. Source conditions were: end plate offset at -500 V; capillary at -4500 V; nebulizer gas (N_2) at 1.6 bar; dry gas (N_2) at $8 \text{ L}\cdot\text{min}^{-1}$; dry temperature at $180 \text{ }^\circ\text{C}$. Ion transfer conditions were: ion funnel RF at 400 Vpp; multiple RF at 400 Vpp; quadrupole low mass set at 455 m/z; collision energy at 5.0 eV; collision RF at 1200 Vpp; ion cooler RF at 250-600 Vpp; transfer time set at 121 μs ; pre-pulse storage time set at 15 μs . Calibration was completed with sodium formate (10 mM).

FTIR spectra were acquired using a Bruker Vector 22 FTIR spectrometer with a Golden Gate diamond attenuated total reflection cell. A total of 64 scans were collected on samples in their native (dry) state.

SEC analysis was performed on one of two systems:

(i) **Dimethylformamide:** Varian 390-LC MDS system equipped with a PL-AS RT/MT autosampler, a PL-gel 3 μm ($50 \times 7.5 \text{ mm}$) guard column, two PL-gel 5 μm ($300 \times 7.5 \text{ mm}$) mixed-D columns using DMF with 5 mM NH_4BF_4 at $50 \text{ }^\circ\text{C}$ as the eluent at a flow rate of $1.0 \text{ mL}\cdot\text{min}^{-1}$. The system was equipped with ultraviolet (UV)

(set at 280 nm) and differential refractive index (DRI) detectors. Narrow molecular weight PMMA standards ($200 - 1.0 \times 10^6 \text{ g.mol}^{-1}$) were used for calibration using a second order polynomial fit.

(ii) **Tetrahydrofuran:** Varian 390-LC MDS system equipped with a PL-AS RT/MT autosampler, a PL-gel 3 μm ($50 \times 7.5 \text{ mm}$) guard column, two PL-gel 5 μm ($300 \times 7.5 \text{ mm}$) mixed-D columns equipped with a differential refractive index and a Shimadzu SPD-M20A diode array detector, using THF (including 2 % TEA) as the eluent at a flow rate of 1.0 mL.min^{-1} . Narrow molecular weight PMMA standards ($200 - 1.0 \times 10^6 \text{ g.mol}^{-1}$) were used for calibration using a second order polynomial fit.

The cloud points were measured using an Optimelt MPA100 system (Stanford Research Systems). The recorded turbidimetry curve was normalised between values of 0 and 1. The cloud point was defined as the temperature corresponding to a normalised absorbance of 0.5. A polymer concentration of 5 mg.mL^{-1} and a constant heating rate of $1 \text{ }^\circ\text{C.min}^{-1}$ were used in all experiments.

UV-Vis measurements were undertaken on a Biotech Synergy HT and processed using the Gen5 software package.

2.5.3 Procedures

2.5.3.1 Synthesis of hydroxyethyl pyridyldisulfide

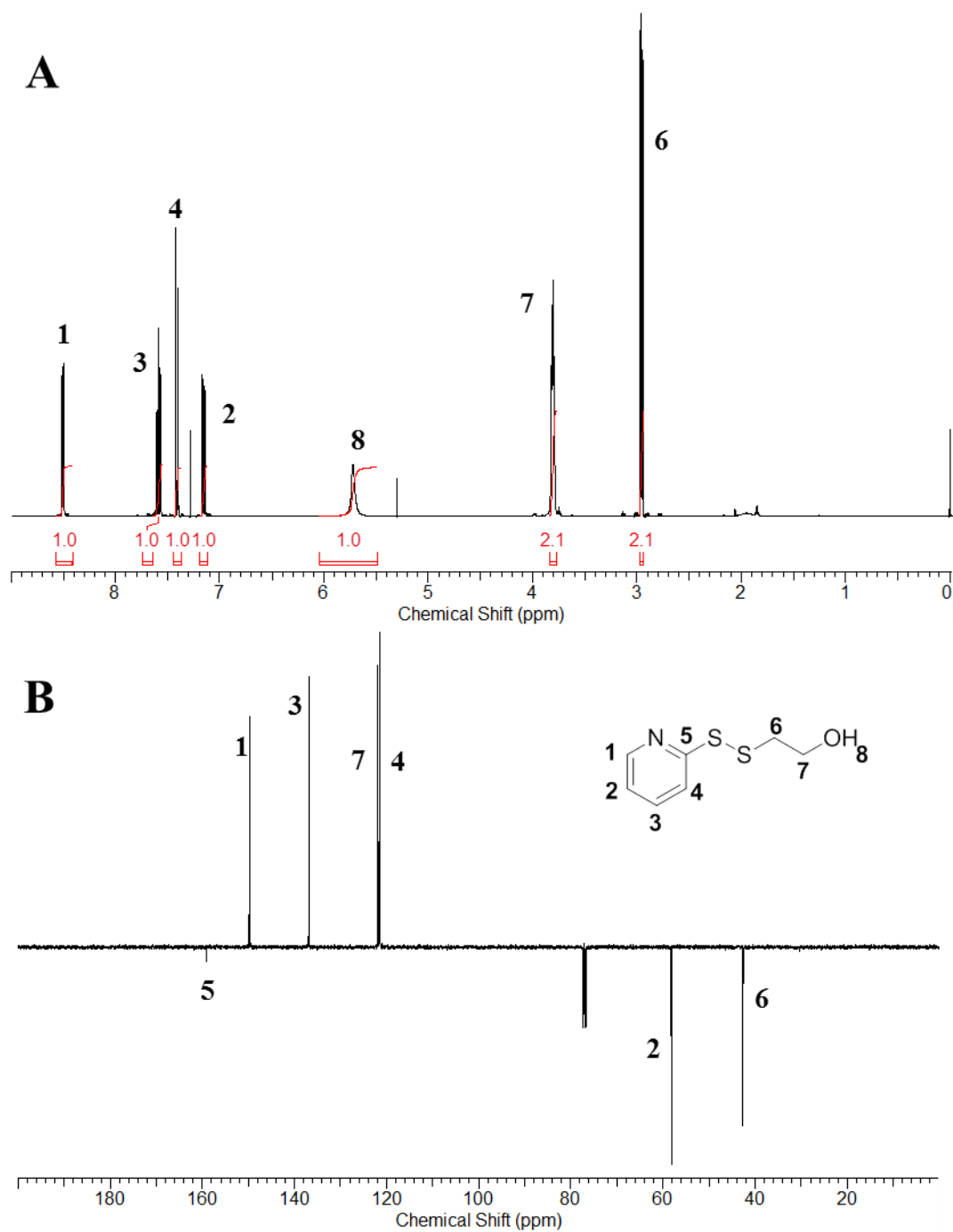
Aldrithiol-2 (10 g, 45.40 mmol) was dissolved in methanol (50 mL) and glacial acetic acid (1.50 mL) was then added. To this mixture, a solution of 2-mercaptoethanol (2.36 g, 2.12 mL, 30.23 mmol) in methanol (10 mL) was added dropwise over 45 mins with continuous stirring. After this time, the reaction mixture had turned bright yellow. The reaction mixture was left to stir overnight under ambient conditions. The solution was concentrated under vacuum to leave the crude product as a yellow oil. Purification by column chromatography (hexane: ethyl acetate, 85:15) yielded the title product as a pale yellow oil (3.40 g, 60 %).

¹H NMR (400.05 MHz, CDCl₃) δ_{ppm}: 8.50 (1H, d, $J_{1-2} = 5.04$ Hz, H¹); 7.59 (1H, td, $J_{3-2}, J_{3-4} = 8.04$ Hz, $J_{3-1} = 2.00$ Hz, H³); 7.41 (1H, d, $J_{4-3} = 8.04$ Hz, H⁴); 7.15 (1H, ddd, $J_{2-3} = 8.04$ Hz, $J_{2-1} = 5.04$ Hz, $J_{2-4} = 1.00$ Hz, H²); 5.72 (1H, s, br., H⁸); 3.81 (2H, t, $J_{7-6} = 5.28$ Hz, H⁷); 2.95 (2H, t, $J_{6-7} = 5.28$ Hz, H⁶).

¹³C NMR (100.58 MHz, CDCl₃) δ_{ppm}: 159.13 (C⁵); 149.85 (C¹); 136.87 (C³); 121.91 (C⁴); 121.52 (C²); 58.27 (C⁷); 42.68 (C⁶).

IR cm⁻¹: 3303 (br., O-H stretch); 3048 (aryl-H stretch); 2922 (alkyl C-H stretch).

MS (ESI +) m/z: 188.1 [M+H]⁺; 210.0 [M+Na]⁺



2.5.3.2 Synthesis of 2-(dodecylthiocarbonothioylthio)-2-methylpropanoic acid

Dodecane thiol (4.00 g, 4.73 mL, 19.76 mmol) was added dropwise to a stirred suspension of tribasic potassium phosphate (4.20 g, 19.76 mmol) in acetone (60 mL) over 25 mins. Carbon disulfide (4.10 g, 3.24 mL, 53.85 mmol) was added and the solution turned bright yellow. After stirring for ten mins 2-bromo-2-methylpropionic acid (3.00 g, 17.96 mmol) was added and a precipitation of KBr was noted. After stirring for 16 hrs, the solvent was removed under reduced pressure and the residue was extracted into dichloromethane (2 x 200 mL) from 1M HCl (200 mL). The organic extracts were washed with water (200 mL) and brine (200 mL) and further dried over magnesium sulfate. The solvent was removed under reduced pressure and the residue was purified by column chromatography on silica using an eluent comprising 75:24:1 40 – 60 °C petroleum ether: diethyl ether: acetic acid to yield a bright yellow solid (4.01 g, 61 %).

¹H NMR (500.133 MHz, CDCl₃) δ_{ppm}: 3.22 (2H, t, $J_{12-11} = 7.55$ Hz, H¹²); 1.66 (6H, s, H¹⁵); 1.60 (2H, p, $J_{11-10, 11-12} = 7.70$ Hz, H¹¹); 1.31 (2H, p, $J_{10-9, 10-11} = 7.70$ Hz, H¹⁰); 1.24-1.19 (16H, m, H²⁻⁹); 0.81 (3H, t, $J_{1-2} = 7.25$ Hz, H¹).

¹³C NMR (125.721 MHz, CDCl₃) δ_{ppm}: 220.92 (C¹³); 177.17 (C¹⁶); 55.46 (C¹⁴); 37.10 (C¹²); 31.93, 29.71, 29.64, 29.57, 29.46, 29.35, 29.12, 22.70 (C²⁻⁹); 28.97 (C¹⁰); 27.82 (C¹¹); 25.26 (C¹⁵); 14.13 (C¹).

IR cm⁻¹: 2955 (alkyl-H stretch); 1712 (C=O stretch); 1069 (S-(C=S)-S stretch).

HRMS (ESI +) m/z: 365.1632 [M+H]⁺; expected 365.1637 (C₁₇H₃₃O₂S₃).

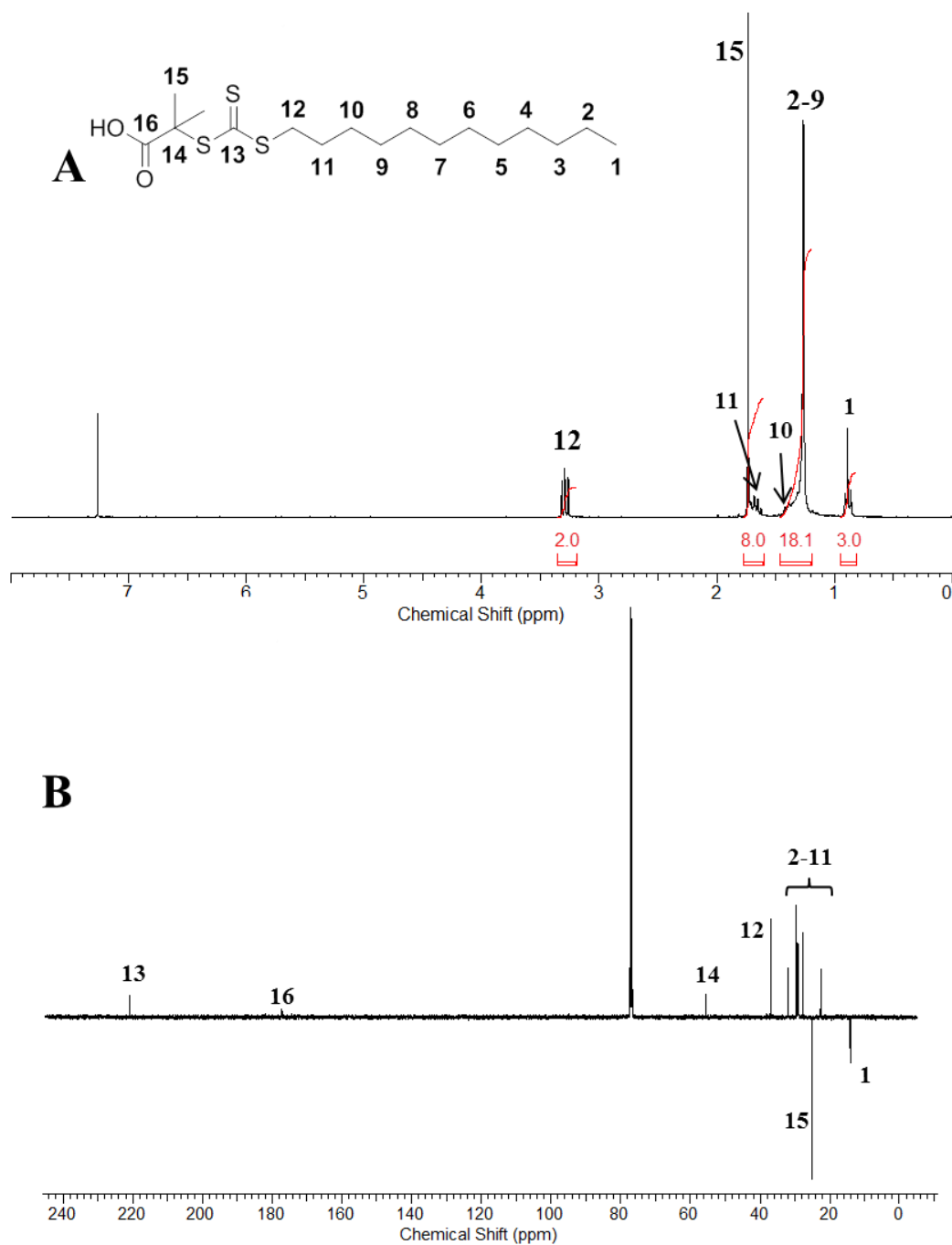


Figure 2.18 NMR spectroscopic characterisation of 2-(dodecylthiocarbonothioylthio)-2-methylpropanoic acid in CDCl_3 : (A) ^1H NMR and (B) ^{13}C NMR spectra.

2.5.3.3 Synthesis of 2-(pyridyldisulfanyl) ethyl 2-(dodecylthiocarbonothioylthio)-2-methylpropanoate

2-(pyridyldisulfanyl) ethyl 2-(dodecylthiocarbonothioylthio)-2-methylpropanoate was prepared using a method similar to that already reported.⁵⁴ Hydroxyethyl pyridyl disulfide (1.61 g, 8.57 mmol), 2-(dodecylthiocarbonothioylthio)-2-methylpropanoic acid (2.50 g, 6.86 mmol) and 4-dimethylaminopyridine (0.25 g, 2.06 mmol) were dissolved in dichloromethane (50 mL). *N,N'*-Diisopropylcarbodiimide (1.08 g, 1.33 mL, 8.57 mmol) was added to the solution under ice and dropwise over a period of 20 mins. The mixture was left to warm to room temperature and stirred for 24 hrs. The observed precipitate was removed by gravity filtration and the solvent concentrated *in vacuo*. The resulting yellow residue was purified by column chromatography using silica gel as the stationary phase and 49:1 hexane: ethyl acetate mixture as eluent to yield a yellow/orange oil (2.85 g, 78 % yield).

¹H NMR (600.132 MHz, CDCl₃) δ_{ppm} : 8.47 (1H, d, $J_{23-22} = 4.14$ Hz, H²³); 7.73 (1H, d, $J_{20-21} = 7.86$ Hz, H²⁰); 7.66 (1H, t, $J_{21-20, 21-22} = 7.71$ Hz, H²¹); 7.10 (1H, t, $J_{22-21, 22-23} = 6.24$ Hz, H²²); 4.36 (2H, t, $J_{17-18} = 6.36$ Hz, H¹⁷); 3.27 (2H, t, $J_{12-11} = 7.56$ Hz, H¹²); 3.03 (2H, t, $J_{18-17} = 6.36$ Hz, H¹⁸); 1.70 (6H, s, H¹⁵); 1.65 (2H, p, $J_{11-12, 11-10} = 7.50$ Hz, H¹¹); 1.37 (2H, p, $J_{10-11, 10-9} = 7.50$ Hz, H¹⁰); 1.23-1.31 (16 H, m, H²⁻⁹); 0.88 (3H, t, $J_{1-2} = 6.96$ Hz, H¹).

¹³C NMR (150.864 MHz, CDCl₃) δ_{ppm} : 221.48 (C¹³); 177.80 (C¹⁶); 159.90 (C¹⁹); 149.68 (C²³); 137.09 (C²¹); 120.77 (C²²); 119.76 (C²⁰); 63.36 (C¹⁷); 55.79 (C¹⁴); 37.21 (C¹⁸); 37.00 (C¹²); 31.91, 29.71, 29.62, 29.55, 29.44, 29.34, 29.10, 22.69 (C²⁻⁹); 28.93 (C¹⁰); 27.86 (C¹¹); 25.34 (C¹⁵); 14.13 (C¹).

IR cm^{-1} : 3049 (aryl-H stretch); 2923 (alkyl-H stretch); 1735 (C=O stretch); 1063 (S-(C=S)-S stretch).

HRMS (ESI +) m/z : 534.1661[M+H]⁺; expected 534.1657 (C₂₄H₄₀NO₂S₅).

2.5.3.4 Synthesis of 2-(pyridyldisulfanyl) ethyl 4-cyano-4-(phenylcarbonothioylthio)pentanoate

Hydroxyethyl pyridyl disulfide (0.66 g, 3.52 mmol), 2-(dodecylthiocarbonothioylthio)-2-methylpropanoic acid (0.48 g, 1.32 mmol) were dissolved in dichloromethane (20 mL). *N,N'*-Diisopropylcarbodiimide (0.56 g, 0.69 mL, 4.42 mmol) was added to the solution under ice and dropwise over a period of 10 mins; a precipitate was observed. The mixture was left to warm to room temperature and stirred overnight. Precipitate was removed by gravity filtration and solvent removed *in vacuo*. The pink/red residue was purified by column chromatography using silica gel as the stationary phase and 49:1 dichloromethane: diethyl ether mixture as eluent to yield a pink oil (0.10 g, 13 % yield).

¹H NMR (600.132 MHz, CDCl₃) δ_{ppm} : 8.48 (1H, d, $J_{18-17} = 4.86$ Hz, H¹⁸); 7.91 (2H, d, $J_{3-2} = 8.28$ Hz, H³); 7.66 (2H, m, H^{15,16}); 7.57 (1H, t, $J_{1-2} = 7.50$ Hz, H¹); 7.40 (2H, t, $J_{2-1} = 7.50$ Hz, H²); 7.11 (1H, m, H¹⁷); 4.39 (2H, t, $J_{12-13} = 6.36$ Hz, H¹²); 3.06 (2H, t, $J_{13-12} = 6.36$ Hz, H¹³); 2.69-2.65 (2H, m, H¹⁰); 2.63 – 2.58, 2.45-2.40 (2H, m, H⁹); 1.94 (3H, s, H⁸).

¹³C NMR (150.864 MHz, CDCl₃) δ_{ppm} : 222.23 (C⁵); 171.23 (C¹¹); 159.49 (C¹⁴); 149.80 (C¹⁸); 144.5 (C⁴); 137.1 (C¹⁶); 133.1 (C¹); 128.6 (C²); 126.7 (C³); 121.0 (C¹⁷); 120.0 (C¹⁵); 118.5 (C⁷); 62.8 (C¹²); 45.7 (C⁶); 37.2 (C¹³); 33.3 (C⁹); 29.7 (C¹⁰); 24.2 (C⁸).

IR cm^{-1} : 3049 (aryl-H stretch); 2975 (alkyl-H stretch); 2233 ($\text{C}\equiv\text{N}$ stretch); 1736 ($\text{C}=\text{O}$ stretch); 1179 ($\text{C}=\text{S}$) stretch.

HRMS (ESI +) m/z : 471.0302 $[\text{M}+\text{Na}]^+$; expected 471.0300 ($\text{C}_{20}\text{H}_{20}\text{N}_2\text{O}_2\text{S}_4\text{Na}$).

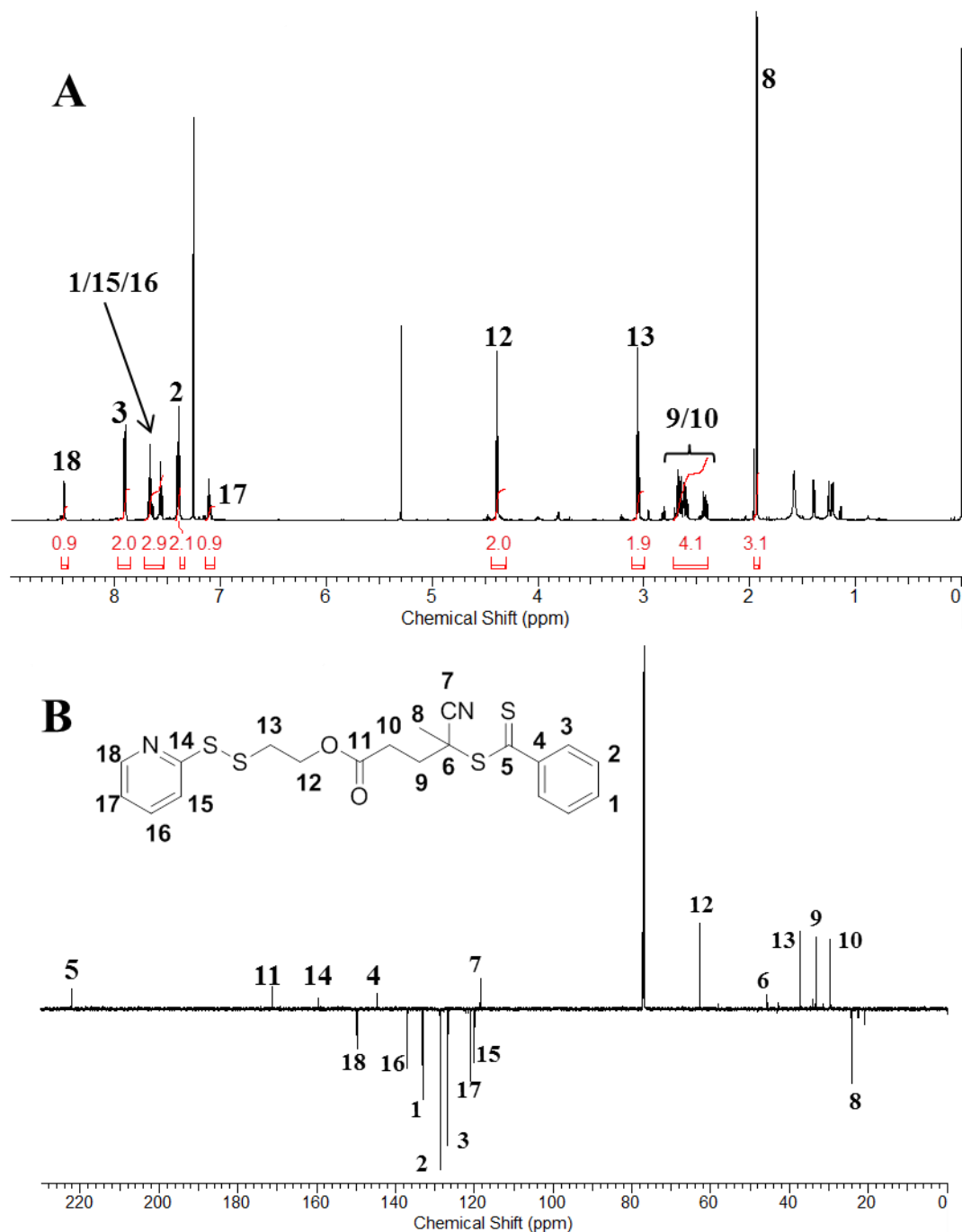


Figure 2.19 NMR spectroscopic characterisation of 2-(pyridyldisulfanyl) ethyl 4-cyano-4-(phenylcarbonothioylthio)pentanoate in CDCl_3 : (A) ^1H and (B) ^{13}C spectra.

2.5.3.5 Polymerisation of *N*-isopropylacrylamide

In a typical procedure *N*-isopropylacrylamide (0.25 g, 2.21 mmol), 2-(pyridyldisulfanyl) ethyl 2-(dodecylthiocarbonothioylthio)-2-methylpropanoate (59.0 mg, 110.69 μmol) and 4,4'-azobis(4-cyanovaleric acid) (6.19 mg, 22.10 μmol) were dissolved in methanol: toluene (1:1) (4 mL) in a glass vial containing a stir bar. Mesitylene (100 μL) was added as an internal reference and the mixture stirred (5 mins). An aliquot of this starting mixture was removed for ^1H NMR spectroscopic analysis. The vial was fitted with a rubber septum and degassed by bubbling with nitrogen gas (30 mins). The vial was then placed in an oil bath thermostated at 70 $^\circ\text{C}$. After 4 hrs the reaction mixture was opened to air and quenched in liquid nitrogen. An aliquot was removed and conversion determined by ^1H NMR spectroscopy. The product was purified three times by precipitation from toluene into diethyl ether, isolated by centrifugation and dried under vacuum overnight to give a yellow solid. The overall monomer conversion was determined from the ^1H NMR spectrum by measuring the decrease in intensity of the vinyl peaks associated with the monomer relative to mesitylene. Conversion (NMR): 91.7 %; M_n (theoretical): 2100 $\text{g}\cdot\text{mol}^{-1}$; M_n (SEC) 2000 $\text{g}\cdot\text{mol}^{-1}$; M_w/M_n (SEC): 1.18.

2.5.3.6 Polymerisation of oligo(ethylene glycol) methyl ether methacrylate

Oligo(ethylene glycol, average $M_n = 300 \text{ g}\cdot\text{mol}^{-1}$) methyl ether methacrylate (0.92 g, 2.3 mmol), 2-(pyridyldisulfanyl) ethyl 2-(dodecylthiocarbonothioylthio)-2-methylpropanoate (81.95 mg, 153.75 μmol) and 4,4'-azobis(4-cyanovaleric acid) (8.60 mg, 30.68 μmol) were dissolved in dioxane (3 mL) in a glass vial containing a stir bar. Mesitylene (100 μL) was added as an internal reference and the mixture stirred (5 mins). An aliquot of this starting mixture was removed for ^1H NMR

spectroscopic analysis. The vial was fitted with a rubber septum and degassed by bubbling with nitrogen gas (30 mins). The vial was then placed in an oil bath thermostated at 70 °C. After 4 hrs the reaction mixture was opened to air and quenched in liquid nitrogen. An aliquot was removed and conversion determined by ^1H NMR spectroscopy. The product was purified three times by precipitation from dioxane into diethyl ether, isolated by centrifugation and dried under vacuum overnight to give a waxy, yellow solid. Conversion (NMR): 89.9 %; M_n (theoretical): 5400 $\text{g}\cdot\text{mol}^{-1}$; M_n (SEC) 18300 $\text{g}\cdot\text{mol}^{-1}$; M_w/M_n (SEC): 1.12.

2.5.3.7 Polymerisation of oligo(ethylene glycol) methyl ether acrylate

Oligo(ethylene glycol, average $M_n = 480 \text{ g}\cdot\text{mol}^{-1}$) methyl ether methacrylate (0.64 g, 1.13 mmol), 2-(pyridyldisulfanyl) ethyl 2-(dodecylthiocarbonothioylthio)-2-methylpropanoate (27.82 mg, 52.11 μmol) and 4,4'-azobis(4-cyanovaleric acid) (2.92 mg, 10.42 μmol) were dissolved in dioxane (3 mL) in a glass vial containing a stir bar. Mesitylene (100 μL) was added as an internal reference and the mixture stirred (5 mins). An aliquot of this starting mixture was removed for ^1H NMR spectroscopic analysis. The vial was fitted with a rubber septum and degassed by bubbling with nitrogen gas (30 mins). The vial was then placed in an oil bath thermostated at 70 °C. After 4 hrs the reaction mixture was opened to air and quenched in liquid nitrogen. An aliquot was removed and conversion determined by ^1H NMR spectroscopy. The product was purified three times by precipitation from dioxane into diethyl ether, isolated by centrifugation and dried under vacuum overnight to give a waxy, yellow solid. Conversion (NMR): 85.1 %; M_n (theoretical): 10600 $\text{g}\cdot\text{mol}^{-1}$; M_n (SEC) 9600 $\text{g}\cdot\text{mol}^{-1}$; M_w/M_n (SEC): 1.10.

2.5.3.8 Polymerisation of diethyleneglycol methyl ether methacrylate

Diethyleneglycol methyl ether methacrylate (1.04 g, 5.49 mmol), 2-(pyridyldisulfanyl) ethyl 2-(dodecylthiocarbonothioylthio)-2-methylpropanoate (0.15 g, 281.43 μmol) and 4,4'-azobis(4-cyanovaleric acid) (15.40 mg, 54.95 μmol) were dissolved in dioxane (4 mL) in a glass vial containing a stir bar. Mesitylene (200 μL) was added as an internal reference and the mixture stirred (5 mins). An aliquot of this starting mixture was removed for ^1H NMR spectroscopic analysis. The vial was fitted with a rubber septum and degassed by bubbling with nitrogen gas (30 mins). The vial was then placed in an oil bath thermostated at 70 °C. After 3 hrs the reaction mixture was opened to air and quenched in liquid nitrogen. An aliquot was removed and conversion determined by ^1H NMR spectroscopy. The product was purified three times by precipitation from dioxane into diethyl ether, isolated by centrifugation and dried under vacuum overnight to give a waxy, yellow solid. Conversion (NMR): 80.4 %; M_n (theoretical): 3000 $\text{g}\cdot\text{mol}^{-1}$; M_n (SEC) 23000 $\text{g}\cdot\text{mol}^{-1}$; M_w/M_n (SEC): 1.24.

2.5.3.9 Polymerisation of methyl methacrylate

Methyl methacrylate (0.52 g, 5.19 mmol), 2-(pyridyldisulfanyl) ethyl 2-(dodecylthiocarbonothioylthio)-2-methylpropanoate (94.70 mg, 177.67 μmol) and 4,4'-azobis(4-cyanovaleric acid) (9.70 mg, 34.61 μmol) were dissolved in dioxane (3 mL) in a glass vial containing a stir bar. Mesitylene (200 μL) was added as an internal reference and the mixture stirred (5 mins). An aliquot of this starting mixture was removed for ^1H NMR spectroscopic analysis. The vial was fitted with a rubber septum and degassed by bubbling with nitrogen gas (30 mins). The vial was then placed in an oil bath thermostated at 70 °C. After 3.5 hrs the reaction mixture was

opened to air and quenched in liquid nitrogen. An aliquot was removed and conversion determined by ^1H NMR spectroscopy. The product was purified three times by precipitation from dioxane into diethyl ether, isolated by centrifugation and dried under vacuum overnight to give a pale yellow solid. Conversion (NMR): 58.2 %; M_n (theoretical): $1700 \text{ g}\cdot\text{mol}^{-1}$; M_n (SEC) $6400 \text{ g}\cdot\text{mol}^{-1}$; M_w/M_n (SEC): 1.38.

2.5.3.10 Polymerisation of *tert*-butyl acrylate

Tert-butyl acrylate (0.67 g, 5.23 mmol), 2-(pyridyldisulfanyl) ethyl 2-(dodecylthiocarbonothioylthio)-2-methylpropanoate (139.54 mg, 261.37 μmol) and 4,4'-azobis(4-cyanovaleric acid) (14.65 mg, 52.27 μmol) were dissolved in dioxane (5 mL) in a glass vial containing a stir bar. Mesitylene (200 μL) was added as an internal reference and the mixture stirred (5 mins). An aliquot of this starting mixture was removed for ^1H NMR spectroscopic analysis. The vial was fitted with a rubber septum and degassed by bubbling with nitrogen gas (30 mins). The vial was then placed in an oil bath thermostated at $70 \text{ }^\circ\text{C}$. After 3 hrs the reaction mixture was opened to air and quenched in liquid nitrogen. An aliquot was removed and conversion determined by ^1H NMR spectroscopy. The product was purified by precipitation once from dioxane into water and three times from THF into a 30:70 methanol: water mixture. The solid was isolated by centrifugation and dried under vacuum overnight to give a waxy, yellow solid. Conversion (NMR): 91.0 %; M_n (theoretical): $2300 \text{ g}\cdot\text{mol}^{-1}$; M_n (SEC) $2500 \text{ g}\cdot\text{mol}^{-1}$; M_w/M_n (SEC): 1.16.

2.5.3.11 Polymerisation of *N,N*-dimethylacrylamide with 2-(pyridyldisulfanyl) ethyl 2-(dodecylthiocarbonothioylthio)-2-methylpropanoate

N,N-dimethylacrylamide (0.55 g, 5.55 mmol), 2-(pyridyldisulfanyl) ethyl 2-(dodecylthiocarbonothioylthio)-2-methylpropanoate (87.12 mg, 163.18 μmol) and

4,4'-azobis(4-cyanovaleric acid) (9.15 mg, 32.64 μmol) were dissolved in methanol: toluene (1:1) (4 mL) in a glass vial containing a stir bar. Mesitylene (230 μL) was added as an internal reference and the mixture stirred (5 mins). An aliquot of this starting mixture was removed for ^1H NMR spectroscopic analysis. The vial was fitted with a rubber septum and degassed by bubbling with nitrogen gas (30 mins). The vial was then placed in an oil bath thermostated at 70 $^\circ\text{C}$. After 1.5 hrs the reaction mixture was opened to air and quenched in liquid nitrogen. An aliquot was removed and conversion determined by ^1H NMR spectroscopy. The product was purified three times by precipitation from toluene into diethyl ether, isolated by centrifugation and dried under vacuum overnight to give a yellow solid. Conversion (NMR): 93.1 %; M_n (theoretical): 3000 $\text{g}\cdot\text{mol}^{-1}$; M_n (SEC) 2800 $\text{g}\cdot\text{mol}^{-1}$; M_w/M_n (SEC): 1.10.

2.5.3.12 Polymerisation of *N,N*-dimethylacrylamide with 2-(pyridyldisulfanyl) ethyl 4-cyano-4-(phenylcarbonothioylthio)pentanoate

N,N-dimethylacrylamide (0.36 g, 3.63 mmol), 2-(pyridyldisulfanyl) ethyl 4-cyano-4-(phenylcarbonothioylthio)pentanoate (16.27 mg, 36.32 μmol) and 4,4'-azobis(4-cyanovaleric acid) (2.04 mg, 7.26 μmol) were dissolved in methanol: toluene (1:1) (3.3 mL) in a glass vial containing a stir bar. Mesitylene (160 μL) was added as an internal reference and the mixture stirred (5 mins). An aliquot of this starting mixture was removed for ^1H NMR spectroscopic analysis. The vial was fitted with a rubber septum and degassed by bubbling with nitrogen gas (30 mins). The vial was then placed in an oil bath thermostated at 70 $^\circ\text{C}$. After 8 hrs the reaction mixture was opened to air and quenched in liquid nitrogen. An aliquot was removed and conversion determined by ^1H NMR spectroscopy. The product was purified three times by precipitation from toluene into diethyl ether, isolated by centrifugation and

dried under vacuum overnight to give a pink solid. Conversion (NMR): 56.7 %; M_n (theoretical): 5700 g.mol⁻¹; M_n (SEC) 3700 g.mol⁻¹; M_w/M_n (SEC): 1.18.

2.5.3.13 General polycondensation procedure

Polymer with pyridyl disulfide end-group (170 mg) was dissolved in tetrahydrofuran (2 mL) in a Schlenk tube equipped with a stir bar and rubber septum. This solution was degassed by a minimum of three freeze-pump-thaw cycles. A separate solution containing ethanolamine (5 equivalents) and triethylamine (2 equivalents) was degassed by a minimum of three freeze-pump-thaw cycles. The amine solution was added to the polymer solution by a syringe purged with dry nitrogen, and the solution left to stir at room temperature for five days. After this time, the mixture had turned bright yellow. The polymer was purified by multiple precipitations from tetrahydrofuran into diethyl ether and the product isolated by centrifugation. After drying overnight under vacuum, a white solid was achieved. This product was then analysed by SEC. The same sample was also treated with tributyl phosphine (2 drops) and re-analysed by SEC to confirm disulfide-bond presence.

2.5.4 Assay Conditions

2.5.4.1 General procedure for turbidimetry-monitored, glutathione-mediated degradation of disulfide-containing polymers

A 5 mg.mL⁻¹ stock solution of pNIPAM (theoretical $M_n = 4000$ g.mol⁻¹) in water was prepared. 3 x 180 μ L aliquots of this stock were transferred into three individual wells of a 96-well plate. The plate was left to incubate at 37 °C in the plate reader until all samples had precipitated out of solution. Once this had been observed, the plate was removed and the well volume made to 200 μ L with distilled water or glutathione solution to give final glutathione concentrations of 0, 1 μ M and 1 mM.

The plate was re-incubated at 37 °C and the absorbance at 650 nm recorded for a further 2.5 hrs.

2.5.4.2 General procedure for SEC evaluation of glutathione-mediated degradation

Polycondensed pNIPAM (theoretical $M_n = 40000 \text{ g}\cdot\text{mol}^{-1}$, 16 mg) was dissolved in distilled water (3.96 mL) in a glass vial (vial A). 1.98 mL of this stock solution was transferred to a separate vial (vial B). To vial A, 20 μL of a 100 μM glutathione solution was added, and to vial B 20 μL of a 100 mM glutathione solution to give final concentrations of 1 μM and 1 mM respectively. Both vials were left to stir at ambient conditions with a 4 mg aliquot removed after 24 and 72 hrs. Aliquots were freeze-dried and subsequently analysed by SEC (DMF).

2.6 References

- 1 Stuart, M. A. C.; Huck, W. T. S.; Genzer, J.; Muller, M.; Ober, C.; Stamm, M.; Sukhorukov, G. B.; Szleifer, I.; Tsukruk, V. V.; Urban, M.; Winnik, F.; Zauscher, S.; Luzinov, I.; Minko, S. Emerging applications of stimuli-responsive polymer materials. *Nat. Mater.* **2010**, *9*, 101-113.
- 2 Bawa, P. P., V.; Choonara, Y. E.; du Toit, L. C. Stimuli-Responsive Polymers and their Applications in Drug Delivery. *Biomed. Mater.* **2009**, *4*, 022001.
- 3 Shim, M. S.; Kwon, Y. J. Stimuli-responsive polymers and nanomaterials for gene delivery and imaging applications. *Adv. Drug Deliv. Rev.* **2012**, *64*, 1046-1059.
- 4 Chan, G.; Mooney, D. J. New materials for tissue engineering: towards greater control over the biological response. *Trends Biotechnol.* **2008**, *26*, 382-392.
- 5 Akimoto, J.; Nakayama, M.; Sakai, K.; Okano, T. Thermally Controlled Intracellular Uptake System of Polymeric Micelles Possessing Poly(N-isopropylacrylamide)-Based Outer Coronas. *Mol. Pharm.* **2010**, *7*, 926-935.
- 6 Saaka, Y.; Deller, R. C.; Rodger, A.; Gibson, M. I. Exploiting Thermoresponsive Polymers to Modulate Lipophilicity: Interactions With Model Membranes. *Macromol. Rapid Commun.* **2012**, *33*, 779-784.
- 7 Chilkoti, A.; Dreher, M. R.; Meyer, D. E.; Raucher, D. Targeted drug delivery by thermally responsive polymers. *Adv. Drug Deliv. Rev.* **2002**, *54*, 613-630.
- 8 Lutz, J.-F. Polymerization of oligo(ethylene glycol) (meth)acrylates: Toward new generations of smart biocompatible materials. *J. Polym. Sci. A: Polym. Chem.* **2008**, *46*, 3459-3470.
- 9 Weber, C.; Hoogenboom, R.; Schubert, U. S. Temperature responsive biocompatible polymers based on poly(ethylene oxide) and poly(2-oxazoline)s. *Prog. Polym. Sci.* **2012**, *37*, 686-714.
- 10 Schild, H. G. Poly(N-isopropylacrylamide): experiment, theory and application. *Prog. Polym. Sci.* **1992**, *17*, 163-249.
- 11 Jeong, N. S.; Redhead, M.; Bosquillon, C.; Alexander, C.; Kelland, M.; O'Reilly, R. K. The Missing Lactam-Thermoresponsive and Biocompatible

- Poly(N-vinylpiperidone) Polymers by Xanthate-Mediated RAFT Polymerization. *Macromolecules* **2011**, *44*, 886-893.
- 12 Heath, F.; Saeed, A. O.; Pennadam, S. S.; Thurecht, K. J.; Alexander, C. 'Isothermal' phase transitions and supramolecular architecture changes in thermoresponsive polymers via acid-labile side-chains. *Polym. Chem.* **2010**, *1*, 1252-1262.
- 13 Magnusson, J. P.; Khan, A.; Pasparakis, G.; Saeed, A. O.; Wang, W.; Alexander, C. Ion-Sensitive "Isothermal" Responsive Polymers Prepared in Water. *J. Am. Chem. Soc.* **2008**, *130*, 10852-10853.
- 14 Steinhauer, W.; Hoogenboom, R.; Keul, H.; Moeller, M. Copolymerization of 2-Hydroxyethyl Acrylate and 2-Methoxyethyl Acrylate via RAFT: Kinetics and Thermoresponsive Properties. *Macromolecules* **2010**, *43*, 7041-7047.
- 15 Shepherd, J.; Sarker, P.; Swindells, K.; Douglas, I.; MacNeil, S.; Swanson, L.; Rimmer, S. Binding Bacteria to Highly Branched Poly(N-isopropyl acrylamide) Modified with Vancomycin Induces the Coil-to-Globule Transition. *J. Am. Chem. Soc.* **2010**, *132*, 1736-1737.
- 16 Jochum, F. D.; zur Borg, L.; Roth, P. J.; Theato, P. Thermo- and Light-Responsive Polymers Containing Photoswitchable Azobenzene End Groups. *Macromolecules* **2009**, *42*, 7854-7862.
- 17 Jochum, F. D.; Theato, P. Temperature- and Light-Responsive Polyacrylamides Prepared by a Double Polymer Analogous Reaction of Activated Ester Polymers. *Macromolecules* **2009**, *42*, 5941-5945.
- 18 Buller, J.; Laschewsky, A.; Lutz, J.-F.; Wischerhoff, E. Tuning the lower critical solution temperature of thermoresponsive polymers by biospecific recognition. *Polym. Chem.* **2011**, *2*, 1486-1489.
- 19 Guo, Z.; Feng, Y.; Wang, Y.; Wang, J.; Wu, Y.; Zhang, Y. A novel smart polymer responsive to CO₂. *Chem. Commun.* **2011**, *47*, 9348-9350.
- 20 Summers, M. J.; Phillips, D. J.; Gibson, M. I. "Isothermal" LCST transitions triggered by bioreduction of single polymer end-groups. *Chem. Commun.* **2013**, *49*, 4223-4225.
- 21 Fox, M. E.; Szoka, F. C.; Fréchet, J. M. J. Soluble Polymer Carriers for the Treatment of Cancer: The Importance of Molecular Architecture. *Acc. Chem. Res.* **2009**, *42*, 1141-1151.

- 22 Han, S.-o.; Mahato, R. I.; Sung, Y. K.; Kim, S. W. Development of Biomaterials for Gene Therapy. *Mol. Ther.* **2000**, *2*, 302-317.
- 23 Ulery, B. D.; Nair, L. S.; Laurencin, C. T. Biomedical applications of biodegradable polymers. *J. Polym. Sci. B: Polym. Phys.* **2011**, *49*, 832-864.
- 24 Okada, M. Chemical syntheses of biodegradable polymers. *Prog. Polym. Sci.* **2002**, *27*, 87-133.
- 25 Schafer, F. Q.; Buettner, G. R. Redox environment of the cell as viewed through the redox state of the glutathione disulfide/glutathione couple. *Free Radic. Biol. Med.* **2001**, *30*, 1191-1212.
- 26 Albertsson, A. C.; Karlsson, S. Degradable polymers for the future. *Acta Polym.* **1995**, *46*, 114-123.
- 27 Pounder, R. J.; Dove, A. P. Towards poly(ester) nanoparticles: recent advances in the synthesis of functional poly(ester)s by ring-opening polymerization. *Polym. Chem.* **2010**, *1*, 260-271.
- 28 Gibson, M. I.; Cameron, N. R. Experimentally facile controlled polymerization of N-carboxyanhydrides (NCAs), including O-benzyl-L-threonine NCA. *J. Polym. Sci. A: Polym. Chem.* **2009**, *47*, 2882-2891.
- 29 Kim, T.-i.; Kim, S. W. Bioreducible polymers for gene delivery. *React. Funct. Polym.* **2011**, *71*, 344-349.
- 30 Moad, G.; Rizzardo, E.; Thang, S. H. Toward Living Radical Polymerization. *Acc. Chem. Res.* **2008**, *41*, 1133-1142.
- 31 Phillips, D. J.; Gibson, M. I. Degradable thermoresponsive polymers which display redox-responsive LCST Behaviour. *Chem. Commun.* **2012**, *48*, 1054-1056.
- 32 Zhang, Q.; Noh, S. M.; Nam, J. H.; Jung, H. W.; Park, J. M.; Oh, J. K. Dual Temperature and Thiol-Responsive POEOMA-Multisegmented Polydisulfides: Synthesis and Thermoresponsive Properties. *Macromol. Rapid Commun.* **2012**, *33*, 1528-1534.
- 33 Anderson, M. E. Glutathione: an overview of biosynthesis and modulation. *Chem. Biol. Interact.* **1998**, *111-112*, 1-14.
- 34 Jones, D. P.; Carlson, J. L.; Samiec, P. S.; Sternberg Jr, P.; Mody Jr, V. C.; Reed, R. L.; Brown, L. A. S. Glutathione measurement in human plasma: Evaluation of sample collection, storage and derivatization conditions for

- analysis of dansyl derivatives by HPLC. *Clin. Chim. Acta* **1998**, 275, 175-184.
- 35 Ou, M.; Xu, R.; Kim, S. H.; Bull, D. A.; Kim, S. W. A family of bio-reducible poly(disulfide amine)s for gene delivery. *Biomaterials* **2009**, 30, 5804-5814.
- 36 Oupický, D.; Parker, A. L.; Seymour, L. W. Laterally Stabilized Complexes of DNA with Linear Reducible Polycations: Strategy for Triggered Intracellular Activation of DNA Delivery Vectors. *J. Am. Chem. Soc.* **2001**, 124, 8-9.
- 37 Vader, P.; van der Aa, L. J.; Engbersen, J. F. J.; Storm, G.; Schiffelers, R. M. Physicochemical and Biological Evaluation of siRNA Polyplexes Based on PEGylated Poly(amido amine)s. *Pharm. Res.* **2012**, 29, 352-361.
- 38 Cho, H. Y.; Srinivasan, A.; Hong, J.; Hsu, E.; Liu, S.; Shrivats, A.; Kwak, D.; Bohaty, A. K.; Paik, H.-j.; Hollinger, J. O.; Matyjaszewski, K. Synthesis of Biocompatible PEG-Based Star Polymers with Cationic and Degradable Core for siRNA Delivery. *Biomacromolecules* **2011**, 12, 3478-3486.
- 39 Cai, X.; Dong, C.; Dong, H.; Wang, G.; Pauletti, G. M.; Pan, X.; Wen, H.; Mehl, I.; Li, Y.; Shi, D. Effective Gene Delivery Using Stimulus-Responsive Cationic Polymer Designed with Redox-Sensitive Disulfide and Acid-Labile Imine Linkers. *Biomacromolecules* **2012**, 13, 1024-1034.
- 40 Li, S.; Wang, Y.; Wang, S.; Zhang, J.; Wu, S.-F.; Wang, B.-L.; Zhu, W.; Yu, X.-Q. Biodegradable cyclen-based linear and cross-linked polymers as non-viral gene vectors. *Bioorg. Med. Chem.* **2012**, 20, 1380-1387.
- 41 Cheng, R.; Feng, F.; Meng, F.; Deng, C.; Feijen, J.; Zhong, Z. Glutathione-responsive nano-vehicles as a promising platform for targeted intracellular drug and gene delivery. *J. Control. Rel.* **2011**, 152, 2-12.
- 42 Ryu, J.-H.; Roy, R.; Ventura, J.; Thayumanavan, S. Redox-Sensitive Disassembly of Amphiphilic Copolymer Based Micelles. *Langmuir* **2010**, 26, 7086-7092.
- 43 Ren, T.-B.; Feng, Y.; Zhang, Z.-H.; Li, L.; Li, Y.-Y. Shell-sheddable micelles based on star-shaped poly(ϵ -caprolactone)-SS-poly(ethyl glycol) copolymer for intracellular drug release. *Soft Matter* **2011**, 7, 2329-2331.
- 44 Wang, Y.-C.; Li, Y.; Sun, T.-M.; Xiong, M.-H.; Wu, J.; Yang, Y.-Y.; Wang, J. Core-Shell-Corona Micelle Stabilized by Reversible Cross-Linkage for

- Intracellular Drug Delivery. *Macromol. Rapid Commun.* **2010**, *31*, 1201-1206.
- 45 Koo, A. N.; Lee, H. J.; Kim, S. E.; Chang, J. H.; Park, C.; Kim, C.; Park, J. H.; Lee, S. C. Disulfide-cross-linked PEG-poly(amino acid)s copolymer micelles for glutathione-mediated intracellular drug delivery. *Chem. Commun.* **2008**, 6570-6572.
- 46 Li, Y.-L.; Zhu, L.; Liu, Z.; Cheng, R.; Meng, F.; Cui, J.-H.; Ji, S.-J.; Zhong, Z. Reversibly Stabilized Multifunctional Dextran Nanoparticles Efficiently Deliver Doxorubicin into the Nuclei of Cancer Cells. *Angew. Chem. Int. Ed.* **2009**, *48*, 9914-9918.
- 47 Jiang, X.; Li, L.; Liu, J.; Hennink, W. E.; Zhuo, R. Facile Fabrication of Thermo-Responsive and Reduction-Sensitive Polymeric Micelles for Anticancer Drug Delivery. *Macromol. Biosci.* **2012**, *12*, 703-711.
- 48 Skey, J.; O'Reilly, R. K. Facile one pot synthesis of a range of reversible addition-fragmentation chain transfer (RAFT) agents. *Chem. Commun.* **2008**, 4183-4185.
- 49 Lutz, J.-F.; Akdemir, Ö.; Hoth, A. Point by Point Comparison of Two Thermosensitive Polymers Exhibiting a Similar LCST: Is the Age of Poly(NIPAM) Over? *J. Am. Chem. Soc.* **2006**, *128*, 13046-13047.
- 50 Luzon, M.; Boyer, C.; Peinado, C.; Corrales, T.; Whittaker, M.; Tao, L.; Davis, T. P. Water-soluble, thermoresponsive, hyperbranched copolymers based on PEG-methacrylates: Synthesis, characterization, and LCST behavior. *J. Polym. Sci. A: Polym. Chem.* **2010**, *48*, 2783-2792.
- 51 Xu, J.; He, J.; Fan, D.; Wang, X.; Yang, Y. Aminolysis of Polymers with Thiocarbonylthio Termini Prepared by RAFT Polymerization: The Difference between Polystyrene and Polymethacrylates. *Macromolecules* **2006**, *39*, 8616-8624.
- 52 Roth, P. J.; Boyer, C.; Lowe, A. B.; Davis, T. P. RAFT Polymerization and Thiol Chemistry: A Complementary Pairing for Implementing Modern Macromolecular Design. *Macromol. Rapid Commun.* **2011**, *32*, 1123-1143.
- 53 Jeong, N. S.; Hasan, M.; Phillips, D. J.; Saaka, Y.; O'Reilly, R. K.; Gibson, M. I. Polymers with molecular weight dependent LCSTs are essential for cooperative behaviour. *Polym. Chem.* **2012**, *3*, 794-799.

- 54 Ryu, J.-H.; Park, S.; Kim, B.; Klaukherd, A.; Russell, T. P.; Thayumanavan, S. Highly Ordered Gold Nanotubes Using Thiols at a Cleavable Block Copolymer Interface. *J. Am. Chem. Soc.* **2009**, *131*, 9870-9871.

Chapter 3

3. Glutathione-Triggered Disassembly of Isothermally Responsive Polymer

Nanoparticles Obtained by

Nanoprecipitation of Hydrophilic Polymers

3.1 Chapter Summary

The encapsulation and selective delivery of therapeutic compounds within polymeric nanoparticles offers hope for the treatment of a variety of diseases. Traditional approaches to trigger selective cargo release typically rely on polymer degradation which itself is a nonspecific process. In this report, we prepare nanoparticles from thermoresponsive polymers with a ‘solubility release catch’ at the chain-end. This release catch is exclusively activated in the presence of intracellular glutathione, triggering an ‘*isothermal*’ response and promoting a change in polymer solubility. This solubility switch leads to specific and rapid nanoparticle disassembly, release of encapsulated cargo and produces completely soluble polymeric side-products.

3.2 Introduction

The application of polymeric nanoparticles for the delivery of therapeutic compounds exhibiting poor pharmacological profiles (e.g. low solubility and high toxicity) holds exciting promise for the treatment of many diseases, particularly cancer.¹⁻⁵ Nanomedicine approaches should enable improved patient compliance by reducing side-effects and administration frequency. To achieve this aim it is preferable that the nanoparticles can release their cargo specifically at the site of action (normally in the cytosol). Typical release mechanisms include the GFLG peptide sequence, which is sensitive to lysosomal cathepsins,⁶ or more commonly the degradation of main-chains or cross-links within the constituent polymers.⁷ Ester and amide linkages are routinely employed for this purpose as they slowly hydrolyse in biological milieu with the assistance of ester-/peptid-ases. For example, Harth and co-workers have reported cross-linked polyesters with potential for intracellular delivery.^{8, 9} These particles have been used to entrap high concentrations of hydrophobic therapeutics whilst displaying linear degradation characteristics dependent on their crystallinity. When functionalised with a targeting peptide, these particles were used successfully to deliver paclitaxel to tumours exposed to ionising radiation.¹⁰ Yang *et al.* reported the use of polyester/DNA nanoparticles to deliver the gene for vascular endothelial growth factor into stem cells to promote limb growth in mice,¹¹ and Palamoor and Jablonski exploited the gradual degradation of poly(orthoesters) for ocular applications, achieving delivery of epinephrine over a period of several months.¹²

Perhaps the most appealing feature of polyesters is for sustained (slow) release applications. For example, cross-linked polyester nanoparticles required ~ 10 days to

degrade by 82.5 % in the best case,⁸ whilst emulsion-derived polyesters degraded by only ~ 50 % after several months.¹³ However, the non-specific degradation mechanism of such functionality poses two challenges: unwanted, non-specific cargo leaching of targeted delivery agents, and the generation of acidic side-products due to ester hydrolysis.^{14, 15} For instance, the generation of acid within degrading microparticles of poly(lactic-*co*-glycolic acid) led to regions with a pH as low as 1.5 after several days.¹⁶ An alternative degradable linkage is the disulfide bond which is sensitive to the primary *in vivo* reducing agent glutathione (GSH). GSH is attractive given the 1000-fold concentration differential between intra- and extracellular environments.¹⁷ This gradient has been exploited to ensure nanocarriers are stable in the circulation, but rapidly disassemble in the intracellular environment.¹⁸⁻²¹ Zhong and co-workers compared the rate of doxorubicin release from poly(ethyleneglycol)-*block*-poly(caprolactone) micelles with and without a disulfide linker in a reducing environment. Complete drug release from the disulfide-containing micelles occurred after 10 hrs whilst only 20 % doxorubicin was released *via* ester hydrolysis from the non-disulfide containing structures, highlighting the advantage of bioreduction over ester hydrolysis when rapid release is desirable.^{22, 23} However, introduction of disulfide linkages between two distinct polymer blocks typically requires macromolecular coupling reactions which are not always efficient and require extensive purification.²² We have previously incorporated a disulfide linkage into thermoresponsive polymers whereby the lower critical solution temperature (LCST) can be modulated in response to intracellularly-relevant concentrations of GSH. This enabled the soluble-insoluble transition associated with an LCST to be manipulated using biochemical triggers rather than temperature changes, an “isothermal” transition.²⁴⁻²⁷ Other examples of isothermal responses include the use of salt

gradients,²⁸ redox-active spin labels²⁹ and bacterial binding,³⁰ the key advantage of which is that known responsive polymers can be easily modified to initiate complex responses under more biologically relevant conditions.

The incorporation of redox and thermally responsive components into nanoparticles *via* complex block copolymer self-assembly can be synthetically challenging. However, nanoprecipitation (or interfacial deposition) has emerged as a facile alternative for the preparation of nanoparticles requiring only a hydrophobic polymer. To process polymers in this way, two methodologies are generally employed: (i) Dialysis of polymer solvent against non-solvent and (ii) dropwise addition of polymer solution to the non-solvent. The latter method is particularly useful when using volatile solvents that can be removed by simple evaporation whilst dialysis may be better where less volatile solvents are concerned (Figure 3.1).³¹

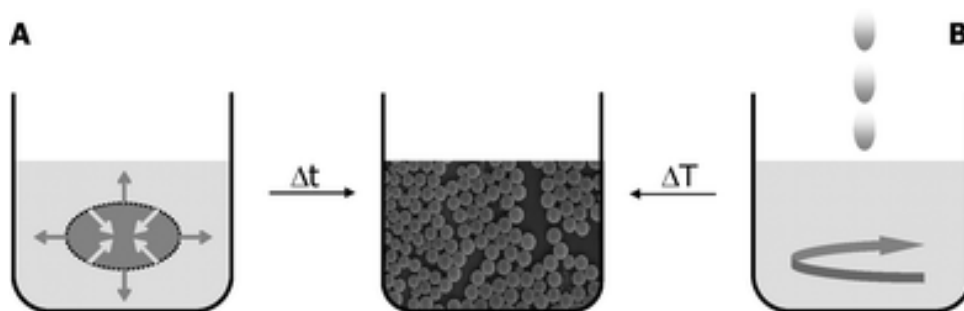


Figure 3.1 Nanoprecipitation as a route towards nanoparticle preparation using: (A) Dialysis and (B) dropping methods.³¹

Applications of this technique, which generally describe the precipitation of a dissolved material following exposure to a miscible non-solvent, have been prevalent for decades. The polyolefin industry has, for example, used nanoprecipitation as an effective tool for purifying synthetic polyolefins from the reaction solvent in a

simpler, lower energy process to the otherwise extensive heating (sometimes under vacuum) that was required.³² It was however in the late 1980's that Fessi *et al.* patented the nanoprecipitation technique as a means of preparing dispersible colloidal systems of a polymeric substance in the form of nanoparticles, exemplified by their report describing the preparation of indomethacin-loaded nanocapsules of poly(lactide).^{33, 34} Today, nanoprecipitation enables the processing of nanoparticles from polymeric starting materials quickly and easily with control over particle size and cargo molecule loading.^{35, 36} Typically however, hydrophobic polymers or at least the need for polymers containing significant hydrophobic portions has essentially constrained this technique to the likes of functionalised-dextrans,³⁷ poly(esters)^{38, 39} plus some examples of poly(styrenes)^{36, 40, 41} and amphiphilic copolymers.⁴²

Here, nanoparticles are prepared from hydrophilic, thermoresponsive polymers containing a disulfide-linked 'solubility release catch' at their chain-end by the nanoprecipitation technique. This release catch is designed to promote rapid nanoparticle disassembly and cargo release upon encountering intracellular levels of GSH. Furthermore, reduction of the end-group switches the material's LCST rendering the polymer and resulting by-products fully hydrophilic.

3.3 Results and Discussion

It was reasoned that thermoresponsive polymers displaying an LCST could be used to prepare particles *via* nanoprecipitation if they were held above their transition temperature. Furthermore, by introducing a redox-responsive chain-end ‘solubility release catch’ to generate an isothermal response, it should be possible to programme the polymer such that its LCST increases in the presence of intracellular GSH. This will allow the particle solubility to switch, triggering disassembly and cargo release using only end-group reduction events rather than random degradation of the polymer backbone. Ultimately, the released polymer will be hydrophilic and of sufficiently low molecular weight to be removed by renal elimination, without the need for further polymer degradation (Figure 3.2).

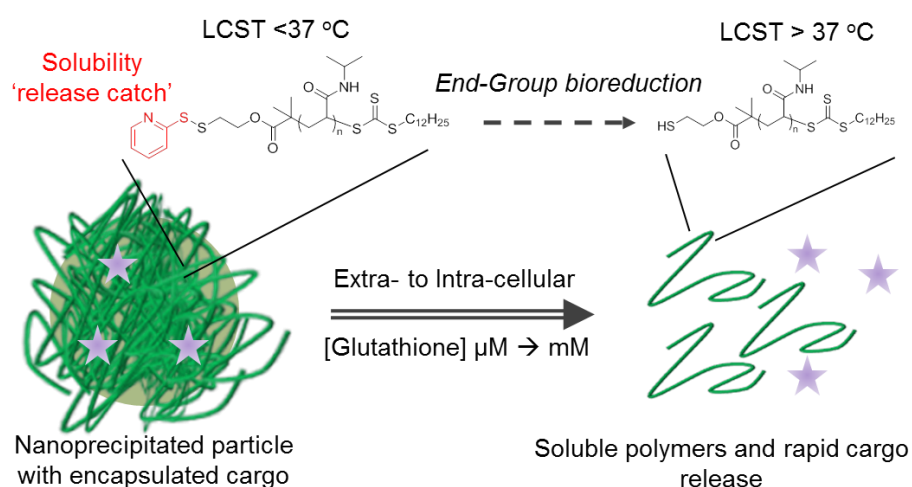
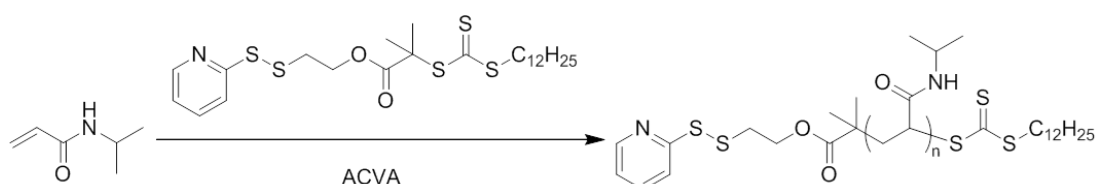


Figure 3.2 Isothermal disassembly concept: Glutathione reduction of the disulfide end-group shifts the LCST to induce a solubility switch and triggers cargo release.

In this study poly(*N*-isopropylacrylamide), pNIPAM, was selected as the responsive polymer given its strong shift in cloud point (measurable property of the LCST) upon polymer end-group modification provides the desired ‘solubility release

catch',^{24, 25, 30} **pNIPAM-1** was prepared using the Reversible Addition-Fragmentation Chain Transfer (RAFT) methodology and the pyridyl disulfide (PDS) end-group installed using a pre-functionalised chain transfer agent (Scheme 3.1, Table 3.1). The polymer was characterised by SEC (Figure 3.3A), turbidimetry (Figure 3.3B) and ¹H NMR spectroscopy (Figure 3.3C). The latter confirmed the successful installation of the pyridyl disulfide α -end-group, as seen by peaks at 7.7 and 8.5 ppm corresponding to the aromatic protons, and the trithiocarbonate ω -end-group given the peak at 0.85 ppm corresponding to the terminal methyl group.



Scheme 3.1 Synthesis of **pNIPAM-1**: Pyridyl disulfide end-group installed using a pre-functionalised RAFT chain transfer agent.

Table 3.1 Characterisation of **pNIPAM-1**.

Polymer ^a	[NIPAM]: Conversion		$M_{n, \text{Theo}}$ (g.mol ⁻¹) ^b	$M_{n, \text{SEC}}$ (g.mol ⁻¹) ^c	M_w/M_n ^c	CP (°C) ^d
	[CTA]	(%) ^b				
pNIPAM-1	488:1	73.3	40500	25400	1.24	31.5

^aNIPAM = *N*-isopropylacrylamide, ^bDetermined by ¹H NMR spectroscopy relative to an internal standard (mesitylene); ^cDetermined by SEC (DMF inc. 5 mM NH₄BF₄) relative to PMMA standards; ^dCP = Cloud Point at polymer concentration of 0.5 mg.mL⁻¹.

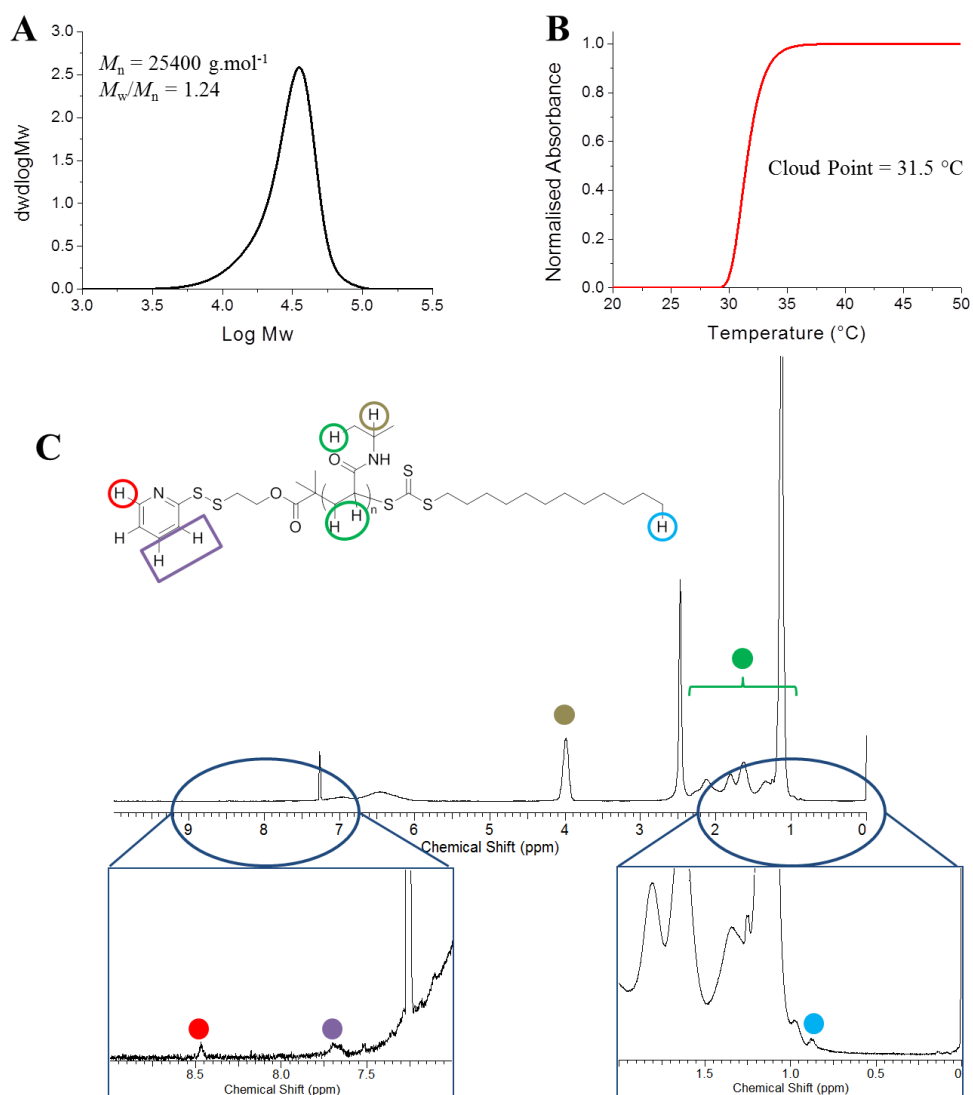


Figure 3.3 Characterisation of **pNIPAM-1**: (A) SEC Characterisation using DMF inc. 5 mM NH_4BF_4 as eluent, relative to PMMA standards; (B) Turbidimetry analysis and (C) ^1H NMR spectrum in CDCl_3 .

PNIPAM-1 with $M_n = 25,400 \text{ g.mol}^{-1}$, $M_w/M_n = 1.24$ and cloud point $\sim 32 \text{ }^{\circ}\text{C}$ was dissolved in acetone (1 mg.mL^{-1}) and added dropwise into water at $50 \text{ }^{\circ}\text{C}$ to give a pale blue, opalescent suspension, indicative of nanoparticle formation. Dynamic light scattering (DLS) at $50 \text{ }^{\circ}\text{C}$ revealed nanoparticles with an average hydrodynamic diameter of 197 nm (polydispersity 0.2, Figure 3.4A) and demonstrated colloidal stability for 7 days without aggregation. To further characterise these particles,

transmission electron microscopy (TEM) was initially employed. Whilst the occasional particle was observed, the vast majority of structures resembled amorphous polymer material (Figure 3.4B). This observation was speculated to be a result of the drying involved in this technique during which time, the temperature of the particles will have decreased below their cloud point prompting re-solubilisation.

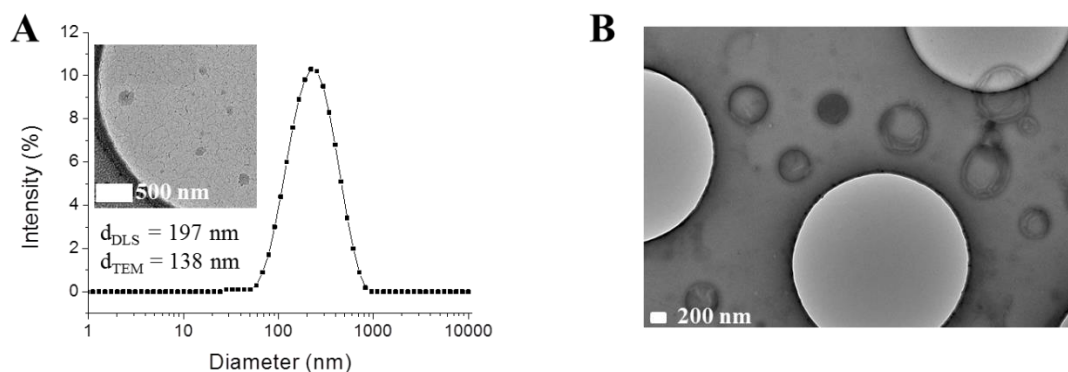


Figure 3.4 Characterisation of nanoparticles prepared from **pNIPAM-1**: (A) Dynamic light scattering and (inset) example cryo-TEM image; (B) TEM image.

Hence, for the particles to be imaged properly, we determined the sample must be held above the polymer cloud point to maintain its hydrophobicity. Cryogenic transmission electron microscopy (cryo-TEM) with rapid vitrification was therefore used. Cryo-TEM takes a snapshot of the system in its “real” state by rapidly cooling (vitrifying) the system, thus eliminating any sample deformation or destruction possible upon sample drying.⁴³ This technique enabled the structural integrity of our particles to be maintained and imaging revealed a number average particle size (determined using ImageJ software) of 138 nm. An example cryo-TEM image together with the particle size is included in Figure 3.4A for ease of comparison whilst a greater selection of the cryo-TEM images recorded is shown in Figure 3.5A. As each individual image contained relatively few nanoparticles, data analysis was performed using multiple images (Figure 3.5B). The particle sizes by both DLS and

cryo-TEM were in broad agreement. Differences in particle size between the two techniques may be rationalised by considering the average particle size provided by cryo-TEM is a number average compared to the z-average (*i.e.* intensity weighted harmonic mean size) provided by DLS. Moreover the swelling of particles dispersed in the solvent of analysis is also possible.

It is also worth noting that although no work designed to tune the size of these particles was undertaken here, there are multiple reports on the influence of various factors on the size of particles produced by the nanoprecipitation technique. Legrand *et al.* found the choice of good solvent affected the particle sizes obtained from linear poly(DL-lactic acid): Smaller particles were always produced when the polymer was initially dissolved in acetone compared to THF as a result of its increased polarity.⁴⁴ Kissel and co-workers made a similar observation in the aqueous nanoprecipitation of poly(lactic-*co*-glycolic acid), PLGA, using acetone, acetonitrile and THF as good solvents. Particles from acetone and acetonitrile produced particles of similar size whilst when THF was used, significantly larger particles were produced. This observation was accounted for by the lower diffusion coefficient and higher viscosity of THF resulting in slower solvent diffusion and hence larger nanoparticles.⁴⁵ Concentration is also an important factor with larger particles routinely observed at higher concentrations of the starting polymer solution as this increased solution viscosity, lowering velocity of diffusion and maintaining a higher ratio of polymer molecules to solvent molecules.^{46, 47} The ability to control nanoparticle synthesis using modern technology platforms such as microfluidics has also been demonstrated by Farokhzad and co-workers who were able to tune the particle size of a PLGA-*b*-PEG copolymer in acetonitrile/water by altering the flow rate.⁴⁸

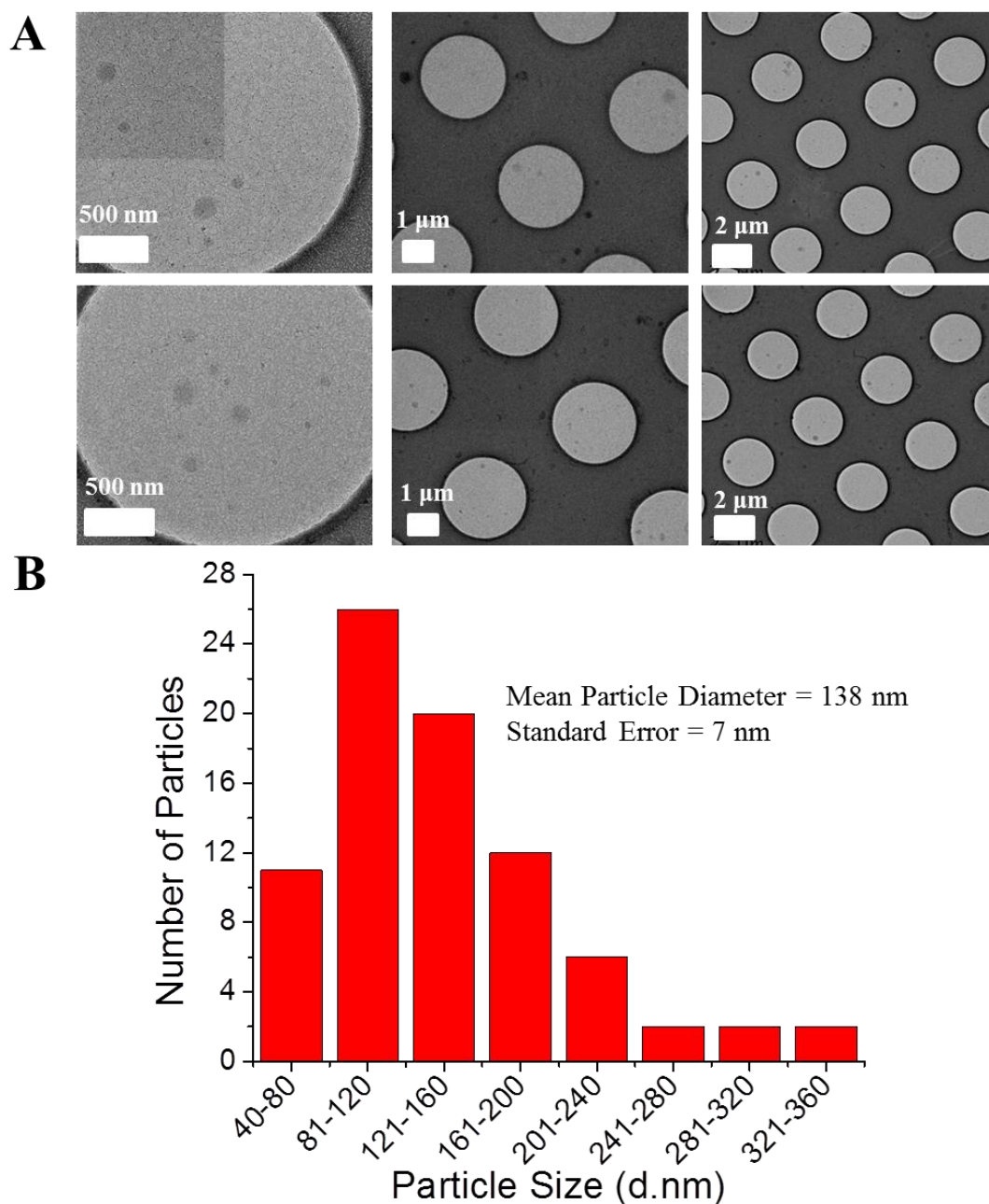


Figure 3.5 (A) Cryo-TEM images of nanoparticles prepared from **pNIPAM-1**. Some discontinuity was noticed in the ice layer which has been previously attributed to over blotting;⁴⁹ (B) Particle size (D_n determined using ImageJ) analysis of nanoparticles prepared from **pNIPAM-1**. The size distribution can be used to determine D_w ($\sum D^2 / \sum D$) = 168 nm or D_z ($\sum D^6 / \sum D^5$) = 281 nm size averages which are more appropriate for comparison with the DLS result of $D_H = 200$ nm.

To ensure that the resulting particles retained the intrinsic thermo-responsiveness of their constituent polymer, temperature-dependent DLS was conducted (Figure 3.6). As the nanoparticles were cooled from 50 to 20 °C a decrease in scattering intensity (count rate) was observed indicating disassembly of the particles. This was also confirmed by the visual change from an opalescent suspension to a colourless solution. An overlay of this DLS data with turbidimetric analysis of **pNIPAM-1** indicated that disassembly correlated with the cloud point of the polymer.

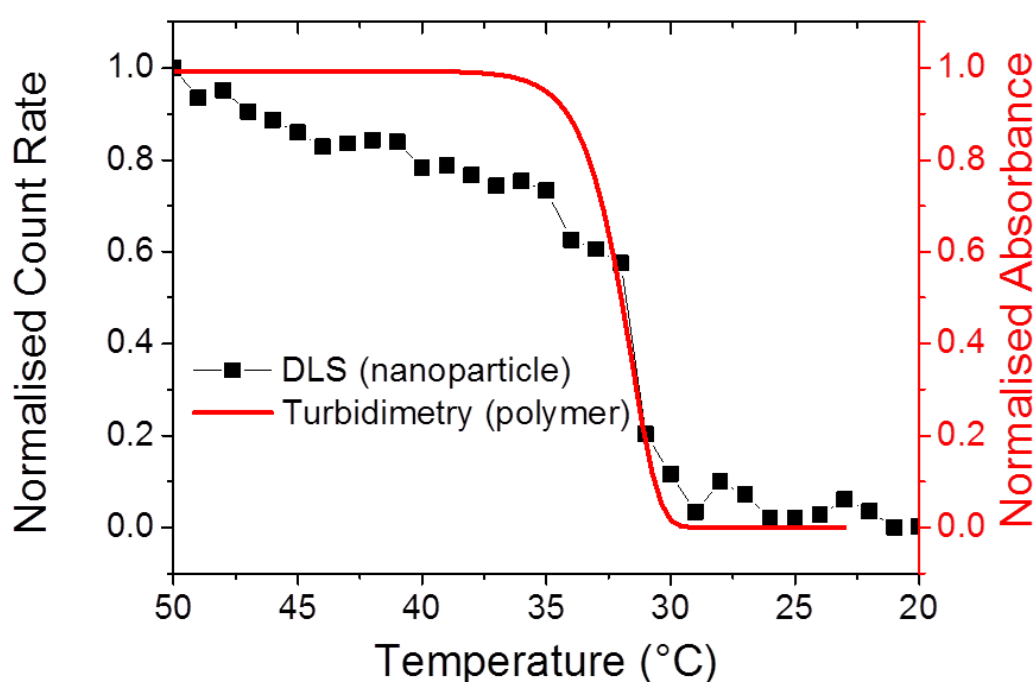


Figure 3.6 Thermal disassembly of nanoparticles (black, DLS) and turbidimetry data of linear **pNIPAM-1** (red). Concentration = 0.5 mg.mL⁻¹.

The principal aim of this study was to evaluate whether the nanoparticles would specifically disassemble in response to intracellular levels of GSH *via* reduction of the PDS solubility release catch. To verify a GSH-induced physical response, the nanoparticles were held at 50 °C, GSH was added at 10 µM (extracellular) or 1 mM (intracellular) and the particle size measured. Addition of 10 µM GSH showed no changes visually, or by DLS. In contrast, addition of 1 mM GSH resulted in rapid

precipitation of the nanoparticles and a significant increase in the particle size to ca. 1.5 microns (Figure 3.7). It should be noted that this experiment is not intended to mimic *in vivo* conditions, but to demonstrate the concept of isothermal disassembly. Hence, aggregation is observed as the experimental temperature, which is above the cloud point of both the original and GSH-modified polymer (Table 3.1), means the resulting disassembled polymer chains exist in a globular conformation. Further exemplification under more physiological conditions leading to dissolution of the polymers is described later (*vide infra*).

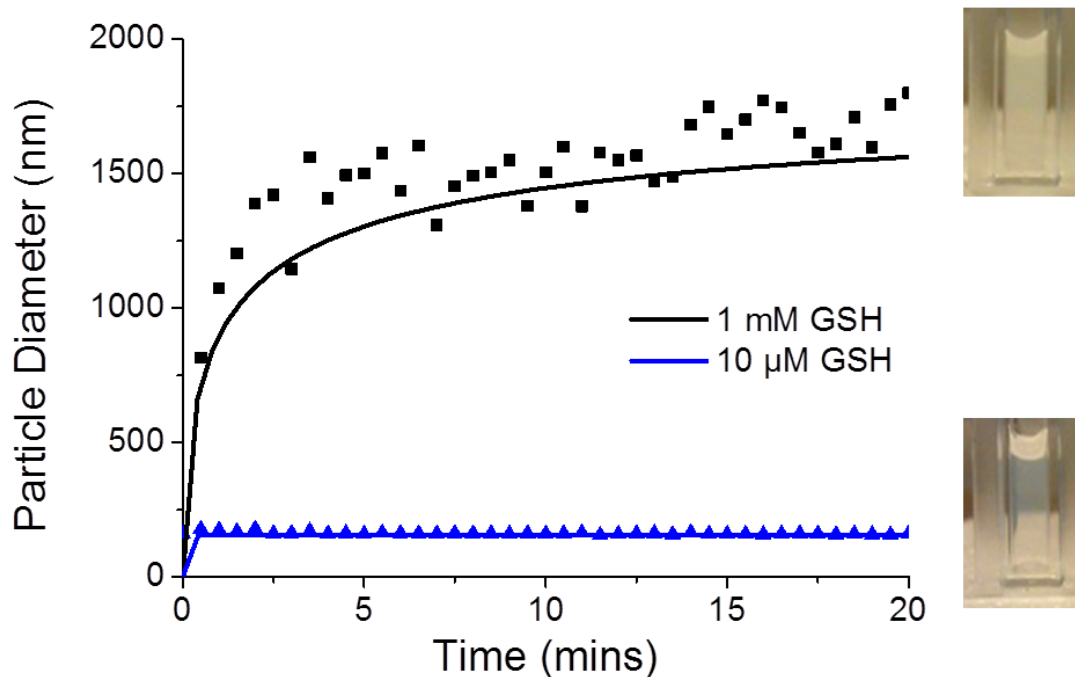


Figure 3.7 DLS-monitored, GSH-triggered disassembly of nanoparticles prepared from **pNIPAM-1**: Temperature = 50 °C; line of best fit shown as solid curve (inset: nanoparticle appearance following GSH addition).

A fluorescent probe, diphenylhexatriene (DPH), was encapsulated in the particle by co-precipitation as a model cargo. DPH only fluoresces in hydrophobic environments allowing direct observation of its release into an aqueous

environment.⁵⁰ Addition of up to 10 μM GSH caused no decrease in fluorescence intensity, with the slight increase observed attributable to evaporation given the elevated (50 $^{\circ}\text{C}$) temperatures being used. Addition of 1 mM GSH led to an almost immediate decrease in fluorescence intensity demonstrating that particles assembled from thermoresponsive polymers are capable of releasing a cargo in response to a biochemical stimulus (Figure 3.8). The observed release agreed with DLS data and confirmed the polymer phase transition as the trigger. Release was both specific, yet significantly faster than that observed with disulfide-linked micelles which required over 10 hrs⁷ or 40 hrs⁵¹ to release their cargo. We believe the fast release kinetics may be due to the co-operative nature of pNIPAM's LCST; if a small fraction of the polymer chains undergo an increase in their LCST (due to bioreduction), then the LCST of those remaining is also raised, facilitating disassembly.⁵² This co-operative LCST behaviour is not found with all thermoresponsive polymers, such as poly[oligo (ethyleneglycol)methacrylates], highlighting the importance of the choice of pNIPAM. Other polymers with co-operative LCST behaviour include elastin-side chain poly(methacrylates)⁵³ and poly(*N*-vinyl lactams). The observation may also be explained by considering the location of encapsulated material in different nanoparticle structures. For example, cross-linked micelles contain hydrophobic cargo within the core. In our particles however, we expect the cargo molecules to be diffusely spread throughout the structure, meaning cargo release occurs as soon as the outer polymers pass through their phase transition.

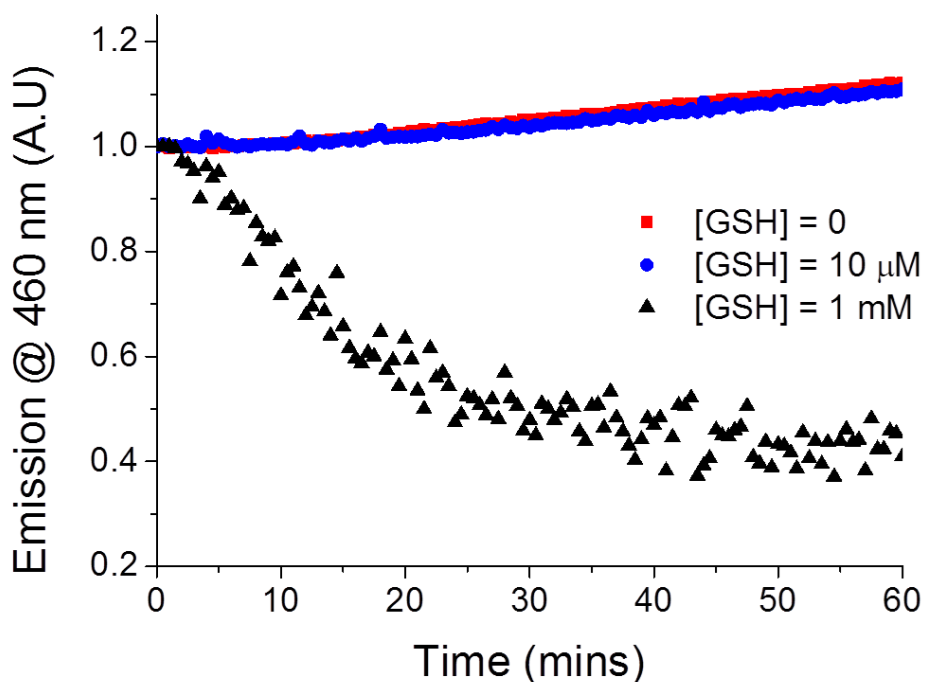
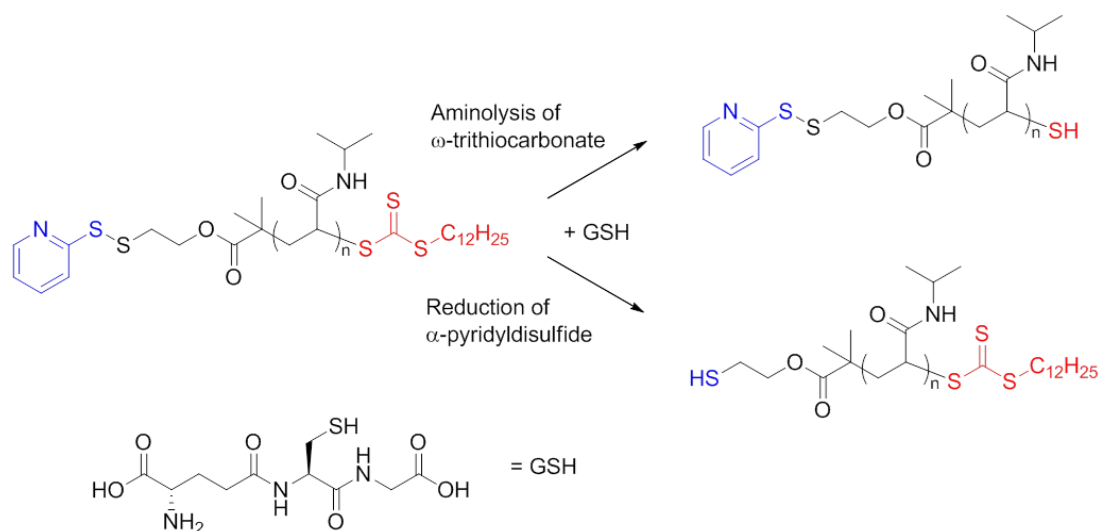


Figure 3.8 GSH-triggered disassembly of cargo-loaded nanoparticles prepared from **pNIPAM-1**: Fluorescence change of DPH-containing nanoparticles incubated with GSH.

GSH contains two functional groups capable of potentially altering the structure of a RAFT-derived polymer: (i) reduction of the pyridyl disulfide α -end-group by the cysteine residue and (ii) aminolysis of the trithiocarbonate ω -end-group by the glutamic acid residue (Scheme 3.2). The latter reaction seems unlikely given the likelihood of GSH existing as a zwitterion in aqueous solutions whereby the amino group will be protonated ($pK_a(\text{NH}_2) = 8.75$) and rendered non-nucleophilic. However, to confirm that the isothermal particle disassembly process was triggered solely by the reduction reaction, additional UV-visible spectrophotometry experiments were performed. UV-Visible spectra of **pNIPAM-2** and **pNIPAM-3**, two polymers of similar molecular weights containing a trithiocarbonate end-group and either a *tert*-butyl carbamate (**pNIPAM-2**) or pyridyl disulfide (**pNIPAM-3**)

end-group (Table 3.2, Figure 3.9), were obtained as a function of GSH concentration, at the same concentration ($0.5 \text{ mg}\cdot\text{mL}^{-1}$) at which the particles were prepared.



Scheme 3.2 Potential reactions of glutathione with RAFT-derived pNIPAM: Aminolysis (top) or disulfide reduction (bottom). Inset: Chemical structure of glutathione.

Table 3.2 Characterisation of polymers used for UV-Visible spectrophotometry experiments.

Polymer ^a	[M]:[CTA]	Conversion (%) ^b	$M_{n(\text{th})}$	$M_{n(\text{SEC})}$	M_w/M_n^c
			($\text{g}\cdot\text{mol}^{-1}$) ^b	($\text{g}\cdot\text{mol}^{-1}$) ^c	
pNIPAM-2	237:1	80.0	21500	18000	1.13
pNIPAM-3	450:1	27.4	14000	19200	1.19

^aNIPAM = *N*-isopropylacrylamide; ^bDetermined by ^1H NMR spectroscopy relative to an internal standard (mesitylene); ^cDetermined by SEC (DMF inc. 5 mM NH_4BF_4) relative to PMMA standards.

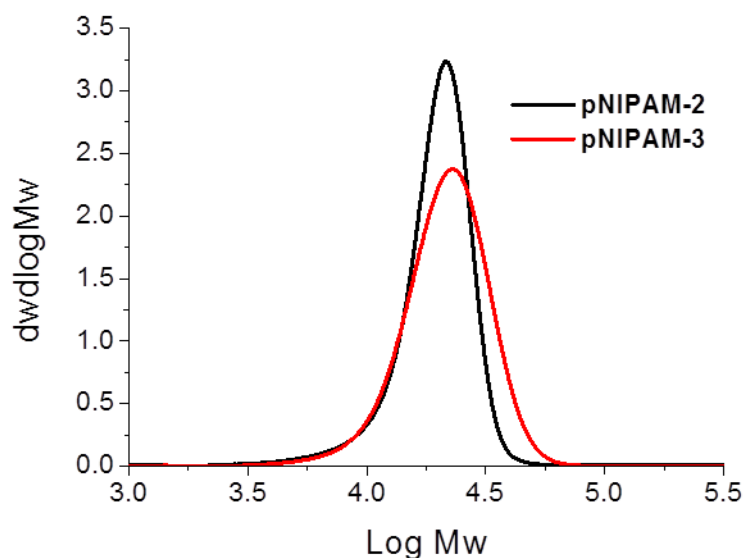
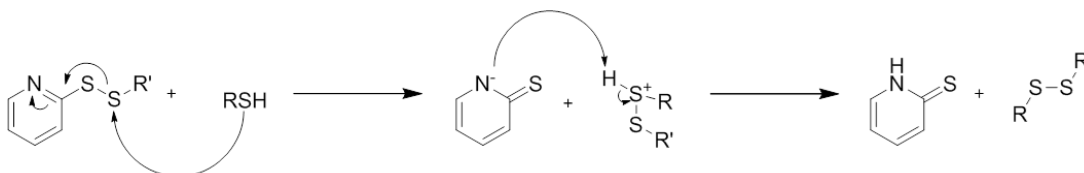


Figure 3.9 SEC Characterisation of pNIPAM-2/3.

The trithiocarbonate end-group and pyridine thione (by-product of the reaction of a thiol with pyridyl disulfide, Scheme 3.3) have distinct peaks in the UV-visible spectrum ($\lambda_{\text{max}} = 309 \text{ nm}$ and 343 nm respectively) providing a useful tool for determining the nature of the interaction between polymer and GSH.



Scheme 3.3 Thiol-disulfide exchange reaction between a thiol and pyridyl disulfide to yield a mixed disulfide and pyridine thione.

At all concentrations of GSH there was no significant change in absorbance at 309 nm for either polymer after 1 hour indicating that the trithiocarbonate end-group is stable to aqueous solutions of GSH. The small increase in absorbance at 309 nm observed in Figure 3.10 can be attributed to the release of pyridine thione, whose spectrum exhibits some absorbance overlap with that of the trithiocarbonate. Spectra obtained after 20 hrs revealed no additional change.

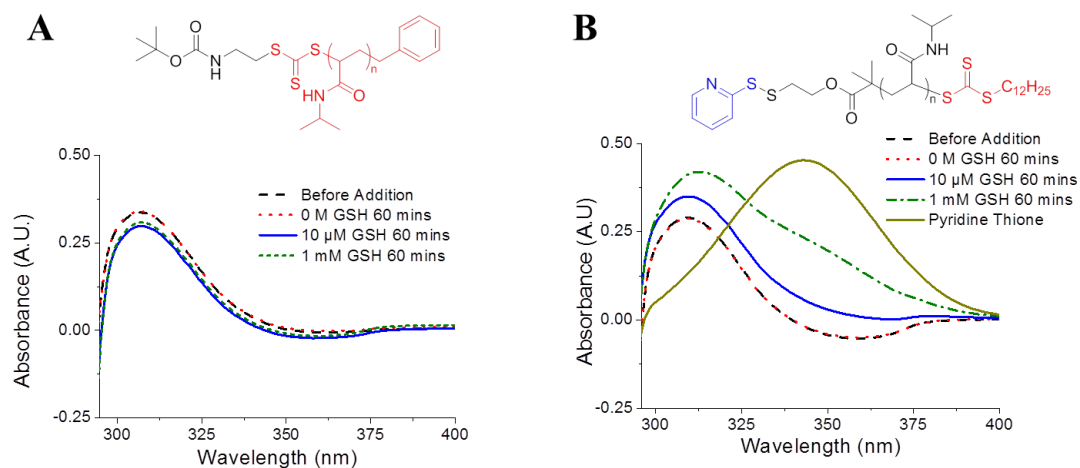


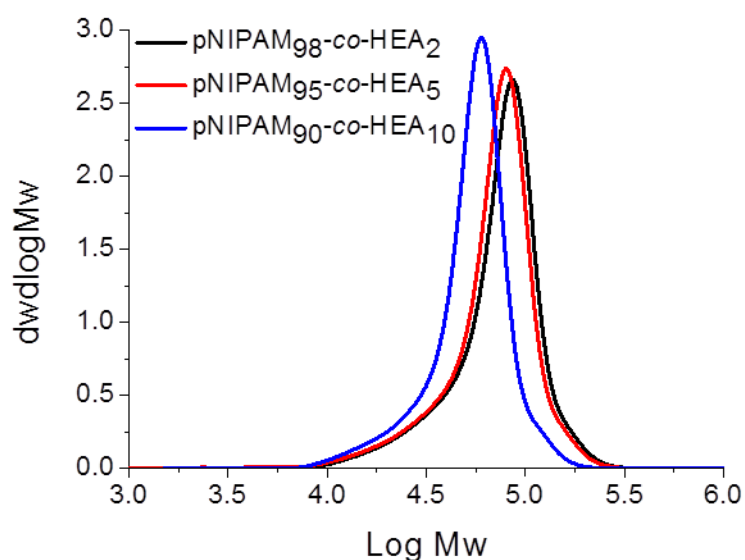
Figure 3.10 UV-visible spectra as a function of GSH concentration of (A) **pNIPAM-2** and (B) **pNIPAM-3**. Concentration = 0.5 mg.mL^{-1} .

The motivation for using an isothermally responsive polymer nanoparticle, as opposed to a conventional hydrophobic polymer, lies in the solubility switch observed upon end-group bioreduction. **PNIPAM-1** had an LCST $\sim 32 \text{ }^\circ\text{C}$ which is not suitable for *in vivo* applications therefore statistical copolymers of NIPAM and *N*-hydroxyethyl acrylamide (HEA) were prepared and their thermoresponsivity measured (Table 3.3, Figure 3.11).

Table 3.3 Characterisation of pNIPAM-*co*-HEA samples prepared in this study.

Polymer ^a	[NIPAM]: [HEA]: [CTA]	Conversion (%) ^b	$M_{n(th)}$ (g.mol ⁻¹) ^d	$M_{n(SEC)}$ (g.mol ⁻¹) ^e	M_w/M_n ^e	CP: 0
						(1 mM) GSH (°C) ^f
pNIPAM ₉₈ - <i>co</i> -HEA ₂	439:9:1	84.8/N _d ^c	-	60300	1.31	33.5 (-)
pNIPAM ₉₅ - <i>co</i> -HEA ₅	404:21:1	79.9/89.2	38700	56900	1.31	35.3 (37.1)
pNIPAM ₉₀ - <i>co</i> -HEA ₁₀	407:45:1	76.1/88.8	39600	45600	1.25	38.2 (39.3)

^aNIPAM = *N*-isopropylacrylamide, HEA = *N*-Hydroxyethylacrylamide; ^bx/y = % conversion NIPAM/HEA; ^cN_d = Not determined due to low intensity of NMR peaks preventing quantitative determination; ^dDetermined by ¹H NMR spectroscopy relative to an internal standard (mesitylene); ^eDetermined by SEC (DMF inc. 5 mM NH₄BF₄) relative to PMMA standards; ^fCP = Cloud Point at polymer concentration of 0.5 mg.mL⁻¹ in 0 (1 mM) GSH solution.

**Figure 3.11** SEC Characterisation of pNIPAM-*co*-HEA.

It is well established that the overall LCST of a system can be increased and decreased by the incorporation of hydrophilic or hydrophobic co-monomers respectively.^{54, 55} In this case, the co-polymerisation of NIPAM with increasing proportions of the hydrophilic monomer HEA led to an increase in cloud point from 33.5 °C to 35.2 °C to 38.2 °C as the mol% of HEA in the polymerisation mixture increased from 2 % to 5 % to 10 %. Importantly, the co-polymerisation of a 95:5 mol% NIPAM:HEA produced a polymer with a cloud point which, when reduced with 1 mM GSH, increased to 37 °C. Nanoparticles with diameter ~ 200 nm were then produced following the nanoprecipitation method used previously. Example cryo-TEM images (Figure 3.12A) and DLS data (Figure 3.12B) for these nanoparticles are shown below. Note that there were not enough particles seen to plot a histogram in this case. Furthermore, the smaller objects seen in Figure 3.12A are crystalline ice contamination on the surface of the vitrified ice layer in which the 200 nm particles are embedded.

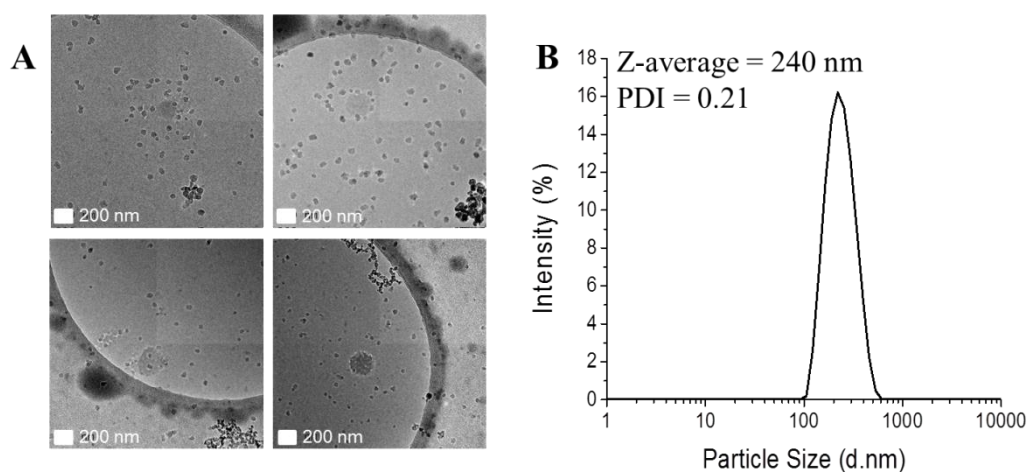


Figure 3.12 (A) Cryogenic Transmission Electron Microscopy (magnification = 20000x) and (B) Dynamic Light Scattering of nanoparticles prepared from **pNIPAM₉₅-co-HEA₅**.

Like the homopolymer, nanoparticles based on the co-polymer were found to be stable at 37 °C in the presence of 10 μM GSH, the extracellular concentration. Increasing the GSH concentration to 1 mM (as found in many intracellular compartments) resulted in particle disassembly (blue suspension to colourless solution) and dye release experiments showed quenching of DPH fluorescence (Figure 3.13). This observation demonstrates that by fine-tuning the polymer structure and hence transition temperature, isothermal disassembly can be employed to trigger cargo release from nanoparticles specifically in response to biochemical triggers. We anticipate that this concept could also be translated to degradable thermoresponsive polymers such as elastin-based peptides⁵⁶ or poly(phosphoesters).⁵⁷

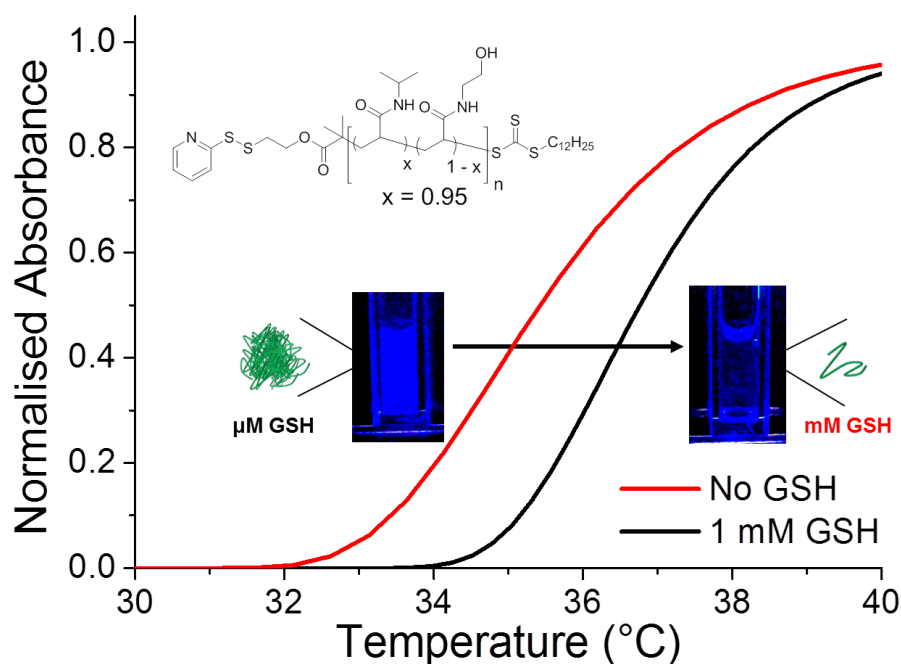


Figure 3.13 Turbidimetric response of linear p(NIPAM₉₅-co-HEA₅) with and without addition of 1 mM GSH. Inset: Visual change in the fluorescence of nanoparticles (37 °C), before and after addition of 1 mM GSH. Fluorescence change is due to DPH release and quenching.

3.4 Conclusions

To summarise, this chapter demonstrates the use of isothermally responsive polymers which are capable of shifting their phase behaviour upon the application of the specific biochemical stimulus glutathione. Nanoparticles were formed by holding pNIPAM above its transition temperature allowing the use of nanoprecipitation; a method typically associated with hydrophobic polymers. The nanoparticles were shown to specifically disassemble and release a cargo upon exposure to intracellular levels of glutathione with complete release in around 30 mins. The fast, but highly specific release kinetics offers a significant advantage over other reducible carriers such as micelles. Importantly the particles were stable for extended periods in the presence of circulatory-levels of glutathione which is essential for a disulfide-linked delivery system where cargo leaching is undesirable. The mechanism of disassembly was shown to be due to the isothermal phase transition of the pNIPAM, caused by rapid and selective cleavage of the disulfide-linked end-group. The ability to tune this transition temperature using simple co-polymerisation methodologies was also demonstrated to generate responses at physiological temperatures. This report represents a powerful strategy to generate nanoparticles from hydrophilic polymers, without the need for cross-linking or block copolymers. Furthermore, these structures can be tuned to trigger release in response to specific cellular stimuli without requiring a non-specific polymer degradation step. Future work will include the *in vitro* assessment of the nanoparticles as drug delivery vehicles and the incorporation of degradable/targeting functionalities into the polymer main-chain.

3.5 Experimental

3.5.1 Materials

All chemicals were used as supplied unless stated. Methanol, hexane, ethyl acetate, dichloromethane, toluene, acetone, 40-60 °C petroleum ether, tetrahydrofuran, diethyl ether and glacial acetic acid (analytical reagent grade) were all purchased from Fisher Scientific at laboratory reagent grade unless otherwise stated. Deuterated chloroform (99.9 atom % D), aldrithiol-2 (98.0 %), 2-mercaptoethanol (≥ 99.0 %), dodecane thiol (≥ 98.0 %), 2-(*boc*-amino) ethanethiol (97.0 %), tribasic potassium phosphate (reagent grade, ≥ 98.0 %), carbon disulfide, 2-bromo-2-methylpropionic acid (98.0 %), benzyl bromide (98.0 %), 4-dimethylaminopyridine (≥ 99.0 %), *N,N'*-diisopropylcarbodiimide (99.0 %), *N*-isopropylacrylamide (97.0 %), *N*-hydroxyethyl acrylamide (97.0 %), mesitylene (analytical standard), glutathione (99.0 % reduced) and 1,6-diphenyl-1,3,5-hexatriene (98.0 %) were all purchased and used as received from Sigma-Aldrich. Hydroxyethyl pyridyl disulfide, 2-(dodecylthiocarbonothioylthio)-2-methylpropanoic acid and 2-(pyridyldisulfanyl) ethyl 2-(dodecylthiocarbonothioylthio)-2-methylpropanoate were synthesised as described in Chapter 2.

3.5.2 Analytical Methods

NMR spectroscopy (^1H , ^{13}C) was conducted on a Bruker DPX-400, Bruker DRX-500, a Bruker AV III-600 or a Bruker AV II-700 spectrometer. Deuterated chloroform was used with all chemical shifts reported in ppm (δ) relative to that solvent.

High resolution mass spectra were recorded on a Bruker Electrospray Ultra-High Resolution tandem TOF mass spectrometer using electrospray ionization (ESI) in positive mode on samples prepared in methanol. FTIR spectra were acquired using a Bruker Vector 22 FTIR spectrometer with a Golden Gate diamond attenuated total reflection cell. A total of 64 scans were collected on samples in their native (dry) state. UV-visible spectra were obtained using an Agilent Cary 60 UV-visible spectrophotometer at a “medium” scan-speed.

SEC analysis was performed on a Varian 390-LC MDS system equipped with a PL-AS RT/MT autosampler, a PL-gel 3 μm (50×7.5 mm) guard column, two PL-gel 5 μm (300×7.5 mm) mixed-D columns using DMF with 5 mM NH_4BF_4 at 50 $^\circ\text{C}$ as the eluent at a flow rate of 1.0 $\text{mL}\cdot\text{min}^{-1}$. The GPC system was equipped with ultraviolet (UV) (set at 280 nm) and differential refractive index (DRI) detectors. Narrow molecular weight PMMA standards ($200 - 1.0 \times 10^6$ $\text{g}\cdot\text{mol}^{-1}$) were used for calibration using a second order polynomial fit.

The cloud points were measured using an Optimelt MPA100 system (Stanford Research Systems). The recorded turbidimetry curve was normalised between values of 0 and 1. The cloud point was defined as the temperature corresponding to a normalised absorbance of 0.5. A polymer concentration of 0.5 $\text{mg}\cdot\text{mL}^{-1}$ and a constant heating rate of 1 $^\circ\text{C}\cdot\text{min}^{-1}$ were used for all experiments.

Fluorescence measurements were performed using a Biotech Synergy HT and processed using the Gen5 software package version 1.11.

Particle size analysis was determined by Dynamic Light Scattering using a Malvern Zetasizer Nano ZS instrument. A 4 mW He-Ne 633 nm laser module was used and scattered light was measured at 173° (back scattering). The attenuator and position were selected automatically by the instrument.

For Transmission Electron Microscopy, images were obtained on a JEOL 2000fx microscope, 200 kV, LaB6 instrument operated with a beam current of ~115 mA; images were captured using a Gatan Orius 11 megapixel camera. Samples were prepared by applying a small volume (typically 4 μ L) of sample to a GO-TEM grid⁴³ held with a pair of tweezers. The water was wicked away with a piece of filter paper and the grid left to dry.

Cryogenic Transmission Electron Microscopy samples (0.5 mg/mL in water) were examined using a Jeol 2010F TEM operated at 200 kV and imaged using a GatanUltrascan 4000 camera. Images were captured using Digital Micrograph software (Gatan). A 3 μ L droplet of the sample solution held at 50 °C was rapidly transferred to a holey carbon-coated copper grid, and the grid was blotted to remove excess solution. Subsequently, the grid was plunged into liquid ethane to vitrify the sample. The temperature of the cryogenic stage was maintained below -170 °C, using liquid nitrogen, during imaging. Where appropriate, particle size analysis was performed using ImageJ version 1.48a.

3.5.3 Procedures

3.5.3.1 Synthesis of benzyl 2-[(*tert*-butoxycarbonyl)amino]ethyl trithiocarbonate

2-(Boc-amino)ethanethiol (1.00 g, 0.95 mL, 5.64 mmol) was added dropwise to a stirred suspension of tribasic potassium phosphate (1.32 g, 6.21 mmol) in acetone (20 mL) over 25 mins. Carbon disulfide (1.29 g, 1.02 mL, 16.94 mmol) was added and the solution turned bright yellow. After stirring for 10 mins benzyl bromide (0.97 g, 0.67 mL, 5.64 mmol) was added. After stirring for 16 hrs, the solvent was removed under reduced pressure and the residue was purified by column chromatography on silica using a 40 – 60 °C petroleum ether – ethyl acetate gradient to yield a bright yellow solid (1.20 g, 62 %).

¹H NMR (700.134 MHz, CDCl₃) δ_{ppm}: 7.29 - 7.37 (5H, m, H¹⁰⁻¹²); 4.84 (1H, s, br., H⁴); 4.64 (2H, s, H⁸); 3.57 (2H, t, *J*₆₋₅ = 6.44 Hz, H⁶); 3.46 (2H, t, *J*₅₋₆ = 6.44 Hz, H⁵); 1.47 (9H, s, H¹).

¹³C NMR (176.008 MHz, CDCl₃) δ_{ppm}: 223.3 (C⁷); 155.9 (C³); 135.0 (C⁹); 129.4, 128.9, 128.0 (C¹⁰⁻¹²); 79.9 (C²); 41.8 (C⁸); 39.3 (C⁵); 36.7 (C⁶); 28.5 (C¹).

FTIR cm⁻¹: 3368 (N-H stretch); 2975, 2922, 2873 (Alkyl C-H stretch); 1681 (C=O stretch); 1523 (Aryl C=C stretch); 1070 (C=S stretch).

HRMS (ESI +) *m/z*: 366.0623 [M+Na]⁺; expected 366.0627 (C₁₅H₂₁NO₂S₃Na).

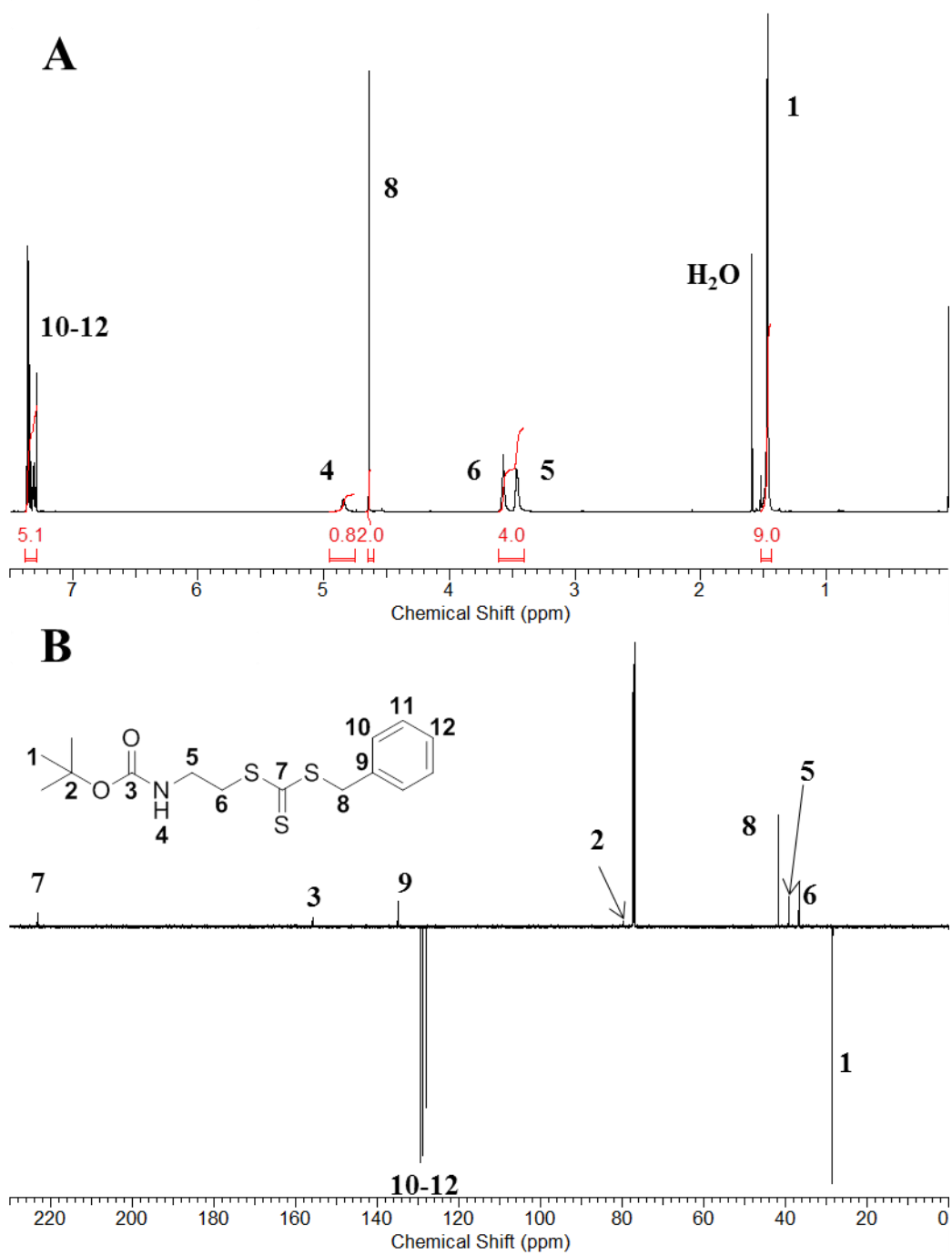


Figure 3.14 NMR spectroscopic characterisation of benzyl 2-[(*tert*-butoxycarbonyl)amino]ethyl trithiocarbonate: A) ^1H NMR and B) ^{13}C NMR spectra.

3.5.3.2 Polymerisation of *N*-isopropylacrylamide using 2-(pyridyldisulfanyl) ethyl 2-(dodecylthiocarbonothioylthio)-2-methylpropanoate

In a typical procedure *N*-isopropylacrylamide (2.16 g, 19.09 mmol), 2-(pyridyldisulfanyl) ethyl 2-(dodecylthiocarbonothioylthio)-2-methylpropanoate (20.90 mg, 39.15 μmol) and 4,4'-azobis(4-cyanovaleric acid) (1.79 mg, 6.39 μmol) were dissolved in methanol: toluene (1:1) (4 mL) in a glass vial containing a stir bar. Mesitylene (100 μL) was added as an internal reference and the mixture stirred (5 mins). An aliquot of this starting mixture was removed for ^1H NMR spectroscopic analysis. The vial was fitted with a rubber septum and degassed by bubbling with nitrogen gas (30 mins). The vial was then placed in an oil bath thermostated at 70 $^{\circ}\text{C}$. After 3 hrs the reaction mixture was opened to air and quenched in liquid nitrogen. An aliquot was removed and conversion determined by ^1H NMR spectroscopy. The product was purified three times by precipitation from tetrahydrofuran into cold diethyl ether, isolated by centrifugation and dried under vacuum overnight to give a pale yellow solid. The overall monomer conversion was determined from the ^1H NMR spectrum by measuring the decrease in intensity of the vinyl peaks associated with the monomer relative to mesitylene. Conversion (NMR): 73.3 %; M_n (theoretical): 40500 $\text{g}\cdot\text{mol}^{-1}$; M_n (SEC) 25400 $\text{g}\cdot\text{mol}^{-1}$; M_w/M_n (SEC): 1.24.

3.5.3.3 Polymerisation of (*N*-isopropylacrylamide) using benzyl 2-[(*tert*-butoxycarbonyl)amino]ethyl trithiocarbonate

N-isopropylacrylamide (1.00 g, 8.84 mmol), benzyl 2-[(*tert*-butoxycarbonyl)amino]ethyl trithiocarbonate (12.80 mg, 37.26 μmol) and 4,4'-azobis(4-cyanovaleric acid) (2.10 mg, 7.49 μmol) were dissolved in methanol:

toluene (1:1) (4 mL) in a glass vial containing a stir bar. Mesitylene (200 μL) was added as an internal reference and the mixture stirred (5 mins). An aliquot of this starting mixture was removed for ^1H NMR spectroscopic analysis. The vial was fitted with a rubber septum and degassed by bubbling with nitrogen gas (30 mins). The vial was then placed in an oil bath thermostated at 70 $^\circ\text{C}$. After 1.5 hrs the reaction mixture was opened to air and quenched in liquid nitrogen. An aliquot was removed and conversion determined by ^1H NMR spectroscopy. The product was purified three times by precipitation from tetrahydrofuran into cold diethyl ether, isolated by centrifugation and dried under vacuum overnight to give a pale yellow solid. The overall monomer conversion was determined from the ^1H NMR spectrum by measuring the decrease in intensity of the vinyl peaks associated with the monomer relative to mesitylene. Conversion (NMR): 80.0 %; M_n (theoretical): 21500 $\text{g}\cdot\text{mol}^{-1}$; M_n (SEC) 18000 $\text{g}\cdot\text{mol}^{-1}$; M_w/M_n (SEC): 1.13.

3.5.3.4 Co-polymerisation of *N*-isopropylacrylamide and *N*-hydroxyethylacrylamide

In a typical procedure *N*-isopropylacrylamide (1.25 g, 11.05 mmol), *N*-hydroxyethyl acrylamide (66.7 mg, 579.35 μmol), 2-(pyridyldisulfanyl) ethyl 2-(dodecylthiocarbonothioylthio)-2-methylpropanoate (14.5 mg, 27.16 μmol) and 4,4'-azobis(4-cyanovaleric acid) (2.50 mg, 8.92 μmol) were dissolved in methanol: toluene (1:1) (2.7 mL) in a glass vial containing a stir bar. Mesitylene (200 μL) was added as an internal reference and the mixture stirred (5 mins). An aliquot of this starting mixture was removed for ^1H NMR spectroscopic analysis. The vial was fitted with a rubber septum and degassed by bubbling with nitrogen gas (30 mins). The vial was then placed in an oil bath thermostated at 70 $^\circ\text{C}$. After 40 mins the

reaction mixture was opened to air and quenched in liquid nitrogen. An aliquot was removed and conversion determined by ^1H NMR spectroscopy. The product was purified four times by precipitation from tetrahydrofuran into cold diethyl ether, isolated by centrifugation and dried under vacuum overnight to give a pale yellow solid. The overall monomer conversion was determined from the ^1H NMR spectrum by measuring the decrease in intensity of the vinyl peaks associated with the monomer relative to mesitylene. Conversion (NMR): 79.9 % (NIPAM); 89.2 % (HEA); M_n (theoretical): $38700 \text{ g}\cdot\text{mol}^{-1}$; M_n (SEC) $56900 \text{ g}\cdot\text{mol}^{-1}$; M_w/M_n (SEC): 1.31.

3.5.3.5 General Procedure for nanoparticle preparation

Polymer (5 mg) was dissolved in acetone (5 mL) and added dropwise to a round bottom flask containing a stir bar and deionised water (10 mL) held at $50 \text{ }^\circ\text{C}$ over a period of one hr. The flask was left stirring, open to air at $50 \text{ }^\circ\text{C}$ for several hrs to allow acetone to evaporate. The resulting pale blue, partially turbid solution was used within 7 days. The preparation of 1,6-diphenyl-1,3,5-hexatriene (DPH)-loaded nanoparticles followed the same methodology only DPH was dissolved alongside polymer in acetone at a concentration of $0.05 \text{ mg}\cdot\text{mL}^{-1}$.

3.5.4 Assay Conditions

3.5.4.1 DLS assay

Nanoparticles ($570 \text{ }\mu\text{L}$) were transferred to a low volume, disposable polycarbonate cuvette and incubated at $50 \text{ }^\circ\text{C}$ in the Zetasizer Nano ZS for 30 mins. After this time $30 \text{ }\mu\text{L}$ of a concentrated glutathione solution was added to give the desired final

glutathione concentration. A measurement was recorded every 30 seconds (5 scans x 5 seconds).

3.5.4.2 Nanoparticle fluorescence assay

A generalised procedure for the fluorescence assay is as follows. Nanoparticles (190 μL) were incubated in a 96-well plate at 50 $^{\circ}\text{C}$ for 1 hr. 10 μL water or concentrated glutathione solution was added to give final glutathione concentrations of 0, 0.01 and 1 mM and the fluorescence monitored over a period of 2 hrs. Excitation wavelength set at 360 nm, emission wavelength at 460 nm and the plate maintained at 50 $^{\circ}\text{C}$ throughout.

3.5.4.3 UV-Visible spectrophotometric experiments

For each polymer tested, 2.5 mL of a 0.5 $\text{mg}\cdot\text{mL}^{-1}$ polymer solution was transferred to three disposable, polycarbonate cuvettes and a UV-visible spectrum recorded. Water or concentrated glutathione solution was added to give final glutathione concentrations of 0, 0.01 and 1 mM. The cuvettes were stirred at ambient conditions and their UV-visible spectra re-recorded after one hour and twenty hrs.

3.6 References

- 1 Duncan, R. The dawning era of polymer therapeutics. *Nat. Rev. Drug Discov.* **2003**, 2, 347-360.
- 2 Duncan, R.; Gaspar, R. Nanomedicine(s) under the Microscope. *Mol. Pharm.* **2011**, 8, 2101-2141.
- 3 Petros, R. A.; DeSimone, J. M. Strategies in the design of nanoparticles for therapeutic applications. *Nat. Rev. Drug Discov.* **2010**, 9, 615-627.
- 4 Peer, D.; Karp, J. M.; Hong, S.; Farokhzad, O. C.; Margalit, R.; Langer, R. Nanocarriers as an emerging platform for cancer therapy. *Nat. Nano.* **2007**, 2, 751-760.
- 5 Elsbahy, M.; Wooley, K. L. Design of polymeric nanoparticles for biomedical delivery applications. *Chem. Soc. Rev.* **2012**, 41, 2545-2561.
- 6 Duncan, R.; Lloyd, J. B.; Kopeček, J. Degradation of side chains of N-(2-hydroxypropyl) methacrylamide copolymers by lysosomal enzymes. *Biochem. Biophys. Res. Commun.* **1980**, 94, 284-290.
- 7 Abulateefeh, S. R.; Spain, S. G.; Thurecht, K. J.; Aylott, J. W.; Chan, W. C.; Garnett, M. C.; Alexander, C. Enhanced uptake of nanoparticle drug carriers via a thermoresponsive shell enhances cytotoxicity in a cancer cell line. *Biomater. Sci.* **2013**, 1, 434-442.
- 8 Ende, A. E. v. d.; Kravitz, E. J.; Harth, E. Approach to Formation of Multifunctional Polyester Particles in Controlled Nanoscopic Dimensions. *J. Am. Chem. Soc.* **2008**, 130, 8706-8713.
- 9 van der Ende, A. E.; Sathiyakumar, V.; Diaz, R.; Hallahan, D. E.; Harth, E. Linear release nanoparticle devices for advanced targeted cancer therapies with increased efficacy. *Polym. Chem.* **2010**, 1, 93-96.
- 10 Passarella, R. J.; Spratt, D. E.; van der Ende, A. E.; Phillips, J. G.; Wu, H.; Sathiyakumar, V.; Zhou, L.; Hallahan, D. E.; Harth, E.; Diaz, R. Targeted Nanoparticles That Deliver a Sustained, Specific Release of Paclitaxel to Irradiated Tumors. *Cancer Res.* **2010**, 70, 4550-4559.
- 11 Yang, F.; Cho, S.-W.; Son, S. M.; Bogatyrev, S. R.; Singh, D.; Green, J. J.; Mei, Y.; Park, S.; Bhang, S. H.; Kim, B.-S.; Langer, R.; Anderson, D. G. Genetic engineering of human stem cells for enhanced angiogenesis using

- biodegradable polymeric nanoparticles. *Proc. Natl. Acad. Sci. U.S.A.* **2010**, *107*, 3317-3322.
- 12 Palamoor, M.; Jablonski, M. M. Poly(ortho ester) Nanoparticle-Based Targeted Intraocular Therapy for Controlled Release of Hydrophilic Molecules. *Mol. Pharm.* **2012**, *10*, 701-708.
- 13 Musyanovych, A.; Schmitz-Wienke, J.; Mailänder, V.; Walther, P.; Landfester, K. Preparation of Biodegradable Polymer Nanoparticles by Miniemulsion Technique and Their Cell Interactions. *Macromol. Biosci.* **2008**, *8*, 127-139.
- 14 Vert, M. Aliphatic Polyesters: Great Degradable Polymers That Cannot Do Everything. *Biomacromolecules* **2004**, *6*, 538-546.
- 15 Putnam, D. Drug delivery: The heart of the matter. *Nat. Mater.* **2008**, *7*, 836-837.
- 16 Fu, K.; Pack, D.; Klibanov, A.; Langer, R. Visual Evidence of Acidic Environment Within Degrading Poly(lactic-co-glycolic acid) (PLGA) Microspheres. *Pharm. Res.* **2000**, *17*, 100-106.
- 17 Wu, C.; Belenda, C.; Leroux, J.-C.; Gauthier, M. A. Interplay of Chemical Microenvironment and Redox Environment on Thiol–Disulfide Exchange Kinetics. *Chem. Eur. J.* **2011**, *17*, 10064-10070.
- 18 Cheng, R.; Feng, F.; Meng, F.; Deng, C.; Feijen, J.; Zhong, Z. Glutathione-responsive nano-vehicles as a promising platform for targeted intracellular drug and gene delivery. *J. Control. Rel.* **2011**, *152*, 2-12.
- 19 Kim, T.-i.; Kim, S. W. Bioreducible polymers for gene delivery. *React. Funct. Polym.* **2011**, *71*, 344-349.
- 20 Khorsand Sourkahi, B.; Cunningham, A.; Zhang, Q.; Oh, J. K. Biodegradable Block Copolymer Micelles with Thiol-Responsive Sheddable Coronas. *Biomacromolecules* **2011**, *12*, 3819-3825.
- 21 Aleksanian, S.; Khorsand, B.; Schmidt, R.; Oh, J. K. Rapidly thiol-responsive degradable block copolymer nanocarriers with facile bioconjugation. *Polym. Chem.* **2012**, *3*, 2138-2147.
- 22 Sun, H.; Guo, B.; Cheng, R.; Meng, F.; Liu, H.; Zhong, Z. Biodegradable micelles with sheddable poly(ethylene glycol) shells for triggered intracellular release of doxorubicin. *Biomaterials* **2009**, *30*, 6358-6366.

- 23 Li, Y.-L.; Zhu, L.; Liu, Z.; Cheng, R.; Meng, F.; Cui, J.-H.; Ji, S.-J.; Zhong, Z. Reversibly Stabilized Multifunctional Dextran Nanoparticles Efficiently Deliver Doxorubicin into the Nuclei of Cancer Cells. *Angew. Chem. Int. Ed.* **2009**, *48*, 9914-9918.
- 24 Phillips, D. J.; Gibson, M. I. Degradable thermoresponsive polymers which display redox-responsive LCST Behaviour. *Chem. Commun.* **2012**, *48*, 1054-1056.
- 25 Phillips, D. J.; Gibson, M. I. Biodegradable Poly(disulfide)s Derived from RAFT Polymerization: Monomer Scope, Glutathione Degradation, and Tunable Thermal Responses. *Biomacromolecules* **2012**, *13*, 3200-3208.
- 26 Summers, M. J.; Phillips, D. J.; Gibson, M. I. "Isothermal" LCST transitions triggered by bioreduction of single polymer end-groups. *Chem. Commun.* **2013**, *49*, 4223-4225.
- 27 Gibson, M. I.; O'Reilly, R. K. To aggregate, or not to aggregate? considerations in the design and application of polymeric thermally-responsive nanoparticles. *Chem. Soc. Rev.* **2013**, *42*, 7204-7213.
- 28 Magnusson, J. P.; Khan, A.; Pasparakis, G.; Saeed, A. O.; Wang, W.; Alexander, C. Ion-Sensitive "Isothermal" Responsive Polymers Prepared in Water. *J. Am. Chem. Soc.* **2008**, *130*, 10852-10853.
- 29 Fu, H.; Policarpio, D. M.; Batteas, J. D.; Bergbreiter, D. E. Redox-controlled 'smart' polyacrylamide solubility. *Polym. Chem.* **2010**, *1*, 631-633.
- 30 Shepherd, J.; Sarker, P.; Swindells, K.; Douglas, I.; MacNeil, S.; Swanson, L.; Rimmer, S. Binding Bacteria to Highly Branched Poly(N-isopropyl acrylamide) Modified with Vancomycin Induces the Coil-to-Globule Transition. *J. Am. Chem. Soc.* **2010**, *132*, 1736-1737.
- 31 Hornig, S.; Heinze, T.; Becer, C. R.; Schubert, U. S. Synthetic polymeric nanoparticles by nanoprecipitation. *J. Mater. Chem.* **2009**, *19*, 3838-3840.
- 32 Schubert, S.; Delaney, J. J. T.; Schubert, U. S. Nanoprecipitation and nanoformulation of polymers: from history to powerful possibilities beyond poly(lactic acid). *Soft Matter* **2011**, *7*, 1581-1588.
- 33 Fessi, H. D., J. P.; Puisieux, F.; Thies, C.; Devissaguet, J. P. *US Pat.*, 5118528. **1988**.

- 34 Fessi, H.; Puisieux, F.; Devissaguet, J. P.; Ammoury, N.; Benita, S. Nanocapsule formation by interfacial polymer deposition following solvent displacement. *Int. J. Pharm.* **1989**, *55*, R1-R4.
- 35 Govender, T.; Stolnik, S.; Garnett, M. C.; Illum, L.; Davis, S. S. PLGA nanoparticles prepared by nanoprecipitation: drug loading and release studies of a water soluble drug. *J. Control. Rel.* **1999**, *57*, 171-185.
- 36 Zhang, C.; Pansare, V. J.; Prud'homme, R. K.; Priestley, R. D. Flash nanoprecipitation of polystyrene nanoparticles. *Soft Matter* **2012**, *8*, 86-93.
- 37 Liebert, T.; Hornig, S.; Hesse, S.; Heinze, T. Nanoparticles on the Basis of Highly Functionalized Dextrans. *J. Am. Chem. Soc.* **2005**, *127*, 10484-10485.
- 38 Bilati, U.; Allémann, E.; Doelker, E. Development of a nanoprecipitation method intended for the entrapment of hydrophilic drugs into nanoparticles. *Eur. J. Pharm. Sci.* **2005**, *24*, 67-75.
- 39 Slater, R. A.; McDonald, T. O.; Adams, D. J.; Draper, E. R.; Weaver, J. V. M.; Rannard, S. P. Architecture-driven aqueous stability of hydrophobic, branched polymer nanoparticles prepared by rapid nanoprecipitation. *Soft Matter* **2012**, *8*, 9816-9827.
- 40 Babiuch, K.; Pretzel, D.; Tolstik, T.; Vollrath, A.; Stanca, S.; Foertsch, F.; Becer, C. R.; Gottschaldt, M.; Biskup, C.; Schubert, U. S. Uptake of Well-Defined, Highly Glycosylated, Pentafluorostyrene-Based Polymers and Nanoparticles by Human Hepatocellular Carcinoma Cells. *Macromol. Biosci.* **2012**, *12*, 1190-1199.
- 41 Becer, C. R.; Babiuch, K.; Pilz, D.; Hornig, S.; Heinze, T.; Gottschaldt, M.; Schubert, U. S. Clicking Pentafluorostyrene Copolymers: Synthesis, Nanoprecipitation, and Glycosylation. *Macromolecules* **2009**, *42*, 2387-2394.
- 42 Dutta, P.; Shrivastava, S.; Dey, J. Amphiphilic Polymer Nanoparticles: Characterization and Assessment as New Drug Carriers. *Macromol. Biosci.* **2009**, *9*, 1116-1126.
- 43 Patterson, J. P.; Sanchez, A. M.; Petzetakis, N.; Smart, T. P.; Epps, I. I. I. T. H.; Portman, I.; Wilson, N. R.; O'Reilly, R. K. A simple approach to characterizing block copolymer assemblies: graphene oxide supports for high contrast multi-technique imaging. *Soft Matter* **2012**, *8*, 3322-3328.
- 44 Legrand, P.; Lesieur, S.; Bochet, A.; Gref, R.; Raatjes, W.; Barratt, G.; Vauthier, C. Influence of polymer behaviour in organic solution on the

- production of polylactide nanoparticles by nanoprecipitation. *Int. J. Pharm.* **2007**, *344*, 33-43.
- 45 Beck-Broichsitter, M.; Rytting, E.; Lehardt, T.; Wang, X.; Kissel, T. Preparation of nanoparticles by solvent displacement for drug delivery: A shift in the “ouzo region” upon drug loading. *Eur. J. Pharm. Sci.* **2010**, *41*, 244-253.
- 46 Hornig, S.; Heinze, T. Efficient Approach To Design Stable Water-Dispersible Nanoparticles of Hydrophobic Cellulose Esters. *Biomacromolecules* **2008**, *9*, 1487-1492.
- 47 Perevyazko, I. Y.; Delaney, J. T.; Vollrath, A.; Pavlov, G. M.; Schubert, S.; Schubert, U. S. Examination and optimization of the self-assembly of biocompatible, polymeric nanoparticles by high-throughput nanoprecipitation. *Soft Matter* **2011**, *7*, 5030-5035.
- 48 Karnik, R.; Gu, F.; Basto, P.; Cannizzaro, C.; Dean, L.; Kyei-Manu, W.; Langer, R.; Farokhzad, O. C. Microfluidic Platform for Controlled Synthesis of Polymeric Nanoparticles. *Nano Lett.* **2008**, *8*, 2906-2912.
- 49 Cui, H.; Hodgdon, T. K.; Kaler, E. W.; Abezgauz, L.; Danino, D.; Lubovsky, M.; Talmon, Y.; Pochan, D. J. Elucidating the assembled structure of amphiphiles in solution via cryogenic transmission electron microscopy. *Soft Matter* **2007**, *3*, 945-955.
- 50 Saaka, Y.; Deller, R. C.; Rodger, A.; Gibson, M. I. Exploiting Thermoresponsive Polymers to Modulate Lipophilicity: Interactions With Model Membranes. *Macromol. Rapid Commun.* **2012**, *33*, 779-784.
- 51 Klaikherd, A.; Nagamani, C.; Thayumanavan, S. Multi-Stimuli Sensitive Amphiphilic Block Copolymer Assemblies. *J. Am. Chem. Soc.* **2009**, *131*, 4830-4838.
- 52 Jeong, N. S.; Hasan, M.; Phillips, D. J.; Saaka, Y.; O'Reilly, R. K.; Gibson, M. I. Polymers with molecular weight dependent LCSTs are essential for cooperative behaviour. *Polym. Chem.* **2012**, *3*, 794-799.
- 53 Fernandez-Trillo, F.; van Hest, J. C. M.; Thies, J. C.; Michon, T.; Weberskirch, R.; Cameron, N. R. Fine-tuning the transition temperature of a stimuli-responsive polymer by a simple blending procedure. *Chem. Commun.* **2008**, 2230-2232.

- 54 Eggenhuisen, T. M.; Becer, C. R.; Fijten, M. W. M.; Eckardt, R.; Hoogenboom, R.; Schubert, U. S. Libraries of Statistical Hydroxypropyl Acrylate Containing Copolymers with LCST Properties Prepared by NMP. *Macromolecules* **2008**, *41*, 5132-5140.
- 55 Takei, Y. G.; Aoki, T.; Sanui, K.; Ogata, N.; Okano, T.; Sakurai, Y. Temperature-responsive bioconjugates. 2. Molecular design for temperature-modulated bioseparations. *Bioconjugate Chem.* **1993**, *4*, 341-346.
- 56 Shah, M.; Hsueh, P.-Y.; Sun, G.; Chang, H. Y.; Janib, S. M.; MacKay, J. A. Biodegradation of elastin-like polypeptide nanoparticles. *Protein Sci.* **2012**, *21*, 743-750.
- 57 Wang, Y.-C.; Tang, L.-Y.; Li, Y.; Wang, J. Thermoresponsive Block Copolymers of Poly(ethylene glycol) and Polyphosphoester: Thermo-Induced Self-Assembly, Biocompatibility, and Hydrolytic Degradation. *Biomacromolecules* **2008**, *10*, 66-73.

Chapter 4

4. Isothermally-Responsive Polymers Triggered by Selective Binding of Fe³⁺ to Siderophoric Catechol End-Groups

4.1 Chapter Summary

Thermo-responsive polymers have attracted huge interest in the development of smart/adaptable materials for bio-medicine, particularly due to changes in their solubility above the Lower Critical Solution Temperature. However, temperature is not always an appropriate or desirable stimulus given the variety of other cellular microenvironments that exist including pH, redox potentials, ionic strength and metal ion concentration. Here we achieve a highly specific, isothermal solubility switch for poly(*N*-isopropylacrylamide) by application of ferric iron (Fe³⁺), a species implicated in a range of neurodegenerative conditions. This is achieved by the site-specific incorporation of (Fe³⁺-binding) catechol units onto the polymer chain-end, inspired by the mechanism by which bacterial siderophores sequester iron from mammalian hosts. The ability to manipulate the hydrophilicity of responsive systems without the need for a temperature gradient offers an exciting approach towards preparing increasingly selective, targeted polymeric materials.

4.2 Introduction

The design of systems which respond to small changes in local environment has been mastered by Nature. Within the human body for instance, the pancreas reacts to modulate our blood sugar levels; we intrinsically respond to repair wounds and muscular reflex reactions react to pain to protect the body from further damage. Inspired by this, synthetic stimuli-responsive or “smart” materials have increasingly found themselves at the forefront of scientific and technological innovation.¹ Such systems can undergo significant macroscopic property changes in response to a wide range of stimuli such as redox potentials, pH and commonly temperature, where aqueous polymer solutions can reversibly precipitate, often upon heating through a Lower Critical Solution Temperature (LCST).² This property has been applied to a number of areas such as for catalysis,³ purification⁴ and to control cell culture and adhesion.⁵ Moreover, the biological potential of these systems, either for controlled release⁶ or to modulate interactions with biological membranes,^{7, 8} is obvious given the wide range of microenvironments found in the body. These environments can also be combined to produce increasingly complex materials eliciting multiple responses in a parallel or sequential manner.⁹ To exemplify a thermo-responsive polymer, the associated solubility switch can be manipulated without the need for a temperature change (*i.e. isothermally*) by using alternative triggers to control the systems’ hydrophilic-hydrophobic balance. This has been achieved using stimuli such as redox potentials,^{10, 11} light,¹² pH^{13, 14} and ionic strength.¹⁵

A lesser studied stimulus is that of host-guest complexation based on metal ion binding. Metal ions have also been implicated as biomarkers in certain disease states providing an attractive precedent for targeted, responsive systems.¹⁶ Chiper *et al.*

have prepared terpyridine-terminated p(*N*-isopropylacrylamide), pNIPAM, samples where the LCST is dependent on the addition of Zn^{2+} and Fe^{2+} to trigger metallo-supramolecular dimer formation.¹⁷ Sharma and Srivastava have used metal ions to cross-link thermosensitive polyaspartamides containing propylimidazole pendants, lowering the LCST through stabilisation of the globular form.¹⁸ Rimmer and co-workers have functionalised hyperbranched pNIPAM samples with imidazole end-groups and observed an increase in LCST in the presence of Cu^{2+} due to an increased hydrophilicity of the polymer.¹⁹ Crown ethers have been used to modulate the LCST depending on the binding affinity of the metal ion employed,^{20, 21} and thermo-responsive ratiometric fluorescent indicators have been prepared for the detection of Cu^{2+} , Zn^{2+} , Pb^{2+} and K^+ .²²⁻²⁴

Another metal of biological interest is iron given its role in a variety of functions such as oxygen transport, metabolic processes and the association of undesirable iron levels with conditions such as anaemia, Alzheimer's and Parkinson's.^{25, 26} Ferric iron (Fe^{3+}) predominates in aerobic conditions but, given its propensity to form compounds with poor aqueous solubility in these conditions ($\sim 10^{-18}$ M), requires proteins like transferrin, or heme for efficient transportation.²⁷ Bacteria are also dependent on Fe^{3+} to survive where it is obtained through competitive abstraction from mammalian hosts using siderophores.²⁸ These low molecular weight compounds contain functional groups such as α -hydroxycarboxylates, hydroxamates and catecholates capable of binding Fe^{3+} with association constants in excess of 10^{50} M, mimics of which have provided the basis for pharmaceutical and antibiotic drug targeting devices.^{29, 30} Enterobactin remains one of the best-understood siderophores where three catecholate functionalities linked to a triserine macrocycle are used to coordinate iron.³¹ We hypothesised that the catechol- Fe^{3+} binding motif could be

applied to responsive polymers in order to influence the hydrophilic-hydrophobic balance of a polymer system *isothermally*. One of the few examples exhibiting a response to Fe^{3+} has been demonstrated by Yin and co-workers who prepared an isothermal, thermochromic sensor based on a co-polymer containing porphyrin groups in the side-chain. This system exhibited thermochromic characteristics in the presence of a variety of ions,³² though multiple side-chain interactions were required to achieve the observed response. Alternatively, polymer function can be elegantly manipulated using simple alterations in polymer end-group functionality. In this fashion, absolute control over a polymer property, such as solubility, can be maintained using only one or two functionalisation events, rather than the multiple reactions required on a polymer side-chain. This concept is also easily accessible given the development of controlled radical processes such as Reversible Addition-Fragmentation Chain Transfer (RAFT) polymerisation which afford high levels of control over polymer structure.³³ End-groups can therefore be installed with high degrees of fidelity and can be easily accessed based on the chain transfer agent used, or through post polymerisation modification techniques.³⁴

Despite this, few reports pursuing this approach exist. Jochum *et al.* have prepared azobenzene chain-end functional poly[(oligo ethylene glycol) methyl ether methacrylate], allowing the LCST to be modulated by the wavelength of applied light.³⁵ Rimmer and co-workers have functionalised hyperbranched pNIPAM samples with vancomycin or polymyxin end-groups which, in the presence of Gram-positive and Gram-negative bacteria respectively, undergo a coil-to-globule phase transition.^{36, 37} Stayton and co-workers have used pH to alter the ionisation state of carboxylic acid-terminated pNIPAM-propylacrylic acid co-polymers and hence the LCST,³⁸ whilst we have applied the anti-oxidant glutathione to trigger isothermal

transitions in both linear systems and polymer nanoparticles containing reduction-sensitive disulfide bonds.^{39, 40} Herein, we seek to exploit isothermal polymer technologies in combination with the biologically-relevant catechol binding motif to prepare systems whereby the solubility can be controlled in response to the presence of Fe^{3+} as an alternative to temperature changes (Figure 4.1).

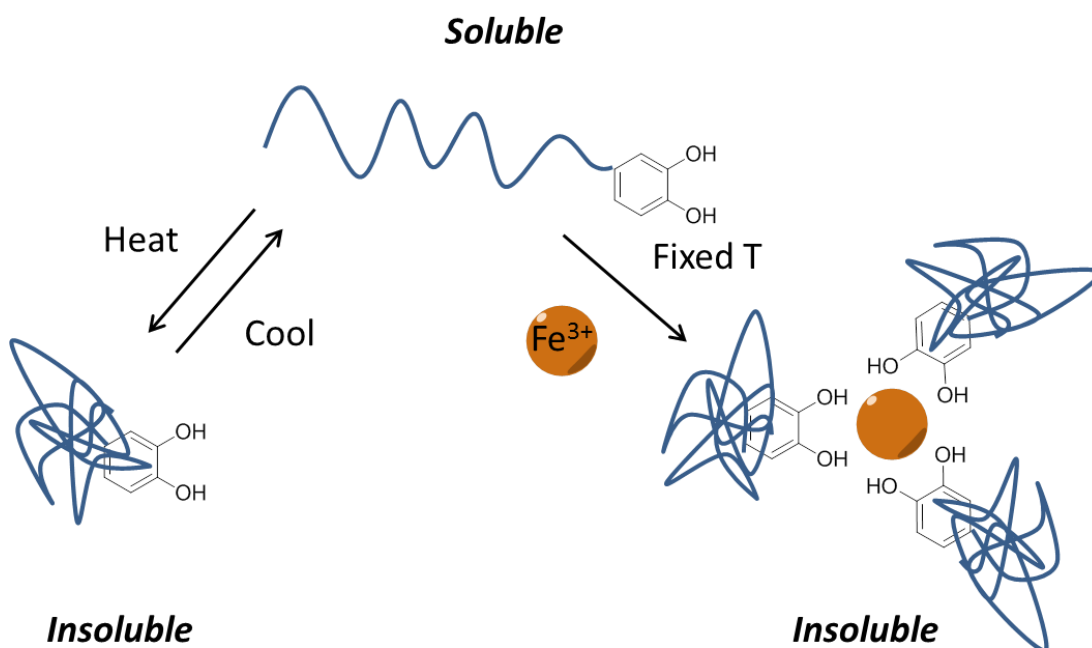
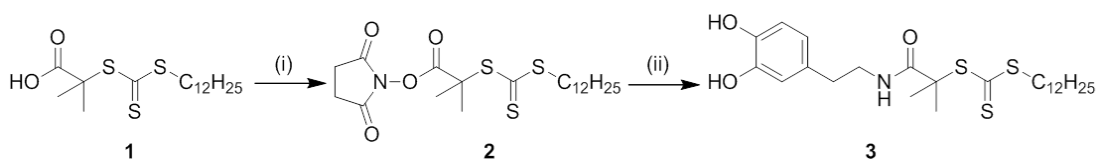


Figure 4.1 Isothermal concept: An LCST and polymer conformational change can be induced through catechol- Fe^{3+} binding, rather than using a temperature change.

4.3 Results and Discussion

To prepare catechol-functional polymers, a new chain-transfer agent was synthesised based on an adaptation of the method described by Zobrist *et al.*⁴¹ First, 2-(dodecylthiocarbonothioylthio)-2-methylpropanoic acid, **1**, was prepared by the reaction of dodecane thiol with carbon disulfide and 2-bromo methyl propionic acid in the presence of potassium phosphate, as described by Skey and O'Reilly.⁴² Standard coupling chemistry using *N,N'*-diisopropylcarbodiimide (DIC) and *N*-hydroxysuccinimide (NHS) was then employed to furnish the activated ester **2** which was finally reacted with a slight excess of dopamine hydrochloride (Dop.HCl), in the presence of triethylamine (TEA), to furnish **3** in good yield (Scheme 4.1).



Scheme 4.1 Synthetic scheme for preparation of catechol-functional CTA **3**: (i) NHS/DIC, THF, 0 °C → r.t, 16 hrs; (ii) Dop.HCl/TEA, MeOH, r.t, 48 hrs.

Importantly, the product could be isolated by precipitation in hexane, negating the need for column chromatography which may be complicated by the presence of an unprotected catechol unit. Moreover, no by-product generated by aminolysis of the trithiocarbonate was observed,^{11, 34} as confirmed by ¹H and ¹³C NMR spectroscopy (Figure 4.2). To exemplify the former, signature catechol aromatic peaks 6.78, 6.67 and 6.57 ppm were observed, together with peaks corresponding to the dodecyl chain between 0.88 and 1.69 ppm.

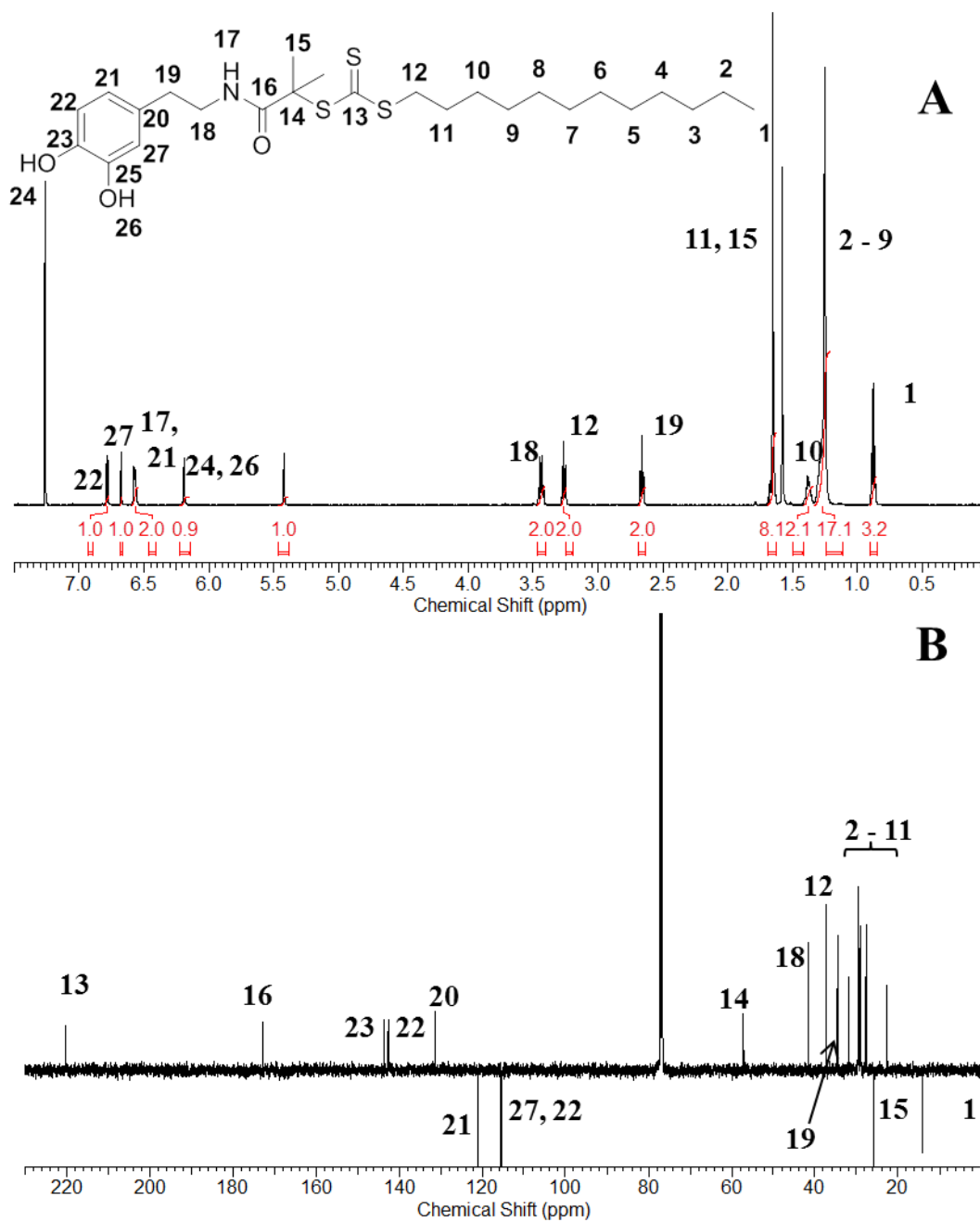


Figure 4.2 NMR spectroscopic characterisation of 1-((3,4-dihydroxyphenethyl)amino)2-methyl-1-oxopropan-2-yl dodecyl carbonotrithioate in CDCl_3 : A) ^1H and B) ^{13}C spectra.

Infrared spectroscopy can also be used to follow the successful preparation of chain transfer agent **3** (Figure 4.3). Activation of the carboxylic acid terminus of **1** with an NHS ester was confirmed by the loss of the C=O stretch at 1700 cm^{-1} and replacement with two C=O stretches at 1735 and 1776 cm^{-1} . Elaboration to catechol-functional chain transfer agent **3** is reflected in the gain of an N-H stretch at 3342 cm^{-1} and an O-H stretch at 3196 cm^{-1} . Furthermore, the two C=O stretches at 1735 and 1776 cm^{-1} have been replaced by two characteristic amide stretches at 1623 and 1523 cm^{-1} .

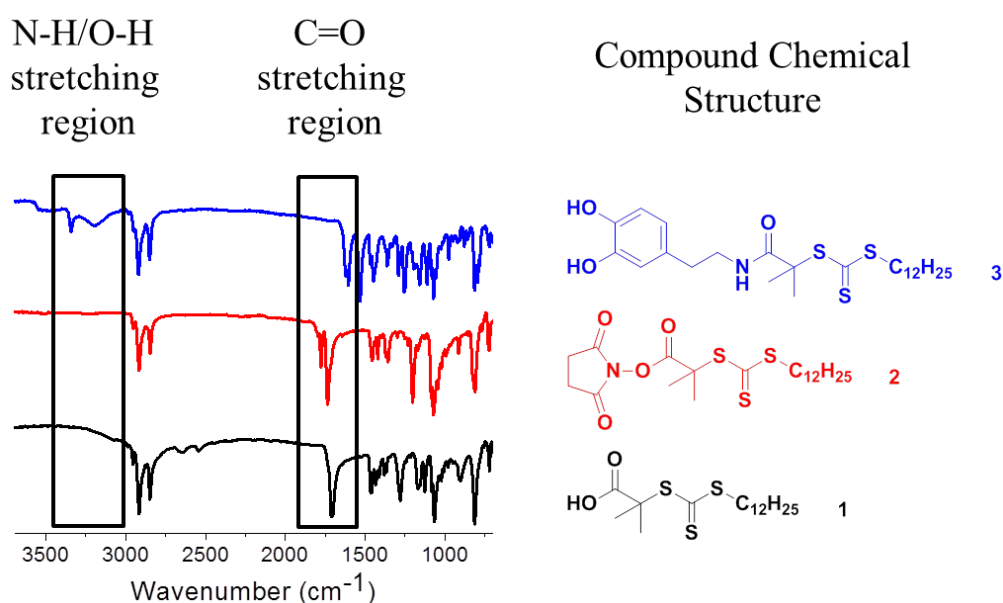


Figure 4.3 Infrared spectra showing the sequential modification of the carboxylic acid terminus of CTA **1** to the activated ester **2** and catechol **3**.

N-isopropylacrylamide (NIPAM) was then polymerised using chain transfer agent **3** as a model thermoresponsive material to give polymers of two different molecular weights (Table 4.1, Figure 4.4). The polymerisation kinetics of **pNIPAM-1** are shown in Figure 4.4. High conversion was reached quickly (> 70% after 1 hour, Figure 4.5A) and first order kinetics were observed (Figure 4.5B), as expected in a controlled radical process such as RAFT. Good agreement between the theoretical and SEC-determined molecular weights was observed, albeit with the final polymer (180 mins, 98.0 % conversion) giving a slightly higher SEC value (Figure 4.5C/D). This may be due to a small amount of radical-radical coupling, commonly observed by RAFT given its free radical initiation step, and is also seen as a small, high molecular weight shoulder.⁴³

Table 4.1 Characterisation of catechol-terminated pNIPAM samples prepared in this study.

Polymer	[M]:[CTA]	Conversion	$M_{n(th)}$	$M_{n(SEC)}$	M_w/M_n^b
		(%) ^a	(g.mol ⁻¹) ^a	(g.mol ⁻¹) ^b	
pNIPAM-1	115	98.0	12500	14000	1.12
pNIPAM-2	60	44.4	3000	5100	1.09

^aDetermined by ¹H NMR spectroscopy relative to an internal standard (mesitylene);

^bDetermined by SEC (DMF inc. 5 mM NH₄BF₄) relative to PMMA standards.

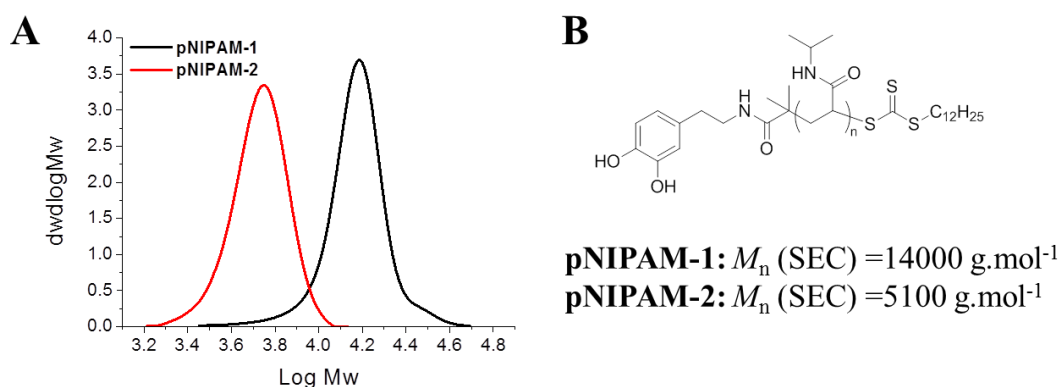


Figure 4.4 (A) SEC characterisation of **pNIPAM-1/2**; (B) Polymer structure.

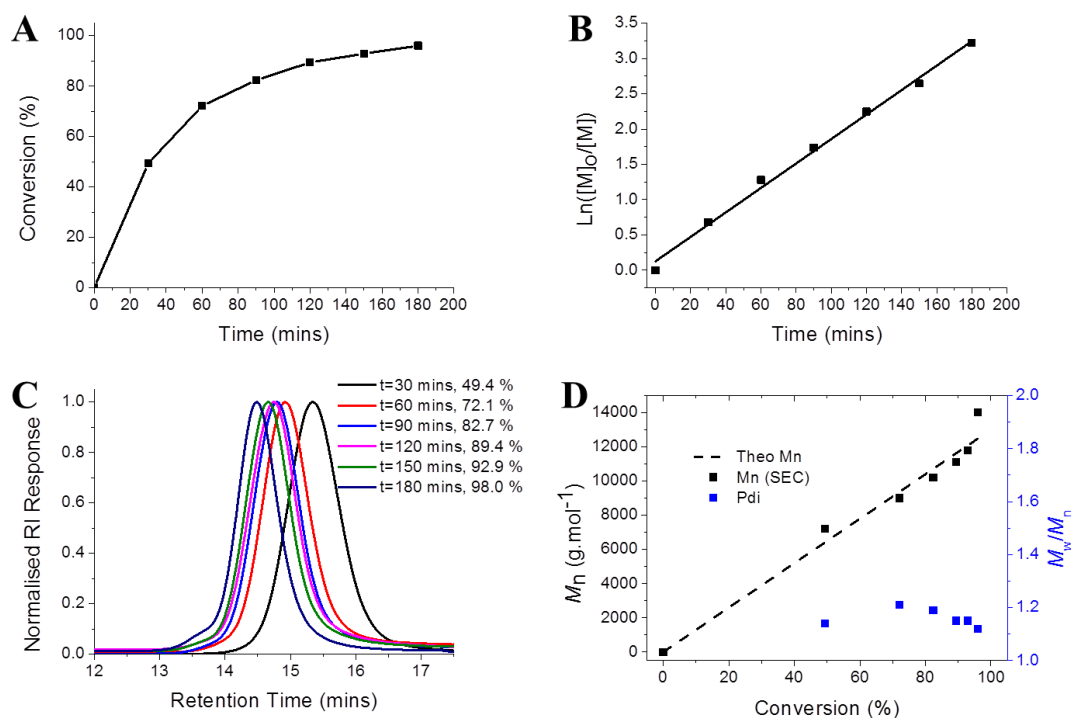


Figure 4.5 Results from RAFT polymerisation of **NIPAM-1**: (A) the time-dependent monomer conversion; (B) pseudo first order kinetic plot; (C) SEC traces of polymer at different polymerisation times and (D) evolution of M_n and M_w/M_n values of the polymer as a function of monomer conversion.

Representative MALDI-ToF data for **pNIPAM-2** confirmed the successful installation of the desired catechol end-group where a distribution corresponding to sodium adducts was observed (Figure 4.6). A secondary distribution at low m/z was also observed relating to sodium adducts of pNIPAM chains with no end-groups, presumably derived from the free radical-like initiation process. ^1H NMR spectroscopic analysis of **pNIPAM-2** further highlights successful polymer synthesis with broad peaks at 6.7 ppm and 4.0 ppm corresponding to the aromatic protons and isopropyl proton in the polymer repeat unit respectively being observed (Figure 4.7).

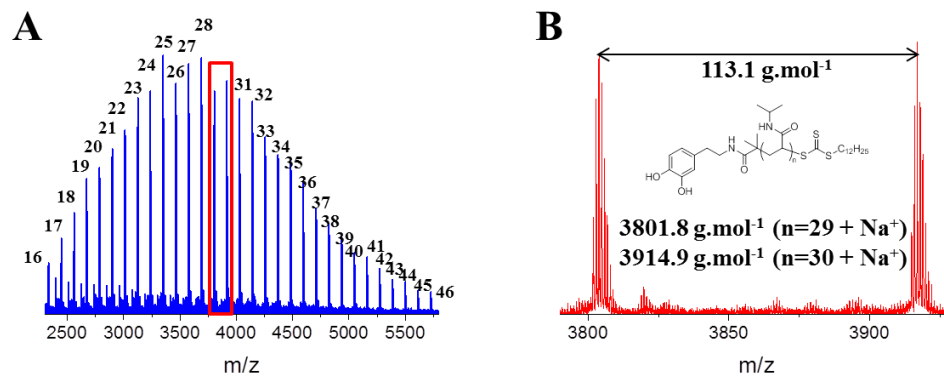


Figure 4.6 MALDI-ToF mass spectrum of **pNIPAM-2**: (A) Full spectrum with labels defining number of repeat units in each peak; (B) Representative example of peak spacing and its assignment.

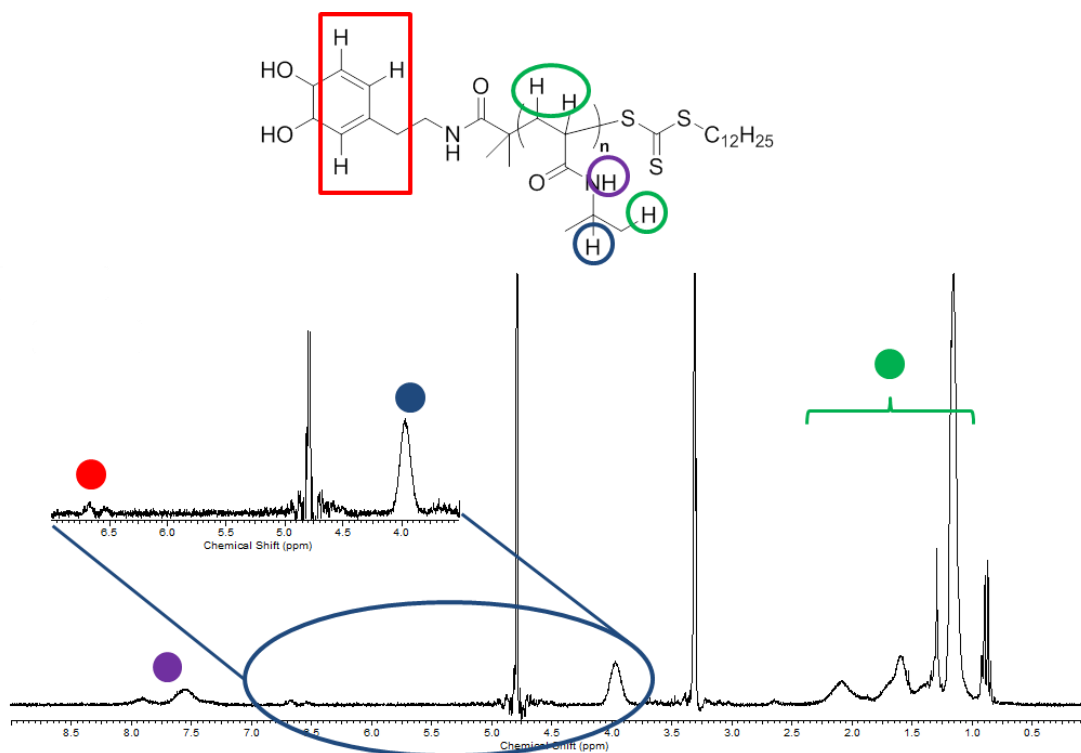
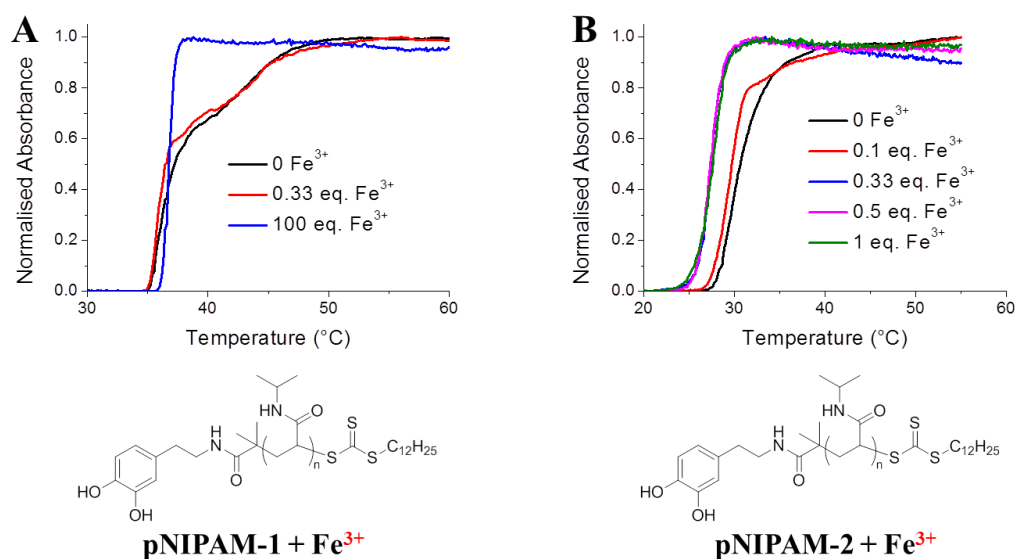


Figure 4.7 ^1H NMR spectrum of **pNIPAM-2** in MeOD.

With functional polymers to hand, **pNIPAM-1** was dissolved in water at a concentration of 1 mg.mL^{-1} and the cloud point (the measurable property of the LCST) was determined by turbidimetry to be $37.3 \text{ }^\circ\text{C}$ (Figure 4.8A/C). Next, the influence of Fe^{3+} on the polymer solution was investigated. The interaction between

catechol and tri-basic metal cations usually involves the displacement of 6 protons, hence Fe^{3+} is widely accepted to bind in an octahedral geometry generated by 3 catechol functions.²⁸ The aqueous polymer solution was therefore doped with 0.33 equivalents of $\text{FeCl}_3 \cdot 6\text{H}_2\text{O}$, giving a 3:1 ratio of catechol units: Fe^{3+} , and the cloud point measured (Figure 4.8A/C). A slight decrease was observed (0.5 °C) which did not change further, even upon the introduction of a large amount (100 equivalents) of the iron salt (Figure 4.8A/C). Interestingly, the shape of the turbidimetry curve in the latter case was noticeably sharper, potentially due to the extra water ordering afforded by the excess of salt in solution. To better assess whether the decrease described above was due to the desired binding motif, and in a bid to promote a greater cloud point shift in the presence of iron, the smaller **pNIPAM-2** was next employed. This was selected given the effect of polymer end-group on the cloud point is generally observed to increase with decreasing molecular weight. This occurs as the end-groups contribute a higher percentage of the total structure and hence any effect is amplified.^{44, 45} The cloud point of this sample at 1 mg.mL^{-1} was determined to be 30.7 °C (Figure 4.8B/C), lower than that of **pNIPAM-1** suggesting the large hydrophobic character of the catechol and dodecane end-groups outweighs the inversely proportional relationship previously reported between pNIPAM cloud point and molecular weight.⁴⁶ Pleasingly, the addition of 0.1 equivalents Fe^{3+} promoted a decrease in cloud point to 29.8 °C which was lowered further to 27.4 °C in the presence of 0.33 equivalents Fe^{3+} (Figure 4.8B/C). This result provided strong indication of catechol binding with the decreased cloud point potentially rationalised by either an increased ordering of the system afforded upon the formation of multimeric species bound to an Fe^{3+} core, or due to an elevated local polymer concentration, as has been previously observed with branched polymers.⁴⁷

Interestingly, the addition of extra Fe^{3+} (up to 1 equivalent) had no further effect on the cloud point suggesting 0.33 equivalents was sufficient to introduce a maximum system change, implicit of octahedral binding, and confirming the decrease was not a simple “salting-out” effect.⁴⁸

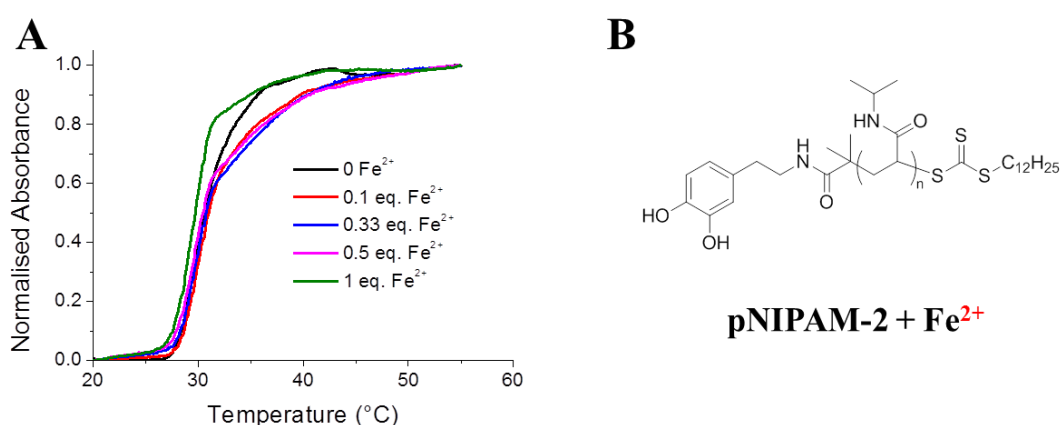


C	Equivalents Fe^{3+}/Cloud Point (°C)					
	0	0.1	0.33	0.5	1	100
pNIPAM-1	37.3	-	36.8	-	-	36.8
pNIPAM-2	30.7	29.8	27.4	27.4	27.4	-

Figure 4.8 Polymer structures and cloud points with Fe^{3+} of: (A) **pNIPAM-1** and (B) **pNIPAM-2**; (C) Tabulated summary of cloud points (polymer concentration = 1 mg.mL^{-1}).

To further probe the specificity of this response **pNIPAM-2** was also investigated with $\text{FeCl}_2 \cdot 4\text{H}_2\text{O}$ (Figure 4.9). The binding of catecholate-based siderophores to Fe^{2+} is significantly weaker than that of Fe^{3+} due to the reduced charge density on the coordinated cation.²⁸ This is important as one of the main known mechanisms for the release of iron from siderophores comprises the reduction of siderophore-bound Fe^{3+}

to Fe^{2+} followed by spontaneous release or competitive sequestration of this reduced species.⁴⁹ As anticipated, minimal change in cloud point at Fe^{2+} concentrations up to 0.5 equivalents was observed. A slight decrease of 0.7 °C occurred in the presence of 1 eq. Fe^{2+} which, given these measurements are performed in aerobic conditions, may be the result of partial oxidation to Fe^{3+} and hence some minimal complexation with the catechol units.



C

	Equivalents Fe^{2+} /Cloud Point (°C)				
	0	0.1	0.33	0.5	1
pNIPAM-2	30.6	30.7	30.7	30.6	29.9

Figure 4.9 (A) Cloud point data and (B) Polymer structure of **pNIPAM-2** with Fe^{2+} ; (C) Tabulated summary of cloud points (polymer concentration = 1 mg.mL⁻¹).

Secondly, to confirm the role of the catechol functionality, a benzyl-terminated pNIPAM of similar molecular weight to that of pNIPAM-2 (**pNIPAM-3**, M_n (SEC) = 5500 g.mol⁻¹, Table 4.2, Figure 4.10) was prepared as a negative control. The cloud point of this polymer was determined (Figure 4.11) as 35.6 °C with minimal change noted at any Fe^{3+} concentration. Taken together, these controls highlight that the change in cloud point observed in Figure 4.7B was due to selective catechol- Fe^{3+} binding rather than through non-specific interactions.

Table 4.2 Characterisation of benzyl-terminated pNIPAM.

Polymer	[M]:[CTA]	Conversion (%) ^a	$M_{n(th)}$ (g.mol ⁻¹) ^a	$M_{n(SEC)}$ (g.mol ⁻¹) ^b	M_w/M_n ^b
pNIPAM-3	50	76.3	4300	5500	1.08

^aDetermined by ¹H NMR relative to an internal standard (mesitylene); ^bDetermined by SEC (DMF inc. 5 mM NH₄BF₄) relative to PMMA standards.

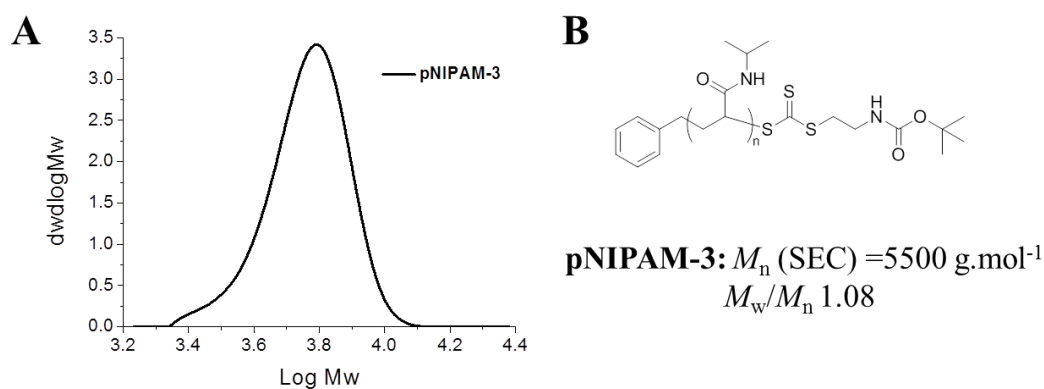


Figure 4.10 (A) SEC characterisation of pNIPAM-3; (B) Polymer structure.

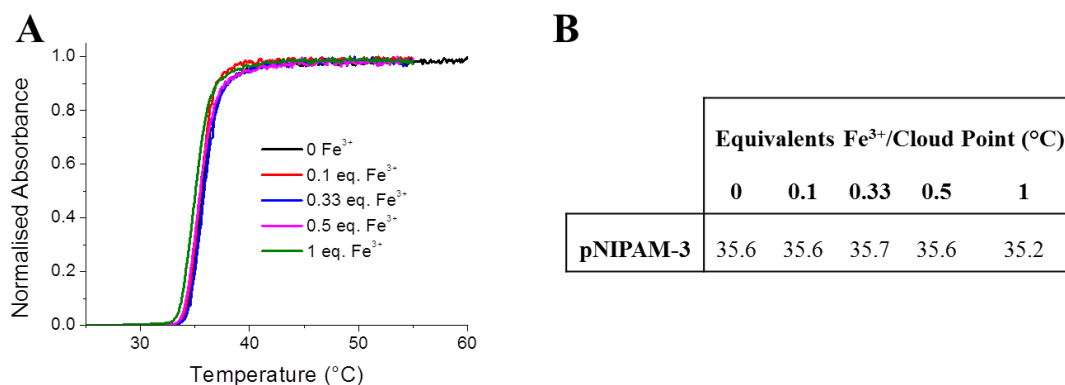


Figure 4.11 (A) Cloud point data and (B) Tabulated summary of cloud points for pNIPAM-3 (concentration = 1 mg.mL⁻¹) and Fe³⁺.

Importantly the introduction of 0.33 eq. Fe^{3+} triggered a decrease in **pNIPAM-2** cloud point of 3.3 °C, providing a window in which an isothermal transition could be achieved. To verify this, the following turbidimetry experiment was devised. A 1 $\text{mg}\cdot\text{mL}^{-1}$ polymer solution was transferred to wells of a 96-well plate and incubated at 25 °C. This was selected to be below the cloud point of the polymer alone but above that observed in the presence of 0.33 equivalents of Fe^{3+} (Figure 4.8B). The absorbance at 650 nm was then monitored for 25 mins to confirm no spontaneous polymer precipitation. After this time, the iron salt was added to one well and, as a control, water to the other. A rapid and significant increase in absorbance by approximately 0.35 units was observed upon the addition of Fe^{3+} indicative of precipitation. By comparison, no change was observed in the absence of iron (Figure 4.12).

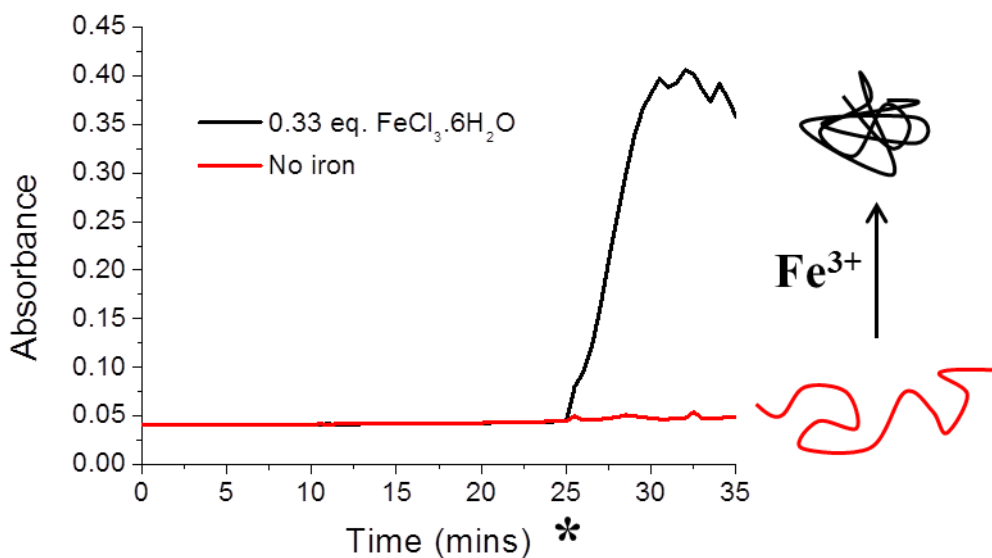


Figure 4.12 Isothermal turbidimetry data for **pNIPAM-2** (polymer concentration = 1 $\text{mg}\cdot\text{mL}^{-1}$). Temperature = 25 °C, $\text{FeCl}_3\cdot 6\text{H}_2\text{O}$ added at time indicated by asterisk.

Inset: Addition of Fe^{3+} triggers a coil-to-globule transition.

4.4 Conclusions

Inspired by the action of siderophores, we have presented a method for controlling the cloud point of a polymeric system exploiting, for the first time, the powerful catechol-Fe³⁺ binding motif. This was achieved using an elegant, single chain-end binding event with the effect amplified in lower molecular weight polymers. The addition of Fe³⁺ stimulated a decrease in transition temperature with maximum change observed with a catechol:Fe³⁺ ratio of 3:1. This phenomenon, not noted in the presence of Fe²⁺, was subsequently exploited to promote isothermal polymer precipitation. Careful tuning of this temperature through judicious selection of polymer, molecular weight and concentration will be a focus for future study. A promising application of this system may lie in selective cell uptake given the pre-existing precedent for hydrophobic polymers to readily cross biological barriers.^{7,8}

4.5 Experimental

4.5.1 Materials

All chemicals were used as supplied. Diethyl ether, ethyl acetate, hexane, methanol, tetrahydrofuran, triethylamine and toluene were all purchased from Fisher Scientific at laboratory reagent grade. Deuterated chloroform (99.8 atom % D), deuterium oxide (99.9 atom % D), *N*-hydroxysuccinimide (98.0 %), *N,N*-diisopropylcarbodiimide (99.0 %), *N*-isopropylacrylamide (97.0 %), 4,4'-azobis(4-cyanovaleric acid) (≥ 98.0 %), mesitylene (97.0 %), iron(III) chloride hexahydrate (97.0 %) and iron(II) tetrahydrate (98.0 %) were all purchased from Sigma-Aldrich. Dopamine hydrochloride (99.0 %) was purchased from VWR International Ltd. 2-(Dodecylthiocarbonothioylthio)-2-methylpropanoic acid (Chapter 2) and benzyl 2-[(*tert*-butoxycarbonyl)amino]ethyl trithiocarbonate (Chapter 3) were synthesised as described in previous chapters.

4.5.2 Analytical Methods

NMR spectroscopy (^1H , ^{13}C) was conducted on a Bruker AV-250, Bruker DRX-500 or Bruker AV III-600 spectrometer using deuterated chloroform or deuterium oxide as solvent. All chemical shifts are reported in ppm (δ) relative to the solvent used.

High resolution mass spectra were recorded on a Bruker Electrospray Ultra-High Resolution tandem TOF mass spectrometer using electrospray ionization (ESI) in positive mode on samples prepared in methanol. MALDI-ToF (matrix-assisted laser desorption ionisation time-of-flight mass spectrometry) was obtained using a Bruker Daltonics Ultraflex Extreme MALDI-ToF mass spectrometer, equipped with a SmartBeam 2 laser. Positive ion ToF detection was performed using an accelerating

voltage of 25 kV. Samples were prepared by layering *trans*-2-[3-(4-*tert*-butylphenyl)-2-methyl-2-propenylidene]malonitrile (DCTB, 0.5 μL of a saturated 50% methanolic solution) followed by polymer (0.5 μL of a 1 $\text{mg}\cdot\text{mL}^{-1}$ solution in THF).

FTIR spectra were acquired using a Bruker Vector 22 FTIR spectrometer with a Golden Gate diamond attenuated total reflection cell. A total of 64 scans were collected on samples in their native (dry) state.

SEC analysis was performed on a Varian 390-LC MDS system equipped with a PL-AS RT/MT autosampler, a PL-gel 3 μm (50×7.5 mm) guard column, two PL-gel 5 μm (300×7.5 mm) mixed-D columns using DMF with 5 mM NH_4BF_4 at 50 $^\circ\text{C}$ as the eluent at a flow rate of 1.0 $\text{mL}\cdot\text{min}^{-1}$. The GPC system was equipped with ultraviolet (UV) (set at 280 nm) and differential refractive index (DRI) detectors. Narrow molecular weight PMMA standards ($200 - 1.0 \times 10^6$ $\text{g}\cdot\text{mol}^{-1}$) were used for calibration using a second order polynomial fit.

Turbidimetric analysis was performed by UV-visible spectrophotometry using an Agilent Cary 60 UV/visible spectrophotometer. The absorbance was set at 650 nm and a heating rate of 1 $^\circ\text{C}\cdot\text{min}^{-1}$ was applied. Data were normalised between 0 and 1 and the cloud point defined as the temperature at which the normalised absorbance equals 0.5.

4.5.3 Procedures

4.5.3.1 Synthesis of 2,5-dioxopyrrolidin-1-yl 2-(((dodecylthio)carbonothioyl)thio)-2-methylpropanoate (2)

N-hydroxysuccinimide (0.47 g, 4.11 mmol) and 2-(dodecylthiocarbonothioylthio)-2-methylpropanoic acid (1.00 g, 2.74 mmol) were dissolved in anhydrous tetrahydrofuran (20 mL) in a 100 mL 3-necked flask purged with nitrogen. The flask was cooled to 10 °C and *N,N'*-diisopropylcarbodiimide (0.52 g, 0.64 mL, 4.11 mmol) was added dropwise over 10 mins. The reaction mixture was stirred at room temperature overnight. After this time, solvent was removed *in vacuo* and the crude solid was re-dissolved in ethyl acetate. The organic layer was washed with saturated sodium hydrogencarbonate solution, twice with water, once with brine and dried over magnesium sulfate. Removal of the solvent left a yellow solid which was recrystallised from ethyl acetate/hexane and washed with water to yield yellow crystals (1.10 g, 86.6 %).

¹H NMR (250.132 MHz, CDCl₃) δ_{ppm}: 3.31 (2H, t, *J*₁₂₋₁₁ = 7.57 Hz, H¹²); 2.81 (4H, d, H¹⁸); 1.88 (6H, s, H¹⁵); 1.69 (2H, p, *J*_{11-12, 11-10} = 7.57 Hz, H¹¹); 1.20 – 1.45 (18H, m, H²⁻¹⁰); 0.89 (3H, t, *J*₁₋₂ = 6.93 Hz, H¹).

¹³C NMR (75.432 MHz, CDCl₃) δ_{ppm}: 218.7 (C¹³); 169.1 (C¹⁶); 168.7 (C¹⁷); 54.3 (C¹⁴); 37.2 (C¹²); 30.9 (C¹⁵); 27.8 (C¹¹); 24.5 (C¹⁸); 31.9, 29.6, 29.5, 29.4, 29.3, 29.1, 29.0, 25.6, 22.7 (C²⁻¹⁰); 14.1 (C¹).

IR cm⁻¹: 2951, 2916, 2847 (alkyl-H stretch); 1776, 1735 (C=O stretch); 1073 (C=S stretch).

HRMS (ESI +) *m/z*: 484.1619 [M+Na]⁺; expected 484.1620 (C₂₁H₃₅NO₄S₃Na).

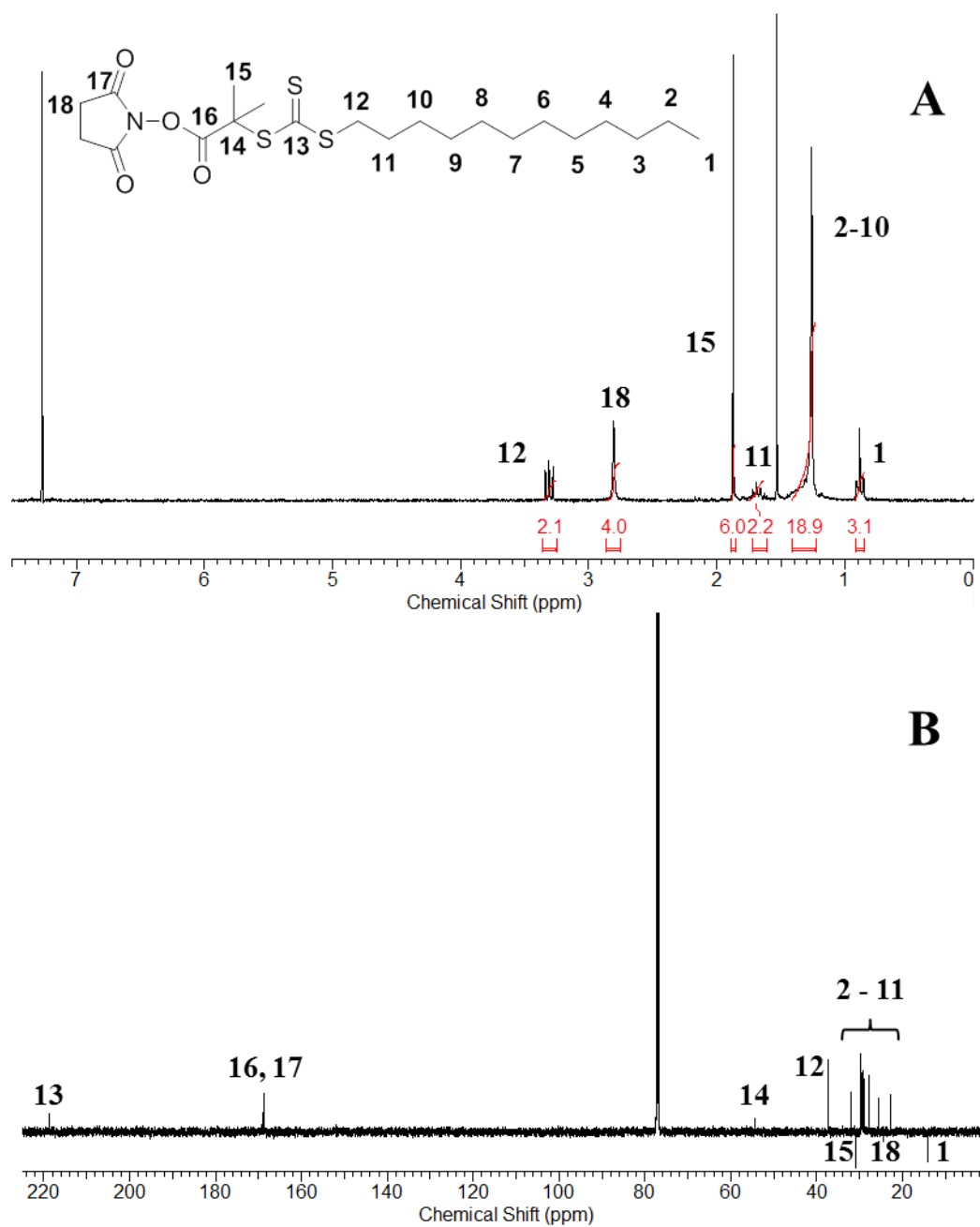


Figure 4.13 NMR spectroscopic characterisation of 2,5-dioxopyrrolidin-1-yl 2-(((dodecylthio)carbonothioyl)thio)-2-methylpropanoate in CDCl_3 : A) ^1H and B) ^{13}C spectra.

4.5.3.2 Synthesis of 1-((3,4-dihydroxyphenethyl)amino)2-methyl-1-oxopropan-2-yl dodecyl carbonotrithioate (3)

Compound **2** (0.9 g, 1.95 mmol) and dopamine hydrochloride (0.41 g, 2.14 mmol) were added to a 100 mL round bottomed flask. Anhydrous methanol (40 mL) was added and stirred to dissolution under nitrogen. Triethylamine (0.24 g, 0.30 mL, 2.34 mmol) was added and the yellow solution stirred at room temperature for 2 days. After this time, solvent was removed *in vacuo* and the yellow residue was re-dissolved in diethyl ether and extracted three times with 1M HCl, twice with water, once with brine and dried over magnesium sulfate. The solvent was removed to give an orange oil (0.9 g) to which hexane (100 mL) was added. The mixture was stirred for 30 mins, after which time a yellow precipitate was observed. This was collected by filtration (gravity) (0.65 g, 67.0 %).

¹H NMR (500 MHz, CDCl₃) δ_{ppm}: 6.78 (1H, d, $J_{24-25} = 8.04$ Hz, H²²); 6.67 (1H, d, $J_{21-25} = 2.00$ Hz, H²⁷); 6.57 (2H, m, H^{17, 21}); 6.18, 5.42 (2H, s br., H^{24, 26}); 3.44 (2H, q, $J_{18-19} = 7.04$ Hz, H¹⁸); 3.26 (2H, t, $J_{12-11} = 7.56$ Hz, H¹²); 2.66 (2H, t, $J_{19-18} = 7.04$ Hz, H¹⁹); 1.63-1.69 (8H, m, H^{11, 15}); 1.38 (2H, p, $J_{10-9, 10-11} = 7.28$ Hz, H¹⁰); 1.20-1.37 (16H, m, H²⁻⁹); 0.88 (3H, t, $J_{1-2} = 7.04$ Hz, H¹).

¹³C NMR (125.721 MHz, CDCl₃) δ_{ppm}: 220.1 (C¹³); 172.8 (C¹⁶); 143.8 (C²³); 142.7 (C²²); 131.2 (C²⁰); 121.0 (C²¹); 115.5 (C²⁷); 115.4 (C²²); 57.1 (C¹⁴); 41.6 (C¹⁸); 37.2 (C¹²); 34.6 (C¹⁹); 31.9, 29.7, 29.6, 29.5, 29.3, 29.1, 29.0, 28.9, 27.7, 22.7 (C²⁻¹¹); 25.9 (C¹⁵); 14.3 (C¹).

IR cm⁻¹: 3342 (N-H stretch); 3196 (O-H stretch); 3042 (aryl-H stretch); 2920, 2850 (alkyl-H stretch); 1623, 1532 (C=O stretch); 1605 (aromatic ring); 1361 (O-H bend); 1071 (S-(C=S)-S) stretch.

HRMS (ESI +) m/z: 522.2138[M+Na]⁺; expected 522.5141 (C₂₅H₄₁NO₃S₃Na).

4.5.3.3 Example polymerisation of *N*-isopropylacrylamide using 1-((3,4-dihydroxyphenethyl)amino)2-methyl-1-oxopropan-2-yl dodecyl carbonotrithioate

N-isopropylacrylamide (1.00 g, 8.84 mmol), compound **3** (38.50 mg, 76.84 μmol) and 4,4'-azobis(4-cyanovaleric acid) (4.90 mg, 15.34 μmol) were added to a vial fitted with stir bar and rubber septum and dissolved in methanol:toluene (50:50) (4 mL). Mesitylene (0.25 mL) was added as internal reference and the mixture stirred (5 mins). An aliquot of this starting mixture was removed for ^1H NMR spectroscopic analysis. The mixture was degassed by bubbling through nitrogen gas for 30 mins and placed in an oil bath thermostated at 70 °C. Samples were removed every 30 mins for 3 hrs after which time the reaction was quenched in liquid nitrogen. An aliquot was removed to determine final conversion by ^1H NMR spectroscopy. The product was purified three times by precipitation from tetrahydrofuran into cold diethyl ether, the solid isolated by centrifugation and dried to yield a pale yellow solid. Conversion (NMR): 98.0 %; M_n (theoretical): 12500 $\text{g}\cdot\text{mol}^{-1}$; M_n (SEC): 14000 $\text{g}\cdot\text{mol}^{-1}$; M_w/M_n (SEC): 1.12.

4.5.3.4 Polymerisation of *N*-isopropylacrylamide using 2-[(*tert*-butoxycarbonyl)amino]ethyl trithiocarbonate

N-isopropylacrylamide (1.00 g, 8.84 mmol), compound **3** (60.70 mg, 179.74 μmol) and 4,4'-azobis(4-cyanovaleric acid) (9.91 mg, 35.36 μmol) were added to a vial fitted with stir bar and rubber septum and dissolved in methanol:toluene (50:50) (4 mL). Mesitylene (0.20 mL) was added as internal reference and the mixture stirred (5 mins). An aliquot of this starting mixture was removed for ^1H NMR spectroscopic analysis. The mixture was degassed by bubbling through nitrogen gas for 30 mins

and placed in an oil bath thermostated at 70 °C for 1 hr. The reaction was quenched in liquid nitrogen, an aliquot removed and conversion determined by ^1H NMR spectroscopy. The product was purified three times by precipitation from tetrahydrofuran into cold diethyl ether, the solid isolated by centrifugation and dried to yield a pale yellow solid. Conversion (NMR): 76.3 %; M_n (theoretical): 4300 $\text{g}\cdot\text{mol}^{-1}$; M_n (SEC): 5500 $\text{g}\cdot\text{mol}^{-1}$; M_w/M_n (SEC): 1.08.

4.5.4 Assay Conditions

4.5.4.1 General procedure for the turbidimetry-monitored, Fe^{3+} -mediated isothermal precipitation of pNIPAM-2

A $1.01 \text{ mg}\cdot\text{mL}^{-1}$ stock solution of **pNIPAM-2** in water was prepared. 2 x 198 μL aliquots of this stock were transferred into two individual wells of a 96-well plate. The plate was left to incubate at 25 °C for 25 mins. The plate was then removed and the well volume made to 200 μL with distilled water or a concentrated solution of $\text{FeCl}_3\cdot 6\text{H}_2\text{O}$ in water. The plate was re-incubated at 25 °C and the absorbance at 650 nm was recorded for an additional 10 mins.

4.6 References

- 1 Liu, F.; Urban, M. W. Recent advances and challenges in designing stimuli-responsive polymers. *Prog. Polym. Sci.* **2010**, *35*, 3-23.
- 2 Roy, D.; Brooks, W. L. A.; Sumerlin, B. S. New directions in thermoresponsive polymers. *Chem. Soc. Rev.* **2013**, *42*, 7214-7243.
- 3 Bergbreiter, D. E. Soluble Polymers as Tools in Catalysis. *ACS Macro Lett.* **2014**, *3*, 260-265.
- 4 Chang, C.-W.; Nguyen, T. H.; Maynard, H. D. Thermoprecipitation of Glutathione S-Transferase by Glutathione–Poly(N-isopropylacrylamide) Prepared by RAFT Polymerization. *Macromol. Rapid Commun.* **2010**, *31*, 1691-1695.
- 5 Tsai, H.-Y.; Vats, K.; Yates, M. Z.; Benoit, D. S. W. Two-Dimensional Patterns of Poly(N-isopropylacrylamide) Microgels to Spatially Control Fibroblast Adhesion and Temperature-Responsive Detachment. *Langmuir* **2013**, *29*, 12183-12193.
- 6 Hastings, C. L.; Kelly, H. M.; Murphy, M. J.; Barry, F. P.; O'Brien, F. J.; Duffy, G. P. Development of a thermoresponsive chitosan gel combined with human mesenchymal stem cells and desferrioxamine as a multimodal pro-angiogenic therapeutic for the treatment of critical limb ischaemia. *J. Contr. Rel.* **2012**, *161*, 73-80.
- 7 Chung, J. E.; Yokoyama, M.; Yamato, M.; Aoyagi, T.; Sakurai, Y.; Okano, T. Thermo-responsive drug delivery from polymeric micelles constructed using block copolymers of poly(N-isopropylacrylamide) and poly(butylmethacrylate). *J. Contr. Rel.* **1999**, *62*, 115-127.
- 8 Meyer, D. E.; Shin, B. C.; Kong, G. A.; Dewhirst, M. W.; Chilkoti, A. Drug targeting using thermally responsive polymers and local hyperthermia. *J. Contr. Rel.* **2001**, *74*, 213-224.
- 9 Schattling, P.; Jochum, F. D.; Theato, P. Multi-stimuli responsive polymers - the all-in-one talents. *Polym. Chem.* **2014**, *5*, 25-36.
- 10 Fu, H.; Policarpio, D. M.; Batteas, J. D.; Bergbreiter, D. E. Redox-controlled 'smart' polyacrylamide solubility. *Polym. Chem.* **2010**, *1*, 631-633.

- 11 Phillips, D. J.; Gibson, M. I. Biodegradable Poly(disulfide)s Derived from RAFT Polymerization: Monomer Scope, Glutathione Degradation, and Tunable Thermal Responses. *Biomacromolecules* **2012**, *13*, 3200-3208.
- 12 Shimoboji, T.; Larenas, E.; Fowler, T.; Kulkarni, S.; Hoffman, A. S.; Stayton, P. S. Photoresponsive polymer–enzyme switches. *Proc. Natl. Acad. Sci. U.S.A.* **2002**, *99*, 16592-16596.
- 13 Heath, F.; Saeed, A. O.; Pennadam, S. S.; Thurecht, K. J.; Alexander, C. 'Isothermal' phase transitions and supramolecular architecture changes in thermoresponsive polymers via acid-labile side-chains. *Polym. Chem.* **2010**, *1*, 1252-1262.
- 14 Tran, N. T. D.; Jia, Z.; Truong, N. P.; Cooper, M. A.; Monteiro, M. J. Fine Tuning the Disassembly Time of Thermoresponsive Polymer Nanoparticles. *Biomacromolecules* **2013**, *14*, 3463-3471.
- 15 Bloksma, M. M.; Bakker, D. J.; Weber, C.; Hoogenboom, R.; Schubert, U. S. The Effect of Hofmeister Salts on the LCST Transition of Poly(2-oxazoline)s with Varying Hydrophilicity. *Macromol. Rapid Commun.* **2010**, *31*, 724-728.
- 16 Que, E. L.; Domaille, D. W.; Chang, C. J. Metals in Neurobiology: Probing Their Chemistry and Biology with Molecular Imaging. *Chem. Rev.* **2008**, *108*, 1517-1549.
- 17 Chipper, M.; Fournier, D.; Hoogenboom, R.; Schubert, U. S. Thermosensitive and Switchable Terpyridine-Functionalized Metallo-Supramolecular Poly(N-isopropylacrylamide). *Macromol. Rapid Commun.* **2008**, *29*, 1640-1647.
- 18 Sharma, A.; Srivastava, A. Pronounced influence of pH, metal-ion and solvent isotope on the thermoresponse of synthetic amphiphilic polypeptides. *Polym. Chem.* **2013**, *4*, 5119-5128.
- 19 Carter, S.; Hunt, B.; Rimmer, S. Highly Branched Poly(N-isopropylacrylamide)s with Imidazole End Groups Prepared by Radical Polymerization in the Presence of a Styryl Monomer Containing a Dithioester Group. *Macromolecules* **2005**, *38*, 4595-4603.
- 20 Mi, P.; Chu, L.-Y.; Ju, X.-J.; Niu, C. H. A Smart Polymer with Ion-Induced Negative Shift of the Lower Critical Solution Temperature for Phase Transition. *Macromol. Rapid Commun.* **2008**, *29*, 27-32.

- 21 Wiktorowicz, S.; Duchene, R.; Tenhu, H.; Aseyev, V. Multi-stimuli responsive poly(azodibenzo-18-crown-6-ether)s. *Polym. Chem.* **2014**, *5*, 4693-4700.
- 22 Du, J.; Yao, S.; Seitz, W. R.; Bencivenga, N. E.; Massing, J. O.; Planalp, R. P.; Jackson, R. K.; Kennedy, D. P.; Burdette, S. C. A ratiometric fluorescent metal ion indicator based on dansyl labeled poly(N-isopropylacrylamide) responds to a quenching metal ion. *Analyst* **2011**, *136*, 5006-5011.
- 23 Yao, S.; Jones, A. M.; Du, J.; Jackson, R. K.; Massing, J. O.; Kennedy, D. P.; Bencivenga, N. E.; Planalp, R. P.; Burdette, S. C.; Seitz, W. R. Intermolecular approach to metal ion indicators based on polymer phase transitions coupled to fluorescence resonance energy transfer. *Analyst* **2012**, *137*, 4734-4741.
- 24 Yin, J.; Li, C.; Wang, D.; Liu, S. FRET-Derived Ratiometric Fluorescent K⁺ Sensors Fabricated from Thermoresponsive Poly(N-isopropylacrylamide) Microgels Labeled with Crown Ether Moieties. *J. Phys. Chem. B* **2010**, *114*, 12213-12220.
- 25 Winterbourn, C. C. Toxicity of iron and hydrogen peroxide: the Fenton reaction. *Toxicol. Lett.* **1995**, *82-83*, 969-974.
- 26 Andrews, N. C. Disorders of Iron Metabolism. *New Engl. J. Med.* **1999**, *341*, 1986-1995.
- 27 Skaar, E. P. The Battle for Iron between Bacterial Pathogens and Their Vertebrate Hosts. *PLoS Pathog.* **2010**, *341*, e1000949.
- 28 Hider, R. C.; Kong, X. Chemistry and biology of siderophores. *Nat. Prod. Rep.* **2010**, *27*, 637-657.
- 29 Lu, Y.; Miller, M. J. Syntheses and studies of multiwarhead siderophore-5-fluorouridine conjugates. *Bioorg. Med. Chem.* **1999**, *7*, 3025-3038.
- 30 Zheng, T.; Nolan, E. M. Enterobactin-Mediated Delivery of β -Lactam Antibiotics Enhances Antibacterial Activity against Pathogenic *Escherichia coli*. *J. Am. Chem. Soc.* **2014**, *136*, 9677-9691.
- 31 Raymond, K. N.; Dertz, E. A.; Kim, S. S. Enterobactin: An archetype for microbial iron transport. *Proc. Natl. Acad. Sci. U.S.A.* **2003**, *100*, 3584-3588.
- 32 Yan, Q.; Yuan, J.; Kang, Y.; Cai, Z.; Zhou, L.; Yin, Y. Dual-sensing porphyrin-containing copolymer nanosensor as full-spectrum colorimeter and ultra-sensitive thermometer. *Chem. Commun.* **2010**, *46*, 2781-2783.

- 33 Chiefari, J.; Chong, Y. K.; Ercole, F.; Krstina, J.; Jeffery, J.; Le, T. P. T.; Mayadunne, R. T. A.; Meijs, G. F.; Moad, C. L.; Moad, G.; Rizzardo, E.; Thang, S. H. Living Free-Radical Polymerization by Reversible Addition–Fragmentation Chain Transfer: The RAFT Process. *Macromolecules* **1998**, *31*, 5559-5562.
- 34 Willcock, H.; O'Reilly, R. K. End group removal and modification of RAFT polymers. *Polym. Chem.* **2010**, *1*, 149-157.
- 35 Jochum, F. D.; zur Borg, L.; Roth, P. J.; Theato, P. Thermo- and Light-Responsive Polymers Containing Photoswitchable Azobenzene End Groups. *Macromolecules* **2009**, *42*, 7854-7862.
- 36 Shepherd, J.; Sarker, P.; Swindells, K.; Douglas, I.; MacNeil, S.; Swanson, L.; Rimmer, S. Binding Bacteria to Highly Branched Poly(N-isopropyl acrylamide) Modified with Vancomycin Induces the Coil-to-Globule Transition. *J. Am. Chem. Soc.* **2010**, *132*, 1736-1737.
- 37 Sarker, P.; Shepherd, J.; Swindells, K.; Douglas, I.; MacNeil, S.; Swanson, L.; Rimmer, S. Highly Branched Polymers with Polymyxin End Groups Responsive to *Pseudomonas aeruginosa*. *Biomacromolecules* **2010**, *12*, 1-5.
- 38 Yin, X.; Hoffman, A. S.; Stayton, P. S. Poly(N-isopropylacrylamide-co-propylacrylic acid) Copolymers That Respond Sharply to Temperature and pH. *Biomacromolecules* **2006**, *7*, 1381-1385.
- 39 Summers, M. J.; Phillips, D. J.; Gibson, M. I. "Isothermal" LCST transitions triggered by bioreduction of single polymer end-groups. *Chem. Commun.* **2013**, *49*, 4223-4225.
- 40 Phillips, D. J.; Patterson, J. P.; O'Reilly, R. K.; Gibson, M. I. Glutathione-triggered disassembly of isothermally responsive polymer nanoparticles obtained by nanoprecipitation of hydrophilic polymers. *Polym. Chem.* **2014**, *5*, 126-131.
- 41 Zobrist, C.; Sobocinski, J.; Lyskawa, J.; Fournier, D.; Miri, V.; Traisnel, M.; Jimenez, M.; Woisel, P. Functionalization of Titanium Surfaces with Polymer Brushes Prepared from a Biomimetic RAFT Agent. *Macromolecules* **2011**, *44*, 5883-5892.
- 42 Skey, J.; O'Reilly, R. K. Facile one pot synthesis of a range of reversible addition-fragmentation chain transfer (RAFT) agents. *Chem. Commun.* **2008**, 4183-4185.

- 43 Keddie, D. J. A guide to the synthesis of block copolymers using reversible-addition fragmentation chain transfer (RAFT) polymerization. *Chem. Soc. Rev.* **2014**, *43*, 496-505.
- 44 Duan, Q.; Miura, Y.; Narumi, A.; Shen, X.; Sato, S.-I.; Satoh, T.; Kakuchi, T. Synthesis and thermoresponsive property of end-functionalized poly(N-isopropylacrylamide) with pyrenyl group. *J. Polym. Sci. A: Polym. Chem.* **2006**, *44*, 1117-1124.
- 45 Steinhauer, W.; Hoogenboom, R.; Keul, H.; Moeller, M. Copolymerization of 2-Hydroxyethyl Acrylate and 2-Methoxyethyl Acrylate via RAFT: Kinetics and Thermoresponsive Properties. *Macromolecules* **2010**, *43*, 7041-7047.
- 46 Phillips, D. J.; Gibson, M. I. Degradable thermoresponsive polymers which display redox-responsive LCST Behaviour. *Chem. Commun.* **2012**, *48*, 1054-1056.
- 47 Liu, M.; Tirino, P.; Radivojevic, M.; Phillips, D. J.; Gibson, M. I.; Leroux, J.-C.; Gauthier, M. A. Molecular Sieving on the Surface of a Protein Provides Protection Without Loss of Activity. *Adv. Funct. Mater.* **2013**, *23*, 2007-2015.
- 48 Magnusson, J. P.; Khan, A.; Pasparakis, G.; Saeed, A. O.; Wang, W.; Alexander, C. Ion-Sensitive “Isothermal” Responsive Polymers Prepared in Water. *J. Am. Chem. Soc.* **2008**, *130*, 10852-10853.
- 49 Miethke, M.; Marahiel, M. A. Siderophore-Based Iron Acquisition and Pathogen Control. *Microbiol. Mol. Biol. Rev.* **2007**, *71*, 413-451.

Chapter 5

5. Siderophore-Inspired Nanoparticle-based Biosensor for the Selective Detection of Fe³⁺

5.1 Chapter Summary

Inspired by nature's exploitation of the 1,2-dihydroxybenzene (or catechol) unit in mammalian and bacterial siderophores, this chapter reports the first example of a nanoparticle sensing system which utilises the strong catechol-Fe³⁺ binding motif to trigger nanoparticle aggregation, promoting a powerful optical response. Gold nanoparticles were functionalised with RAFT polymerisation-prepared, water-soluble poly(*N*-hydroxyethylacrylamide) containing a catechol moiety at the α -chain-end. A strong red-to-purple colorimetric response occurred in the presence of Fe³⁺ at serum concentrations (8 – 25 μ M) in saline solution. The addition of sodium chloride was critical in generating a strong optical output, as was the length of the polymer used to coat the nanoparticles. This behaviour was also demonstrated to be selective for Fe³⁺ over a host of other biologically relevant ions. Therefore, these highly selective and sensitive nanocomposites provide a route towards a simple, cheap and highly applicable Fe³⁺ biosensor.

5.2 Introduction

Iron is the most abundant metal in the body with the average adult requiring a total of around 5 g, using it for a range of functions including oxygen transport, electron transport and metabolic processes.¹ The *in vivo* concentration is, however, carefully regulated to avoid serious health implications. For example, anaemia is caused by insufficient dietary intake and absorption of iron, whilst elevated iron concentrations, such as those present in genetic disorders such as hemochromatosis, can produce excess levels of reactive oxygen species *via* Fenton chemistry.^{2, 3} Undesirable iron levels have been linked to a variety of diseases including Alzheimer's and Parkinson's,⁴ making the effective detection of iron species a critical area of study.

The ability to sequester iron in the human body is complicated by the poor bioavailability of the ferric ion (Fe^{3+}), which predominates in aerobic conditions forming complexes exhibiting a solubility of approximately 10^{-18} M.⁵ To overcome this, it is sequestered within the porphyrin ring of heme and as a co-factor in haemoglobin and myoglobin, whilst its passage into cells depends heavily on transport proteins such as transferrin.^{6, 7} Bacteria also require sufficient levels of the metal to survive and grow, abstracting it from their mammalian hosts with siderophores - low molecular weight complexes that bind iron with an association constant in excess of 10^{50} M allowing effective competition with the host for iron sequestration.^{7, 8}

A large number of bacterial siderophores are known in comparison to the single mammalian siderophore, siderocalin,⁶ which counteracts bacterial uptake by sequestering the bacterial siderophore-iron complex.⁹⁻¹¹ The majority of these species are divided into three groups: α -hydroxycarboxylates, hydroxamates and

catecholates, examples of which are deoxymugineic acid, rhodotorulic acid and enterobactin respectively (Figure 5.1). These functionalities have inspired the development of a number of compounds such as deferoxamine, deferiprone and deferasirox for use in iron chelation therapies,^{12, 13} and have provided a focus for investigations into the use of siderophore (mimics) as pharmaceutical and antibiotic drug targeting devices.¹⁴⁻¹⁷

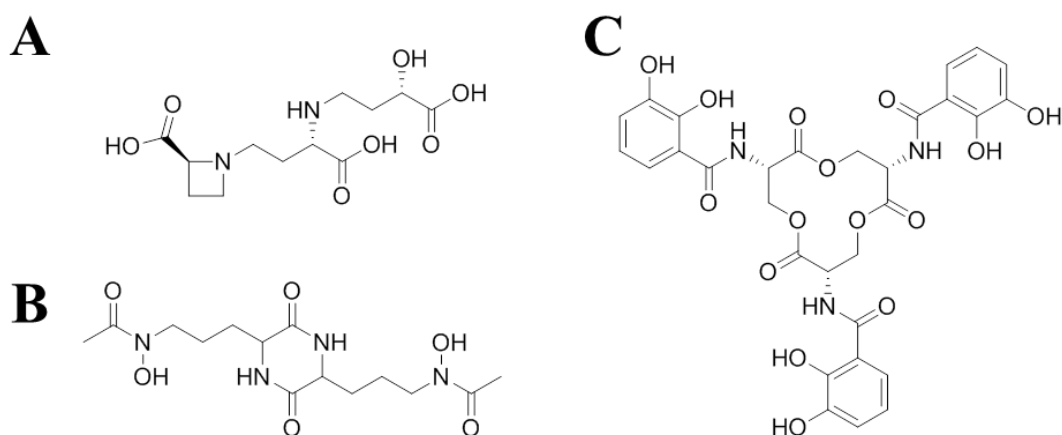


Figure 5.1 Chemical structures (and classification) of example siderophores: (A) Deoxymugineic acid (α -hydroxycarboxylates); (B) rhodotorulic acid (hydroxamate) and (C) enterobactin (catecholate).

The development of sensors capable of detecting a variety of metal ions is a popular field of research.^{18, 19} Such detection is important for a variety of applications such as environmental monitoring, clinical toxicology and as a diagnostic tool.²⁰⁻²² Several sensing platforms/responses have been described to date, including proteins and DNA,^{23, 24} metal electrodes^{25, 26} and graphene oxide,²⁷ whilst the ability to trigger a fluorescent response upon metal ion binding has received significant study.^{28, 29} A further, particularly attractive platform is that of gold nanoparticles (AuNPs) due to their facile preparation, control over size, ease of surface functionalisation through

simple coating strategies and, most importantly for sensing applications, the resulting impact on optical properties.³⁰⁻³² Specifically, the extent of nanoparticle dispersion/aggregation has a significant effect on the nanoparticle colour due to shifts in surface plasmon resonance (SPR). This signature has been applied for the detection of a variety of metal ions including lithium,³³ mercury,^{34, 35} potassium,³⁶ aluminium,³⁷ lead³⁸ and chromium.³⁹ However, there are few instances of the application of AuNPs capable of detecting iron which have been reported. Bai *et al.* functionalised gold nanoparticles with a hydrophilic ligand, to ensure water solubility, and a 4-piperazinyl-1,8-naphthalimide-based ligand which was able to complex with Fe³⁺ generating a colorimetric and fluorescent output.⁴⁰ Tripathy *et al.* have prepared a colorimetric detection system based on gold, whereby the addition of iron(III) in the presence of thiourea and hydrochloric acid catalyses leaching of the gold, damping the SPR and hence resulting in a visible colour change.⁴¹ Wu *et al.* have functionalised gold nanoparticles with pyrophosphate which underwent a pink-to-violet change in the presence of Fe³⁺, showing selectivity for Fe³⁺ over a host of other ions.⁴²

Further inspired by the structure and action of siderophores, we hypothesised that the binding between catechols⁴³ and Fe³⁺ may be sufficient to affect the aggregation behaviour of a gold nanoparticle suspension in order to generate an optical response. To date, catechol groups have been used in the formulation of nanoparticles as a way of stabilising the metallic cores, but not such that the catechol unit is readily available to undergo further chemistry.^{44, 45} They have also been grafted onto mesoporous silica nanoparticles⁴⁶ and have been used as a stabiliser in the synthesis of gold nanoparticles from their parent Au(III) salt due to the redox chemistry involved with the interchange of catechol to quinone groups.⁴⁷⁻⁴⁹ To the best of our

knowledge however, there are few examples whereby (gold) nanoparticles have been prepared with a catechol group protruding from the particle surface, allowing active use.⁵⁰ This is surprising given developments in controlled (living) radical polymerisation (C(L)RP) methodologies over the past two decades have enabled the routine generation of vast arrays of polymeric architectures with high levels of control over functionality, chain-end structure and topology. Moreover, polymers derived from the Reversible Addition-Fragmentation Chain Transfer (RAFT) methodology⁵¹ are ideally suited for further reaction with gold nanoparticles given the inherent affinity between gold and the thiol groups derived from the ω -end of the preceding polymer chains.³² It is therefore possible, through judicious selection of the chain transfer agent used, to install the desired catechol functional group at the α -end of a polymer chain which will be subsequently available on the gold nanoparticle surface.

Herein, inspired by the structure and biological importance of siderophores, we detail the first example of a gold nanoparticle-based system capable of sensing subtle changes in physiological Fe^{3+} concentration through the powerful catechol- Fe^{3+} binding motif.

5.3 Results and Discussion

To prepare catechol-functional polymers, the chain-transfer agent described in chapter 4 was employed.⁵² To effectively furnish catechol-functional gold nanoparticles, a water-soluble polymer was first required, hence *N*-hydroxyethyl acrylamide (HEA) was selected for use here. This polymer was also deliberately chosen as it does not possess thermo-responsive behaviour and hence removes any potential complication of particle aggregation behaviour given the transition temperature of thermo-responsive polymers is known to change when tethered to gold nanoparticles.⁵³ The polymerisation conditions used afforded rapid polymerisation rates (at least 75 % conversion after 35 mins) and polymers of a range of molecular weights were prepared and characterised by SEC and ¹H NMR spectroscopy (Table 5.1, Figure 5.2). Narrow dispersities (≤ 1.20) were observed, an attractive feature of the RAFT technique.

Table 5.1 Characterisation of pHEA samples prepared in this study.

Polymer	[M]:[CTA]	Conversion (%) ^a	$M_{n(th)}$ (g.mol ⁻¹) ^a	$M_{n(SEC)}$ (g.mol ⁻¹) ^b	M_w/M_n ^b
pHEA-1	30	83.1	2900	4800	1.14
pHEA-2	75	78.5	6800	9700	1.17
pHEA-3	200	74.7	17200	17500	1.20
pHEA-4 ^c	75	74.1	6400	10200	1.16

^aDetermined by ¹H NMR spectroscopy relative to an internal standard (mesitylene);

^bDetermined by SEC (DMF inc. 5 mM NH₄BF₄) relative to PMMA standards; ^cA control polymer used later in study (*vide infra*).

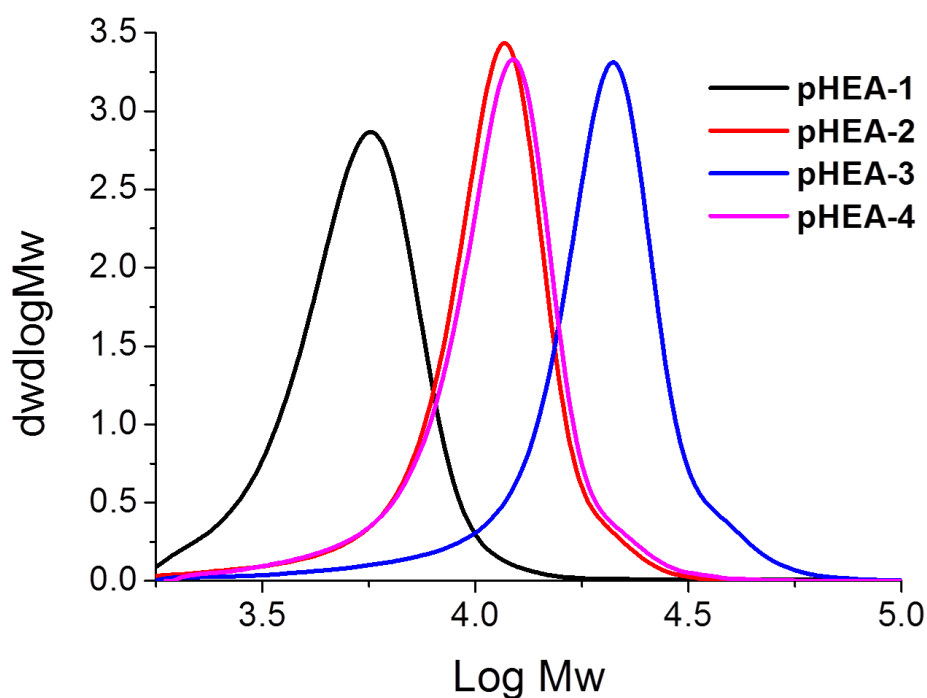
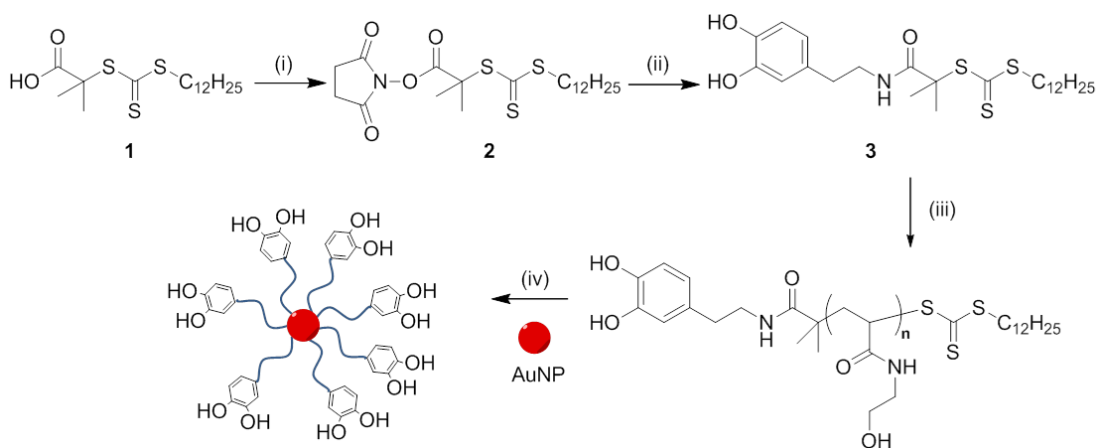


Figure 5.2 SEC characterisation of **pHEA-1/2/3/4**.

Nanoparticles can be routinely synthesized from Au^{3+} salts and are ideally suited for RAFT-derived polymers given the strong affinity between thiols, which are derived from the ω -trithiocarbonate terminus, and gold. This can be used to prepare self-assembled monolayers and has been previously exploited to generate large nanoparticle libraries.⁵⁴ Commercially available citrate-coated nanoparticles with a diameter of 40 nm (**AuNP₄₀**) were used as a starting material and coated with the polymers by a simple mixing procedure, washing several times by centrifugation to remove excess polymer yielding **pHEA-1/2/3@AuNP₄₀** (Scheme 5.1).



Scheme 5.1 Synthetic scheme for the preparation of catechol-functional gold nanoparticles: (i) NHS/DIC, THF, 0 °C → r.t, 16 hrs; (ii) Dop.HCl/TEA, MeOH, r.t, 48 hrs; (iii) HEA, **3**, ACVA, MeOH/Toluene, 70 °C, 35 mins; (iv) Polymer/AuNP, 5 °C, 16 hrs.

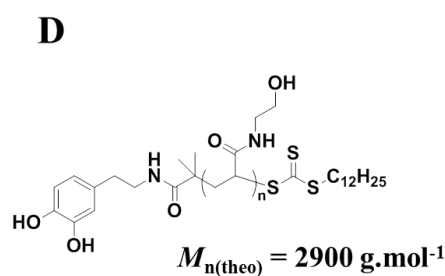
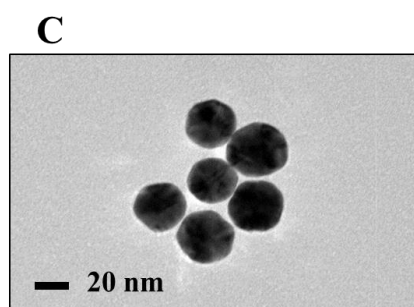
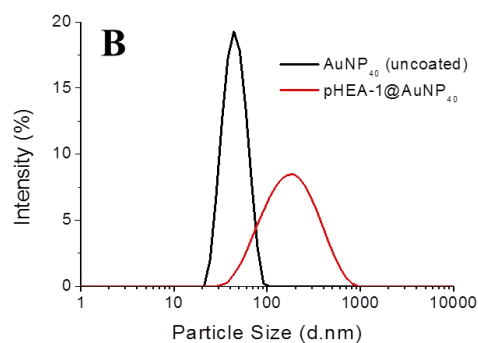
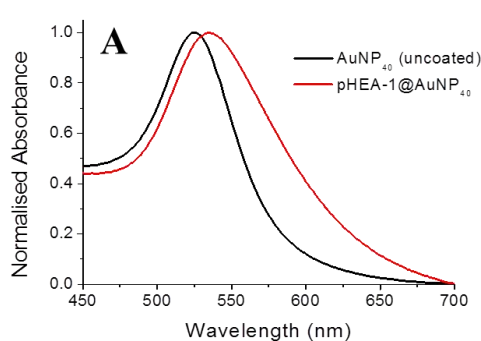
Successful functionalisation of the nanoparticles was confirmed by several techniques. UV-visible spectrophotometry revealed a distinctive red shift in maximum wavelength from 525 nm for the uncoated particles to between 531-534 nm following polymer addition, implicit of a change in refractive index of the coating (Figure 5.3A/E/I/M). DLS analysis also indicated an increase in particle size from 41.5 ± 0.2 nm for the uncoated particles to between 80 and 126 nm when coated with polymer, with the size increasing with polymer length (Figure 5.3B/F/J/N). TEM confirmed particle sizes of ~ 40 nm (Table 5.2, Figure 5.3C/G/K/O) with narrow size distributions in all cases. Due to the low degrees of surface loading employed herein, the surface polymer coating was not clearly observed by this technique. Particle sizes are larger for polymer-coated particles due to the presence of the hydrophilic polymer layer contributing to the particles' hydrodynamic diameter as the functionalised particles undergo Brownian motion. The larger particle sizes observed for **pHEA-1/2@AuNP₄₀** by DLS may also suggest

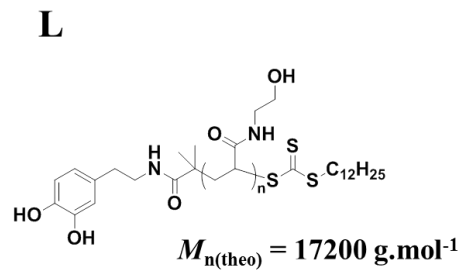
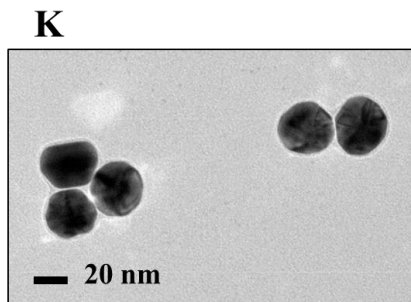
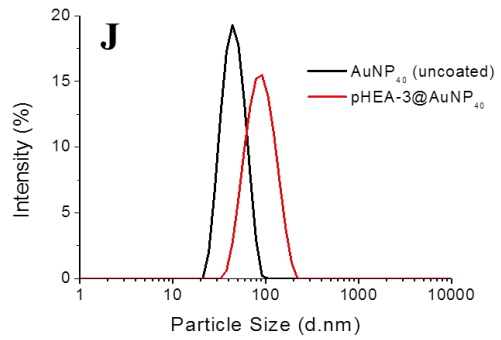
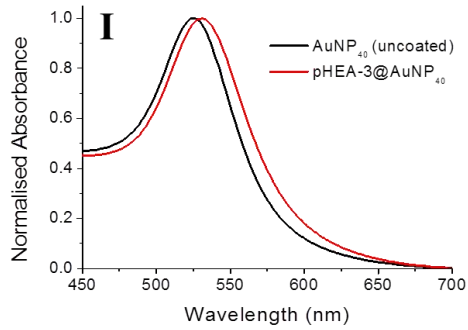
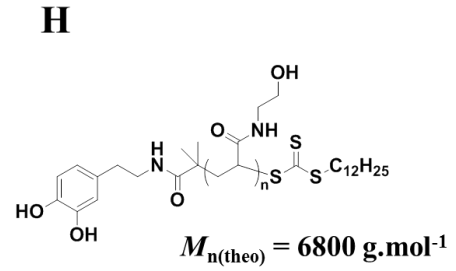
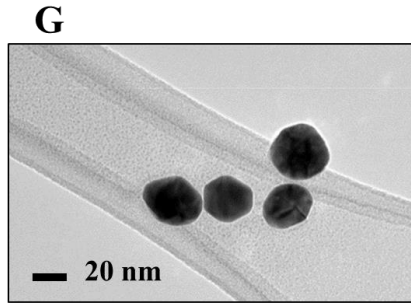
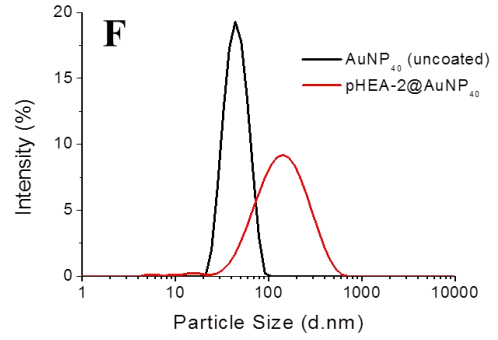
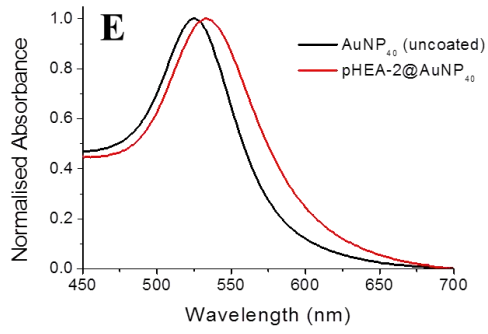
a small degree of aggregation resulting during the polymer coating process. However, given the lack of a significant colour change to either blue (associated with large scale AuNP aggregation) or colourless (associated with AuNP precipitation), these particles were still deemed sufficiently dispersed for further testing.

Table 5.2 Characterisation of gold nanoparticles used in this study.

Code	Diameter (DLS) (nm)	Diameter (TEM)	
		(nm) ^a	SPR _{max} (nm)
AuNP ₄₀ (uncoated)	41.5 ± 0.2	36.2 ± 3.8	525
pHEA-1@ AuNP ₄₀	126.0 ± 2.6	38.0 ± 4.4	534
pHEA-2@ AuNP ₄₀	113.7 ± 3.2	39.0 ± 4.1	532
pHEA-3@ AuNP ₄₀	79.5 ± 0.4	38.2 ± 2.8	531
pHEA-4@ AuNP ₄₀ ^b	59.6 ± 3.5	37.5 ± 4.0	530

^aAverage particle sizes by TEM were calculated by counting a minimum of 60 particles; ^bControl particles used later in study (*vide infra*).





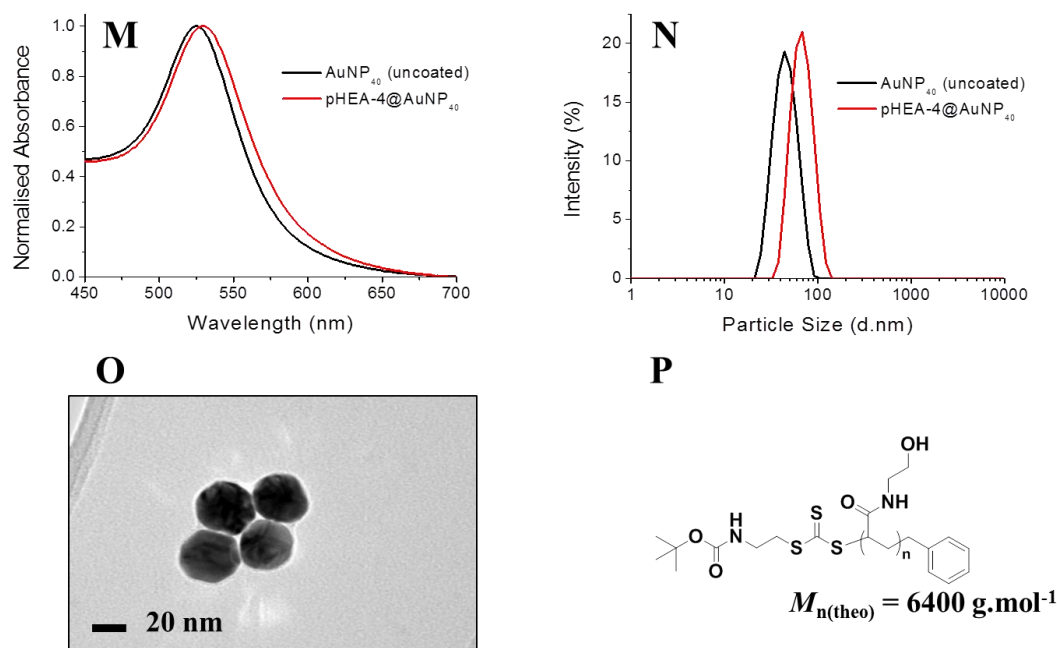


Figure 5.3 Characterisation of **pHEA-1/2/3/4@AuNP₄₀**: (A, E, I, M) UV/visible spectra; (B, F, J, N) DLS analysis; (C, G, K, O) Transmission electron microscope (TEM) image of polymer-functionalised gold nanocomposites, scale bar 20 nm; (D, H, L, P) Chemical structure of polymer used to coat particles.

These catechol-functionalised nanoparticles were then probed for their ability to detect Fe^{3+} in aqueous solution. **PHEA-2@AuNP₄₀** was incubated with varying concentrations (100 μM – 1 nM) of $\text{FeCl}_3 \cdot 6\text{H}_2\text{O}$ for 30 mins at room temperature and the UV/visible spectrum between 450 and 700 nm was measured (Figure 5.4A). Two points of reference are often used to assess any change in the aggregation behaviour of gold: (i) any change in maximum SPR_{max} , where aggregation results in a shift to longer wavelengths and (ii) any change in absorbance at 700 nm ($\text{Abs}@700 \text{ nm}$), which may also be accompanied by a decrease in intensity of SPR_{max} .⁵⁵ Unfortunately, no change in either of these properties was observed at any iron concentration indicating either no catechol-iron binding was occurring, or any binding was insufficient to trigger a change in the particle aggregation state. This

was not entirely unexpected given a literature precedent which suggests the modulation of ionic strength is important to tune particle aggregation *via* interparticle electrostatic repulsion. For instance, Zhang and Wang demonstrated an ability to control the growth of charged gold nanoparticle chains by altering the ionic strength of the dispersion medium. When thioglycolic acid-coated AuNPs of 14 nm core diameter were placed in NaCl solutions of increasing concentration, a noticeable increase in intensity of the peak at 600 nm was observed by UV/visible spectrophotometry. Subsequent TEM analysis revealed 1D self-assembled AuNP chains with a chain length proportional to the concentration of salt used.⁵⁶ The addition of salt to a suspension of AuNPs has also been shown to be critical if the thermo-responsive behaviour of gold nanoparticles functionalised with a poly(*N*-isopropylacrylamide), pNIPAM corona is to be visualised. Yusa *et al.* noted that the heating of these functional particles in water failed to cause a change in SPR, even when above the transition temperature of the corona. However, a considerable red shift from 523 nm to 580 nm was observed when the suspension was heated in a 50 mM NaCl solution.⁵⁷ Hoogenboom, De Geest and co-workers have also noted the importance of salt requiring a 0.1 M NaCl solution to trigger an SPR shift from 530 nm at 25 °C to 565 nm at 40 °C.⁵⁸ These results suggest that the presence of salt is necessary to screen the electrostatic charges on the surface of the AuNPs and hence allow the dehydrated pNIPAM chains to aggregate above their transition temperature.

Considering this information, the assay was doped with 50 mM NaCl and repeated (Figure 5.4B). Gratifyingly, we now saw some response, notably in the presence of 10 μM Fe^{3+} where a shift in SPR_{max} from 532 to 547 nm was observed, together with

an increase in Abs@700 nm from 0.288 to 0.602. Interestingly, minimal response was seen in the presence of any other iron concentration (*vide infra*).

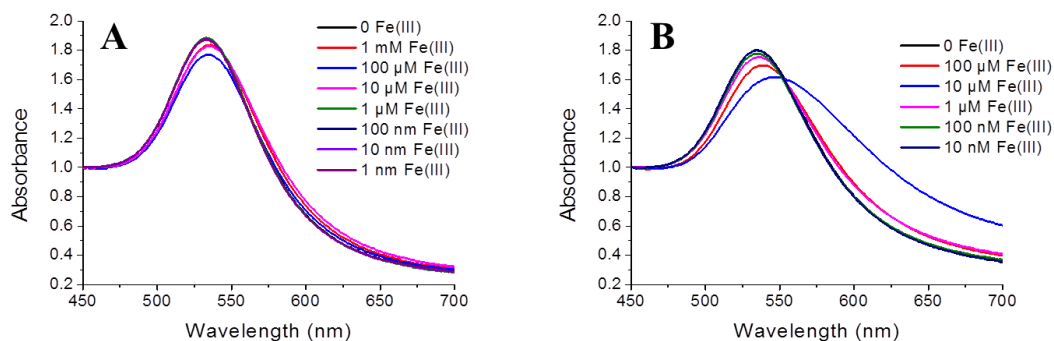


Figure 5.4 UV/visible spectra showing response of **pHEA-2@AuNP₄₀** in the presence of various concentrations of Fe³⁺ and (A) 0 NaCl, (B) 50 mM NaCl.

This behaviour was further tuned by fixing the concentration of FeCl₃·6H₂O at 10 μM and varying the concentration of NaCl in the AuNP suspensions up to saline concentrations (150 mM). A noticeable, non-linear increase in both SPR_{max} and Abs@700 nm with increasing levels of NaCl was observed, likely due to an increased screening of any negative charge on the particle surface which allowed greater interparticle interactions. Therefore, in the presence 150 mM NaCl (saline) amplified optical shifts were noted (SPR_{max} shifted by 20 nm and Abs@700 nm by 0.412 compared to in the absence of salt) due to the ionic environment (Figure 5.5A/B). As the optical responses in 150 mM NaCl were significantly larger, providing a noticeable change in appearance (Figure 5.5C), these conditions were employed in the rest of this study. Particle stability over time in 150 mM NaCl was confirmed by DLS with minimal increase in particle size after 8 hrs (Figure 5.5D). This was important as it confirmed the results were not complicated by non-specific aggregation processes within the assay time-scale.

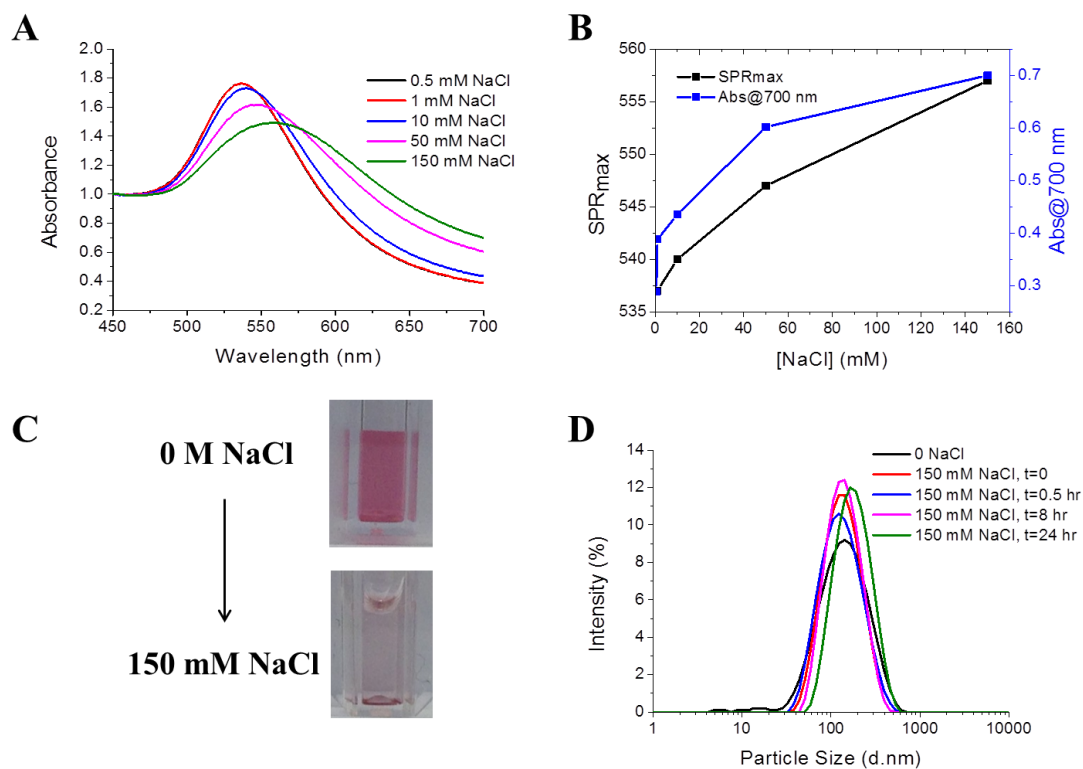


Figure 5.5 Response of **pHEA-2@AuNP₄₀** in the presence of 10 μM Fe³⁺ and various NaCl concentrations: (A) UV/visible spectra; (B) Change in SPR_{max} and Abs@700 nm as a function of NaCl concentration; (C) Appearance of **pHEA-2@AuNP₄₀** in the presence of 10 μM Fe³⁺ and either 0 or 150 mM NaCl; (D) DLS in the presence of 150 mM NaCl at various time-points.

The initial Fe³⁺ assay was next repeated in 150 mM NaCl solution. Interestingly, a linear trend in SPR_{max} and Abs@700 nm with increasing Fe³⁺ concentration was not observed. There was a noticeable increase with increasing Fe³⁺ concentration up to a concentration of 10 μM; however, further increases in concentration led to a decreased optical response (Figure 5.6A). The fact that the same general trend is observed for both SPR_{max} and Abs@700 nm indicated the applicability of both data points as a tool for assessing the aggregation behaviour of AuNPs (Figure 5.6B).

Aggregation behaviour was confirmed by DLS analysis (Figure 5.6C). A significant increase in particle size was first observed at 10 μM Fe^{3+} , peaking at 25 μM Fe^{3+} before decreasing when the concentration reached 100 μM . The selective response to certain iron concentrations is in keeping with results reported previously by Bai *et al.* who rationalised AuNP dispersion at high Fe^{3+} concentrations by an excess of Fe^{3+} and hence positive charges in the system, promoting Coulombic repulsion.⁴⁰ The change in both particle size and Abs@700 nm with respect to iron concentration yielded a very similar trend (Figure 5.6D), indicative of aggregation due to catechol- Fe^{3+} binding rather than due to non-specific response of the polymer chains.

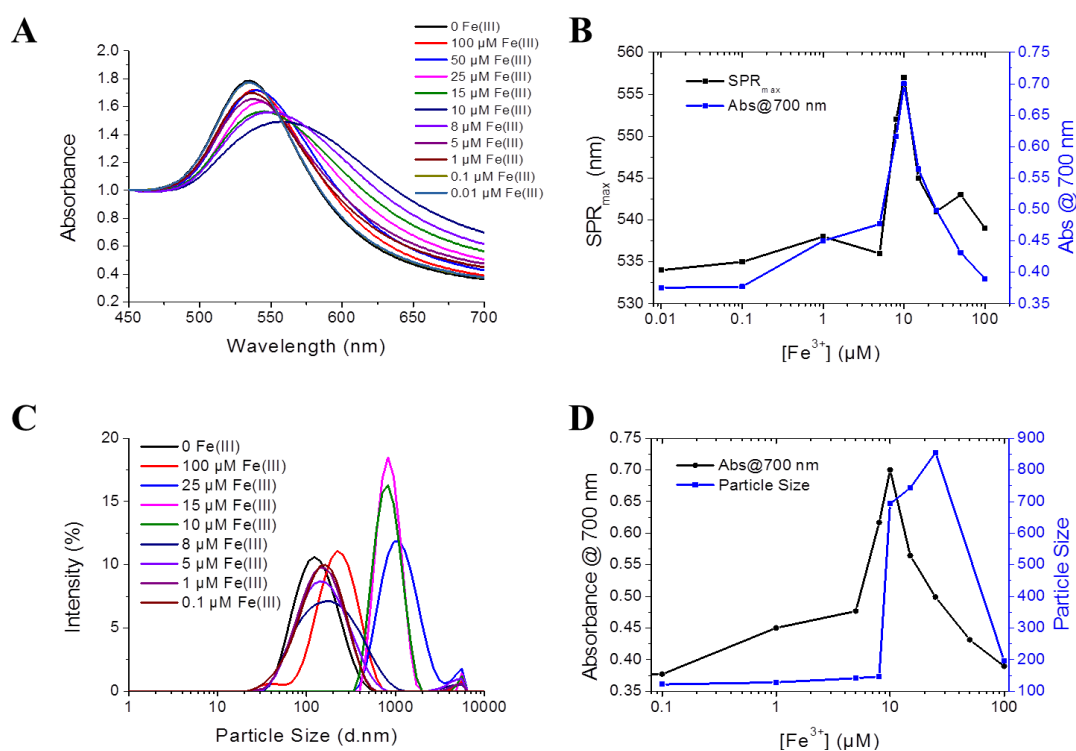


Figure 5.6 Response of pHEA-2@AuNP₄₀ in 150 mM NaCl to various concentrations of Fe^{3+} : (A) UV/visible spectra and (C) DLS traces; (B) SPR_{max}, Abs@700 nm and (D) Comparison of Abs@700 nm (UV/vis) and particle size (DLS) as a function of Fe^{3+} concentration.

Several control studies were carried out to further confirm that the observed response was due to selective catechol-Fe³⁺ binding. Incubation of **pHEA-2@AuNP₄₀** in 150 mM NaCl with FeCl₂.4H₂O resulted in no significant change in either SPR_{max} or Abs@700 nm. No change in aggregation behaviour was expected in this case as the binding of catecholate-based siderophores to Fe²⁺ is significantly weaker than that of Fe³⁺ due to the reduced charge density on the coordinated cation⁸. A slight increase in Abs@700 nm was observed with increasing Fe²⁺ (difference of 0.076 with 100 μM Fe²⁺) which may be due to reduced particle stability leading to the beginnings of a “salting-out” phenomenon (Figure 5.7A).

A polymer of similar molecular weight containing a benzyl end-group was prepared as a negative control to directly compare against the catechol end-group containing polymers (**pHEA-4**, Table 5.1). AuNPs were functionalised with **pHEA-4** using the same coating technique (**pHEA-4@AuNP₄₀**, Table 5.2) to yield particles with a diameter of 59.6 ± 3.5 nm (DLS). Incubation with Fe³⁺ revealed no response to any concentration tested proving that the catechol end-group is necessary to promote cross-linking and hence optical responsive behaviour (Figure 5.7B). A summary of the incubation of **pHEA-2/4@AuNP₄₀** with Fe²⁺ and Fe³⁺ is shown in Scheme 5.2.

In a bid to further tune the selectivity of the nanoparticles to the presence of iron, the effect of polymer molecular weight on aggregation behaviour was investigated. AuNPs coated with a shorter polymer (molecular weight $\sim 3000 \text{ g}\cdot\text{mol}^{-1}$ **pHEA-1@AuNP₄₀**) showed poor saline stability, with aggregation and precipitation occurring within 30 mins, even at low NaCl concentrations, and a colour change from red/pink to blue/purple (Figure 5.8). This precipitation is most likely due to the shorter polymer chain failing to offer sufficient steric stabilisation in the presence of the electrolyte.

Coating the particles with a longer polymer (molecular weight $\sim 17000 \text{ g}\cdot\text{mol}^{-1}$; **pHEA-3@AuNP₄₀**) provided good saline stability; however no aggregation occurred at any Fe^{3+} concentration (Figure 5.8). The importance of polymer linker length on AuNP-based detection systems has been demonstrated previously: Richards *et al.* noted that glycosylated AuNPs, designed for the detection of FimH positive bacteria, required the addition of a poly(ethylene glycol) spacer between the nanoparticle core and carbohydrate extremity in order to increase saline stability and specificity for bacterial binding.⁵⁵

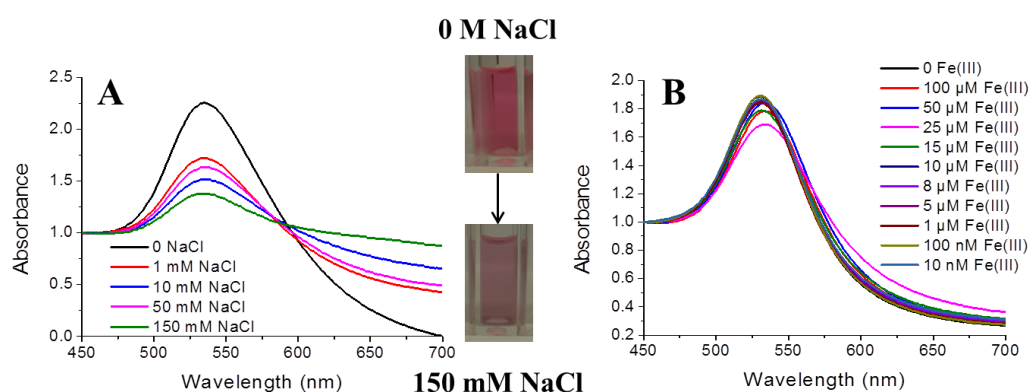


Figure 5.8 (A) UV/visible spectra showing response of **pHEA-1@AuNP₄₀** to NaCl (inset: Appearance at 0 and 150 mM NaCl); (B) UV/visible spectra showing response of **pHEA-3@AuNP₄₀** to various concentrations of Fe^{3+} .

In biological systems, a host of metal ions are known to play a variety of different roles.⁵⁹⁻⁶¹ Hence, the specificity of the nanocomposites with respect to Fe^{3+} was investigated by carrying out a comparative assay with a range of biologically relevant cations. (Figure 5.9). Pleasingly, the response to Fe^{3+} , as assessed by the change in $\text{Abs}@700\text{ nm}$, was 5-fold greater than the closest competitive ion (Fe^{2+}) and over 10-fold greater than all other ions tested. Furthermore, minimal response was observed in the presence of Gd^{3+} , another tribasic metal ion, further highlighting the specificity of a catechol unit to Fe^{3+} .

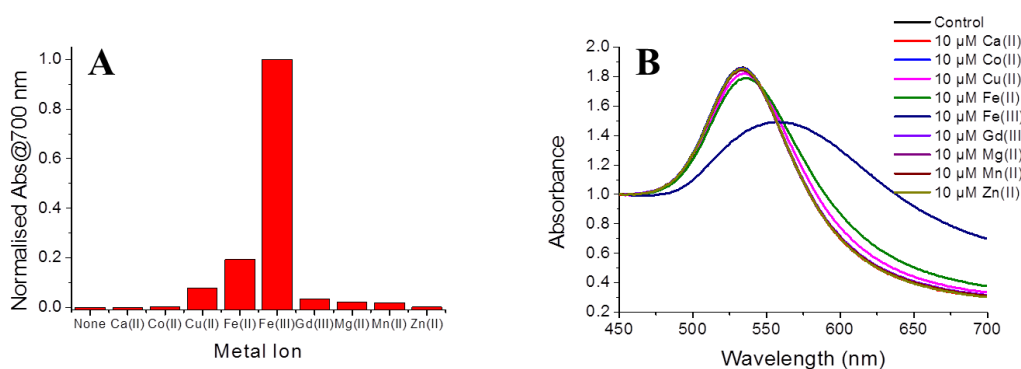


Figure 5.9 Response of **pHEA-2@AuNP₄₀**, doped with 150 mM NaCl, to a variety of metal ions: (A) Bar chart showing change in $\text{Abs}@700\text{ nm}$ in the presence of metal ions (10 μM); data normalised against ion that showed greatest response (Fe^{3+}) and (B) UV/visible spectra.

As a final test, we investigated whether the assay would work in a more complex biological media than saline. **PHEA-2@AuNP₄₀** was centrifuged and the pellet re-suspended in bovine plasma. Successful re-suspension of the AuNPs in this medium was observed, with no signs of aggregation by UV/visible spectrophotometry (it should be noted that attempted DLS of these particles proved unsuccessful, presumably due to interference of proteins in the medium). When incubated with various concentrations of Fe^{3+} for 30 mins, no significant change in either SPR_{max} or

Abs@700 nm was observed (Figure 5.10). It should be noted that no additional NaCl was added to the assay to maintain integrity of the medium. This observation may be as a consequence of the high protein content of the medium which can physisorb to the nanoparticle surface, preventing particle aggregation, even if catechol-iron binding has occurred. Alternatively, the plasma used also contained several common proteins including transferrin. This may have coordinated the iron and hence prevented it being accessed by the catechol units. Clearly therefore, the use of these nanocomposites in physiological media will need further investigation to assess their true versatility.

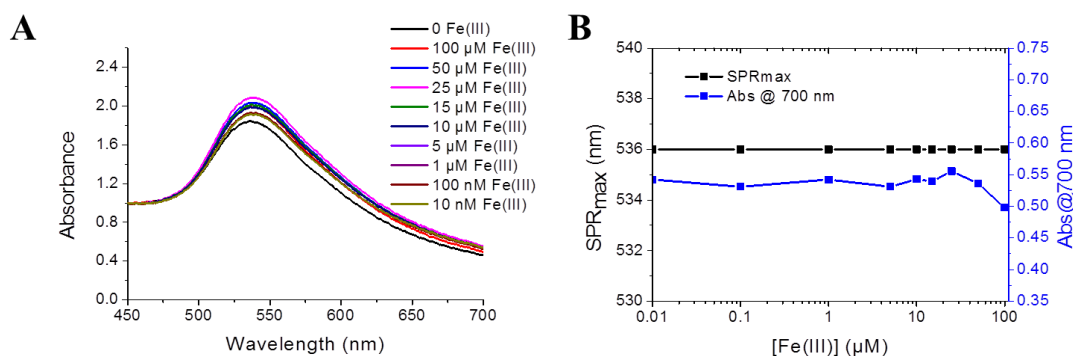


Figure 5.10 Response of pHEA-2@AuNP₄₀, suspended in bovine plasma, with various concentrations of Fe³⁺: (A) UV/visible spectra and (B) SPR_{max} and Abs@700 nm as a function of Fe³⁺ concentration.

5.4 Conclusions

Inspired by Nature's need for iron acquisition, this study presents the first example of the strong catechol-Fe³⁺ binding motif as a route to controlling the dispersion/aggregation behaviour of gold nanoparticles as optical sensing devices. A small library of water-soluble poly(*N*-hydroxyethyl acrylamide) was prepared using an α -chain end, catechol-functional chain transfer agent. These polymers were subsequently used to coat gold nanoparticles with a core diameter of 40 nm and characterised by a range of techniques. The propensity for catechol-Fe³⁺ binding was then assessed using simple UV/visible spectrophotometry and DLS-based assays. The addition of salt was observed to be critical if any aggregation was to be observed due to successful shielding of residual negative charge on the AuNP surface. The response was dependent on the amount of salt used in a non-linear fashion, with physiologically-relevant saline conditions (150 mM NaCl) providing the best response in terms of both optical SPR_{max} band shifting and the observed Abs@700 nm.

With these optimised conditions, a selective response of the gold nanoparticle system to Fe³⁺ concentrations between 8 and 25 μ M was achieved, with the most notable optical response occurring with 10 μ M Fe³⁺. Concentrations above and below this gave minimal indication of aggregation by DLS and UV/visible spectrophotometry. It is suggested that in this current system, a trade-off exists between adding a sufficient concentration of Fe³⁺ to trigger cross-linking and an excess which promotes Coulombic repulsion. Nevertheless, this limitation is minimal given the iron concentrations detected by this current system correspond to those found in

human serum.⁶² Controls including the effect of Fe^{2+} on catechol-functional AuNPs and the effect of Fe^{3+} on AuNPs coated with a simple phenyl end-group confirmed the nature and specificity of the aggregation behaviour. The length of polymer chain on the extent of iron response was also optimised; small chains failed to provide sufficient steric stability resulting in rapid aggregation even at very low concentrations of NaCl, whilst the addition of long chains afforded too much stability and failed to generate any noticeable response. Finally, the nature and specificity of the aggregation behaviour was shown, notably giving at least a 5-fold higher response to Fe^{3+} compared to the other biologically relevant cations tested.

In summary, we have developed a powerful system which exhibits an optimal response between 8 – 25 μM Fe^{3+} and offers valuable sensing potential at physiological concentrations.⁶² Future work will focus on tailoring the nanoparticle surface/surrounding environment to promote a response to a wider range of Fe^{3+} concentrations for use as a sensor in both deprived and iron-rich conditions. Moreover, further study into the suitability of the sensor to more complex biological media is ongoing.

5.5 Experimental

5.5.1 Materials

All chemicals were used as supplied. Diethyl ether, ethyl acetate, hexane, methanol, triethylamine and toluene were all purchased from Fisher Scientific at laboratory reagent grade. Deuterated chloroform (99.8 atom % D), deuterated methanol (99.8 atom % D), *N*-hydroxysuccinimide (98.0 %), *N,N*-diisopropylcarbodiimide (99.0 %), *N*-hydroxyethylacrylamide (97.0 %), 4,4'-azobis(4-cyanovaleric acid) (≥ 98.0 %), mesitylene (97.0 %), calcium chloride dihydrate (≥ 99.0 %), cobalt(II) chloride hexahydrate (98.0 %), copper(II) chloride (≥ 99.0 %), iron(III) chloride hexahydrate (97.0 %), iron(II) chloride tetrahydrate (98.0 %), gadolinium(III) chloride hexahydrate (99.0 %), manganese(II) chloride tetrahydrate (≥ 98.0 %) and bovine plasma were all purchased from Sigma-Aldrich. Gold nanoparticle suspension (40 nm) was purchased from BBI Solutions. 2-(Dodecylthiocarbonothioylthio)-2-methylpropanoic acid (Chapter 2), benzyl 2-[(*tert*-butoxycarbonyl)amino]ethyl trithiocarbonate (Chapter 3), 2,5-dioxopyrrolidin-1-yl 2-(((dodecylthio)carbonothioyl)thio)-2-methylpropanoate (Chapter 5) and 1-((3,4-dihydroxyphenethyl)amino)2-methyl-1-oxopropan-2-yl dodecyl carbonotrithioate (Chapter 5) were synthesised as described in previous chapters.

5.5.2 Analytical Methods

NMR spectroscopy (^1H , ^{13}C) was conducted on a Bruker AV-250, Bruker DRX-500 or Bruker AV III-600 spectrometer using deuterated chloroform or methanol as solvent. All chemical shifts are reported in ppm (δ) relative to the solvent used.

High resolution mass spectra were recorded on a Bruker Electrospray Ultra-High Resolution tandem TOF mass spectrometer using electrospray ionization (ESI) in positive mode on samples prepared in methanol.

FTIR spectra were acquired using a Bruker Vector 22 FTIR spectrometer with a Golden Gate diamond attenuated total reflection cell. A total of 64 scans were collected on samples in their native (dry) state.

UV-visible spectra were obtained using a Biotech Synergy HT and processed using the Gen5 software package version 1.11. “Normalised absorbance” refers to data that has been normalised between 0 and 1. All other data referred to as “absorbance” has been normalised such that the absorbance at 450 nm equals 1.

SEC analysis was performed on a Varian 390-LC MDS system equipped with a PL-AS RT/MT autosampler, a PL-gel 3 μm (50×7.5 mm) guard column, two PL-gel 5 μm (300×7.5 mm) mixed-D columns using DMF with 5 mM NH_4BF_4 at 50 °C as the eluent at a flow rate of 1.0 $\text{mL}\cdot\text{min}^{-1}$. The GPC system was equipped with ultraviolet (UV) (set at 280 nm) and differential refractive index (DRI) detectors. Narrow molecular weight PMMA standards ($200 - 1.0 \times 10^6$ $\text{g}\cdot\text{mol}^{-1}$) were used for calibration using a second order polynomial fit.

Particle size analysis was determined by Dynamic Light Scattering using a Malvern Zetasizer Nano ZS instrument. A 4 mW He-Ne 633 nm laser module was used and scattered light was measured at 173° (back scattering). The attenuator and position was selected automatically by the instrument and particle sizes reported as the average of 4 measurements.

TEM images were obtained on a JEOL 2000fx microscope, 200 kV, LaB₆ instrument operated with a beam current of ~115 mA; images were captured using a Gatan Orius 11 megapixel camera. Samples were prepared by deposition and drying of nanoparticle samples (10 μ L of stock solutions) onto lacey carbon 300-mesh copper TEM grids (Agar Scientific). Diameters were measured using ImageJ version 1.48a; average values were calculated by counting a minimum of 60 particles.

5.5.3 Procedures

5.5.3.1 Example polymerisation of *N*-hydroxyethylacrylamide using 1-((3,4-dihydroxyphenethyl)amino)2-methyl-1-oxopropan-2-yl dodecyl carbonotrithioate

N-hydroxyethylacrylamide (1.00 g, 8.69 mmol), compound **3** (75.90 mg, 115.91 μ mol) and 4,4'-azobis(4-cyanovaleric acid) (6.50 mg, 23.18 μ mol) were added to a vial fitted with stir bar and rubber septum and dissolved in methanol:toluene (50:50) (2 mL). Mesitylene (0.20 mL) was added as internal reference and the mixture stirred (5 mins). An aliquot of this starting mixture was removed for ¹H NMR spectroscopic analysis. The mixture was degassed by bubbling through nitrogen gas for 30 mins and placed in an oil bath thermostated at 70 °C for 35 mins. The reaction was quenched in liquid nitrogen, an aliquot removed and conversion determined by ¹H NMR spectroscopy. The product was purified three times by precipitation from methanol into cold diethyl ether, the solid isolated by centrifugation and dried to yield a pale yellow solid. Conversion (NMR): 78.5 % M_n (theoretical): 6800 g.mol⁻¹; M_n (SEC): 9700 g.mol⁻¹; M_w/M_n (SEC): 1.17.

5.5.3.2 Polymerisation of *N*-hydroxyethylacrylamide using benzyl 2-[(*tert*-butoxycarbonyl)amino]ethyl trithiocarbonate

N-hydroxyethylacrylamide (1.00 g, 8.69 mmol), benzyl 2-[(*tert*-butoxycarbonyl)amino]ethyl trithiocarbonate (39.76 mg, 115.91 μmol), 4,4'-azobis(4-cyanovaleric acid) (6.50 mg, 23.18 μmol) were added to a vial fitted with stir bar and rubber septum and dissolved in methanol:toluene (50:50) (2 mL). Mesitylene (0.20 mL) was added as internal reference and the mixture stirred (5 mins). An aliquot of this starting mixture was removed for ^1H NMR spectroscopic analysis. The mixture was degassed by bubbling through nitrogen gas for 30 mins and placed in an oil bath thermostated at 70 °C for 45 mins. The reaction was quenched in liquid nitrogen, an aliquot removed and conversion determined by ^1H NMR spectroscopy. The product was purified three times by precipitation from methanol into cold diethyl ether, the solid isolated by centrifugation and dried to yield a pale yellow solid. Conversion (NMR): 74.1 % M_n (theoretical): 6400 $\text{g}\cdot\text{mol}^{-1}$; M_n (SEC): 10200 $\text{g}\cdot\text{mol}^{-1}$; M_w/M_n (SEC): 1.16

5.5.3.3 Functionalisation of gold nanoparticles with polymer (pHEA-1/2/3/4@AuNP₄₀)

Polymer was dissolved in citrated coated gold nanoparticle suspension at a concentration of 2 $\text{mg}\cdot\text{mL}^{-1}$ and left at 5 °C overnight. The solution was centrifuged (15 mins, 10000 rpm), supernatant removed and the pellet re-dispersed in distilled water. This washing procedure was repeated a total of 4 times, the pellet re-dispersed in equal volume of distilled water and stored in the fridge until required.

5.5.4 Assay Conditions

5.5.4.1 General procedure for UV/visible spectrophotometry assay of gold nanoparticles

In triplicate in a 96-well plate, polymer-coated gold nanoparticle suspension (95 μL), concentrated sodium chloride solution (5 μL) and freshly-prepared, concentrated iron(III) chloride hexahydrate or iron(II) chloride tetrahydrate solution were added to give the desired final concentrations. After incubation for 30 mins at room temperature, the UV-visible spectrum between 450 and 700 nm was recorded. Data presented is the mean average of three replicates.

5.6 References

- 1 Que, E. L.; Domaille, D. W.; Chang, C. J. Metals in Neurobiology: Probing Their Chemistry and Biology with Molecular Imaging. *Chem. Rev.* **2008**, *108*, 1517-1549.
- 2 Andrews, N. C. Disorders of Iron Metabolism. *New Engl. J. Med.* **1999**, *341*, 1986-1995.
- 3 Winterbourn, C. C. Toxicity of iron and hydrogen peroxide: the Fenton reaction. *Toxicol. Lett.* **1995**, *82–83*, 969-974.
- 4 Bush, A. I. Metals and neuroscience. *Curr. Opin. Chem. Biol.* **2000**, *4*, 184-191.
- 5 Zheng, T.; Nolan, E. M. Siderophore-based detection of Fe(III) and microbial pathogens. *Metallomics* **2012**, *4*, 866-880.
- 6 Correnti, C.; Strong, R. K. Mammalian Siderophores, Siderophore-binding Lipocalins, and the Labile Iron Pool. *J. Biol. Chem.* **2012**, *287*, 13524-13531.
- 7 Skaar, E. P. The Battle for Iron between Bacterial Pathogens and Their Vertebrate Hosts. *PLoS Pathog.* **2010**, *6*, e1000949.
- 8 Hider, R. C.; Kong, X. Chemistry and biology of siderophores. *Nat. Prod. Rep.* **2010**, *27*, 637-657.
- 9 Goetz, D. H.; Holmes, M. A.; Borregaard, N.; Bluhm, M. E.; Raymond, K. N.; Strong, R. K. The Neutrophil Lipocalin NGAL Is a Bacteriostatic Agent that Interferes with Siderophore-Mediated Iron Acquisition. *Mol. Cell* **2002**, *10*, 1033-1043.
- 10 Flo, T. H.; Smith, K. D.; Sato, S.; Rodriguez, D. J.; Holmes, M. A.; Strong, R. K.; Akira, S.; Aderem, A. Lipocalin 2 mediates an innate immune response to bacterial infection by sequestering iron. *Nature* **2004**, *432*, 917-921.
- 11 Allred, B. E.; Correnti, C.; Clifton, M. C.; Strong, R. K.; Raymond, K. N. Siderocalin Outwits the Coordination Chemistry of Vibriobactin, a Siderophore of *Vibrio cholerae*. *ACS Chem. Biol.* **2013**, *8*, 1882-1887.
- 12 Bernhardt, P. V. Coordination chemistry and biology of chelators for the treatment of iron overload disorders. *Dalton Trans.* **2007**, 3214-3220.

- 13 Hanspeter, N. Iron chelation, quo vadis? *Curr. Opin. Chem. Biol.* **2007**, *11*, 419-423.
- 14 Lu, Y.; Miller, M. J. Syntheses and studies of multiwarhead siderophore-5-fluorouridine conjugates. *Bioorg. Med. Chem.* **1999**, *7*, 3025-3038.
- 15 Möllmann, U.; Heinisch, L.; Bauernfeind, A.; Köhler, T.; Ankel-Fuchs, D. Siderophores as drug delivery agents: application of the “Trojan Horse” strategy. *Biometals* **2009**, *22*, 615-624.
- 16 Starr, J.; Brown, M. F.; Aschenbrenner, L.; Caspers, N.; Che, Y.; Gerstenberger, B. S.; Huband, M.; Knafels, J. D.; Lemmon, M. M.; Li, C.; McCurdy, S. P.; McElroy, E.; Rauckhorst, M. R.; Tomaras, A. P.; Young, J. A.; Zaniewski, R. P.; Shanmugasundaram, V.; Han, S. Siderophore Receptor-Mediated Uptake of Lactivicin Analogues in Gram-Negative Bacteria. *J. Med. Chem.* **2014**, *57*, 3845-3855.
- 17 Zheng, T.; Nolan, E. M. Enterobactin-Mediated Delivery of β -Lactam Antibiotics Enhances Antibacterial Activity against Pathogenic *Escherichia coli*. *J. Am. Chem. Soc.* **2014**, *136*, 9677-9691.
- 18 Liu, Z.; He, W.; Guo, Z. Metal coordination in photoluminescent sensing. *Chem. Soc. Rev.* **2013**, *42*, 1568-1600.
- 19 Hancock, R. D. The pyridyl group in ligand design for selective metal ion complexation and sensing. *Chem. Soc. Rev.* **2013**, *42*, 1500-1524.
- 20 Burdette, S. C.; Frederickson, C. J.; Bu, W.; Lippard, S. J. ZP4, an Improved Neuronal Zn^{2+} Sensor of the Zinpyr Family. *J. Am. Chem. Soc.* **2003**, *125*, 1778-1787.
- 21 Lee, J.-S.; Han, M. S.; Mirkin, C. A. Colorimetric Detection of Mercuric Ion (Hg^{2+}) in Aqueous Media using DNA-Functionalized Gold Nanoparticles. *Angew. Chem. Int. Ed.* **2007**, *119*, 4171-4174.
- 22 Agasti, S. S.; Rana, S.; Park, M.-H.; Kim, C. K.; You, C.-C.; Rotello, V. M. Nanoparticles for detection and diagnosis. *Adv. Drug Deliv. Rev.* **2010**, *62*, 316-328.
- 23 Xiang, Y.; Lu, Y. DNA as Sensors and Imaging Agents for Metal Ions. *Inorg. Chem.* **2013**, *53*, 1925-1942.
- 24 Wen, S.; Zeng, T.; Liu, L.; Zhao, K.; Zhao, Y.; Liu, X.; Wu, H.-C. Highly Sensitive and Selective DNA-Based Detection of Mercury(II) with α -Hemolysin Nanopore. *J. Am. Chem. Soc.* **2011**, *133*, 18312-18317.

- 25 Luo, X.; Morrin, A.; Killard, A. J.; Smyth, M. R. Application of Nanoparticles in Electrochemical Sensors and Biosensors. *Electroanal.* **2006**, *18*, 319-326.
- 26 Gooding, J.; Hibbert, D.; Yang, W. Electrochemical Metal Ion Sensors. Exploiting Amino Acids and Peptides as Recognition Elements. *Sensors* **2001**, *1*, 75-90.
- 27 Mei, Q.; Jiang, C.; Guan, G.; Zhang, K.; Liu, B.; Liu, R.; Zhang, Z. Fluorescent graphene oxide logic gates for discrimination of iron (3+) and iron (2+) in living cells by imaging. *Chem. Commun.* **2012**, *48*, 7468-7470.
- 28 Carter, K. P.; Young, A. M.; Palmer, A. E. Fluorescent Sensors for Measuring Metal Ions in Living Systems. *Chem. Rev.* **2014**, *114*, 4564-4601.
- 29 Domaille, D. W.; Que, E. L.; Chang, C. J. Synthetic fluorescent sensors for studying the cell biology of metals. *Nat. Chem. Biol.* **2008**, *4*, 168-175.
- 30 Doria, G.; Conde, J.; Veigas, B.; Giestas, L.; Almeida, C.; Assunção, M.; Rosa, J.; Baptista, P. V. Noble Metal Nanoparticles for Biosensing Applications. *Sensors* **2012**, *12*, 1657-1687.
- 31 Grzelczak, M.; Perez-Juste, J.; Mulvaney, P.; Liz-Marzan, L. M. Shape control in gold nanoparticle synthesis. *Chem. Soc. Rev.* **2008**, *37*, 1783-1791.
- 32 Shan, J.; Tenhu, H. Recent advances in polymer protected gold nanoparticles: synthesis, properties and applications. *Chem. Commun.* **2007**, 4580-4598.
- 33 Obare, S. O.; Hollowell, R. E.; Murphy, C. J. Sensing Strategy for Lithium Ion Based on Gold Nanoparticles. *Langmuir* **2002**, *18*, 10407-10410.
- 34 Yu, C.-J.; Tseng, W.-L. Colorimetric Detection of Mercury(II) in a High-Salinity Solution Using Gold Nanoparticles Capped with 3-Mercaptopropionate Acid and Adenosine Monophosphate. *Langmuir* **2008**, *24*, 12717-12722.
- 35 Jiang, Z.; Fan, Y.; Chen, M.; Liang, A.; Liao, X.; Wen, G.; Shen, X.; He, X.; Pan, H.; Jiang, H. Resonance Scattering Spectral Detection of Trace Hg²⁺ Using Aptamer-Modified Nanogold as Probe and Nanocatalyst. *Anal. Chem.* **2009**, *81*, 5439-5445.
- 36 Patel, G.; Kumar, A.; Pal, U.; Menon, S. Potassium ion recognition by facile dithiocarbamate assembly of benzo-15-crown-5-gold nanoparticles. *Chem. Commun.* **2009**, 1849-1851.

- 37 Chen, S.; Fang, Y.-M.; Xiao, Q.; Li, J.; Li, S.-B.; Chen, H.-J.; Sun, J.-J.; Yang, H.-H. Rapid visual detection of aluminium ion using citrate capped gold nanoparticles. *Analyst* **2012**, *137*, 2021-2023.
- 38 Liu, J.; Lu, Y. A Colorimetric Lead Biosensor Using DNAzyme-Directed Assembly of Gold Nanoparticles. *J. Am. Chem. Soc.* **2003**, *125*, 6642-6643.
- 39 Chen, Y.-C.; Lee, I. L.; Sung, Y.-M.; Wu, S.-P. Triazole functionalized gold nanoparticles for colorimetric Cr³⁺ sensing. *Sensor. Actuat. B: Chem.* **2013**, *188*, 354-359.
- 40 Bai, L.; Zhu, L.; Ang, C. Y.; Li, X.; Wu, S.; Zeng, Y.; Ågren, H.; Zhao, Y. Iron(III)-Quantity-Dependent Aggregation–Dispersion Conversion of Functionalized Gold Nanoparticles. *Chem. Eur. J.* **2014**, *20*, 4032-4037.
- 41 Tripathy, S. K.; Woo, J. Y.; Han, C.-S. Colorimetric detection of Fe(III) ions using label-free gold nanoparticles and acidic thiourea mixture. *Sensor. Actuat. B: Chem.* **2013**, *181*, 114-118.
- 42 Wu, S.-P.; Chen, Y.-P.; Sung, Y.-M. Colorimetric detection of Fe³⁺ ions using pyrophosphate functionalized gold nanoparticles. *Analyst* **2011**, *136*, 1887-1891.
- 43 Kaim, W. S., B.; Klein, A. *Inorganic Biochemistry: Inorganic Elements in the Chemistry of Life*. John Wiley & Sons, Ltd: Chichester, **2013**.
- 44 Yuen, A. K. L.; Hutton, G. A.; Masters, A. F.; Maschmeyer, T. The interplay of catechol ligands with nanoparticulate iron oxides. *Dalton Trans.* **2012**, *41*, 2545-2559.
- 45 Thomas, A.; Bauer, H.; Schilman, A.-M.; Fischer, K.; Tremel, W.; Frey, H. The “Needle in the Haystack” Makes the Difference: Linear and Hyperbranched Polyglycerols with a Single Catechol Moiety for Metal Oxide Nanoparticle Coating. *Macromolecules* **2014**, *47*, 4557-4566.
- 46 Zhu, Y.; Sundaram, H. S.; Liu, S.; Zhang, L.; Xu, X.; Yu, Q.; Xu, J.; Jiang, S. A Robust Graft-to Strategy To Form Multifunctional and Stealth Zwitterionic Polymer-Coated Mesoporous Silica Nanoparticles. *Biomacromolecules* **2014**, *15*, 1845-1851.
- 47 Black, K. C. L.; Liu, Z.; Messersmith, P. B. Catechol Redox Induced Formation of Metal Core–Polymer Shell Nanoparticles. *Chem. Mater.* **2011**, *23*, 1130-1135.

- 48 Marcelo, G.; Fernandez-Garcia, M. Direct preparation of PNIPAM coating gold nanoparticles by catechol redox and surface adhesion chemistry. *RSC Adv.* **2014**, *4*, 11740-11749.
- 49 Lee, Y.; Lee, S. H.; Kim, J. S.; Maruyama, A.; Chen, X.; Park, T. G. Controlled synthesis of PEI-coated gold nanoparticles using reductive catechol chemistry for siRNA delivery. *J. Contr. Rel.* **2011**, *155*, 3-10.
- 50 Inomata, T.; Murase, T.; Ido, H.; Ozawa, T.; Masuda, H. Gold Nanoparticles Modified with Artificial Siderophore–Iron(III) Ion Complexes: Selective Adsorption and Aggregation of Microbes Using “Coordination Programming”. *Chem. Lett.* **2014**, *43*, 1146-1148.
- 51 Chiefari, J.; Chong, Y. K.; Ercole, F.; Krstina, J.; Jeffery, J.; Le, T. P. T.; Mayadunne, R. T. A.; Meijs, G. F.; Moad, C. L.; Moad, G.; Rizzardo, E.; Thang, S. H. Living Free-Radical Polymerization by Reversible Addition–Fragmentation Chain Transfer: The RAFT Process. *Macromolecules* **1998**, *31*, 5559-5562.
- 52 Zobrist, C. d.; Sobocinski, J.; Lyskawa, J. I.; Fournier, D.; Miri, V. r.; Traisnel, M.; Jimenez, M.; Woisel, P. Functionalization of Titanium Surfaces with Polymer Brushes Prepared from a Biomimetic RAFT Agent. *Macromolecules* **2011**, *44*, 5883-5892.
- 53 Gibson, M. I.; Paripovic, D.; Klok, H.-A. Size-Dependent LCST Transitions of Polymer-Coated Gold Nanoparticles: Cooperative Aggregation and Surface Assembly. *Adv. Mater.* **2010**, *22*, 4721-4725.
- 54 Gibson, M. I.; Danial, M.; Klok, H.-A. Sequentially Modified, Polymer-Stabilized Gold Nanoparticle Libraries: Convergent Synthesis and Aggregation Behavior. *ACS Comb. Sci.* **2011**, *13*, 286-297.
- 55 Richards, S.-J.; Fullam, E.; Besra, G. S.; Gibson, M. I. Discrimination between bacterial phenotypes using glyco-nanoparticles and the impact of polymer coating on detection readouts. *J. Mater. Chem. B* **2014**, *2*, 1490-1498.
- 56 Zhang, H.; Wang, D. Controlling the Growth of Charged-Nanoparticle Chains through Interparticle Electrostatic Repulsion. *Angew. Chem. Int. Ed.* **2008**, *47*, 3984-3987.
- 57 Yusa, S.-i.; Fukuda, K.; Yamamoto, T.; Iwasaki, Y.; Watanabe, A.; Akiyoshi, K.; Morishima, Y. Salt Effect on the Heat-Induced Association Behavior of

- Gold Nanoparticles Coated with Poly(*N*-isopropylacrylamide) Prepared via Reversible Addition–Fragmentation Chain Transfer (RAFT) Radical Polymerization. *Langmuir* **2007**, *23*, 12842-12848.
- 58 Zhang, Z.; Maji, S.; Antunes, A. B. d. F.; De Rycke, R.; Zhang, Q.; Hoogenboom, R.; De Geest, B. G. Salt Plays a Pivotal Role in the Temperature-Responsive Aggregation and Layer-by-Layer Assembly of Polymer-Decorated Gold Nanoparticles. *Chem. Mater.* **2013**, *25*, 4297-4303.
- 59 Williams, R. J. P. Role of transition metal ions in biological processes. *R. Inst. Chem., Rev.* **1968**, *1*, 13-38.
- 60 Evenäs, J.; Malmendal, A.; Forsén, S. Calcium. *Curr. Opin. Chem. Biol.* **1998**, *2*, 293-302.
- 61 Kozłowski, H.; Janicka-Kłos, A.; Brasun, J.; Gaggelli, E.; Valensin, D.; Valensin, G. Copper, iron, and zinc ions homeostasis and their role in neurodegenerative disorders (metal uptake, transport, distribution and regulation). *Coord. Chem. Rev.* **2009**, *253*, 2665-2685.
- 62 Porter, R. S. *et al.* (Eds.) *Common Medical Tests. In The Merck Manual Home Health Handbook*. Merck Research Laboratories: Whitehouse Station, NJ, **2009**.

Chapter 6

6. Using an Enzymatic Trigger to Stimulate Isothermal Cell Uptake

6.1 Chapter Summary

The synthesis of polymers bearing phosphate-rich side-chains by Reversible Addition-Fragmentation Chain Transfer (RAFT) polymerisation of a phosphorylated methacrylate (Phos-HEMA) is described. These polymers were shown to be susceptible to the enzyme calf intestinal alkaline phosphatase which cleaves phosphates to hydroxyl-functional groups irrespective of polymer molecular weight up to $11500 \text{ g}\cdot\text{mol}^{-1}$. Phos-HEMA was co-polymerised with diethylene glycol methyl ether methacrylate (DEGMA) to produce thermo-responsive materials with the observed cloud point dependent on the percentage of Phos-HEMA included. The cloud point was also shown to be reduced in the presence of the enzyme due to dephosphorylation of the polymer side-chain allowing a switch in solubility to be achieved isothermally. An MTT assay indicated both pDEGMA-*co*-Phos-HEMA and pNIPAM were biocompatible with MCF7 cells up to at least a concentration of $1.8 \text{ mg}\cdot\text{mL}^{-1}$. The cloud points of these polymers displayed an inversely proportional dependency on polymer concentration and also varied depending on the medium (deionised water, PBS and RPMI 1640) in which they were dissolved. The uptake of these polymers by MCF7 cells was shown to increase when heated above their LCST.

6.2 Introduction

Responsive polymers provide a valuable tool in drug delivery with common stimuli including pH, light, and electric fields.¹⁻³ Enzymes are a particularly attractive stimulus where specific responses are desired given their highly specialised nature and unique localisation to certain tissues. For example, azoreductase is produced by the microbial flora present in the colon;⁴ pepsin is present at high levels in the stomach⁵ and a variety of digestive enzymes exist throughout the gastrointestinal tract.⁶ They can also provide valuable biomarkers with a range of stress and disease states characterised by imbalances in enzyme expression and activity.⁷ For instance, hepsin is a protease overexpressed in the early stages of prostate cancer,⁸ cathepsins are released at inflammatory sites⁹ and matrix metalloproteinases have been linked to vascular disease and tumour growth.^{10, 11}

The use of enzymes to trigger a specific response and hence manipulate the structures and pharmacokinetics of polymer-based materials has recently received increasing attention.¹²⁻¹⁴ A number of groups have utilised enzymes to trigger nanoparticle disassembly such as Rao and Khan who prepared polymeric micelles containing an azoreductase-susceptible azobenzene linkage at the copolymer junction of an amphiphilic diblock copolymer. Treatment of the aqueous-assembled micelle with this enzyme, in the presence of the coenzyme NADPH, cleaved the junction and disrupted the micellar assembly.¹⁵ A similar approach has been employed by Harnoy *et al.* who used penicillin G amidase to disrupt phenyl acetamide-containing micelles.¹⁶ Thayumanavan and co-workers have prepared dendrimer-based amphiphilic nanocontainers containing ester units which are cleaved to release encapsulated guests in the presence of porcine liver esterase.¹⁷

Fuchs *et al.* have prepared nanoparticles from polystyrene-peptide-polystyrene triblock copolymers with the peptide susceptible to different enzymes depending on its sequence: Trypsin or hepsin could be used depending on whether a Gly-Phe-Phe or Arg-Gln-Leu-Arg-Val-Val-Gly-Gly sequence was present respectively.¹⁸ Enzymes have also been shown to promote material assembly. For example, Hu and Messersmith have used transglutaminase – a protein cross-linking enzyme which catalyses an acyl-transfer reaction between the γ -carboxamide group of glutaminy residues and the ϵ -amino group of lysine residues - as a gelation agent in the assembly of hydrogels¹⁹ whilst peroxidases²⁰ and tyrosinases²¹ have also been used. Furthermore, an enzyme-based response has been applied to modulate the mechanical properties of nanofiber networks,²² for triggered release from liposome-based platforms²³ and for surface modification.^{24, 25}

A particularly interesting class of enzyme is that of phosphatases which catalyse the hydrolysis of phosphate monoesters.²⁶ Within this family, alkaline phosphatase (ALP) is found in the liver and bone, as well as in the intestinal lining, placenta and the kidney. ALP is important for a variety of physiological processes such as mineralisation and osteogenesis.^{27, 28} Elevated levels of the enzyme can therefore be implicated in Paget's bone disease,²⁹ whilst depleted levels have been linked with Wilson's disease³⁰ and in a range of cancer types.³¹ Considering this, there is clear incentive for the development of alkaline phosphatase-responsive systems. Xu and co-workers used ALP to trigger hydrogelation by neutralising an ionic group on an amino acid derivative, rendering it a small-molecular hydrogelator.³² Wang *et al.* have prepared a phosphatase-responsive system using electrostatic interactions between a double hydrophilic block copolymer comprising poly(ethylene glycol), poly(L-lysine hydrochloride) and adenosine 5'-triphosphate (ATP) to form a

superamphiphile in aqueous solution. Addition of ALP hydrolyses ATP to single phosphates and a neutral adenine group prompting aggregate disassembly.³³ Zelzer and co-workers have prepared a peptide-based surface whose chemical properties change upon the catalytic action of ALP.³⁴

The ability to combine the specificity of stimuli such as enzymatic action with other complex responses holds great promise for a variety of applications, a concept which has been recently reviewed by Schattling *et al.*³⁵ For example, thermally-responsive systems typically undergo an abrupt solubility change with an aqueous polymer solution either phase separating (LCST), or a phase-separated mixture re-solubilising (UCST) upon heating. To exemplify the LCST, it is well-known that introducing hydrophobicity to the system decreases the transition temperature.^{36, 37} It is therefore reasonable to assume that the phosphatase-driven dephosphorylation of a phosphate to hydroxyl functional group will decrease the hydrophilicity of the system and hence affect the LCST, allowing an isothermal change in polymer solubility. Few examples combining a thermal response with the specificity of enzymes exist in the literature. One example presented by the Ulijn group combines the thermo-responsive properties of poly(2-isopropyl-2-oxazoline) (PiPrOx) with a phosphate-containing fluorenylmethoxycarbonyl-tyrosine (Fmoc-*p*Y). Treatment of Fmoc-*p*Y-PiPrOx with alkaline phosphatase caused a decrease in cloud point by 2 °C due to removal of hydrophilic phosphate, whilst the unmodified polymer saw no change. Phosphate loss was also used to trigger self-assembly (Figure 6.1).³⁸

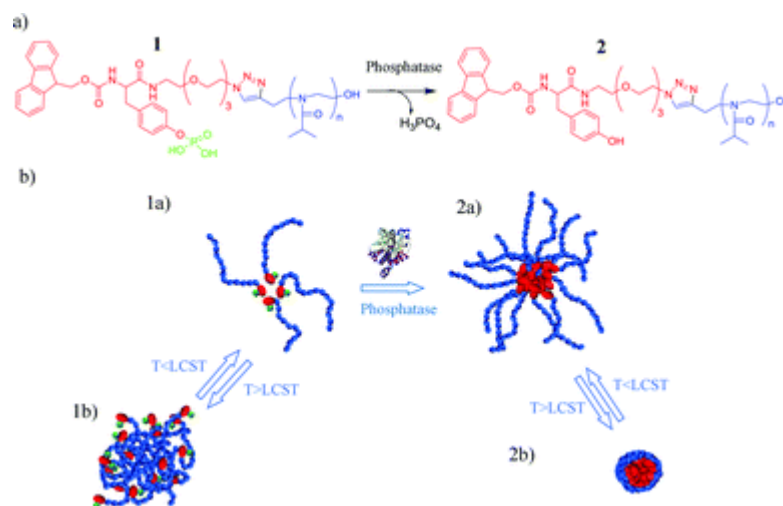


Figure 6.1 (a) Dephosphorylation of Fmoc-*p*Y-PiPrOx catalysed by phosphatase and (b) schematic representation of enzyme- and temperature-induced self-assembly behaviour of the polymer bioconjugate.³⁸

Whilst the solubility switch associated with the LCST has found numerous applications in, for example, catalysis³⁹ and purification,⁴⁰ it has also been used to trigger the uptake of various functional structures into cells due to increased lipophilicity and membrane permeability.⁴¹ For example, Alexander and co-workers have prepared nanoparticles comprising a biodegradable poly(lactide-*co*-glycolide) core, in which paclitaxel was internalised, and a thermo-responsive PEG-based shell. Significantly enhanced uptake and paclitaxel-based cytotoxicity was observed when incubated above the particle thermal transition temperature.⁴² In addition to polymer nanoparticles,⁴¹ other structures which have employed this property to enhance cell uptake include liposomes,⁴³ hydrogel submicron particles⁴⁴ and elastin-like polypeptides.^{45, 46}

An attractive extension of this concept would be to trigger cell uptake using localised biochemical environments, such as local enzyme concentrations, as a polymer solubility modifier. This feature would enhance the selectivity of such systems and

provide an alternative approach to the more traditional, receptor-mediated uptake pathways.⁴⁷⁻⁵¹ Considering this, the following chapter first explores the synthesis of phosphate-functional polymers capable of responding to the presence of alkaline phosphatase and their subsequent elaboration into thermo-responsive structures is assessed. Secondly, the use of an LCST to enhance cell uptake into a human breast adenocarcinoma (MCF7) cell line is determined before finally investigating the ability to selectively trigger uptake using alkaline phosphatase as the LCST modifier.

6.3 Results and Discussion

6.3.1 Synthesis of Phosphorylated Polymers

Polymers containing phosphate moieties in their side-chain can be produced through the polymerisation of ethylene glycol methacrylate phosphate (Phos-HEMA), a commercially available monomer. Very few examples of the polymerisation of this monomer in its native state by controlled radical processes exist. Previous reports on the polymerisation of phosphate-containing monomers by Atom Transfer Radical Polymerisation (ATRP) have described slow polymerisation rates and side reactions as the result of complexation between the metal used in ATRP and the phosphate group.⁵² Zhou and Huck circumvented this by polymerising a deprotonated Phos-HEMA.⁵³ Reports of the RAFT polymerisation of this monomer are also rare with most reports polymerising a protected monomer and generating phosphate groups through subsequent deprotection.⁵⁴ The first polymerisation of Phos-HEMA by RAFT was reported by Suzuki *et al.*⁵⁵ Subsequently, Yusa and co-workers used RAFT polymerisation to prepare Phos-HEMA containing block co-polymers.⁵⁶ In our hands, polymerisation of a commercially available Phos-HEMA by RAFT using 4,4'-azobis(4-cyanovaleric acid) and 4-cyano-4-(phenylcarbonothioylthio) pentanoic acid as initiator and chain-transfer agent respectively produced an insoluble, cross-linked gel within minutes. This observation was initially surprising given the addition of a similar chain transfer agent (CTA) concentration (0.02 M) to that described by Suzuki *et al.*⁵⁵ However, analysis of the "monomeric" starting material by ³¹P NMR spectroscopy revealed three peaks corresponding to free phosphate, orthophosphoric acid (0.91 ppm), phos-HEMA (0.07 ppm) and a diene (-0.74 ppm) in a ratio of 0.5:1:0.5 (Figure 6.2).⁵⁷ Dienes are a common additive where cross-

linking is required⁵⁸ hence the presence of a significant portion (~25 %) of this compound most likely explains the observed gelation.

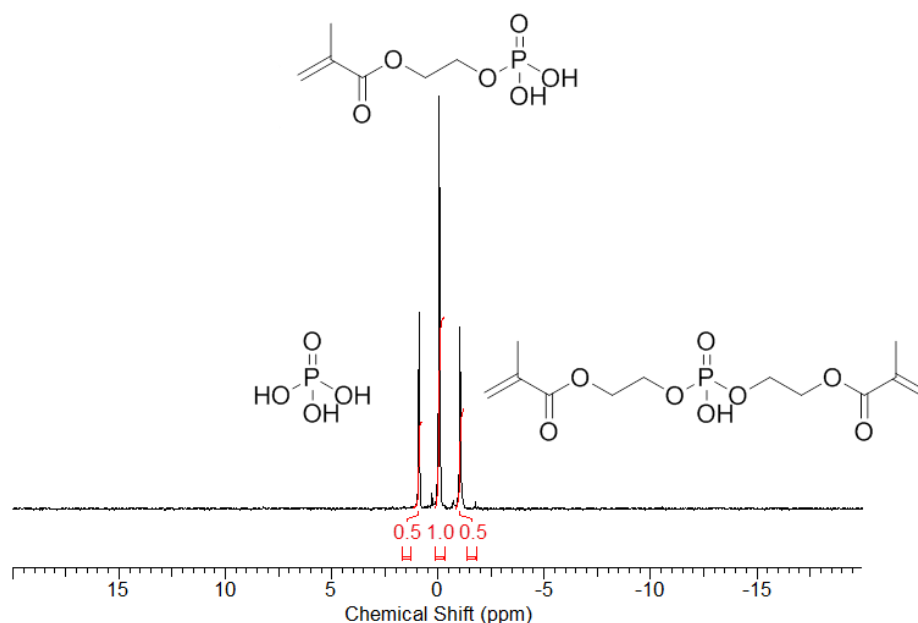
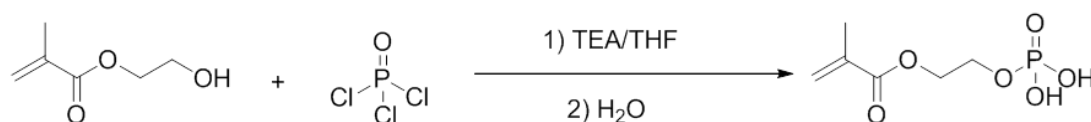


Figure 6.2 ³¹P NMR spectrum of ethylene glycol methacrylate phosphate (commercial product) - assignment based on previous report.⁵⁷

Considering this, a purer monomer was synthesised using phosphorus oxychloride, POCl₃, as phosphorylation agent (Scheme 6.1).⁵⁹



Scheme 6.1 Synthetic scheme for the preparation of Phos-HEMA.

Pleasingly, this reaction produced the desired monomer in good yield, with negligible traces of the undesired diene impurity. ¹H NMR spectroscopic analysis revealed vinyl proton peaks at 6.17 and 5.67 ppm, together with two CH₂ groups and one CH₃ group at 4.37, 4.21 and 1.97 ppm respectively (Figure 6.3A). Doublets at 64.1 and 63.5 ppm observed in the ¹³C NMR spectrum on account of coupling with the phosphorus atom and the single peak observed by ³¹P NMR spectroscopic analysis further confirmed monomer structure and purity (Figure 6.3B/C).

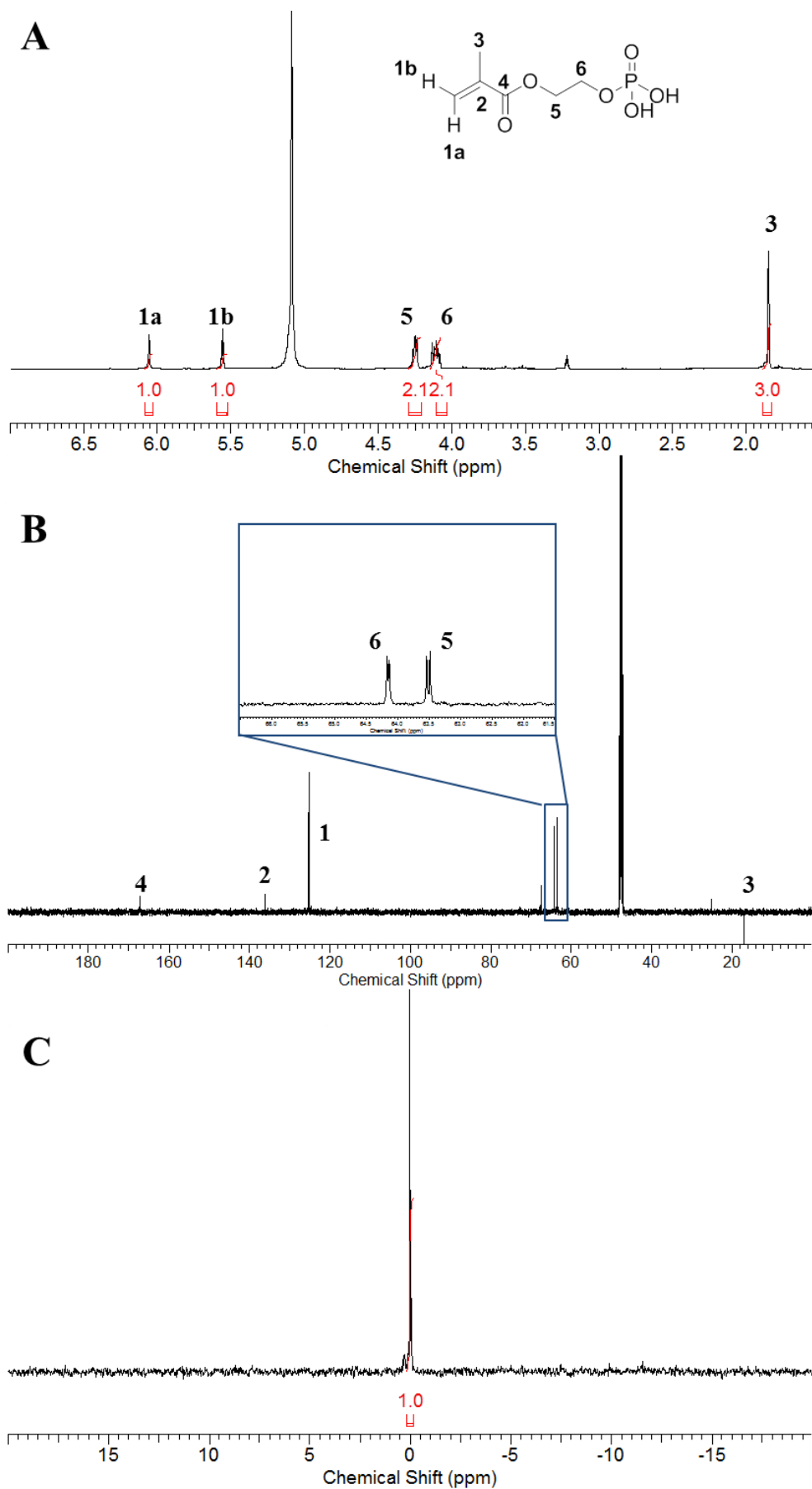


Figure 6.3 NMR characterisation of Phos-HEMA: (A) ^1H ; (B) ^{13}C and (C) ^{31}P NMR.

With phosphorylated monomer in hand, phosphate-functional polymers were prepared by the RAFT process. Given the few reports on this, preliminary experiments were performed to better understand the polymerisation rate, and to check the kinetics adhered to controlled radical polymerisation theory. Two chain transfer agents, 4-cyano-4-(phenylcarbonothioylthio) pentanoic acid and 2-(dodecylthiocarbonothioylthio)-2-methylpropanoic acid were employed in a reaction mixture comprising $[M]:[CTA]:[Initiator] = 100:1:0.2$, and an initial monomer concentration of 1.19 M. Mesitylene was used as an internal standard and conversion was monitored by ^1H NMR spectroscopy, following the change in integral of vinyl proton peak relative to this standard. Polymerisation was observed to be faster using the trithiocarbonate compared to the dithiobenzoate, with approximately 85 % conversion reached after 10 and 24 hours respectively (Figure 6.4A). A key characteristic of controlled radical processes is the progression of first order kinetics.⁶⁰ This was observed in the case of both chain transfer agents (Figure 6.4B).

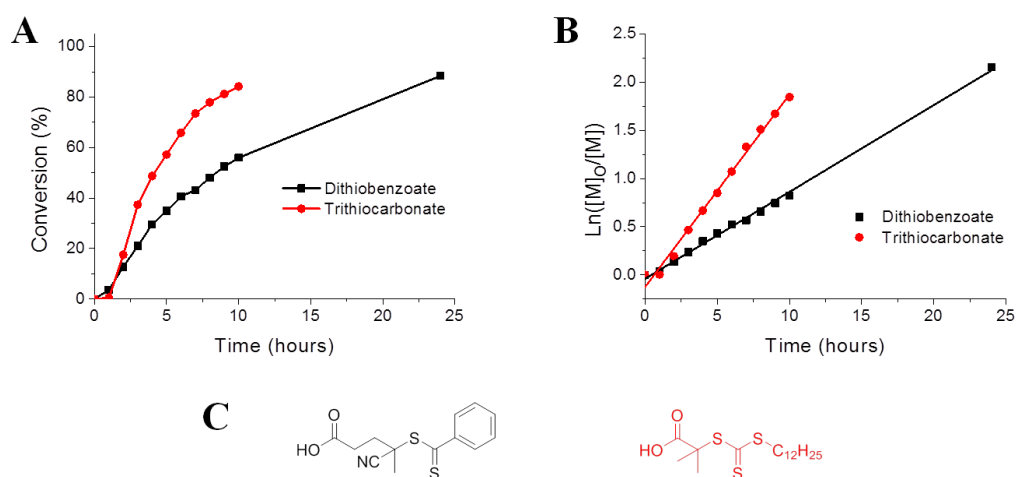


Figure 6.4 Kinetic results from the RAFT polymerisation of Phos-HEMA: (A) time-dependent monomer conversion; (B) pseudo first order kinetic plot with (C) dithiobenzoate and trithiocarbonate chain transfer agents.

With the controlled polymerisation of this monomer by RAFT confirmed, the dithiobenzoate chain transfer agent was used to prepare a series of small molecular weight polymers (Table 6.1, Figure 6.5A). At higher molecular weights, the dispersity becomes broader than typically desired for controlled radical methodologies, with a high molecular weight shoulder beginning to develop. This may be an artefact of the SEC system used – for instance, partial deprotonation of the phosphate functionality may influence the hydrodynamic volume of some polymer chains or, may be the result of the polymerisation methodology employed. If more well-defined polymers are desired, alternative chain transfer agents may be required or different methods towards making the polymer, such as through post-polymerisation modification, may require investigation. For our purpose however, RAFT was simply used as a facile route towards the preparation of phosphate-functional polymers. To confirm the presence of this functional group, ^{31}P NMR analysis of the purified material was performed and revealed a single phosphorus peak, confirming the presence of a phosphate group and hence the suitable application of the RAFT technique (Figure 6.5B). Moreover, the use of a diene-free monomer ensured the poly(diester) observed in previous reports⁵⁵ was not seen in our case.

Table 6.1 Characterisation of pPhos-HEMA samples prepared using 4-cyano-4-(phenylcarbonothioylthio) pentanoic acid in this study.

Polymer	[M]:[CTA]	Conversion (%)^a	$M_{n(\text{th})}$ (g.mol⁻¹)^a	$M_{n(\text{SEC})}$ (g.mol⁻¹)^b	M_w/M_n^b
pPhos-HEMA-1	10	41.2	870	9400	1.24
pPhos-HEMA-2	75	50.8	8000	30900	2.00
pPhos-HEMA-3	100	54.7	11500	38000	2.20

^aDetermined by ^1H NMR spectroscopy relative to an internal standard (mesitylene);

^bDetermined by SEC (aqueous) relative to PEO standards.

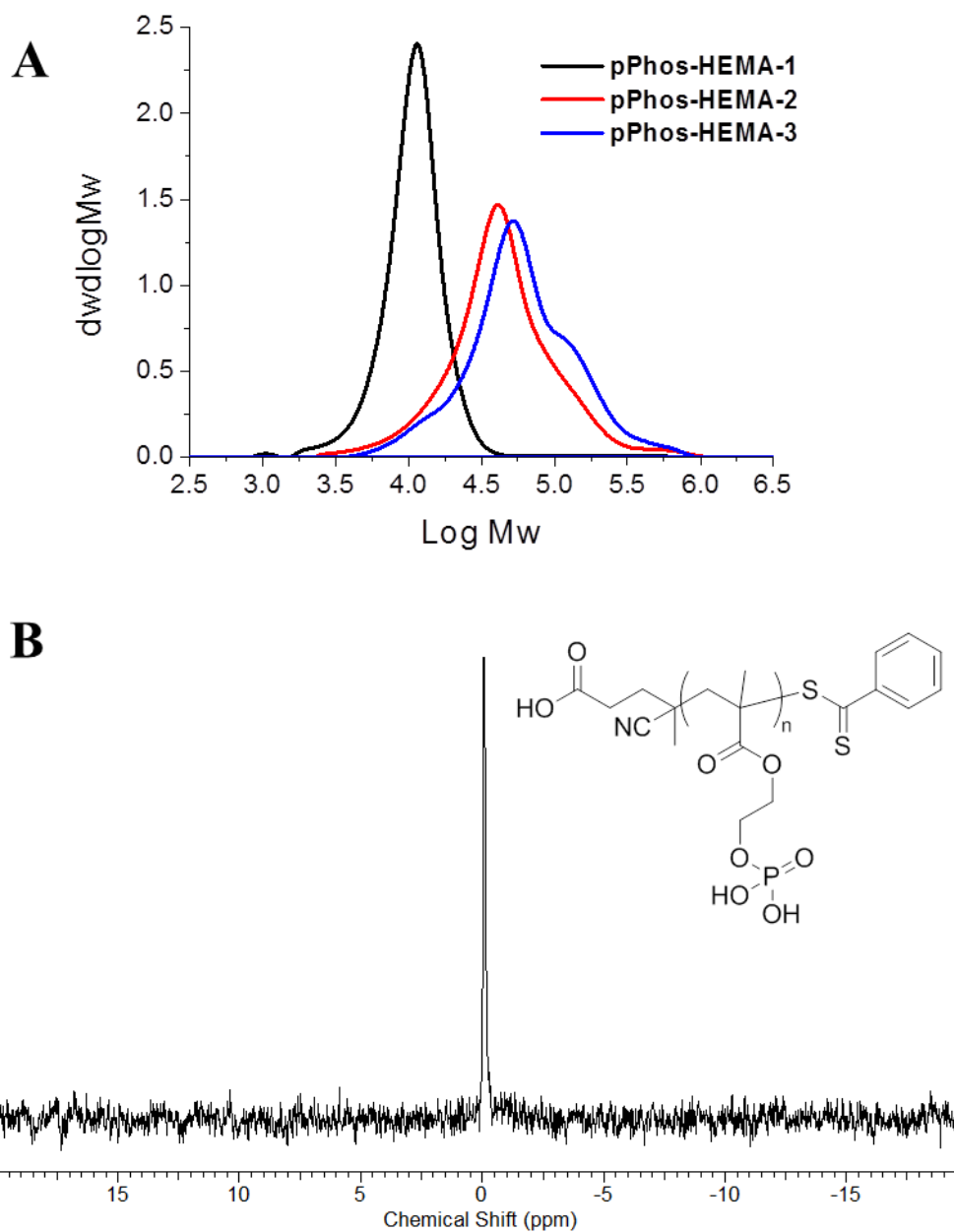


Figure 6.5 (A) SEC characterisation of **pPhos-HEMA-1/2/3**; (B) ^{31}P NMR spectrum of **pPhos-HEMA-1** in MeOD.

Next, the ability of the enzyme calf intestinal alkaline phosphatase (CIALP) to cleave phosphate groups from the functional polymer chain was verified. To do this, a commercially available colorimetric assay was employed. This assay utilises a formulation of malachite green and ammonium molybdate which, in the presence of a phosphate ion, forms a chromogenic complex with an intense absorption band

around 650 nm. The absorbance of this complex was checked using a series of standard solutions up to a known phosphate concentration of 1 mM (Figure 6.6A). A linear relationship between absorbance and phosphate concentration was observed up to a concentration of 25 μM (Figure 6.6B – inset), above which a green/brown precipitate was rapidly produced. Considering this observation, all assays were designed such that a theoretical 100% phosphate release equated to a concentration of 25 μM .

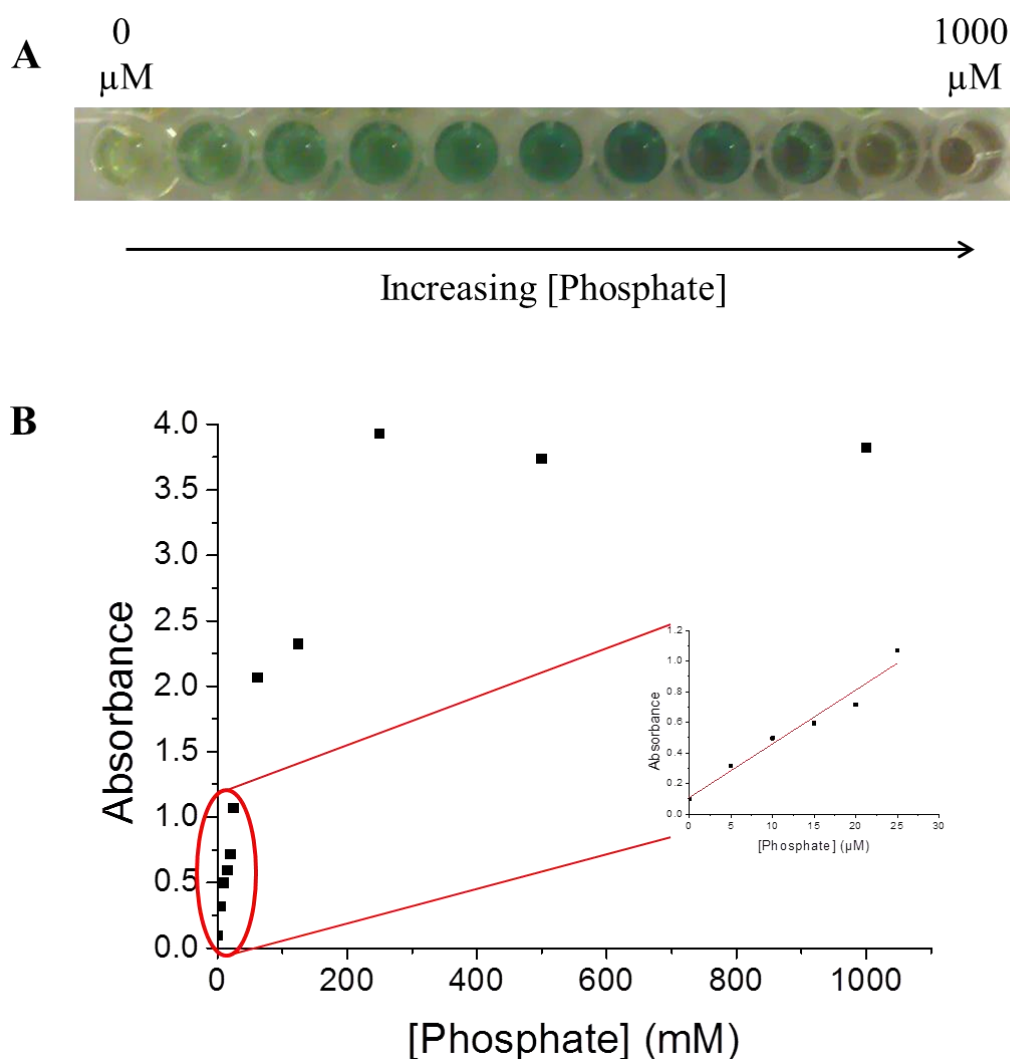


Figure 6.6 (A) Colour observed with increasing phosphate concentration; (B) Absorbance of malachite green/ammonium molybdate in presence of phosphate ion (inset: linear region 0 – 25 μM).

Given the use of a biologically-relevant enzyme, all experiments were performed at 37 °C. Whilst the colour of the assay complex remained relatively constant over a 2 hour period at room temperature, the absorbance at 37 °C was observed to increase for the first 70 mins after reagent addition before plateauing (Figure 6.7A). It is not obvious why this occurred but to minimise measurement-to-measurement error, the reagent/phosphate mixture was left to incubate for 90 mins (*i.e.* after absorbance had plateaued) before a measurement was taken. Importantly, the calibration plot of the standards after 90 mins at 37 °C was still linear within the region of analysis (Figure 6.7B), and no precipitate was observed.

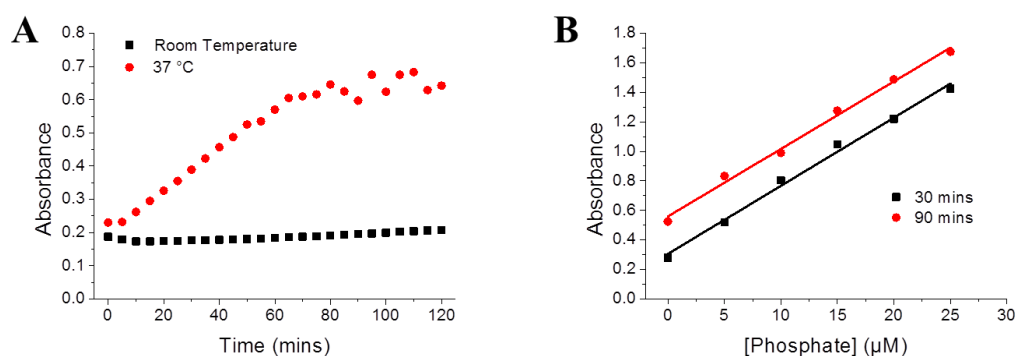


Figure 6.7 Effect of temperature and time on absorbance profile of phosphate detection assay: (A) variation of absorbance with time at room temperature and 37 °C; (B) linear relationship of absorbance with phosphate concentration at 30 mins (supplier recommended reagent incubation time) and 90 mins.

With these conditions optimised, the effect of CIALP on polymer **pPhos-HEMA-3** was assessed. A multi-well plate was used in which a concentrated solution of **pPhos-HEMA-3** was prepared and added to buffer. The enzyme was then added followed by the detection reagent at the required time-points and the absorbance at 650 nm measured after a 90 minute incubation time (Figure 6.8). Phosphate release was observed to be rapid with approximately 38 % released after 30 mins before

plateauing at approximately 60 % after 8 hours. Failure to release more phosphate was initially surprising but could be rationalised as follows. Firstly, the activity of the enzyme, and hence ability to desphosphorylate over the extended time-period of the assay may be influenced by the presence of the polymer. Secondly, the volume of enzyme used in this assay was not optimised and hence more may be required to achieve greater levels of dephosphorylation. Thirdly, complete polymer dephosphorylation would produce poly(hydroxyethyl methacrylate), pHEMA, which is known to be water swellable, rather than water-soluble at chain lengths beyond approximately 20 repeat units.^{61, 62} Whilst no polymer precipitation was observed during the assay, the increasing hydrophobic character obtained upon dephosphorylation may result in the formation of globule-type micro-domains which could limit enzyme access to the remaining phosphate functional groups. A similar observation has been made by Amir *et al.* who used acid phosphate to dephosphorylate a diblock copolymer containing PEG-derived and phosphorylated styrene blocks. Incomplete dephosphorylation was observed which was attributed to the beginnings of a self-assembly process which shielded some phosphate groups from being accessed by the enzyme.⁶³

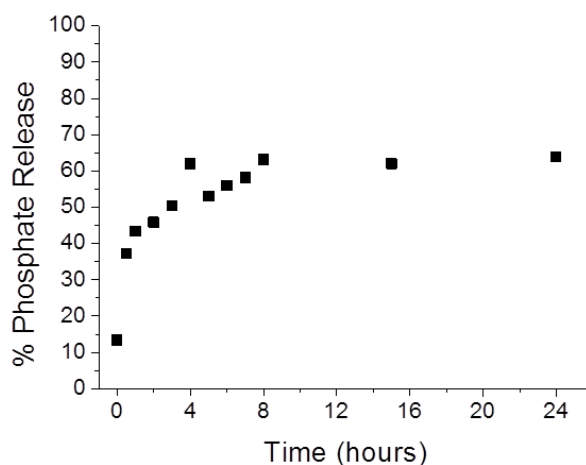


Figure 6.8 Percentage phosphate release from **pPhos-HEMA-3** upon incubation with CIALP.

To investigate whether the polymer chain length could influence the degree of phosphate release, the same assay was performed on polymers **pPhos-HEMA-1** ($M_{n(\text{theo})} = 870 \text{ g.mol}^{-1}$) and **pPhos-HEMA-2** ($M_{n(\text{theo})} = 11500 \text{ g.mol}^{-1}$). In each case, the mass of polymer used was fixed meaning despite the difference in chain length the number of phosphate groups in each sample should theoretically be equal. All samples were incubated for 24 hours and the detection kit used to assess phosphate release with all polymers exhibiting similar release profiles between 55 and 60 % (Figure 6.9). This observation suggests enzyme activity or access to dephosphorylation is similar for all molecular weights tested here. Several controls were also performed to confirm the validity of the assay. Firstly, the absorbance of the kit in buffer was shown to be minimal confirming no interaction between the chromogenic complex and the solution salts (Figure 6.9). Polymer **pPhos-HEMA-3** was also tested in the absence of enzyme. Less than 10 % release was observed indicating the measured absorbance was due to the dephosphorylation of phosphate groups by CIALP, rather than by other non-specific mechanisms such as aqueous phosphate hydrolysis (Figure 6.9). Finally, a non-phosphate containing, water-soluble polymer was also tested – poly[oligo(ethylene glycol)₃₀₀ methyl ether methacrylate], **pOEGMA₃₀₀** (Table 6.2, Figure 6.10). A small change in absorbance which equated to approximately 10 % phosphate release was also observed suggesting the polymer may interfere with the colorimetric assay in some way though this was still significantly less than that observed for **pPhos-HEMA-1/2/3** in the presence of the enzyme (Figure 6.9).

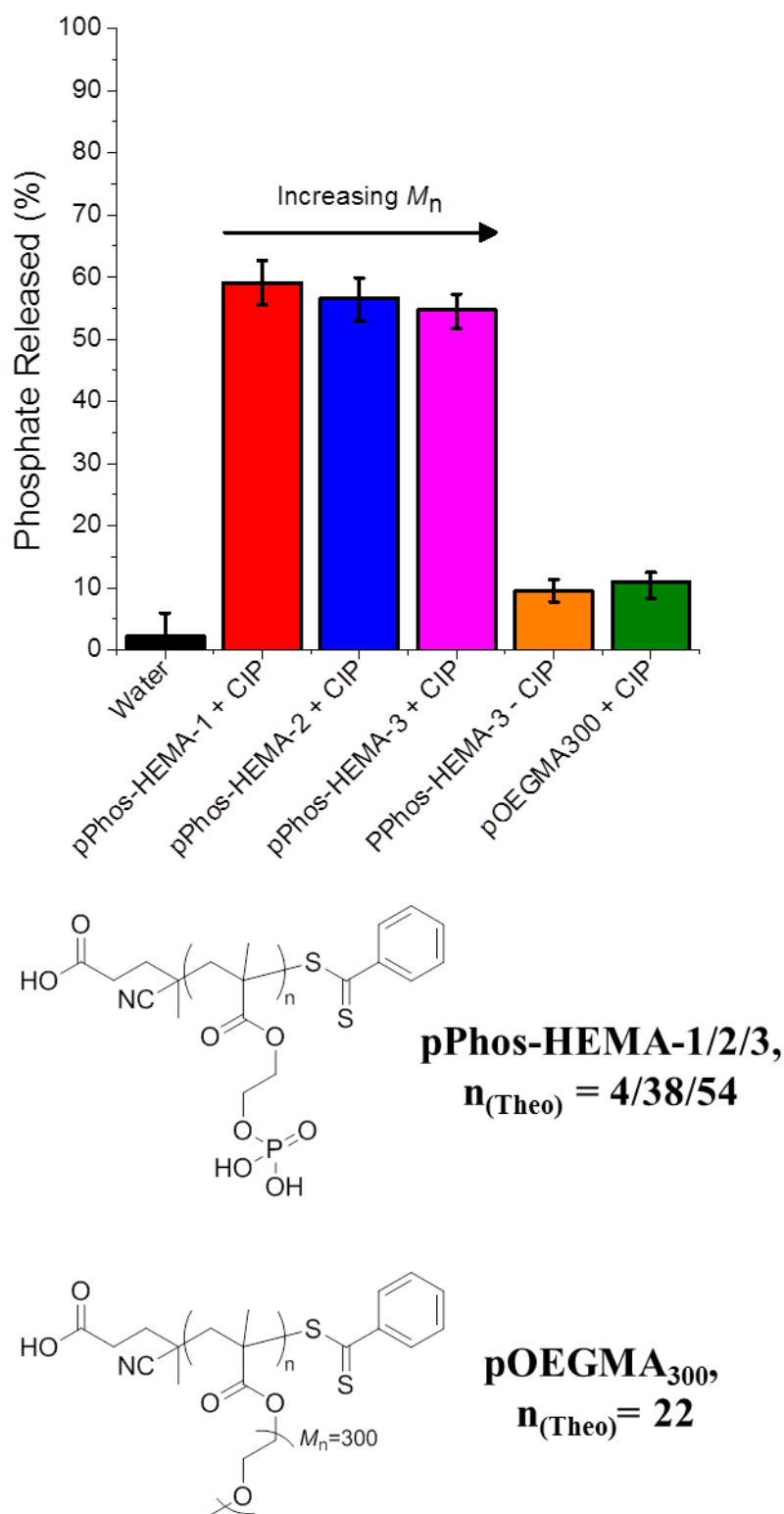


Figure 6.9 (A) Percentage of phosphate released from polymers of various molecular weights and side-chain functionalities in the presence and absence of CIALP; (B) Chemical structures of polymers employed.

Table 6.2 Characterisation of **pOEGMA₃₀₀** prepared using 4-cyano-4-(phenylcarbonothioylthio) pentanoic acid.

Polymer	[M]:[CTA]	Conversion	$M_{n(th)}$	$M_{n(SEC)}$	M_w/M_n^b
		(%) ^a	(g.mol ⁻¹) ^a	(g.mol ⁻¹) ^b	
pOEGMA ₃₀₀	50	44.2	8800	11300	1.18

^aDetermined by ¹H NMR spectroscopy relative to an internal standard (mesitylene);

^bDetermined by SEC (DMF inc. 5 mM NH₄BF₄) relative to PMMA standards.

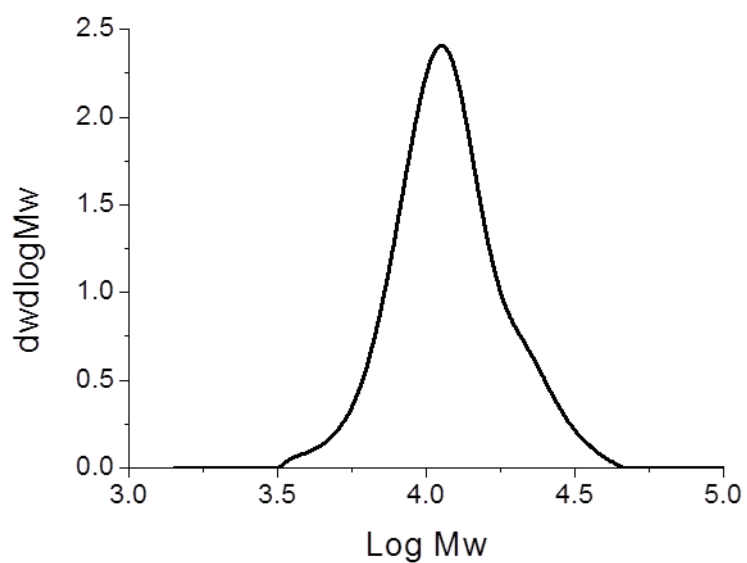


Figure 6.10 SEC characterisation of **pOEGMA₃₀₀**

6.3.2 Phosphate-Containing, Thermally-Responsive Systems

Poly(Phos-HEMA) does not display a thermal transition in aqueous solution within easily accessible experimental temperatures. Hence, to introduce this property into the system, a thermally-responsive unit was added into the polymerisation mixture. The poly[oligo(ethylene glycol) methyl ether methacrylate] family is well known for its thermally-responsive behaviour, the shortest member of which is diethylene glycol methyl ether methacrylate (DEGMA), typically possessing a cloud point of around 26 °C in aqueous solution.^{64, 65} To assess the effect of Phos-HEMA on the cloud point of the DEGMA-based co-polymers, a series of samples was prepared (Table 6.3).

Table 6.3 Characterisation of poly(DEGMA-*co*-Phos-HEMA) samples prepared using 4-cyano-4-(phenylcarbonothioylthio) pentanoic acid in this study.

Polymer	[DEGMA]:[Phos-HEMA]:[CTA]	Conversion (%) ^a	$M_{n(th)}$ (g.mol ⁻¹) ^a	$M_{n(SEC)}$ (g.mol ⁻¹) ^b	M_w/M_n ^b
P _{co} 1%	99:1:1	42.7	8000	7300	1.23
P _{co} 2.5%	97.5:2.5:1	45.9	8600	7200	1.21
P _{co} 5%	95:5:1	46.4	8800	6400	1.21
P _{co} 10%	90:10:1	23.3	4400	6200	1.30

^aDetermined by ¹H NMR spectroscopy relative to an internal standard (mesitylene) assuming equal conversion of DEGMA and Phos-HEMA (Phos-HEMA vinyl proton peaks too poorly resolved for analysis); ^bDetermined by SEC (DMF inc. 5 mM NH₄BF₄) relative to PMMA standards.

Interestingly, to exemplify **P_{co}1%**, **P_{co}2.5%** and **P_{co}5%** (Figure 6.11A) all of which proceeded to similar conversions and showed an increase in theoretical molecular weight, the molecular weights as determined by SEC showed a progressive decrease

in size with increasing Phos-HEMA incorporation, whilst a low molecular weight tail was apparent in all cases (Figure 6.11B). Poly(Phos-HEMA) is insoluble in DMF therefore this observation is likely to be due to the solvation characteristics of the increasingly Phos-HEMA-rich co-polymers in the eluent used. Nevertheless, the incorporation of small degrees of Phos-HEMA was enough to significantly influence the system cloud point. An increase from 35 °C to 45 °C was observed upon increasing the Phos-HEMA proportion from 1 % to 10 % (Figure 6.11C/D), providing evidence of the successful incorporation of the monomer in the co-polymer structure. The very hydrophilic nature of Phos-HEMA means only small proportions are required to produce a cloud point with physiological relevance.

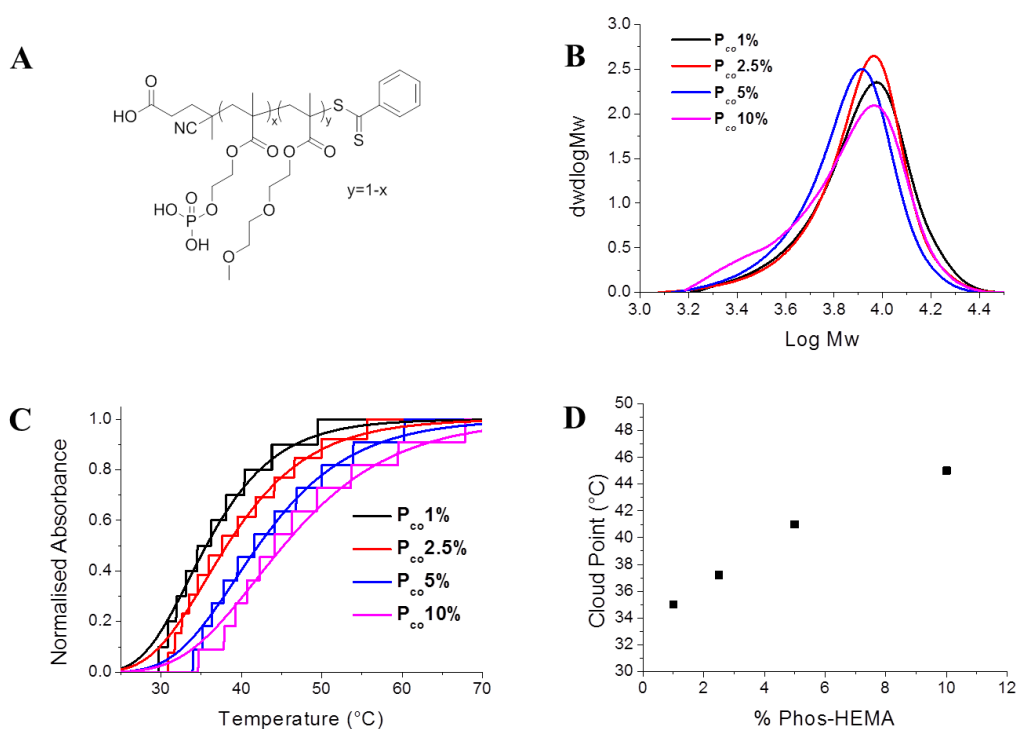


Figure 6.11 Characterisation of pDEGMA-co-Phos-HEMA: (A) Co-polymer chemical structure; (B) SEC characterisation; (C) Cloud point traces at a polymer concentration of 5 mg.mL⁻¹ (solid curves added to guide the eye only); (D) Cloud point as a function of co-polymer composition.

It was anticipated that the action of phosphatase on this polymer would trigger a decrease in cloud point by converting phosphate groups to less hydrophilic hydroxyl moieties (Figure 6.12A). To test this hypothesis, a 5 mg.mL⁻¹ solution of **P_{co}5%** was incubated with CIALP and the sample stirred at 37 °C for 24 hours. This polymer concentration was selected to ensure the change in turbidity observed upon passing through the cloud point would be sufficiently strong for detection by the instrument used (Optimelt) in this case. After this time, the sample was analysed by turbidimetry and, pleasingly, a decrease in the cloud point by 4 °C and 8 °C was observed in the presence of 2 μL (2 units) and 10 μL (10 units) of enzyme respectively (Figure 6.12B).

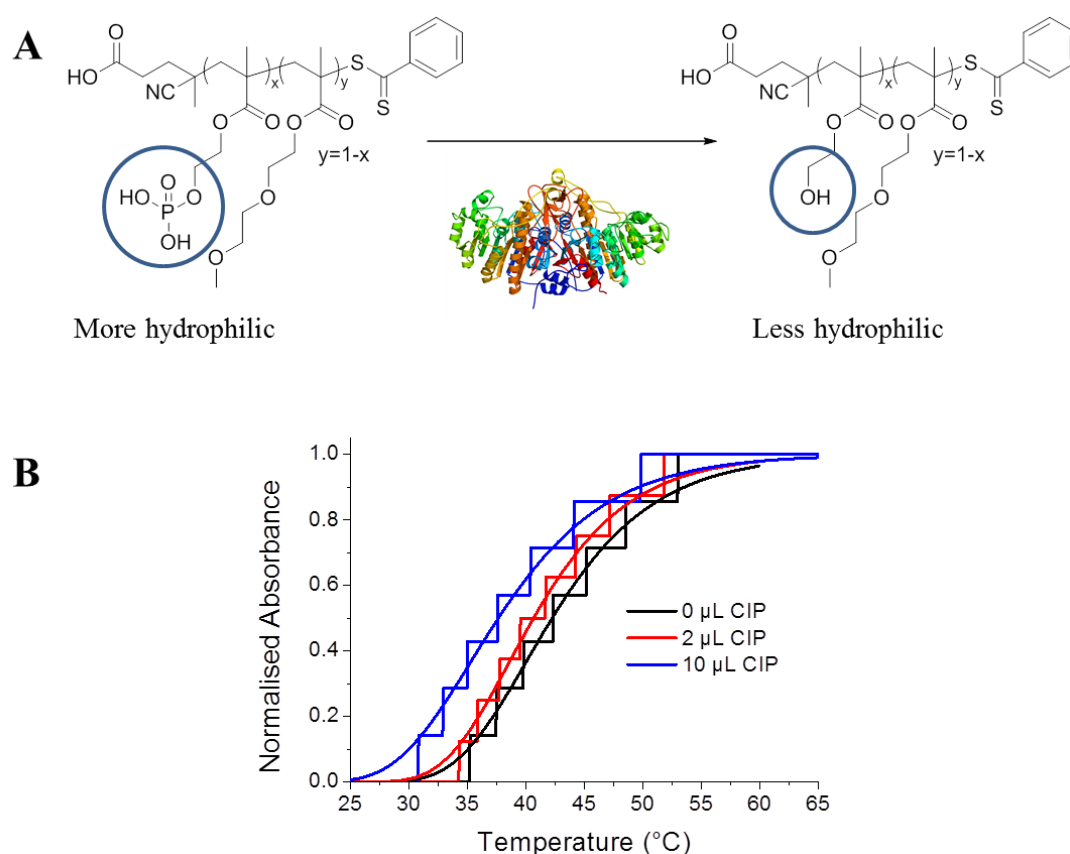


Figure 6.12 (A) Anticipated change in chemical structure of poly(DEGMA-*co*-Phos-HEMA) upon incubation with CIALP; (B) Effect of CIALP on cloud point of **P_{co}5%** (solid curves are to guide the eye).

To confirm this action was due to phosphate removal, two controls were performed. Firstly, the polymer was incubated without enzyme for a period of 24 hours and negligible change in cloud point was observed, confirming any shift is not due to routine hydrolysis of either the phosphate groups or the methacrylate backbone (Figure 6.13A). Moreover, to verify the shift was not simply due to the additives present in the buffer used for analysis the non-phosphate-containing **pOEGMA₃₀₀** was also analysed following 24 hour incubation with 10 μ L CIALP (Figure 6.13B). Minimal change was observed in this case with the cloud point actually increasing slightly, in contrast to the behaviour expected and observed if dephosphorylation was occurring (Figure 6.12B). In comparison to the assays performed on the homopolymers (Figure 6.9A) where a phosphate concentration of 25 μ M was employed, the phosphate concentration in this test was nearly 50 x higher (\sim 1.2 mM) and hence the effect of a larger enzyme volume is perhaps unsurprising.

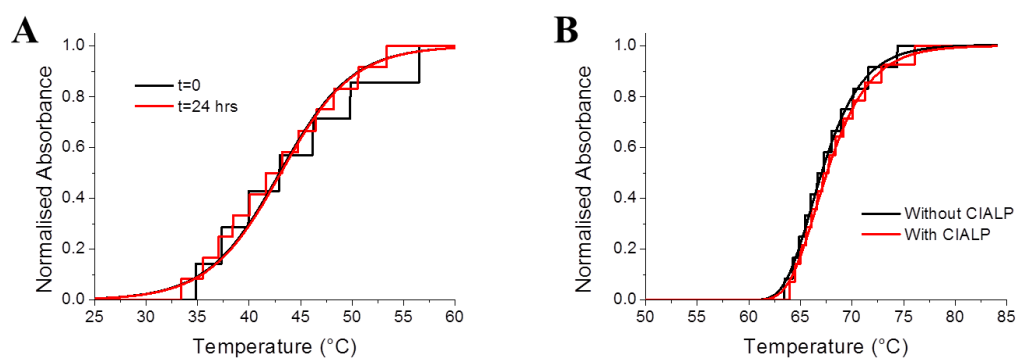


Figure 6.13 (A) Cloud point of **P_{co}5%** in 1x NEBuffer 3 after 24 hours; (B) Cloud point of **pOEGMA₃₀₀** with and without 10 μ L CIALP (solid curves are to guide the eye).

The change in cloud point observed upon the addition of CIALP provided a window for an isothermal transition to be achieved and was tested using a turbidimetric assay (Figure 6.14). The polymer was held at 34 °C, below its cloud point but above that observed in the presence of 10 μ L CIALP. No increase in absorbance was observed until the enzyme was added, at which time a rapid and significant increase in absorbance, concomitant with polymer precipitation was observed. Altering a material's solubility without needing a temperature change is potentially attractive for biomedical applications providing, for example, a route towards improved, controlled targeting of therapeutic delivery vehicles.^{66, 67}

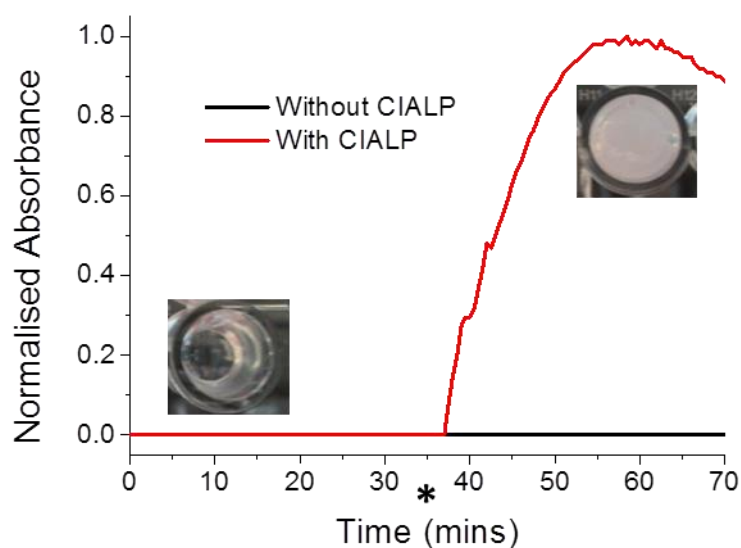


Figure 6.14 Isothermal turbidimetry data for $P_{co}5\%$: Polymer concentration = 5 $\text{mg}\cdot\text{mL}^{-1}$; Temperature = 34 °C; CIALP added at time indicated by asterisk. Black = control (polymer without enzyme); red = polymer with 10 μ L CIALP. Inset = representative photo of wells before and after experiment.

6.3.3 Cell Studies

Having verified the isothermal response of these polymers in the presence of CIALP, we next wanted to investigate their behaviour when applied to cells. Typically, cell uptake is assessed by applying a fluorescently-labelled sample to a cell line and measuring the resulting cell lysate fluorescence. In this study, a small percentage of hostasol methacrylate (HMA) was added to the co-polymerisation mixture given its strong fluorescent characteristics at excitation and emission wavelengths of 461 and 528 nm respectively.⁶⁸ We first wanted to check that the LCST could be used to enhance cell uptake and hence a positive control was required. Poly(*N*-isopropylacrylamide-*co*-HMA), **pNIPAM-*co*-HMA**, was selected for use here given its prevalence in the literature as both a thermo-responsive polymer⁶⁹ and also given it has been applied for cell uptake studies previously.^{41, 70} SEC was used to confirm the successful labelling of the polymer, with a strong absorbance at 461 nm (corresponding to HMA) observed at the same elution time as the polymer peak (Figure 6.15, Table 6.4). It should be noted that the slight difference in retention time between the peaks detected by RI and at 461 nm is due to inter-detector delay.

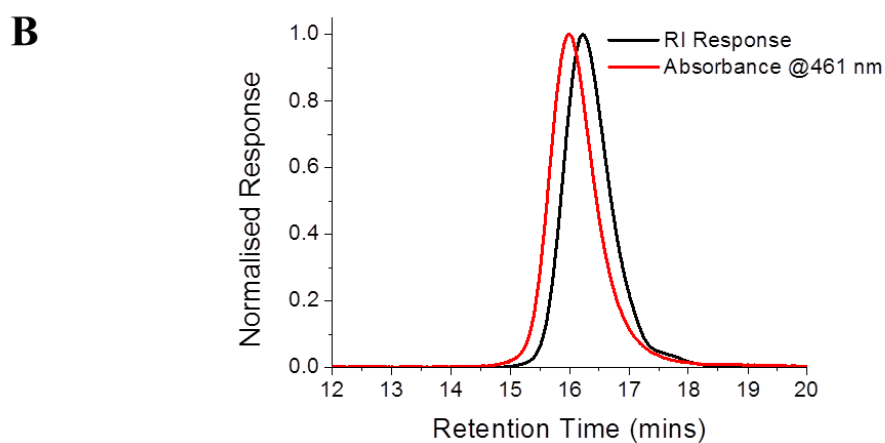
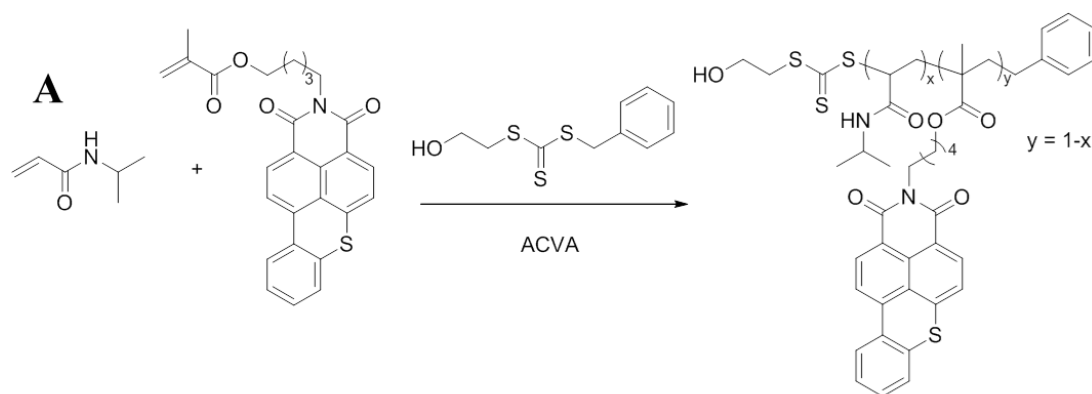


Figure 6.15 (A) Synthesis of **pNIPAM-co-HMA**; (B) SEC characterisation showing successful fluorescent labelling of polymer.

Table 6.4 Characterisation of **pNIPAM-co-HMA** prepared using benzyl 2-hydroxyethyl carbonotrithioate.

Polymer	[NIPAM]:[HMA]:[CTA]	Conversion (%) ^a	$M_{n(th)}$ (g.mol ⁻¹) ^a	$M_{n(SEC)}$ (g.mol ⁻¹) ^b	M_w/M_n ^b
pNIPAM-co-HMA	30:0.01:1	89.3	3000	3800	1.11

^aDetermined by ¹H NMR spectroscopy relative to an internal standard (mesitylene);

^bDetermined by SEC (DMF inc. 5 mM NH₄BF₄) relative to PMMA standards.

The cloud point of this polymer was also characterised in water at various concentrations (Figures 6.16A). In keeping with previous observations, an exponential increase in cloud point was observed with decreasing polymer concentration from 42.8 °C at 1 mg.mL⁻¹ to 55.9 °C at 0.1 mg.mL⁻¹.^{71, 72} In biological systems more complex salt-containing media are encountered. Phosphate buffered saline (PBS) is routinely used as an osmotic mimic of *in vivo* conditions and hence the cloud point in this medium was also determined. A noticeable decrease in cloud point of 4 – 5 °C compared to the polymer in pure water was observed at all concentrations tested due to the high kosmotropic salt content (Figures 6.16B).⁷³ Furthermore, cell culture media are even more complex than simple salt solutions where additional amino acids and sometimes antibiotics are commonly present. To assess the cloud point in such media RPMI 1640 was selected given its prevalence in cell culture processes (Figure 6.16C).⁷⁴ Again, significant deviations from the cloud points in water were observed, generally exhibiting lower values of between 3 and 4 °C. Equally, the cloud point was observed to be approximately 1 °C higher than those obtained in PBS with the exception of a concentration of 0.1 mg.mL⁻¹. Here however, the reduced resolution of the observed curve makes the obtained value unfit for effective comparison. Finally, foetal bovine serum (FBS) is also sometimes added to the growth medium to aid cell proliferation. To mimic this, 5 % w/v bovine serum albumin (BSA) was added and the cloud points measured (Figure 6.16D). Minimal change compared to the value obtained in RPMI 1640 alone was observed, except again at very dilute (0.1 mg.mL⁻¹) concentrations where the curve profile was again poorly resolved. This may be due to a lack of instrument sensitivity at this concentration where the change in visual turbidity will be minimal compared to that seen at the higher polymer concentrations

tested. Nevertheless, these results do show that careful consideration of the solvents/biological media being used, as well as the polymer concentration is required in the design of any material intended for *in vivo* application. Given the plethora of cell culture media available, it is reasonable to expect some differences between media given the variety of additives known to exist in such solutions. A summary of all the cloud points measured is shown in Table 6.5 and Figure 6.17.

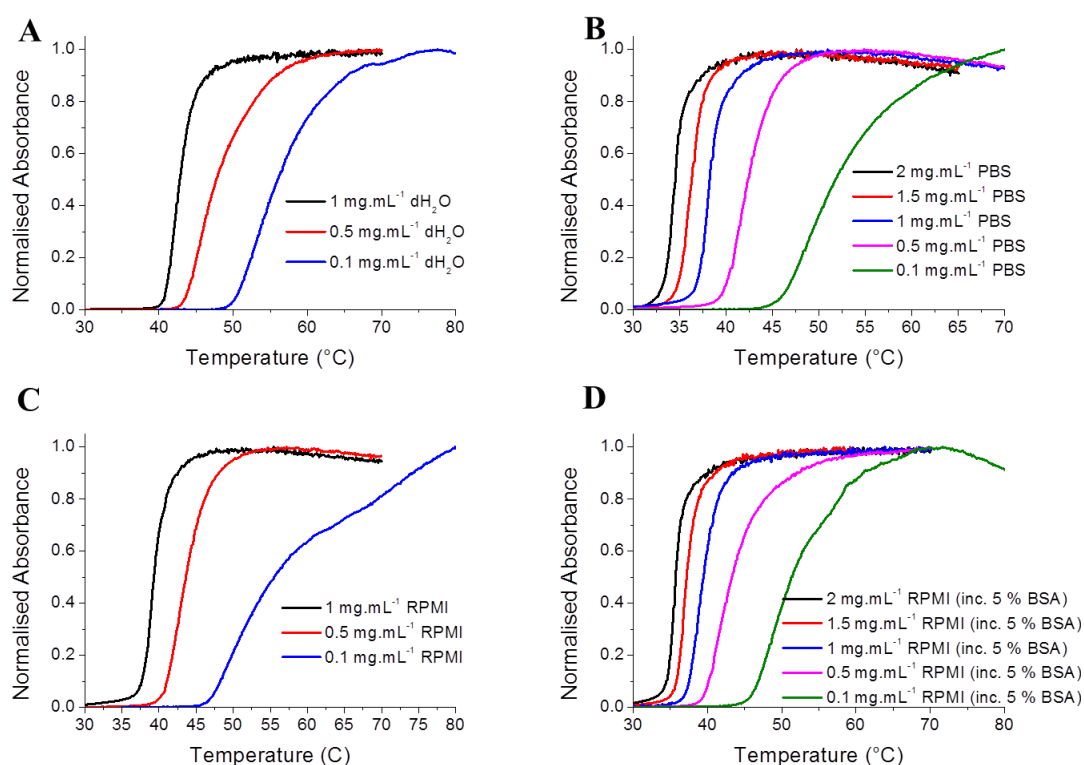


Figure 6.16 Turbidimetric analysis of **pNIPAM-co-HMA** at varying polymer concentrations in different media: (A) Deionised water; (B) PBS; (C) RPMI and (D) RPMI (inc. 5 % BSA).

Table 6.5 Cloud points of **pNIPAM-co-HMA** at various concentrations in different media.

Cloud Point (°C) of pNIPAM-co-HMA		Medium			
		H ₂ O	PBS	RPMI	RPMI inc. 5 % BSA
Polymer Concentration (mg.mL ⁻¹)	2	-	34.6	-	35.7
	1.5	-	36.3	-	37.2
	1	42.8	38.2	39.3	39.5
	0.5	47.7	42.4	43.6	43.3
	0.1	55.9	51.8	55.5	51.3

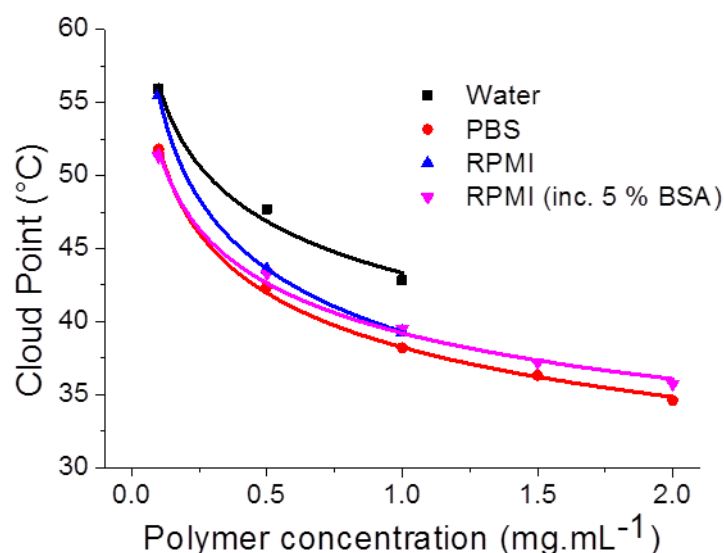


Figure 6.17 Cloud points of **pNIPAM-co-HMA** as a function of polymer concentration in a variety of media.

With the thermo-responsive behaviour of the polymer characterised, the cytotoxicity of an analogous polymer to the cell line of interest (MCF7) was characterised using the 3-(4,5-dimethylthiazol-2-yl)2,5-diphenyl-tetrazolium bromide (MTT) assay. First used by Mosmann to quantitate cellular growth and cytotoxicity in cultured cells in

1983,⁷⁵ the tetrazole ring in MTT, a yellow, water-soluble compound, is reduced to a water-insoluble, purple formazan in metabolically active cells.^{76, 77} The reduction is thought to occur mainly in the mitochondria, through the action of succinate dehydrogenase, and hence provides a measure of mitochondrial function.⁷⁸

To avoid any potential interference with the colorimetric output of the assay, another pNIPAM of similar molecular weight was prepared without any fluorescent label (Figure 6.18, Table 6.6). Given the percentage inclusion the HMA in the copolymer described above was so small (< 1 %), it was assumed this would have little impact on the cytotoxicity of the overall polymer, in keeping with previous reports.⁷⁹

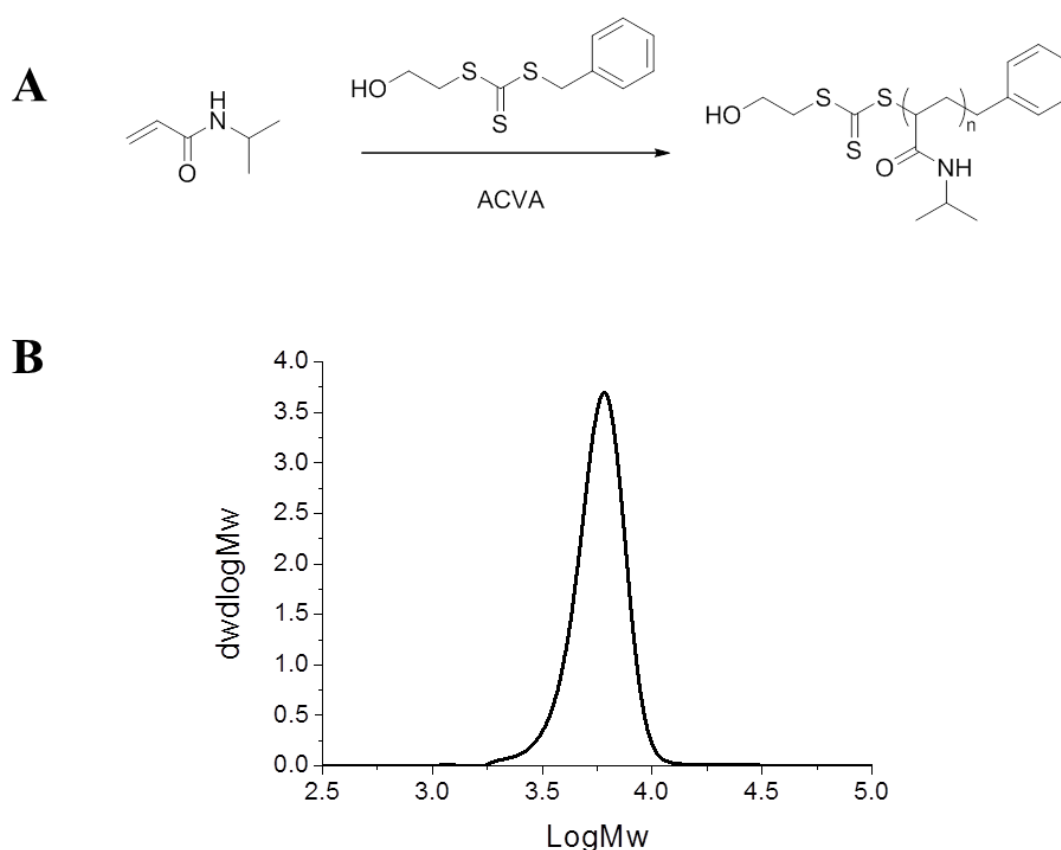


Figure 6.18 (A) Synthesis of pNIPAM; (B) SEC characterisation of polymer

Table 6.6 Characterisation of **pNIPAM** prepared using benzyl 2-hydroxyethyl carbonotrithioate.

Polymer	[M]:[CTA]	Conversion (%) ^a	$M_{n(th)}$ (g.mol ⁻¹) ^a	$M_{n(SEC)}$ (g.mol ⁻¹) ^b	M_w/M_n ^b
pNIPAM	50	63.6	3600	5500	1.08

^aDetermined by ¹H NMR spectroscopy relative to an internal standard (mesitylene);

^bDetermined by SEC (DMF inc. 5 mM NH₄BF₄) relative to PMMA standards.

The cloud points of **pNIPAM** were again determined in the media described above with the cloud point observed to follow a similar trend: deionised water > RPMI 1640 (with BSA) > RPMI 1640 (without BSA) > PBS (Figures 6.19, 6.20 and Table 6.7). It should be noted that the effect of BSA on the cloud point for this polymer was more significant with its presence increasing the cloud point by approximately 0.5 °C at all concentrations, further emphasising the subtle differences in responsive behaviour between polymers.

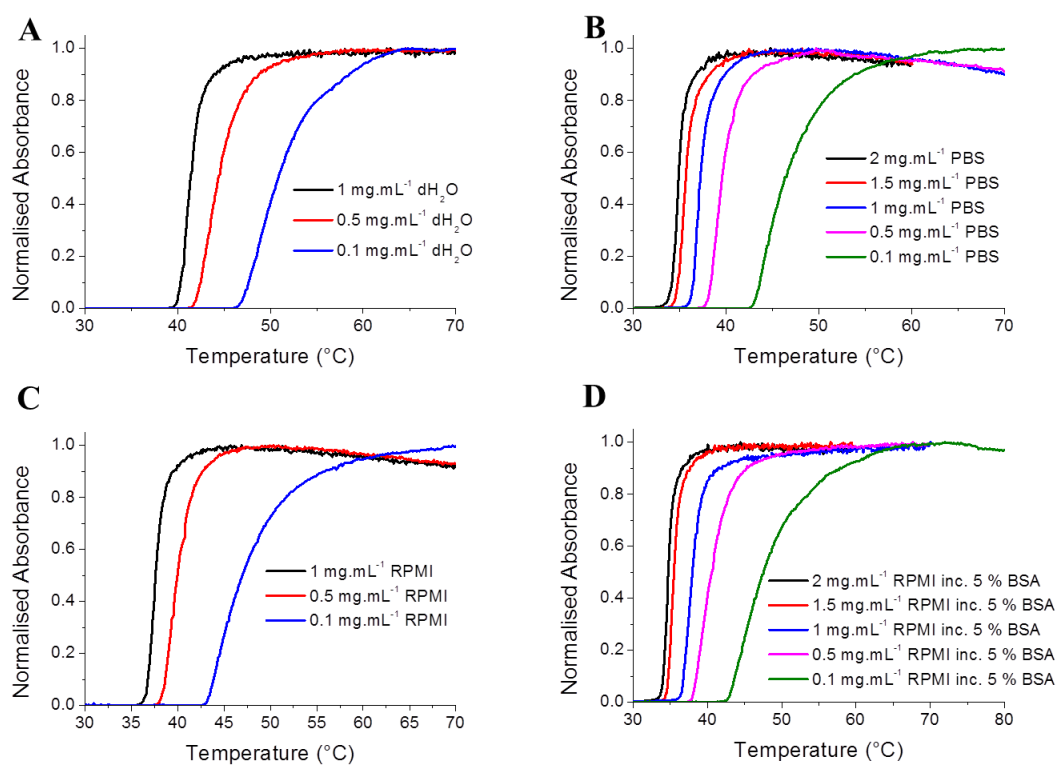


Figure 6.19 Turbidimetric analysis of **pNIPAM** at varying polymer concentrations in different media: (A) Deionised water; (B) PBS; (C) RPMI and (D) RPMI (inc. 5 % BSA).

Table 6.7 Cloud points of **pNIPAM** at various concentrations in different media.

Cloud Point (°C) of pNIPAM		Medium			
		H ₂ O	PBS	RPMI	RPMI inc. 5 % BSA
Polymer Concentration (mg.mL ⁻¹)	2	-	34.8	-	34.7
	1.5	-	35.7	-	35.5
	1	41.4	37.3	37.6	38.0
	0.5	44.4	39.5	40.0	40.5
	0.1	50.8	46.3	47.0	47.6

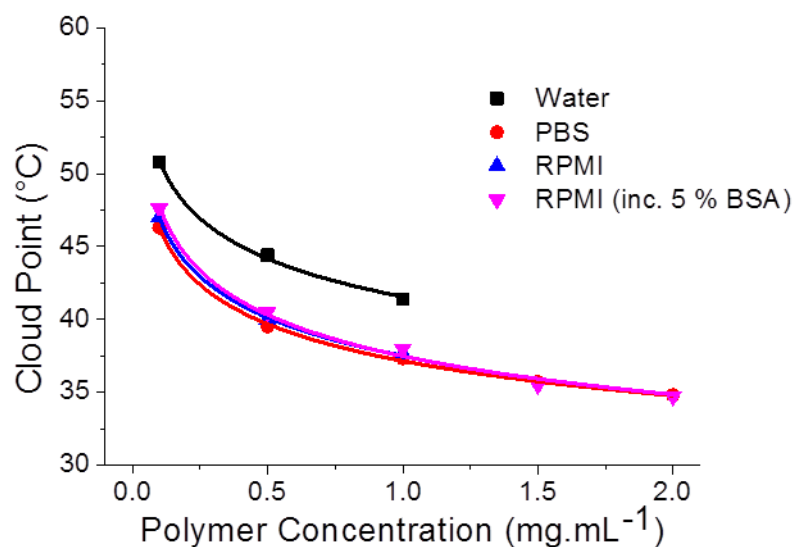


Figure 6.20 Cloud points of pNIPAM as a function of polymer concentration in a variety of media.

Pleasingly, the MTT assay showed no significant toxicity at any polymer concentration with a cell viability greater than 85 % observed at the relatively high concentration of 2 mg.mL⁻¹ (Figure 6.21A). Given the cloud point of 35.7 °C, the ability to trigger cell uptake by heating beyond the polymer LCST was next assessed at this concentration. The polymer was added to cells in two different multi-well plates and incubated at either 30 °C or 38 °C, well below and above the cloud point respectively. The polymer-cell mixture was incubated for one hour after which time the wells were washed thoroughly, lysed and the fluorescence of the cell lysate measured. An increase in fluorescence intensity of 68 % was observed in the cells incubated at a temperature above the LCST suggesting greater cell uptake (Figure 6.21B). A statistical difference between the two data sets was confirmed with a P value of 0.0008, as obtained from a two-tail Student's t-test where a value below 0.05 describes a 95 % confidence interval that the results obtained were not

serendipitous. It is anticipated that greater cell uptake would be observed with longer incubation times.

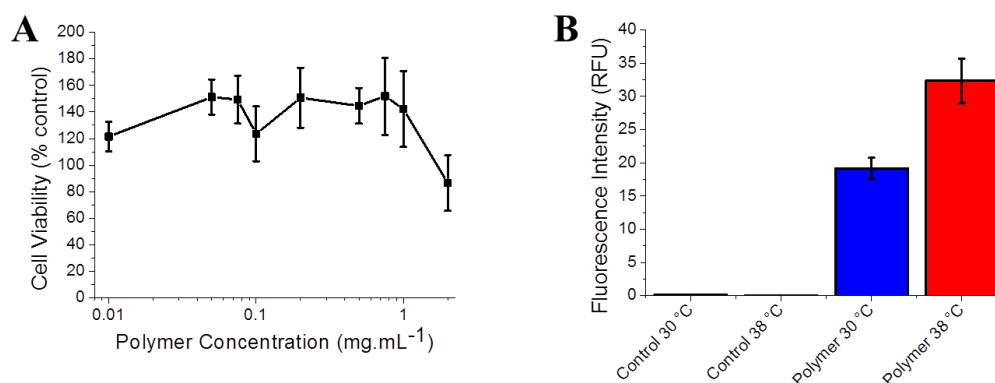


Figure 6.21 (A) MTT assay results of **pNIPAM** incubated with MCF7 cells for 67 hours (mean of 4 replicates shown, error bars = standard error); (B) Fluorescence intensity following cell uptake experiments of **pNIPAM-co-HMA** in MCF7 cells held at 30 °C and 38 °C (polymer concentration = 2 mg.mL⁻¹).

The thermal-triggered uptake of the pDEGMA-co-Phos-HEMA copolymers was next assessed. The cytotoxicity of **pOEGMA₃₀₀** was first tested *via* the MTT assay to verify any cytotoxic contribution of the ethylene glycol component of the copolymer. Importantly, no cytotoxicity was observed (Figure 6.22A) up to a polymer concentration of 2 mg.mL⁻¹ which is well above the concentration employed in this study (*vide infra*). Secondly, **P_{co5%}** was tested and this polymer exhibited an IC₅₀ value - the concentration at which only 50 % of viable cells is present, and hence is regarded as a marker of cytotoxicity - of 1.81 mg.mL⁻¹ (Figure 6.22B). This observation suggests the incorporation of the phosphorylated monomer into the polymer structure is not tolerated so well by the cells used in this study. By extension, the design of polymers for cell studies should contain as little Phos-HEMA as possible.

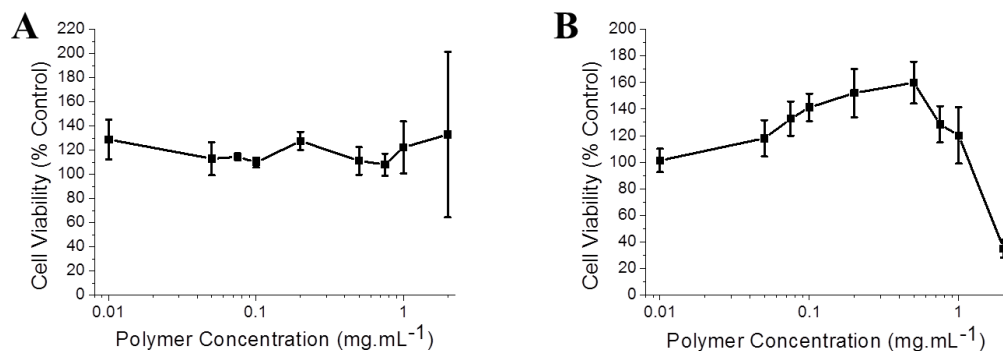
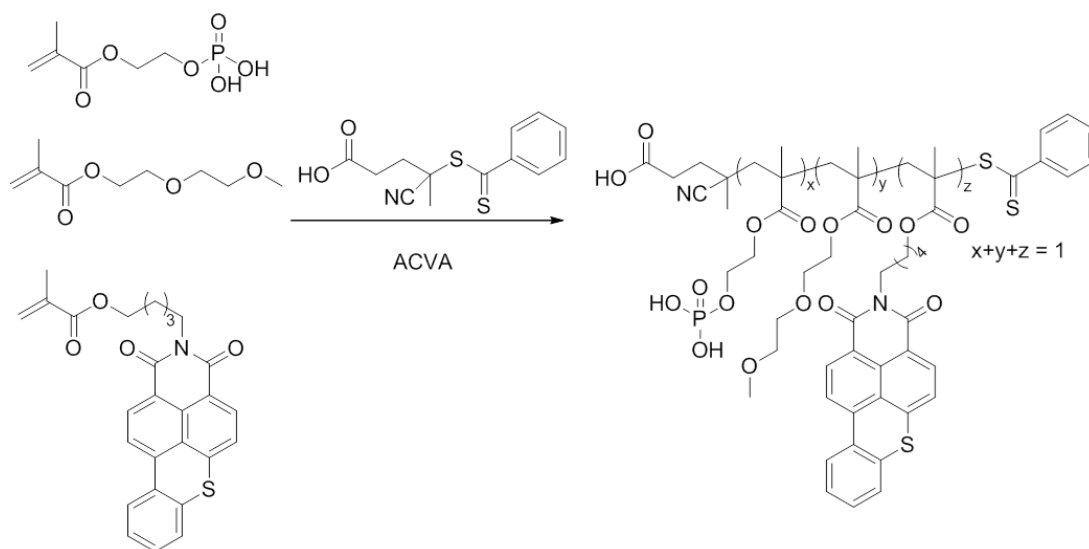


Figure 6.22 MTT assay results of (A) pOEGMA₃₀₀ and (B) P_{co5%} incubated with MCF7 cells for 67 hours (mean of 4 replicates shown, error bars = standard error).

With the lack of toxicity confirmed, a phosphate-functional, fluorescently labelled polymer was prepared by co-polymerising Phos-HEMA, DEGMA and HMA (Scheme 6.2, Table 6.8).



Scheme 6.2 Synthetic scheme for the preparation of a fluorescent, phosphate-labelled thermo-responsive polymer.

Table 6.8 Characterisation of **pDEGMA-co-Phos-HEMA-co-HMA** prepared using benzyl 2-hydroxyethyl carbonotrithioate.

Polymer	[DEGMA]: [Phos-HEMA]: [HMA]:[CTA]	Conversion (%) ^a	$M_{n(th)}$ (g.mol ⁻¹) ^a	$M_{n(SEC)}$ (g.mol ⁻¹) ^b	M_w/M_n ^b
pDEGMA- co-Phos- HEMA-co- HMA	99:1:0.8:1	30.9	5800	13400	1.12

^aDetermined by ¹H NMR spectroscopy relative to an internal standard (mesitylene);

^bDetermined by SEC (DMF inc. 5mM NH₄BF₄) relative to PMMA standards.

Given the indication of some cytotoxicity when Phos-HEMA is incorporated into the co-polymer structure, a polymer comprising only 1 % of the phosphorylated side-chain was isolated by multiple precipitations into cold diethyl ether, as indicated by SEC (Figure 6.23A, Table 6.8). The thermal response of this polymer was then characterised at various concentrations in the cell culture medium-mimic (RPMI 1640, including 5 % BSA, Figure 6.23B).

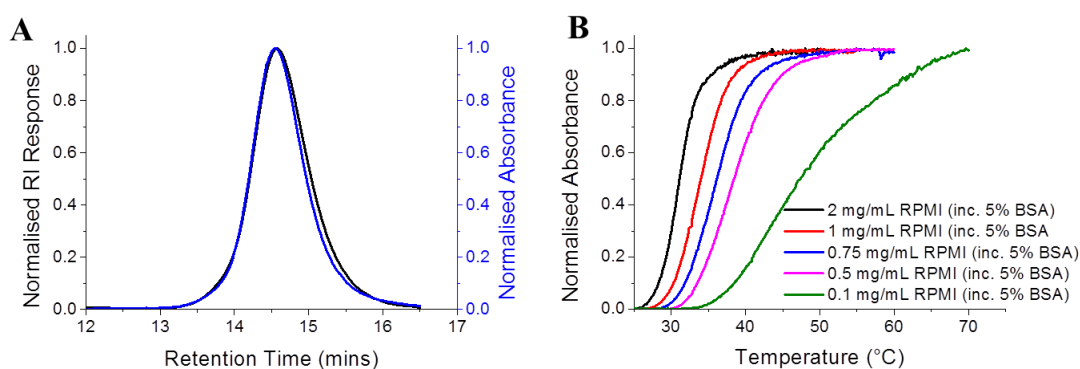


Figure 6.23 (A) SEC characterisation showing fluorescent labelling and (B) Turbidimetric analysis of **pDEGMA-co-Phos-HEMA-co-HMA**.

The uptake of this polymer below and above the LCST was next determined in the same manner as described above (Figure 6.24). Here, a 60 % increase in the fluorescence intensity was observed at 38 °C (above the polymer cloud point) compared to at 30 °C (below the cloud point) suggesting enhanced uptake when the polymer is in its hydrophobic conformation. A P value of 0.01 again confirms the statistical difference between the two data sets. It should be noted that the total fluorescence intensity was less than that observed with the **pNIPAM** sample and is most likely due to the more dilute concentration in which the polymer was applied to the cells.

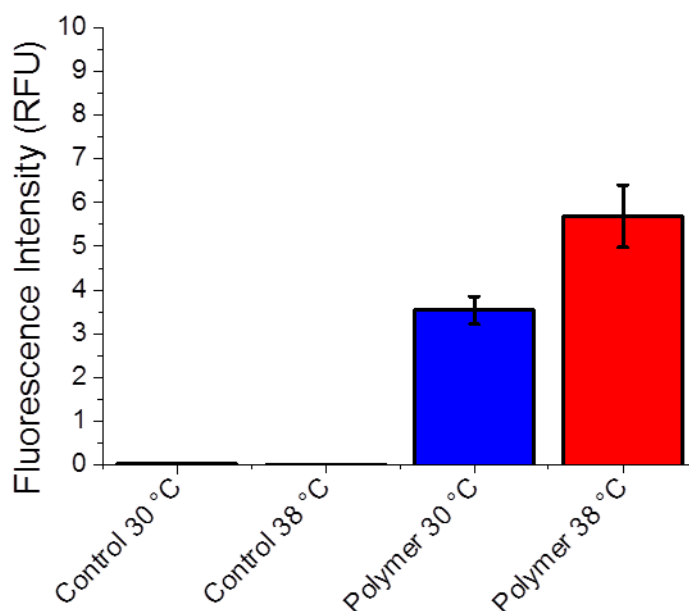


Figure 6.24 Fluorescence intensity following cell uptake experiments of **pDEGMA-co-Phos-HEMA-co-HMA** in MCF7 cells held at 30 °C and 38 °C (polymer concentration = 0.75 mg.mL⁻¹, mean of 3 replicates shown, error bars = standard error).

Finally, the ability to trigger uptake isothermally through enzyme-mediated dephosphorylation was assessed. In this experiment, the polymer was held at 36 °C

at a concentration of 0.75 mg.mL^{-1} given the cloud point of $36.5 \text{ }^\circ\text{C}$ is slightly above physiological temperature. It was then anticipated the addition of CIALP would lower the polymer cloud point below $36 \text{ }^\circ\text{C}$ making the polymer more hydrophobic and hence enhance cell uptake. CIALP was added at two different volumes ($2 \text{ }\mu\text{L}$ and $10 \text{ }\mu\text{L}$) given the precise volume required was not known. Moreover, earlier experiments suggested $10 \text{ }\mu\text{L}$ was enough to promote a significant change in cloud point at a far higher polymer concentration (5 mg.mL^{-1} , Figure 6.12B). The polymer/cell mixture, together with enzyme was incubated for 24 hours, the cells lysed, washed thoroughly and the fluorescence of the resulting cell lysate measured (Figure 6.25). Initial results revealed no statistically significant differences in the fluorescence observed between the cells incubated with polymer alone, or those with added CIALP. The reasoning behind this observation could be as follows: Firstly, the incorporation of 1 % Phos-HEMA in the polymer structure may not be sufficient to trigger a significant change in the polymer cloud point. Given its statistical nature, some chains may contain no phosphorylated groups in the side-chain, for instance. Another reason may be that the cloud point of this polymer without any enzyme was too close to the incubation temperature. There are some reports that define the cloud point as the temperature at which an onset of precipitation is observed,⁸⁰ not the value at which a normalised absorbance is equal to 0.5, as has been employed throughout this thesis. Although the latter definition proved adequate in all other investigations described in this work, it is possible that given the long (24 hour) incubation time in this experiment, some of the polymer solution had already undergone the coil-to-globule transition associated with the LCST hence limiting the influence of the enzyme. Finally, the lack of desired effect may be an artefact of the methodology used here. Specifically, sterile-filtered FBS was used throughout the

cell culturing process. As this may contain traces of alkaline phosphatase, any phosphate units on the polymer backbone will be cleaved, hence negating the intended effect of the subsequently added enzyme. Ways in which to improve upon this are currently being investigated including ensuring the cell culture medium is phosphatase-free, together with the synthesis of additional co-polymers containing higher percentages of the phosphate unit.

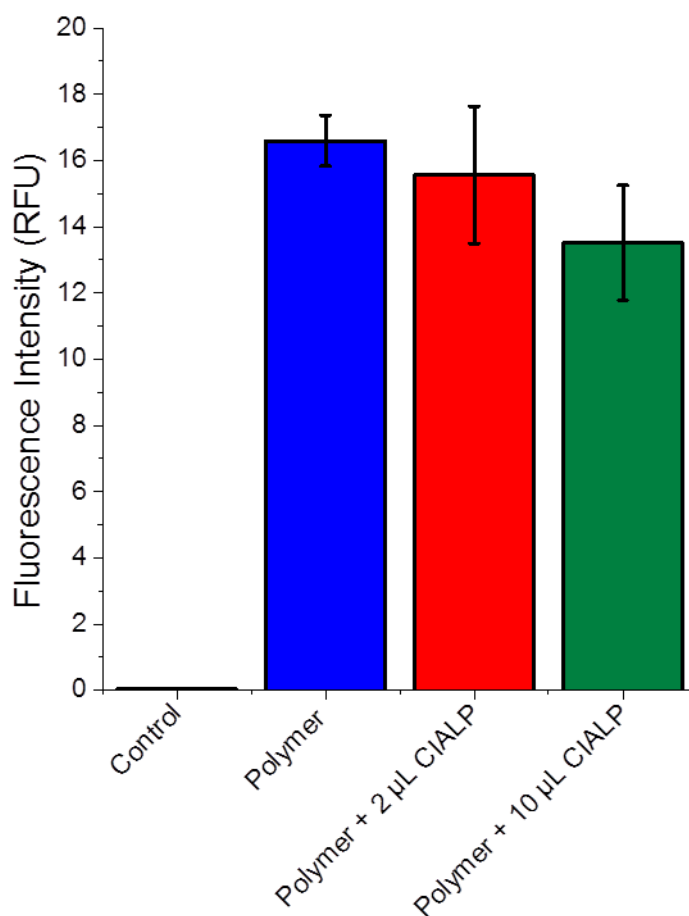


Figure 6.25 Cell uptake results of **pDEGMA-co-Phos-HEMA-co-HMA** in MCF7 cells with added CIAALP at 36 °C (mean of 3 replicates shown, error bars = standard error). Polymer concentration = 0.75 mg.mL⁻¹.

6.4 Conclusions

In summary, this chapter first describes the synthesis of a phosphorylated methacrylate (Phos-HEMA) which is well tolerated by the RAFT methodology to produce phosphate-functional polymers. The susceptibility of these polymers to the action of the enzyme calf intestinal alkaline phosphatase was also demonstrated with no obvious effect of polymer molecular weight on the degradation profiles.

Secondly, the phosphorylated monomer was co-polymerised with diethylene glycol methyl ether methacrylate (DEGMA) to produce thermally-responsive materials. The cloud point of these polymers was proportional to the percentage of Phos-HEMA included with the inclusion of between 1 and 10 % resulting in a cloud point increase from 35 °C to 45 °C. The cloud point of these polymers was also observed to decrease in the presence of calf intestinal alkaline phosphatase due to enzyme-mediated dephosphorylation to the more hydrophobic hydroxyl functional group. This switch was used to modulate the polymer solubility isothermally.

In the third part of this chapter, the interactions of pNIPAM and pDEGMA-co-Phos-HEMA with the MCF7 cell line were assessed. Both polymers were fluorescently labelled using a small percentage of hostasol methacrylate as a co-monomer. Cloud point analysis of these polymers revealed an exponential, inversely-proportional concentration dependence, and was also influenced by variations in aqueous conditions. The cloud point in deionised water was higher than that of PBS whilst subtle differences between PBS and the RPMI 1640 based cell culture medium used in this investigation were also present. This highlights the need to fully characterise any thermally responsive system intended for *in vivo* application in biologically relevant media. The MTT assay was performed on pNIPAM, the

ethylene glycol-rich poly[oligo(ethylene glycol) methyl ether methacrylate], pOEGMA₃₀₀, and a pDEGMA-*co*-Phos-HEMA sample comprising 95 % DEGMA and 5 % Phos-HEMA. All polymers were shown to be biocompatible with the MCF7 cell line up to and including 2 mg.mL⁻¹ except for the co-polymer which exhibited an IC₅₀ value of 1.81 mg.mL⁻¹. This observation suggests that the percentage of phos-HEMA included in polymers intended for biological application should be kept to a minimum.

Finally, initial experiments aimed at investigating the effect of temperature on the uptake of these polymers by MCF7 cells indicated an enhanced uptake at temperatures above the polymer cloud point. Initial attempts to trigger this uptake isothermally, using enzyme-mediated polymer dephosphorylation proved unsuccessful however and will be a focus for future work.

6.5 Experimental

6.5.1 Materials

Phosphorus (V) oxychloride ($\geq 99.0\%$), 2-hydroxyethyl methacrylate (97.0%), triethylamine ($\geq 99.0\%$), *N*-isopropylacrylamide (97.0%), 4-cyano-4-(phenylcarbonothioylthio) pentanoic acid ($> 97.0\%$), 4,4'-azobis(4-cyanovaleric acid) ($\geq 98.0\%$), mesitylene (analytical standard), 2-mercaptoethanol ($\geq 99.0\%$), tribasic potassium phosphate (reagent grade, $\geq 98.0\%$), carbon disulfide ($\geq 99.0\%$) and benzyl bromide (98.0%) were purchased from Sigma-Aldrich. Oligo(ethylene glycol, average $M_n = 300 \text{ g.mol}^{-1}$), methyl ether methacrylate and di(ethylene glycol) methyl ether methacrylate (95.0%) were also purchased from Sigma-Aldrich and inhibitors removed by passing through a column of basic alumina prior to polymerisation. Hostasol methacrylate was kindly donated by the Haddleton group at the University of Warwick. 2-(dodecylthiocarbonothioylthio)-2-methylpropanoic acid was synthesised as described in chapter 2.

Calf Intestinal Alkaline Phosphatase was purchased from New England Biolabs Inc. The enzyme was packaged with a 10x NEBuffer 3. This was diluted 10-fold prior to use with the resulting 1x NEBuffer 3 containing 100 mM NaCl, 50 mM Tris-HCl, 10 mM MgCl₂, 1 mM dithiothreitol, pH 7.9 at 25 °C. The phosphate colorimetric assay kit was purchased from BioVision. A Standard Curve was prepared by diluting 10 μL of the supplied 10 mM Phosphate Standard to 990 μL dH₂O to give a 100 μM working standard. Desired standard concentrations were prepared by mixing the 10 mM standard with deionised water to give a total volume of 200 μL . The colorimetric phosphate reagent was used as received.

A human breast adenocarcinoma MCF7 cell line was sourced from the Tenovus centre for Cancer research (Cardiff, UK) and stored in liquid nitrogen when not in use. RPMI 1640 containing L-glutamine, sterile filtered foetal bovine serum (FBS) and trypsin were purchased from Lonza. Trypan blue 0.4 % was obtained from Gibco and 3-(4,5-dimethylthiazol-2-yl)2,5-diphenyl-tetrazolium bromide, Triton™ X-100 (for molecular biology) and sodium phosphate monobasic dehydrate were obtained from Sigma (UK). Dimethyl sulfoxide, sodium chloride and sodium phosphate dibasic anhydrous were sourced from Fisher Scientific. Phosphate buffer saline (PBS) was prepared freshly and autoclaved. Disposable tissue culture consumables were obtained from Greiner Bio-One and disposable glass ware from Fisher Scientific.

6.5.2 Analytical Methods

SEC analysis was performed on one of two systems:

(i) **Dimethylformamide:** Varian 390-LC MDS system equipped with a PL-AS RT/MT autosampler, a PL-gel 3 μm (50 x 7.5 mm) guard column, two PL-gel 5 μm (300 x 7.5 mm) mixed-D columns using DMF with 5 mM NH_4BF_4 at 50 °C as eluent at a flow rate of 1.0 $\text{mL}\cdot\text{min}^{-1}$. The SEC system was equipped with ultraviolet (UV)/visible (set at 280 and 461 nm) and differential refractive index (DRI) detectors. Narrow molecular weight PMMA standard (200 - 1.0 x 10⁶ $\text{g}\cdot\text{mol}^{-1}$) were used for calibration using a second order polynomial fit.

(ii) **Aqueous:** Varian 390-LC MDS system equipped with a PL-AS RT/MT autosampler, an aquagel-OH (50 x 7.5 mm) guard column, one PL-aquagel-OH 40 μm (300 x 7.5 mm) and one PL-aquagel-OH 30 μm (300 x 7.5 mm) column using a buffer comprising 0.2 M NaNO_3 and 0.01 M $\text{NaH}_2\text{PO}_4\cdot 2\text{H}_2\text{O}$ adjusted to pH 8.2

with 1 M NaOH at 30 °C as eluent at a flow rate of 1.0 mL.min⁻¹). The SEC system was equipped with a differential refractive index (DRO) detector. Narrow molecular weight PEO standards (100 – 1.0 x 10⁵ g.mol⁻¹) were used for calibration using a second order polynomial fit.

NMR spectroscopy (¹H, ¹³C, ³¹P) was conducted on a Bruker DPX-300, Bruker DRX-500 or Bruker AV III 600 spectrometer using deuterated chloroform or deuterated methanol as solvent. All chemical shifts are reported in ppm (δ) relative to the solvent used.

FTIR spectra were acquired using a Bruker Vector 22 FTIR spectrometer with a Golden Gate diamond attenuated total reflection cell. A total of 64 scans were collected on samples in their native state.

High resolution mass spectra were recorded on a Bruker Electrospray Ultra-High Resolution tandem TOF mass spectrometer using electrospray ionisation (ESI) in either positive or negative mode on samples prepared in methanol.

Cloud points were determined by turbidimetric analysis using either an Optimelt MPA100 system (Stanford Research Systems) or an Agilent Cary 60 UV/visible spectrophotometer with the absorbance monitored at 650 nm. A heating rate of 1 °C.min⁻¹ was used in both cases and the recorded turbidimetry curve was normalised between values of 0 and 1. The cloud point was defined as the temperature corresponding to a normalised absorbance of 0.5.

6.5.3 Synthetic Methods

6.5.3.1 Synthesis of 2-(methacryloyloxy)ethyl phosphate

Phosphorous oxychloride (13.90 g, 8.45 mL, 90.65 mmol) was dissolved in tetrahydrofuran (100 mL) in a two-necked round bottomed flask fitted with nitrogen inlet and pressure-equalising dropping funnel and cooled to $-15\text{ }^{\circ}\text{C}$. 2-Hydroxyethyl methacrylate (10.72 g, 10.00 mL, 82.41 mmol) and triethylamine (9.17 g, 12.63 mL, 90.65 mmol) were mixed with tetrahydrofuran (20 mL) in the dropping funnel and added over a period of 60 mins. The reaction mixture was left to stir for a further 90 mins at $-15\text{ }^{\circ}\text{C}$ followed by 90 mins at $0\text{ }^{\circ}\text{C}$. Water (22.5 mL) was added in one portion and the reaction stirred at $0\text{ }^{\circ}\text{C}$ for 1 hr. After this time, the solution was transferred to a separating funnel and extracted three times with brine. The organic layer was dried over magnesium sulfate and solvent removed to leave a viscous colourless liquid (12.64 g, 73.2 %).

$^1\text{H NMR}$ (600.132 MHz, MeOD) δ_{ppm} : 6.17 (1H, s, H^{1a}); 5.67 (1H, s, H^{1b}); 4.37 (2H, t, $J_{5-6} = 4.32\text{ Hz}$, H⁵); 4.21 – 4.24 (2H, m, H⁶); 1.97 (3H, s, H³).

$^{13}\text{C NMR}$ (150.864 MHz, MeOD) δ_{ppm} : 167.2 (C⁴); 136.1 (C²); 125.1 (C¹); 64.1 (d, $^2J_{\text{C-P}} = 4.77\text{ Hz}$, C⁶); 63.5 (d, $^3J_{\text{C-P}} = 8.34\text{ Hz}$, C⁵); 17.0 (C³).

$^{31}\text{P NMR}$ (121.442 MHz, MeOD) δ_{ppm} : 0.1

IR cm^{-1} : 2955 (alkyl-H stretch); 1703 (C=O stretch); 1634 (C=C); 1300 (P=O).

HRMS (ESI $-$) m/z : 209.0226 [M-H] $^-$; expected 209.0220 (C₆H₁₀O₆P).

6.5.3.2 Synthesis of benzyl 2-hydroxyethyl carbonotrithioate

2-Mercaptoethanol (1.00 g, 0.90 mL, 12.80 mmol) was added dropwise to a stirred suspension of K_3PO_4 (3.00 g, 14.13 mmol) in acetone (20 mL) over 20 mins. Carbon disulfide (2.92 g, 2.32 mL, 38.35 mmol) was added and the solution turned bright yellow. After stirring for ten mins, benzyl bromide (2.19 g, 1.52 mL, 12.80 mmol) was added and an immediate precipitation of KBr was noted. After stirring for 2 hours, the suspension was filtered and the cake washed with acetone. The solvent was removed *in vacuo* and the yellow residue was purified by column chromatography on silica using a 40-60 °C petroleum ether/ ethyl acetate gradient to yield a bright yellow oil (2.90 g, 92.9 %).

1H NMR (500.133 MHz, $CDCl_3$) δ_{ppm} : 7.25 – 7.35 (5H, m, H^{7-9}); 4.62 (2H, s, H^5); 3.90 (2H, q, $J_{2-1/2-3} = 7.50$ Hz, H^2); 3.62 (2H, t, $J_{3-2} = 7.50$ Hz, H^3); 1.86 (1H, t, $J_{1-2} = 7.50$ Hz, H^1).

^{13}C NMR (125.721 MHz, $CDCl_3$) δ_{ppm} : 223.5 (C^4); 134.8 (C^6); 129.3, 128.8, 127.9 (C^{7-9}); 60.7 (C^2); 41.7 (C^5); 39.2 (C^3).

IR cm^{-1} : 3345 (O-H stretch); 3084, 3060 (aryl-H stretch); 2921, 2876 (alkyl-H stretch); 1601, 1583, 1494 (aryl vibrations); 1058 (C=S stretch).

HRMS (ESI +) m/z : 266.9939 $[M+Na]^+$; expected 266.9942 ($C_{10}H_{12}NaOS_3$).

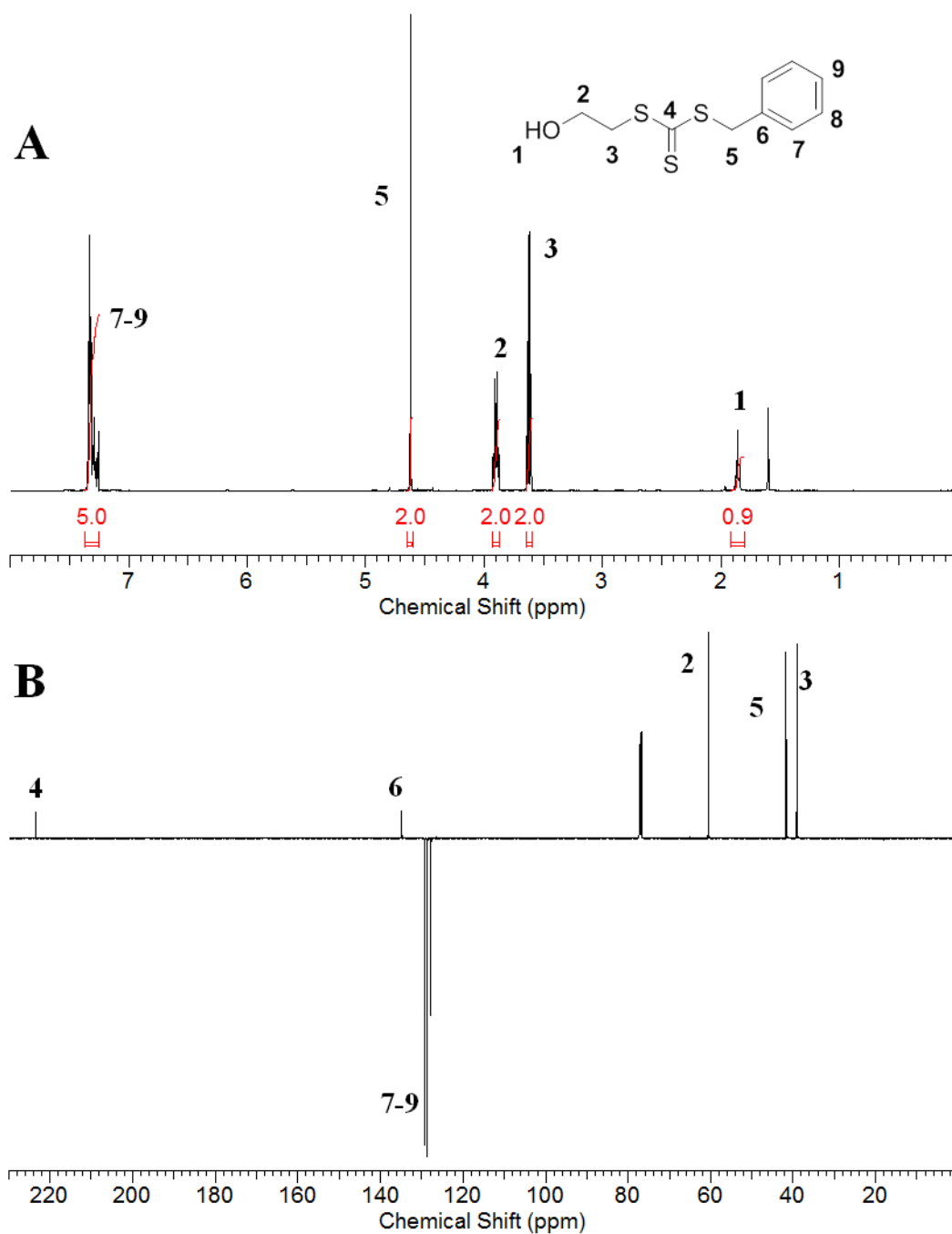


Figure 6.26 NMR spectroscopic characterisation of benzyl 2-hydroxyethyl carbonotrithioate in CDCl_3 : (A) ^1H and (B) ^{13}C spectra.

6.5.3.3 Example polymerisation of 2-(methacryloyloxy)ethyl phosphate using 4-cyano-4-(phenylcarbonothioylthio) pentanoic acid

2-(methacryloyloxy)ethyl phosphate (1.00 g, 4.76 mmol), 4-cyano-4-(phenylcarbonothioylthio) pentanoic acid (13.30 mg, 47.61 μmol) and 4,4'-azobis(4-cyanovaleric acid) (2.70 mg, 9.63 μmol) were added to a vial fitted with stir bar and rubber septum and dissolved in methanol (4 mL). Mesitylene (200 μL) was added as internal reference and the mixture stirred (5 mins). An aliquot of this starting mixture was removed for ^1H NMR spectroscopic analysis. The mixture was degassed by bubbling through nitrogen gas for 30 mins and placed in an oil bath thermostated at 65 °C for 7 hrs. The reaction was quenched in liquid nitrogen, an aliquot removed and conversion determined by ^1H NMR spectroscopy. The product was purified three times by precipitation from methanol into cold diethyl ether, the solid isolated by centrifugation and dried to yield a pale pink solid. Conversion (NMR): 54.7 % M_n (theoretical): 11500 $\text{g}\cdot\text{mol}^{-1}$; M_n (SEC): 38000 $\text{g}\cdot\text{mol}^{-1}$; M_w/M_n (SEC): 2.20.

6.5.3.4 Example polymerisation of 2-(methacryloyloxy)ethyl phosphate using 2-(dodecylthiocarbonothioylthio)-2-methylpropanoic

2-(methacryloyloxy)ethyl phosphate (1.00 g, 4.76 mmol), 2-(dodecylthiocarbonothioylthio)-2-methylpropanoic acid (17.35 mg, 47.58 μmol) and 4,4'-azobis(4-cyanovaleric acid) (2.70 mg, 9.63 μmol) were added to a vial fitted with stir bar and rubber septum and dissolved in methanol (4 mL). Mesitylene (200 μL) was added as internal reference and the mixture stirred (5 mins). An aliquot of this starting mixture was removed for ^1H NMR spectroscopic analysis. The mixture was degassed by bubbling through nitrogen gas for 30 mins and placed in an oil bath thermostated at 65 °C for 10 hrs. The reaction was quenched in liquid nitrogen, an

aliquot removed and conversion determined by ^1H NMR spectroscopy. The product was purified three times by precipitation from methanol into cold diethyl ether, the solid isolated by centrifugation and dried to yield a pale yellow solid. Conversion (NMR): 67.0 % M_n (theoretical): 14100 $\text{g}\cdot\text{mol}^{-1}$; M_n (SEC): 27700 $\text{g}\cdot\text{mol}^{-1}$; M_w/M_n (SEC): 2.17.

6.5.3.5 Polymerisation of oligo(ethylene glycol) methyl ether methacrylate using 4-cyano-4-(phenylcarbonothioylthio) pentanoic acid

Oligo(ethylene glycol, average $M_n = 300 \text{ g}\cdot\text{mol}^{-1}$) methyl ether methacrylate (1.00 g, 2.5 mmol), 4-cyano-4-(phenylcarbonothioylthio) pentanoic acid (13.97 mg, 50.00 μmol) and 4,4'-azobis(4-cyanovaleric acid) (2.80 mg, 10.00 μmol) were added to a vial fitted with stir bar and rubber septum and dissolved in dioxane (3 mL). Mesitylene (100 μL) was added as internal reference and the mixture stirred (5 mins). An aliquot of this starting mixture was removed for ^1H NMR spectroscopic analysis. The mixture was degassed by bubbling through nitrogen gas for 30 mins and placed in an oil bath thermostated at 70 $^\circ\text{C}$ for 4 hrs. The reaction was quenched in liquid nitrogen, an aliquot removed and conversion determined by ^1H NMR spectroscopy. The product was purified three times by precipitation from dioxane into cold diethyl ether, the solid isolated by centrifugation and dried to yield a waxy pink solid. Conversion (NMR): 44.2 %; M_n (theoretical): 8800 $\text{g}\cdot\text{mol}^{-1}$; M_n (SEC): 11300 $\text{g}\cdot\text{mol}^{-1}$; M_w/M_n (SEC): 1.18.

6.5.3.6 Example co-polymerisation of 2-(methacryloyloxy)ethyl phosphate and diethylene glycol methyl ether methacrylate using 4-cyano-4-(phenylcarbonothioylthio) pentanoic acid

Diethylene glycol methyl ether methacrylate (1.03 g, 5.47 mmol), 2-(methacryloyloxy)ethyl phosphate (0.13 g, 607.92 μmol), 4-cyano-4-(phenylcarbonothioylthio) pentanoic acid (17.00 mg, 60.79 μmol) and 4,4'-azobis(4-cyanovaleric acid) (3.41 mg, 12.16 μmol) were added to a vial fitted with stir bar and rubber septum and dissolved in methanol (4 mL). Mesitylene (200 μL) was added as internal reference and the mixture stirred (5 mins). An aliquot of this starting mixture was removed for ^1H NMR spectroscopic analysis. The mixture was degassed by bubbling through nitrogen gas for 30 mins and placed in an oil bath thermostated at 65 $^\circ\text{C}$ for 6.5 hrs. The reaction was quenched in liquid nitrogen, an aliquot removed and conversion determined by ^1H NMR spectroscopy. The product was purified three times by precipitation from methanol into cold diethyl ether, the solid isolated by centrifugation and dried to yield a waxy pink solid. Conversion (NMR): 23.3 %; M_n (theoretical): 4400 $\text{g}\cdot\text{mol}^{-1}$; M_n (SEC): 6200 $\text{g}\cdot\text{mol}^{-1}$; M_w/M_n (SEC): 1.30.

6.5.3.7 Co-polymerisation of *N*-isopropylacrylamide and hostasol methacrylate using benzyl 2-hydroxyethyl carbonotrithioate

N-isopropylacrylamide (1.00 g, 8.84 mmol), hostasol methacrylate (0.04 g, 87.42 μmol), benzyl 2-hydroxyethyl carbonotrithioate (72.00 mg, 294.57 μmol) and 4,4'-azobis(4-cyanovaleric acid) (16.51 mg, 58.91 μmol) were added to a vial fitted with stir bar and rubber septum and dissolved in a 1:1 mixture of methanol:toluene (4 mL). Mesitylene (200 μL) was added as internal reference and the mixture stirred (5 mins). An aliquot of this starting mixture was removed for ^1H NMR spectroscopic

analysis. The mixture was degassed by bubbling through nitrogen gas for 30 mins and placed in an oil bath thermostated at 70 °C for 1.75 hrs. The reaction was quenched in liquid nitrogen, an aliquot removed and conversion determined by ^1H NMR spectroscopy. The product was purified three times by precipitation from tetrahydrofuran into cold diethyl ether, the solid isolated by centrifugation and dried. Deionised water (10 mL) was added to the orange solid and stirred for 30 mins. The resulting suspension was then centrifuged and the supernatant freeze-dried to leave a pale orange solid. Conversion (NMR): 89.3 %; M_n (theoretical): 3000 g.mol $^{-1}$; M_n (SEC): 3800 g.mol $^{-1}$; M_w/M_n (SEC): 1.11.

6.5.3.8 Polymerisation of *N*-isopropylacrylamide using benzyl 2-hydroxyethyl carbonotrithioate.

N-isopropylacrylamide (1.00 g, 8.84 mmol), benzyl 2-hydroxyethyl carbonotrithioate (43.12 mg, 176.74 μmol) and 4,4'-azobis(4-cyanovaleric acid) (9.91 mg, 35.35 μmol) were added to a vial fitted with stir bar and rubber septum and dissolved in a 1:1 mixture of methanol:toluene (4 mL). Mesitylene (200 μL) was added as internal reference and the mixture stirred (5 mins). An aliquot of this starting mixture was removed for ^1H NMR spectroscopic analysis. The mixture was degassed by bubbling through nitrogen gas for 30 mins and placed in an oil bath thermostated at 70 °C for 1 hr. The reaction was quenched in liquid nitrogen, an aliquot removed and conversion determined by ^1H NMR spectroscopy. The product was purified three times by precipitation from tetrahydrofuran into cold diethyl ether, the solid isolated by centrifugation and dried to leave a pale yellow solid. Conversion (NMR): 63.6 %; M_n (theoretical): 3600 g.mol $^{-1}$; M_n (SEC): 5500 g.mol $^{-1}$; M_w/M_n (SEC): 1.08.

6.5.3.9 Co-polymerisation of 2-(methacryloyloxy)ethyl phosphate, diethylene glycol methyl ether methacrylate and hostasol methacrylate using 4-cyano-4-(phenylcarbonothioylthio) pentanoic acid

Diethylene glycol methyl ether methacrylate (1.00 g, 5.32 mmol), 2-(methacryloyloxy)ethyl phosphate (0.01 g, 53.69 μmol), hostasol methacrylate (0.02 g, 43.71 μmol), 4-cyano-4-(phenylcarbonothioylthio) pentanoic acid (15.00 mg, 53.69 μmol) and 4,4'-azobis(4-cyanovaleric acid) (3.01 mg, 10.74 μmol) were added to a vial fitted with stir bar and rubber septum and dissolved in methanol (4 mL). Mesitylene (200 μL) was added as internal reference and the mixture stirred (5 mins). An aliquot of this starting mixture was removed for ^1H NMR spectroscopic analysis. The mixture was degassed by bubbling through nitrogen gas for 30 mins and placed in an oil bath thermostated at 65 $^\circ\text{C}$ for 6.5 hrs. The reaction was quenched in liquid nitrogen, an aliquot removed and conversion determined by ^1H NMR spectroscopy. The product was purified six times by precipitation from tetrahydrofuran into cold diethyl ether, the solid isolated by centrifugation and dried to leave a waxy orange solid. Conversion (NMR): 30.9 %; M_n (theoretical): 5800 $\text{g}\cdot\text{mol}^{-1}$; M_n (SEC): 13400 $\text{g}\cdot\text{mol}^{-1}$; M_w/M_n (SEC): 1.12.

6.5.4 Assay Conditions

6.5.4.1 General assay conditions for colorimetric determination of phosphate release

A 105 $\mu\text{g}\cdot\text{mL}^{-1}$ stock solution of polymer in water was prepared. In a 96-well plate, in triplicate was added 188 μL of 1x NEBuffer 3 solution (diluted from the 10x concentrated solution provided by supplier), 10 μL of polymer solution and 2 μL calf intestinal alkaline phosphatase. The plate was then covered and incubated at 37 $^\circ\text{C}$.

At a given time-point, 30 μL of the phosphate reagent was mixed into each well, incubated at 37 $^{\circ}\text{C}$ for 90 mins and the absorbance at 650 nm measured. The molar concentration and hence percentage of phosphate released was determined by comparing to a known calibration curve.

6.5.4.2 Assay determining the effect of phosphatase on polymer cloud point

Polymer was dissolved in 1x NE Buffer 3 and calf intestinal alkaline phosphatase added to give a final polymer concentration of 5 $\text{mg}\cdot\text{mL}^{-1}$. This mixture was stirred at 37 $^{\circ}\text{C}$ for 24 hrs. After this time, an aliquot of the mixture was transferred to a melting point tube and the cloud point determined at a heating rate of 1 $^{\circ}\text{C}\cdot\text{min}^{-1}$.

6.5.4.3 Turbidimetric assay for phosphatase-mediated isothermal polymer response

A 5.56 $\text{mg}\cdot\text{mL}^{-1}$ solution of polymer in 1x NEBuffer 3 was prepared. 2 x 90 μL aliquots of this stock were transferred into individual wells of a 96-well plate. The plate was left to incubate at 34 $^{\circ}\text{C}$ in the plate reader for 35 mins. The plate was then removed and the well volume made to 100 μL with distilled water or calf intestinal alkaline phosphatase. The plate was re-incubated at 34 $^{\circ}\text{C}$ and the absorbance at 650 nm was recorded for an additional 25 mins.

6.5.5 Cell Culture

6.5.5.1 General cell culture

All cell culture work and experiments were performed in a Class II biosafety cabinet. Cells were cultivated under standard conditions (37 $^{\circ}\text{C}$, humidified atmosphere containing 5 % CO_2). A frozen stock vial (1 mL) containing the MCF7 cell suspension (approximately 10^6 cells) was thawed in warm water (37 $^{\circ}\text{C}$). The

suspension was transferred to a falcon tube containing pre-warmed (37 °C) medium (RPMI 1640, 9 mL), gently mixed with a pipette and centrifuged for 5 mins (1150 rpm). The supernatant was aspirated, cells re-suspended in medium (5 mL) and the whole cell-medium solution was transferred into a 25 cm² tissue culture flask using RPMI 1640 growth medium supplemented with 5 % FBS. The medium was changed every 2-3 days until cells were sufficiently confluent and required passaging. Confluence was assessed by bright field microscopy (Nikon Eclipse TS 100) and cell passaging was performed when 70 – 80 % of the growth area was covered with attached cells. For the passaging of cultured cells, old medium was removed and the cell layer washed with pre-warmed sterile PBS. To detach the cells, trypsin was added and the cells incubated for 3-5 mins. Fresh medium containing FBS was then added to stop the proteolytic action of trypsin. The suspension was collected into a falcon tube and centrifuged for 5 mins (1150 rpm). The supernatant was removed and the cell pellet re-suspended in fresh medium. Aliquots of the suspension were used for either seeding new flasks or multi-well plates after performing a cell count with the haemocytometer (0.1 x 0.0025 mm²) (Marienfeld, Germany).

6.5.5.2 Cytotoxicity testing of polymers: MTT assay

The cells were counted and growth medium added to give a final cell concentration of 4×10^4 cells.mL⁻¹. Multi-well plates (96-well; growth area of 0.34 cm² per well) were seeded using 100 µL of this cell-medium suspension and the plates incubated for 24 hrs under standard conditions. Cells were treated with 100 µL of a sterile filtered stock solution of polymer in FBS-supplemented growth medium (4, 0.4, or 0.02 mg.mL⁻¹) to give the desired concentrations (2.0, 1.0, 0.75, 0.5, 0.2, 0.1, 0.075, 0.05 and 0.01 mg.mL⁻¹). As control, 100 µL growth medium was added instead of a polymer solution. After 67 hrs, 3-[4,5-dimethylthiazol-2-yl]-3,5-diphenyl

tetrazolium bromide (MTT, 20 μL of a 5 $\text{mg}\cdot\text{mL}^{-1}$ solution) was added and the cells were incubated for a further 5 hrs. All media was then aspirated, 100 μL DMSO was added and the plates were incubated for 30 mins to dissolve the formazan crystals. The absorbance was then measured at 570 nm using a Benchmark Microplate Reader (Bio-Rad, UK). Cells treated with complete medium only were taken as a control (100 % viability). Cell viability was expressed using the following equation, where Abs_{exp} and $\text{Abs}_{\text{control}}$ represent the amount of formazan determined for cells treated with the polymer and for control cells respectively.

$$\text{Cell viability (\%)} = \left(\frac{\text{Abs}_{\text{exp}}}{\text{Abs}_{\text{control}}} \right) \times 100$$

A total of four replicates were performed and the results are expressed as mean values \pm standard error.

6.5.5.3 Cell uptake at fixed temperature

The cells were counted and growth medium added to give a final cell concentration of 4×10^4 $\text{cells}\cdot\text{mL}^{-1}$. Multi-well plates (24-well; growth area of 1.9 cm^2 per well) were seeded using 100 μL of this cell-medium suspension and the plates incubated for 24 hrs under standard conditions to allow cell attachment. The medium was removed and the well washed with sterile PBS (1 mL). Fresh medium (1 mL, control) or polymer solution (1 mL, final concentration of pNIPAM-*co*-HMA and pDEGMA-*co*-phos-HEMA-*co*-HMA = 2.0 $\text{mg}\cdot\text{mL}^{-1}$ and 0.75 $\text{mg}\cdot\text{mL}^{-1}$ respectively) was then added. In each case, one plate was incubated at 30 $^{\circ}\text{C}$ and the other at 38 $^{\circ}\text{C}$. After one hr, the polymer solution was removed and the cell layer washed with sterile PBS (3 x 1 mL). Sterile filtered 1 % Triton-X solution (1 mL) was added and plates were incubated at set temperature for 30 mins. After this time, the Triton-X-

cell suspension was transferred into cuvettes; the wells washed with PBS (1.5 mL) and the solution transferred into cuvettes. Fluorescence was measured at excitation and emission wavelengths of 461 nm and 528 nm respectively. A total of three replicates were performed and the results are expressed as mean values \pm standard error.

6.5.5.4 Calf intestinal alkaline phosphatase-driven cell uptake

The cells were counted and growth medium added to give a final cell concentration of 4×10^4 cells.mL⁻¹. Multi-well plates (24-well; growth area of 1.9 cm² per well) were seeded using 100 μ L of this cell-medium suspension and the plates incubated for 24 hrs under standard conditions to allow cell attachment. The medium was removed and the well washed with sterile PBS (1 mL). Fresh medium (1 mL, control) or polymer solution (1 mL, final concentration of 0.75 mg.mL⁻¹) was then added together with the designated volume of enzyme, as required. The plates were incubated at 36 °C for 24 hrs after which time, the polymer solution was removed and the cell layer washed with sterile PBS (3 x 1 mL). Sterile filtered 1 % Triton-X solution (1 mL) was added and plates were incubated at 36 °C for 30 mins. After this time, the Triton-X-cell suspension was transferred into cuvettes; the wells washed with PBS (1.5 mL) and the solution transferred into cuvettes. Fluorescence was measured at excitation and emission wavelengths of 461 nm and 528 nm respectively. Three replicates were performed and the results are expressed as mean values \pm standard error.

6.6 References

- 1 Murdan, S. Electro-responsive drug delivery from hydrogels. *J. Control. Rel.* **2003**, *92*, 1-17.
- 2 Schmaljohann, D. Thermo- and pH-responsive polymers in drug delivery. *Adv. Drug Deliv. Rev.* **2006**, *58*, 1655-1670.
- 3 Ganta, S.; Devalapally, H.; Shahiwala, A.; Amiji, M. A review of stimuli-responsive nanocarriers for drug and gene delivery. *J. Control. Rel.* **2008**, *126*, 187-204.
- 4 Saffran, M.; Kumar, G.; Savariar, C.; Burnham, J.; Williams, F.; Neckers, D. A new approach to the oral administration of insulin and other peptide drugs. *Science* **1986**, *233*, 1081-1084.
- 5 Allen, A.; Flemström, G. Gastroduodenal mucus bicarbonate barrier: protection against acid and pepsin. *Am. J. Physiol. Cell Physiol.* **2005**, *288*, C1-C19.
- 6 Sinha, V. R.; Kumria, R. Microbially triggered drug delivery to the colon. *Eur. J. Pharm.* **2003**, *18*, 3-18.
- 7 Ku, T.-H.; Chien, M.-P.; Thompson, M. P.; Sinkovits, R. S.; Olson, N. H.; Baker, T. S.; Gianneschi, N. C. Controlling and Switching the Morphology of Micellar Nanoparticles with Enzymes. *J. Am. Chem. Soc.* **2011**, *133*, 8392-8395.
- 8 Dhanasekaran, S. M.; Barrette, T. R.; Ghosh, D.; Shah, R.; Varambally, S.; Kurachi, K.; Pienta, K. J.; Rubin, M. A.; Chinnaiyan, A. M. Delineation of prognostic biomarkers in prostate cancer. *Nature* **2001**, *412*, 822-826.
- 9 Meers, P. Enzyme-activated targeting of liposomes. *Adv. Drug Deliv. Rev.* **2001**, *53*, 265-272.
- 10 Raffetto, J. D.; Khalil, R. A. Matrix metalloproteinases and their inhibitors in vascular remodeling and vascular disease. *Biochem. Pharmacol.* **2008**, *75*, 346-359.
- 11 Kessenbrock, K.; Plaks, V.; Werb, Z. Matrix Metalloproteinases: Regulators of the Tumor Microenvironment. *Cell* **2010**, *141*, 52-67.
- 12 Hu, J.; Zhang, G.; Liu, S. Enzyme-responsive polymeric assemblies, nanoparticles and hydrogels. *Chem. Soc. Rev.* **2012**, *41*, 5933-5949.

- 13 Zelzer, M.; Todd, S. J.; Hirst, A. R.; McDonald, T. O.; Ulijn, R. V. Enzyme responsive materials: design strategies and future developments. *Biomater. Sci.* **2013**, *1*, 11-39.
- 14 Hahn, M. E.; Gianneschi, N. C. Enzyme-directed assembly and manipulation of organic nanomaterials. *Chem. Commun.* **2011**, *47*, 11814-11821.
- 15 Rao, J.; Khan, A. Enzyme Sensitive Synthetic Polymer Micelles Based on the Azobenzene Motif. *J. Am. Chem. Soc.* **2013**, *135*, 14056-14059.
- 16 Harnoy, A. J.; Rosenbaum, I.; Tirosh, E.; Ebenstein, Y.; Shaharabani, R.; Beck, R.; Amir, R. J. Enzyme-Responsive Amphiphilic PEG-Dendron Hybrids and Their Assembly into Smart Micellar Nanocarriers. *J. Am. Chem. Soc.* **2014**, *136*, 7531-7534.
- 17 Azagarsamy, M. A.; Sockalingam, P.; Thayumanavan, S. Enzyme-Triggered Disassembly of Dendrimer-Based Amphiphilic Nanocontainers. *J. Am. Chem. Soc.* **2009**, *131*, 14184-14185.
- 18 Fuchs, A. V.; Kotman, N.; Andrieu, J.; Mailander, V.; Weiss, C. K.; Landfester, K. Enzyme cleavable nanoparticles from peptide based triblock copolymers. *Nanoscale* **2013**, *5*, 4829-4839.
- 19 Hu, B.-H.; Messersmith, P. B. Rational Design of Transglutaminase Substrate Peptides for Rapid Enzymatic Formation of Hydrogels. *J. Am. Chem. Soc.* **2003**, *125*, 14298-14299.
- 20 Sofia, S. J.; Singh, A.; Kaplan, D. L. Peroxidase-Catalyzed Crosslinking of Functionalized Polyaspartic Acid Polymers. *J. Macromol. Sci. A: Pure Appl. Chem.* **2002**, *39*, 1151-1181.
- 21 Chen, T.; Embree, H. D.; Brown, E. M.; Taylor, M. M.; Payne, G. F. Enzyme-catalyzed gel formation of gelatin and chitosan: potential for in situ applications. *Biomaterials* **2003**, *24*, 2831-2841.
- 22 Jun, H. W.; Yuwono, V.; Paramonov, S. E.; Hartgerink, J. D. Enzyme-Mediated Degradation of Peptide-Amphiphile Nanofiber Networks. *Adv. Mater.* **2005**, *17*, 2612-2617.
- 23 Davidsen, J.; Vermehren, C.; Frokjaer, S.; Mouritsen, O. G.; Jørgensen, K. Drug delivery by phospholipase A2 degradable liposomes. *Int. J. Pharm.* **2001**, *214*, 67-69.
- 24 Li, H.; He, Q.; Wang, X.; Lu, G.; Liusman, C.; Li, B.; Boey, F.; Venkatraman, S. S.; Zhang, H. Nanoscale-Controlled Enzymatic Degradation

- of Poly(L-lactic acid) Films Using Dip-Pen Nanolithography. *Small* **2011**, *7*, 226-229.
- 25 Guyomard-Lack, A. I.; Delorme, N.; Moreau, C. I.; Bardeau, J.-F. O.; Cathala, B. Site-Selective Surface Modification Using Enzymatic Soft Lithography. *Langmuir* **2011**, *27*, 7629-7634.
- 26 Vincent, J. B.; Crowder, M. W.; Averill, B. A. Hydrolysis of phosphate monoesters: a biological problem with multiple chemical solutions. *Trends Biochem. Sci.* **1992**, *17*, 105-110.
- 27 Siffert, R. S. The Role of Alkaline Phosphatase in Osteogenesis *J. Exp. Med.* **1951**, *93*, 415-426.
- 28 Golub, E. E.; Boesze-Battaglia, K. The role of alkaline phosphatase in mineralization. *Curr. Opin. Orthop.* **2007**, *18*, 444-448.
- 29 Moe, S. M. Disorders Involving Calcium, Phosphorus, and Magnesium. *Prim. Care* **2008**, *35*, 215-237.
- 30 Shaver, W. A.; Bhatt, H.; Combes, B. Low serum alkaline phosphatase activity in Wilson's disease. *Hepatology* **1986**, *6*, 859-863.
- 31 Millán, J. L.; Fishman, W. H.; Stinson, R. Biology of Human Alkaline Phosphatases with Special Reference to Cancer. *Crit. Rev. Clin. Lab. Sci.* **1995**, *32*, 1-39.
- 32 Yang, Z.; Gu, H.; Fu, D.; Gao, P.; Lam, J. K.; Xu, B. Enzymatic Formation of Supramolecular Hydrogels. *Adv. Mater.* **2004**, *16*, 1440-1444.
- 33 Wang, C.; Chen, Q.; Wang, Z.; Zhang, X. An Enzyme-Responsive Polymeric Superamphiphile. *Angew. Chem. Int. Ed.* **2010**, *49*, 8612-8615.
- 34 Zelzer, M.; McNamara, L. E.; Scurr, D. J.; Alexander, M. R.; Dalby, M. J.; Ulijn, R. V. Phosphatase responsive peptide surfaces. *J. Mater. Chem.* **2012**, *22*, 12229-12237.
- 35 Schattling, P.; Jochum, F. D.; Theato, P. Multi-stimuli responsive polymers - the all-in-one talents. *Polym. Chem.* **2014**, *5*, 25-36.
- 36 Xia, Y.; Burke, N. A. D.; Stöver, H. D. H. End Group Effect on the Thermal Response of Narrow-Disperse Poly(N-isopropylacrylamide) Prepared by Atom Transfer Radical Polymerization. *Macromolecules* **2006**, *39*, 2275-2283.
- 37 López-Pérez, P. M.; da Silva, R. M. P.; Pashkuleva, I.; Parra, F.; Reis, R. L.; San Roman, J. Hydrophobic–Electrostatic Balance Driving the LCST Offset

- Aggregation–Redissolution Behavior of N-Alkylacrylamide-Based Ionic Terpolymers. *Langmuir* **2009**, *26*, 5934-5941.
- 38 Caponi, P.-F.; Qiu, X.-P.; Vilela, F.; Winnik, F. M.; Ulijn, R. V. Phosphatase/temperature responsive poly(2-isopropyl-2-oxazoline). *Polym. Chem.* **2011**, *2*, 306-308.
- 39 Bergbreiter, D. E. Soluble Polymers as Tools in Catalysis. *ACS Macro Lett.* **2014**, *3*, 260-265.
- 40 Kanazawa, H. Thermally responsive chromatographic materials using functional polymers. *J. Sep. Sci.* **2007**, *30*, 1646-1656.
- 41 Chung, J. E.; Yokoyama, M.; Yamato, M.; Aoyagi, T.; Sakurai, Y.; Okano, T. Thermo-responsive drug delivery from polymeric micelles constructed using block copolymers of poly(N-isopropylacrylamide) and poly(butylmethacrylate). *J. Control. Rel.* **1999**, *62*, 115-127.
- 42 Abulateefeh, S. R.; Spain, S. G.; Thurecht, K. J.; Aylott, J. W.; Chan, W. C.; Garnett, M. C.; Alexander, C. Enhanced uptake of nanoparticle drug carriers via a thermoresponsive shell enhances cytotoxicity in a cancer cell line. *Biomater. Sci.* **2013**, *1*, 434-442.
- 43 Kono, K.; Nakai, R.; Morimoto, K.; Takagishi, T. Temperature-dependent interaction of thermo-sensitive polymer-modified liposomes with CV1 cells. *FEBS Lett.* **1999**, *456*, 306-310.
- 44 Choi, S. H.; Yoon, J. J.; Park, T. G. Galactosylated Poly(N-isopropylacrylamide) Hydrogel Submicrometer Particles for Specific Cellular Uptake within Hepatocytes. *J. Colloid Interface Sci.* **2002**, *251*, 57-63.
- 45 Bidwell, G. L.; Raucher, D. Application of thermally responsive polypeptides directed against c-Myc transcriptional function for cancer therapy. *Mol. Cancer Ther.* **2005**, *4*, 1076-1085.
- 46 MacEwan, S. R.; Chilkoti, A. Applications of elastin-like polypeptides in drug delivery. *J. Control. Rel.* **2014**, *190*, 314-330.
- 47 Stockert, R. J. The asialoglycoprotein receptor: relationships between structure, function, and expression. *Physiol. Rev.* **1995**, *75*, 591-609.
- 48 Yoo, H. S.; Park, T. G. Folate receptor targeted biodegradable polymeric doxorubicin micelles. *J. Control. Rel.* **2004**, *96*, 273-283.

- 49 Wiley, D. T.; Webster, P.; Gale, A.; Davis, M. E. Transcytosis and brain uptake of transferrin-containing nanoparticles by tuning avidity to transferrin receptor. *Proc. Natl. Acad. Sci. U.S.A.* **2013**, *110*, 8662-8667.
- 50 Qian, Z. M.; Li, H.; Sun, H.; Ho, K. Targeted Drug Delivery via the Transferrin Receptor-Mediated Endocytosis Pathway. *Pharmacol. Rev.* **2002**, *54*, 561-587.
- 51 Bareford, L. M.; Swaan, P. W. Endocytic mechanisms for targeted drug delivery. *Adv. Drug Deliv. Rev.* **2007**, *59*, 748-758.
- 52 Huang, J.; Matyjaszewski, K. Atom Transfer Radical Polymerization of Dimethyl(1-ethoxycarbonyl)vinyl Phosphate and Corresponding Block Copolymers. *Macromolecules* **2005**, *38*, 3577-3583.
- 53 Zhou, F.; Huck, W. T. S. Three-stage switching of surface wetting using phosphate-bearing polymer brushes. *Chem. Commun.* **2005**, 5999-6001.
- 54 Jang, S.; Lee, S.; Kim, H.; Ham, J.; Seo, J.-H.; Mok, Y.; Noh, M.; Lee, Y. Preparation of pH-sensitive CaP nanoparticles coated with a phosphate-based block copolymer for efficient gene delivery. *Polymer* **2012**, *53*, 4678-4685.
- 55 Suzuki, S.; Whittaker, M. R.; Grøndahl, L.; Monteiro, M. J.; Wentrup-Byrne, E. Synthesis of Soluble Phosphate Polymers by RAFT and Their in Vitro Mineralization. *Biomacromolecules* **2006**, *7*, 3178-3187.
- 56 Iwasaki, Y.; Matsumoto, A.; Yusa, S.-i. Optimized Molecular Structure of Photoreactive Biocompatible Block Copolymers for Surface Modification of Metal Substrates. *ACS Appl. Mater. Interfaces* **2012**, *4*, 3254-3260.
- 57 Grondahl, L.; Suzuki, S.; Wentrup-Byrne, E. Influence of a diene impurity on the molecular structure of phosphate-containing polymers with medical applications. *Chem. Commun.* **2008**, 3314-3316.
- 58 Flory, P. J. Effects of Cross-Linking and Branching on the Molecular Constitution of Diene Polymers¹. *J. Am. Chem. Soc.* **1947**, *69*, 2893-2899.
- 59 Lomoschitz, C. J.; Feichtenschlager, B.; Moszner, N.; Puchberger, M.; Müller, K.; Abele, M.; Kickelbick, G. Directing Alkyl Chain Ordering of Functional Phosphorus Coupling Agents on ZrO₂. *Langmuir* **2011**, *27*, 3534-3540.
- 60 Quirk, R. P.; Lee, B. Experimental Criteria for Living Polymerizations. *Polym. Int.* **1992**, *27*, 359-367.

- 61 Hirao, A.; Kato, H.; Yamaguchi, K.; Nakahama, S. Polymerization of monomers containing functional groups protected by trialkylsilyl groups. 5. Synthesis of poly(2-hydroxyethyl methacrylate) with a narrow molecular weight distribution by means of anionic living polymerization. *Macromolecules* **1986**, *19*, 1294-1299.
- 62 Weaver, J. V. M.; Bannister, I.; Robinson, K. L.; Bories-Azeau, X.; Armes, S. P.; Smallridge, M.; McKenna, P. Stimulus-Responsive Water-Soluble Polymers Based on 2-Hydroxyethyl Methacrylate. *Macromolecules* **2004**, *37*, 2395-2403.
- 63 Amir, R. J.; Zhong, S.; Pochan, D. J.; Hawker, C. J. Enzymatically Triggered Self-Assembly of Block Copolymers. *J. Am. Chem. Soc.* **2009**, *131*, 13949-13951.
- 64 Han, S.; Hagiwara, M.; Ishizone, T. Synthesis of Thermally Sensitive Water-Soluble Polymethacrylates by Living Anionic Polymerizations of Oligo(ethylene glycol) Methyl Ether Methacrylates. *Macromolecules* **2003**, *36*, 8312-8319.
- 65 Becer, C. R.; Hahn, S.; Fijten, M. W. M.; Thijs, H. M. L.; Hoogenboom, R.; Schubert, U. S. Libraries of methacrylic acid and oligo(ethylene glycol) methacrylate copolymers with LCST behavior. *J. Polym. Sci. Part A: Polym. Chem.* **2008**, *46*, 7138-7147.
- 66 Alarcon, C. d. I. H.; Pennadam, S.; Alexander, C. Stimuli responsive polymers for biomedical applications. *Chem. Soc. Rev.* **2005**, *34*, 276-285.
- 67 Timko, B. P.; Dvir, T.; Kohane, D. S. Remotely Triggerable Drug Delivery Systems. *Adv. Mater.* **2010**, *22*, 4925-4943.
- 68 Nicolas, J.; Miguel, V. S.; Mantovani, G.; Haddleton, D. M. Fluorescently tagged polymer bioconjugates from protein derived macroinitiators. *Chem. Commun.* **2006**, 4697-4699.
- 69 Schild, H. G. Poly(N-isopropylacrylamide): experiment, theory and application. *Prog. Polym. Sci.* **1992**, *17*, 163-249.
- 70 Akimoto, J.; Nakayama, M.; Sakai, K.; Okano, T. Thermally Controlled Intracellular Uptake System of Polymeric Micelles Possessing Poly(N-isopropylacrylamide)-Based Outer Coronas. *Mol. Pharm.* **2010**, *7*, 926-935.

- 71 Phillips, D. J.; Gibson, M. I. Degradable thermoresponsive polymers which display redox-responsive LCST Behaviour. *Chem. Commun.* **2012**, *48*, 1054-1056.
- 72 Bebis, K.; Jones, M. W.; Haddleton, D. M.; Gibson, M. I. Thermoresponsive behaviour of poly[(oligo(ethyleneglycol methacrylate)]s and their protein conjugates: importance of concentration and solvent system. *Polym. Chem.* **2011**, *2*, 975-982.
- 73 Magnusson, J. P.; Khan, A.; Pasparakis, G.; Saeed, A. O.; Wang, W.; Alexander, C. Ion-Sensitive “Isothermal” Responsive Polymers Prepared in Water. *J. Am. Chem. Soc.* **2008**, *130*, 10852-10853.
- 74 Moore, G. E.; Gerner, R. E.; Franklin, H. Culture of normal human leukocytes. *JAMA* **1967**, *199*, 519-524.
- 75 Mosmann, T. Rapid colorimetric assay for cellular growth and survival: Application to proliferation and cytotoxicity assays. *J. Immunol. Methods* **1983**, *65*, 55-63.
- 76 Lobner, D. Comparison of the LDH and MTT assays for quantifying cell death: validity for neuronal apoptosis? *J. Neurosci. Methods* **2000**, *96*, 147-152.
- 77 Schiller, C. D.; Kainz, A.; Mynett, K.; Gescher, A. Assessment of viability of hepatocytes in suspension using the MTT assay. *Toxicol. In Vitro* **1992**, *6*, 575-578.
- 78 Slater, T. F.; Sawyer, B.; Sträuli, U. Studies on succinate-tetrazolium reductase systems: III. Points of coupling of four different tetrazolium salts III. Points of coupling of four different tetrazolium salts. *Biochim. Biophys. Acta* **1963**, *77*, 383-393.
- 79 Rawlinson, L.-A. B.; Ryan, S. a. M.; Mantovani, G.; Syrett, J. A.; Haddleton, D. M.; Brayden, D. J. Antibacterial Effects of Poly(2-(dimethylamino ethyl)methacrylate) against Selected Gram-Positive and Gram-Negative Bacteria. *Biomacromolecules* **2009**, *11*, 443-453.
- 80 Aseyev, V.; Tenhu, H.; Winnik, F. M. Non-ionic Thermoresponsive Polymers in Water. In *Self Organized Nanostructures of Amphiphilic Block Copolymers II*, Müller, A. H. E.; Borisov, O., Eds.; Springer: Berlin, **2011**; Vol. 242, pp 29-89.

Chapter 7

7. Conclusions

As the burgeoning scope of responsive materials expands to fulfil roles within and beyond biology, the development of systems capable of responding to multiple stimuli remains a profitable challenge. Equipped with an ever-increasing grasp of polymer synthesis, the modern-day chemist has at their disposal a vast toolbox from which increasingly adaptable and complex structures are becoming routinely available.

This work has investigated a variety of (thermo)-responsive polymer-based materials capable of exhibiting a macroscopic property change in response to more than just temperature. First, a facile method for the preparation of thermo-responsive pNIPAM homopolymers containing reduction-sensitive disulfide linkages in the backbone has been developed. This was achieved following an aminolysis-driven, polycondensation-type expansion of polymers containing pyridyl disulfide and thiocarbonylthio moieties at the α - and ω -chain-ends respectively. These linkages were shown to be selectively degraded at intracellular concentrations of the key *in vivo* reducing agent glutathione. The inversely proportional relationship between pNIPAM molecular weight and LCST ensured the degradation of the disulfide-linked “macro” species to smaller chains was accompanied by an increase in LCST, allowing for isothermal solubilisation.

Secondly, glutathione has been applied to shift the phase behaviour of responsive polymer nanoparticles. The particle matrix, prepared by nanoprecipitation of hydrophilic pHEA-*co*-NIPAM chains, could be disassembled by reduction-mediated degradation of the disulfide-functional polymer end-groups to release encapsulated cargo. The increase in LCST observed in this process allowed for re-solubilisation of the polymer matrix and hence removal of insoluble material.

Thirdly, a chain-end modification inspired by the catechol-Fe³⁺ binding motif utilised by bacteria to sequester iron from mammalian hosts has been applied to achieve isothermal precipitation. Beyond thermo-responsive systems, this motif has also been applied to control the dispersion-aggregation behaviour of gold nanoparticles containing surface-accessible catechol units. The addition of physiologically-relevant levels of Fe³⁺ triggered particle cross-linking and a strong colorimetric output, offering valuable biosensor potential.

Finally, thermo-responsive co-polymers containing hydrophilic phosphate linkages throughout the side-chain have been shown to degrade in the presence of calf intestinal alkaline phosphatase. Cleavage to more hydrophobic hydroxyl moieties triggered a decrease in cloud point enabling isothermal polymer precipitation. Initial investigations into the interactions of these polymers with MCF7 cells revealed an increased uptake when the polymers were held in their hydrophobic state.

Ultimately, a single macroscopic response can be routinely controlled by the action of a range of stimuli. Hence, a “scaffold” can be developed from which systems designed to react to a host of environments can be obtained. This work has demonstrated examples whereby simple modifications of a polymer backbone, end-groups and side-chain in response to diverse stimuli such as redox potential, metal

ions and enzyme concentration are able to significantly alter a system's macroscopic response. Future developments in this area are arguably limited only by the imagination of the pursuing scientist. It is hoped the development of new chemistries and structural platforms from which next-generation materials can be produced will soon follow.

Appendix

Redox-Sensitive Materials for Drug

Delivery: Targeting the Correct

Intracellular Environment; Tuning Release

Rates and Appropriate Predictive Systems

The development of redox-sensitive drug delivery systems holds great promise for *in vivo* applications given the wide range of redox gradients found therein. However, these gradients also require careful consideration during material design as subtle differences can significantly alter the behaviour of an intended delivery vehicle. Moreover, the types of model reducing agents used in the development of such systems should also be thoughtfully selected in a bid to achieve behaviour predictive of an *in vivo* setting.

The following “Forum Review Article” was written during the course of my Doctoral studies with the aim of highlighting these points. Although not directly related to the experimental chapters described elsewhere in this thesis, the concepts discussed are of explicit relevance to the design of redox-sensitive materials.

FORUM REVIEW ARTICLE

Redox-Sensitive Materials for Drug Delivery: Targeting the Correct Intracellular Environment, Tuning Release Rates, and Appropriate Predictive Systems

Daniel J. Phillips and Matthew I. Gibson

Abstract

Significance: The development of responsive drug delivery systems (DDS) holds great promise as a tool for improving the pharmacokinetic properties of drug compounds. Redox-sensitive systems are particularly attractive given the rich variety of redox gradients present *in vivo*. These gradients, where the circulation is generally considered oxidizing and the cellular environment is substantially more reducing, provide attractive options for targeted, specific cargo delivery. **Recent Advances:** Experimental evidence suggests that a “one size fits all” redox gradient does not exist. Rather, there are subtle differences in redox potential within a cell, while the chemical nature of reducing agents in these microenvironments varies. Recent works have demonstrated an ability to modulate the degradation rate of redox-susceptible groups and, hence, provide new tools to engineer precision-targeted DDS. **Critical Issues:** Modern synthetic and macromolecular chemistry provides access to a wide range of redox-susceptible architectures. However, in order to utilize these in real applications, the actual chemical nature of the redox-susceptible group, the sub-cellular location being targeted, and the redox microenvironment being encountered should be considered in detail. This is critical to avoid the over-simplification possible when using non-biological reducing agents, which may provide inaccurate kinetic information, and to ensure these materials can be advanced beyond simple “on/off” systems. Furthermore, a strong case can be made for the use of biorelevant reducing agents such as glutathione when demonstrating a materials redox response. **Future Directions:** A further understanding of the complexities of the extra- and intracellular microenvironments would greatly assist with the design and application of DDS. *Antioxid. Redox Signal.* 21, 786–803.

Introduction

Why prepare redox-susceptible materials?

THE USE OF drug delivery systems (DDS) to improve the pharmacokinetics of known therapeutic compounds is a well-established concept (4, 24, 87). This is particularly the case for anti-cancer drugs, where the use of polymeric/nanosopic agents is popular due to the enhanced permeability and retention effect that promotes the passive accumulation of macromolecules into cancerous tissue (34, 65, 85). However, outstanding challenges associated with these systems include maintaining control of release specificity and rate at systemic and sub-cellular levels to ensure maximum therapeutic efficacy and minimal toxicity, and to target non-cancer disease states (28, 38).

Within the human body, a landscape of biochemical gradients exists that can be exploited for targeted delivery and controlled release. These include fluctuations in temperature, pH, osmotic pressure, cell-surface receptors, circulatory biomarkers, and enzymes, to name but a few (2, 9, 58, 73). The variety of *in vivo* redox potentials are a particularly interesting gradient. In simple terms, the intracellular environment is highly reducing relative to the extracellular environment, providing an exciting target for selective intracellular release. Conversely, certain areas such as wound sites are significantly more oxidizing than healthy tissue (113). Given the highly established chemistries associated with oxidation and reduction processes, there is a rapidly expanding interest in incorporating these into DDS.

The key aim of this review is to provide a critical evaluation of current redox-responsive functional groups that have been exploited for drug delivery, with particular focus on reduction-sensitive materials. An analysis of sub-cellular redox gradients and ways in which to tune the cleavage of reduction-sensitive groups to target these regions will be provided. A critical discussion of which appropriate *in vitro* reducing agents might be used when designing new DDS and examples of the variety of reduction-susceptible materials being prepared and applied these days will also be highlighted. To put this into context, a brief description of oxidation-sensitive materials is also included. The individual sections are summarized next:

- Oxidation-susceptible materials
- Cellular redox environments: important redox couples
- Cellular redox environments: variations in *in vivo* gradients
- Selecting an appropriate reducing agent for *in vitro* studies
- Manipulating rates of disulfide reduction
- Bioreducible drug carriers

Oxidation-Susceptible Materials

Reactive oxygen species (ROS) such as hydrogen peroxide (H_2O_2), superoxide, and hydroxyl radical are normal by-products of the eukaryotic metabolism (17). Generally, these species are maintained in a healthy equilibrium by enzymes such as superoxide dismutase, catalase, and glutathione peroxidase and play an important role in a variety of capacities, including cell signaling, homeostasis (30), and wound healing (6). However, when an excess of ROS are produced, localized areas of oxidative stress develop and are considered markers of a variety of diseases such as Alzheimer's, Parkinson's, cardiovascular disease, and some cancers (52, 81, 97, 119, 131). These localized areas, therefore, provide a realistic target for scientists developing responsive biomedical materials. This section seeks to briefly highlight some examples of this approach, to place the reduction-sensitive section in context, though readers are directed to the following detailed reviews for more information (27, 72, 75, 130).

Poly(propylene sulfide) (PPS) is a hydrophobic polymer that readily oxidizes into hydrophilic poly(sulfoxides and sulfones). It has been identified as a matrix for hydrophobic drugs that can be released after oxidation-induced solubilization or swelling. Napoli *et al.* prepared vesicles from ABA block copolymers comprising poly(ethylene glycol) (PEG) and PPS, which could be destabilized by oxidative action (90). Tirelli and co-workers have also investigated responsive particles containing PPS (59, 104). Interestingly, the oxidation character and, hence, cytotoxicity of such materials was shown to be dependent on whether H_2O_2 or sodium hypochlorite (NaOCl), both oxidants present in inflamed tissues, was used (18). Oxidation with H_2O_2 converted thioethers into sulfoxides, while the reaction with NaOCl produced sulfones in addition to sulfoxides, affecting the toxicity of the oxidation products. PPS-based materials have been exploited by Reddy *et al.* to deliver antigen-presenting cells into dendritic cells without the use of a targeting ligand (103) and Allen *et al.*, who triggered the release of hydrophobic cargo from nanoparticles by both chemically- and enzymatically generated ROS (3).

Boronic esters are also oxidatively susceptible and exploited as protecting groups in organic chemistry. Almutairi and co-workers prepared nanoparticles containing aryl boronic ester groups that were oxidized to phenol groups at a biologically relevant H_2O_2 range of 50–100 μM . This triggered main chain degradation *via* a quinone methide rearrangement (31). Song *et al.* (115) prepared pH/oxidation dual-responsive micelle-like nanoparticles comprising ortho ester and phenylboronic ester components. At pH 7.4, hydrolysis of the ortho ester was accelerated by the addition of 50 μM H_2O_2 , as the phenylboronic ester was oxidized to a catalytic carboxylic acid (115). Broaders *et al.* (15) loaded ovalbumin into dextran nanoparticles containing arylboronic ester units and saw payload release with a half life of 36 min. However, this required 1 mM H_2O_2 , which is well above physiological levels. When applied to CD8^+ T cells, a 27-fold increase in exposure of ovalbumin compared with a non-oxidation sensitive control vehicle was observed, suggesting potential application in vaccine therapies (15).

Thioketal-containing nanoparticles have been used by Wilson *et al.* for localized oral delivery of small interfering RNAs to sites of intestinal inflammation while inhibiting gene expression (135). Mahmoud *et al.* (84) combined thioether and ketal functionalities to produce dual-responsive nanoparticles. These were designed to produce a more hydrophilic backbone, due to thioether oxidation, and, hence, enable faster acid-catalyzed ketal degradation than the more hydrophobic ketal-only containing structures. The particles were loaded with ovalbumin, and the greatest cargo release was observed after 24 h in conditions, enabling both responses. Cell studies revealed efficient nanoparticle uptake by macrophages followed by cytoplasmic release of the protein (84).

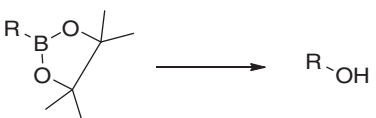
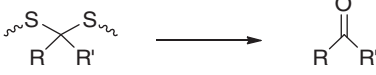
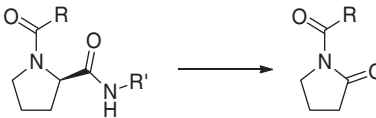
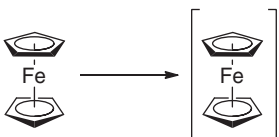
(Di)selenide groups have also been of interest, as they can be both oxidized and reduced. Self-assembled structures from a copolymer containing hydrophobic diselenide-containing and hydrophilic PEG blocks were shown by Ma *et al.* to be stable under ambient conditions but sensitive to a redox trigger (83). Liu *et al.* (79) have prepared an amphiphilic hyperbranched polymer consisting of alternative hydrophobic selenide and hydrophilic phosphate segments in the dendritic backbone. As a secondary benefit, the hydrophilic oxidation products could then be degraded into easily excreted, small-molecular-weight species *via* enzymatic digestion of the phosphate segments (79).

Yu *et al.* prepared proline cross-linked polymeric scaffolds based on PEG and poly(caprolactam) (PCL), which were cleaved by H_2O_2 (142). Peptide-based cleavable groups are particularly attractive, as they can be directly incorporated into recombinant protein-based delivery systems and are composed of canonical and, therefore, resorbable components. Finally, oxidizable "nanopatches" composed of poly(vinylferrocene) blocks distributed in a poly(methyl methacrylate) matrix have been prepared by Staff *et al.* (117). Selective oxidation of the vinylferrocene units enabled release of hydrophobic payloads, while the topography of the nanocapsules post-oxidation was dependent on the oxidizing agent (H_2O_2 or potassium permanganate) used (117). Examples of the variety of oxidizable linkages and their resulting oxidized products are shown in Table 1.

Cellular Redox Environments: Important Redox Couples

The intracellular environment is inherently more reducing than the comparatively oxidative extracellular (circulatory)

TABLE 1. EXAMPLES OF OXIDATION-SENSITIVE GROUPS AND THEIR RESULTING OXIDATION PRODUCTS

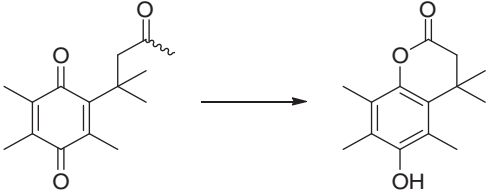
Oxidizable linkages and resulting oxidation products	Reference(s)
$\text{R-S-R}' \longrightarrow \text{R-S(=O)-R}' \quad , \quad \text{R-S(=O)}_2\text{-R}'$	Sulfide \rightarrow sulfoxide/sulfone (3, 18, 59, 84, 90, 103, 104)
	Boronic ester \rightarrow alcohol (15, 31, 115)
	Thioketal \rightarrow ketone (135)
$\text{R-Se-Se-R}' \longrightarrow \text{R-Se-OH}$	Diselenide \rightarrow seleninic acid (83)
$\text{R-Se-R}' \longrightarrow \text{R-Se(=O)}_2\text{-R}'$	Selenide \rightarrow selenone (79)
	Prolyl peptide \rightarrow 2-Pyrrolidone peptide (142)
	Ferrocene \rightarrow ferrocenium ion (117)

environment as a result of redox couples such as nicotinamide adenine dinucleotide phosphate (NADPH/NADP⁺), thioredoxin (TRX_{red}/TRX_{ox}), and glutathione (GSH/GSSG), which are a part of healthy metabolism (62). The interest in developing delivery systems containing reduction-sensitive linkages that are capable of selectively releasing cargo in response to raised reduction potentials is, therefore, an obvious and appealing target for controlled drug delivery. A variety of reducible groups have been incorporated into material structures, including diselenides (83) and trimethyl-locked benzoquinone (23). Graf and Lippard have also recently reviewed the use of prodrugs based on metal complexes that can be activated in the reducing environment of cancer cells (50). Nevertheless, the reducible linkage of choice appears to be the disulfide bond, which is further described in sections

“Cellular redox environments: variations in *in vivo* gradients,” “Selecting an appropriate reducing agent for *in vitro* studies,” “Manipulating rates of disulfide reduction,” and “Bio-reducible drug carriers.” These reducible groups and their resulting reduced products are highlighted in Table 2.

Of the reducing compounds present in the body, the most commonly studied is that of GSH. GSH is a tripeptide containing glutamate, cysteine, and glycine and it is synthesized in the body in two steps. First, γ -glutamylcysteine is synthesized from L-glutamate and cysteine *via* the enzyme γ -glutamylcysteine synthetase and second, glycine is added to the C-terminus of γ -glutamylcysteine *via* the enzyme glutathione synthetase (Fig. 1A). Importantly, it is the most abundant intracellular thiol with a reported concentration of between 0.2 and 10 mM in healthy cells, which is significantly

TABLE 2. EXAMPLES OF REDUCTION-SENSITIVE GROUPS AND THEIR REDUCTION PRODUCTS

Reducible linkages and resulting reduction products	Reference(s)
$\text{R-Se-Se-R}' \longrightarrow \text{R-SeH}$	Diselenide \rightarrow selenol (83)
	Trimethyl-locked benzoquinone \rightarrow lactone (23)
$\text{R-S-S-R}' \longrightarrow \text{R-SH}$	Disulfide \rightarrow Thiol (13, 22, 132)

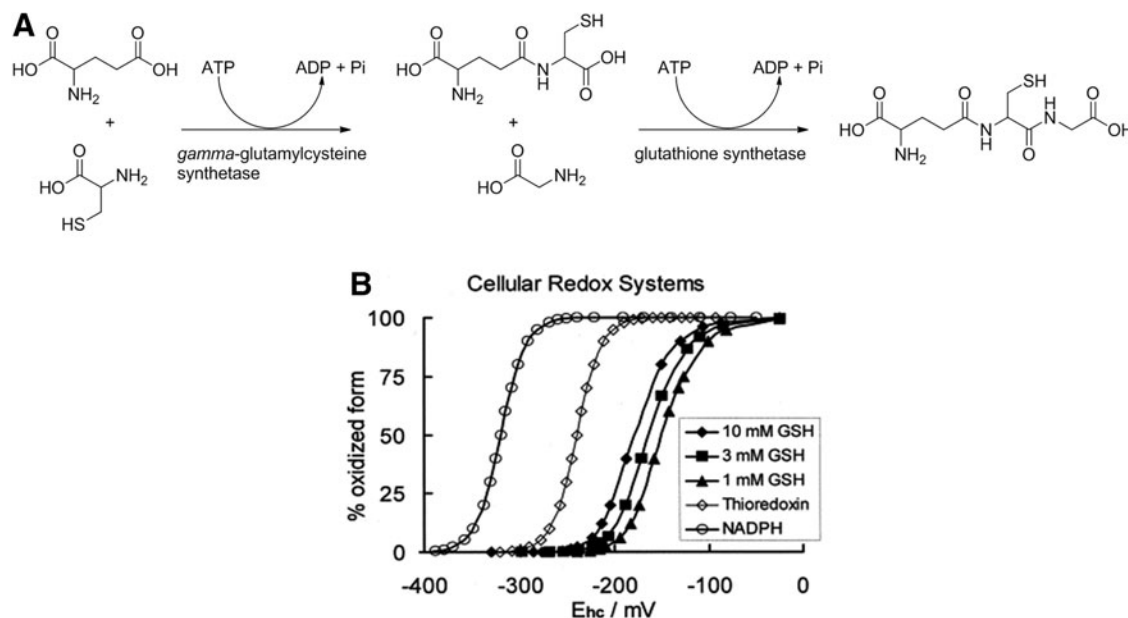


FIG. 1. (A) Biosynthetic scheme for the synthesis of GSH; (B) the redox potential of the couples NADPH, thioredoxin, and GSH as a function of oxidized percentage. Reprinted (adapted) with permission from Schafer and Buettner (112). Copyright (2013) Elsevier. GSH, glutathione; NADPH, nicotinamide adenine dinucleotide phosphate.

higher than any other available redox couple (5, 62). By comparison, the TRX couple exists at an intracellular concentration of $\sim 1\text{--}10\ \mu\text{M}$ in bovine tissue (54) and of approximately $15\ \mu\text{M}$ in bacteria (55), while the intracellular NADPH concentration has been approximated at $0.1\ \text{mM}$ (112). Half-cell potentials of the three linked redox couples NADPH/ NADP^+ ; $\text{TRX}_{\text{red}}/\text{TRX}_{\text{ox}}$; and GSH/GSSG, as estimated using the Nernst equation, are shown in Figure 1B. NADPH, which provides reducing equivalents to the NADPH and TRX couples, is considered the thermodynamic driving force for these two systems though the overall redox environment results primarily from the GSH couple given its significantly higher concentration (112). This definition of redox environment has been used by Deponete to show the reducing capacity of different concentrations of GSH (32). Unlike many other physiological redox couples, the redox potential of the GSH system depends not only on the ratio of oxidized and reduced GSH but also on the actual GSH concentration (32, 70, 112).

In comparison to the intracellular environment, blood plasma retains a more oxidizing characteristic with micromolar concentrations of GSH and cysteine being the main reducing entities (49, 63, 64). The significantly more oxidizing nature of the circulatory system is important in maintaining protein folding and function. A thorough description of GSH concentration in specific organelles has been detailed by Schafer and Buettner (112), though it should be noted that the nature of the reducing environment differs throughout the cell. Considering this, it is necessary to consider *intracellular gradients* as well as organism-level gradients if one is to design a truly targeted therapeutic, as highlighted in the next section.

Cellular Redox Environments: Variations in *In Vivo* Gradients

While GSH is the most abundant reducing agent in the cytosol, organelles such as those within the endocytic path-

way have different redox potentials (Table 3). The endoplasmic reticulum, for example, plays both oxidative and reductive roles (49). Although GSH is the principal redox buffer here, the redox state is 20–100 times more oxidized (GSH concentration estimated at $0.5\text{--}1\ \text{mM}$) than in the cytosol, thus enabling disulfide formation in proteins (61). Protein disulfide isomerase also catalyzes both the oxidation and isomerization of disulfides on nascent polypeptides in the endoplasmic reticulum, while solely catalyzing the reduction of protein disulfides in the cytoplasm, endosomes, and at the cell surface (91). The mechanism of reduction within the endocytic pathway is also likely to be different from that of the cytosol, where reduction by thiol-disulfide exchange dominates. For this mechanism to proceed efficiently, the desired nucleophilic species is a thiolate anion. Although a lack of endosomal acidification has been observed when using monovalent folate conjugates (141), the endocytic pathway is generally considered acidic, negating the formation of this species and leaving reducing agents in their sulfhydryl form. Instead, gamma-interferon-inducible lysosomal thiol

TABLE 3. ORGANELLES EXHIBITING DIFFERENT REDOX CHARACTERISTICS

Organelle	Oxidizing/ reducing	Main reductants	References
Endoplasmic reticulum	Both	GSH, GILT, PDI	(49)
Endosome	Oxidizing Reducing	PDI, GILT	(7, 111) (140)
Golgi apparatus	Reducing	PDI	(39)
Lysosome	Reducing	Cysteine	(19, 26)
Cytosol	Reducing	GSH	(112)

Data assembled from (109).

GILT, gamma-interferon-inducible lysosomal thiol reductase; GSH, glutathione; PDI, protein disulfide isomerase.

reductase, the only known reductase localized in the endocytic pathway, works optimally at acidic pH and can catalyze disulfide bond reduction in this compartment (53). Cell surface sulfhydryls that become oriented at the inner face of the nascent endosome on endocytosis can also mediate reduction. In this manner, disulfide reduction is considered critical in activating diphtheria toxin, for example (107).

The reducing nature of the whole endocytic pathway has been the focus of much debate. For a review detailing where and how a disulfide bond specifically in a bioconjugate is reduced on contact with biological milieu, the reader is directed to a review by Saito *et al.* (109). Austin *et al.* noted a low reductive or even oxidative nature of endosomes (7), which Sauer *et al.* further demonstrated with mesoporous silica nanoparticles (MSNs) containing disulfide-linked cysteine (111). These particles were taken into endosomes of HuH7 cells but saw no reductive release after 49 h. When the photosensitizer TPPS_{2a} was added, endosomal collapse was observed, as the singlet oxygen produced on quenching triplet oxygen with the excited triplet state of TPPS_{2a} was able to oxidize unsaturated fatty acids, cholesterol, and amino acids. This released the nanoparticles into the significantly more reducing cytosol, which triggered disulfide bond cleavage and, hence, release of cysteine. Conversely, Yang *et al.* (140) found the endosome to be sufficiently reducing to cleave the disulfide bond in a fluorescent folate-SS-rhodamine conjugate. Fluorescence studies indicated that reduction began in the endosome and remained active along the entire folate receptor endocytic pathway with a half life of 6 h (140).

Feener *et al.* have suggested that the most probable site of reduction of a membrane absorptive polymer based on tyramine-SS-poly-D-lysine was the Golgi apparatus (39), while Collins *et al.* noted reduction of a conjugate comprising tyrosine linked *via* a disulfide linker to α_2 -macroglobulin only in the lysosome (26), the main reducing agent in which is arguably cysteine (80, 101). Considering this, Cerritelli *et al.* (19) prepared reduction-sensitive disulfide block copolymer vesicles for intracellular drug delivery using cysteine as the reducing agent. A PEG-monothiolate and a PPS-monothiolate were oxidatively combined to produce PEG-SS-PPS. The resulting polymersomes were shown to protect biomolecules in the extracellular environment, be taken into a cell through endocytosis, and demonstrate a burst release in the early endosome on account of disulfide-bond reduction by endosomally relevant cysteine concentrations (19). Van der Vlies *et al.* utilized the same trigger to release tioguanine linked *via* a disulfide bond to block copolymers of PEG-*b*-PPS. Reduction and, hence, tioguanine release was observed in response to

cysteine and serum at a rate dependent on the PPS block length (126).

Selecting an Appropriate Reducing Agent for *In Vitro* Studies

Considering the wide range of redox potentials in the intracellular environment (*vide supra*), it is crucial that the DDS contains a redox-active component which responds *specifically* and *selectively* at the desired site of action. While apparently obvious, a wide variety of chemical and biochemical reducing agents are used in the literature to demonstrate the susceptibility of new DDS to cellular reducing agents, without consideration of their *in vitro* relevance. Some common examples include tris(2-carboxyethyl) phosphine (TCEP), dithiothreitol (DTT), 2-mercaptoethanol (ME), dihydrolipoic acid (DHLA), nicotinamide adenine dinucleotide hydride (NADH), and GSH (Fig. 2).

Each of these reducing agents will likely have different redox potentials and mechanisms of action from those found in the target environment, decreasing the predictive value of initial screen assays. A detailed investigation by Lee *et al.* (74) showed the effect that different reducing agents can have on the results of high-throughput screening, a method used to identify drug leads. A reducing agent is commonly added to the assay to prevent cysteine oxidation in target proteins. An issue with the use of strong reducing agents such as DTT and TCEP is the generation of false positives as a result of H₂O₂ production (14, 51). The authors, therefore, investigated the inhibition of three cysteine proteases tested with a variety of compounds and reducing agents, and observed many non-overlapping hits. The inhibitor potency changed approximately 20-fold depending on the reducing agent used, while DTT produced the most false negatives. For example, the application of inhibitor 3 (Fig. 3) to the NS3/4A target protein revealed a half maximal inhibitory concentration (IC₅₀) value of 48.4 μ M when no reducing agent was present and a similar value of 69.4 μ M when GSH was present. With TCEP, the IC₅₀ value decreased fivefold (12.8 μ M), while no inhibition was observed in the presence of either DTT or ME. The authors also demonstrated that GSH could be reliably used in such assays and is, therefore, the preferred method for predicative chemical reduction compared with TCEP or DTT (74).

In the context of this review article, the earlier study clearly demonstrates that in order to be able to predict the behavior of a DDS *in vitro*, it is essential to use a redox couple which is appropriate to the targeted sub-cellular location. Selected examples of delivery systems in which the effect of the reductant has been probed are discussed next.

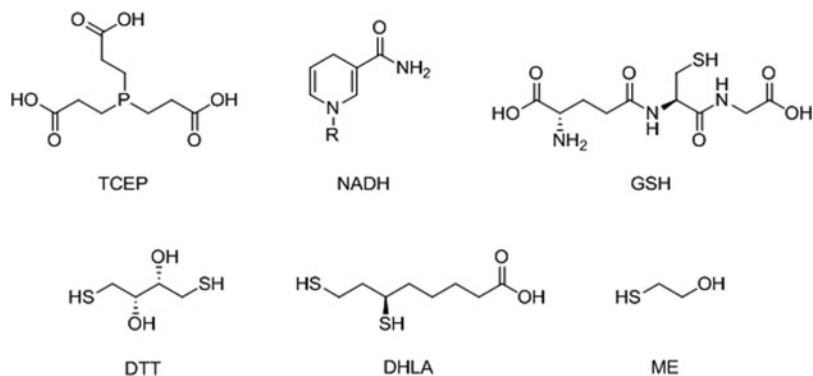


FIG. 2. Chemical structures of commonly used *in vitro* reducing agents. DHLA, dihydrolipoic acid; DTT, dithiothreitol; ME, 2-mercaptoethanol; NADH, nicotinamide adenine dinucleotide hydride; TCEP, tris(2-carboxyethyl) phosphine.

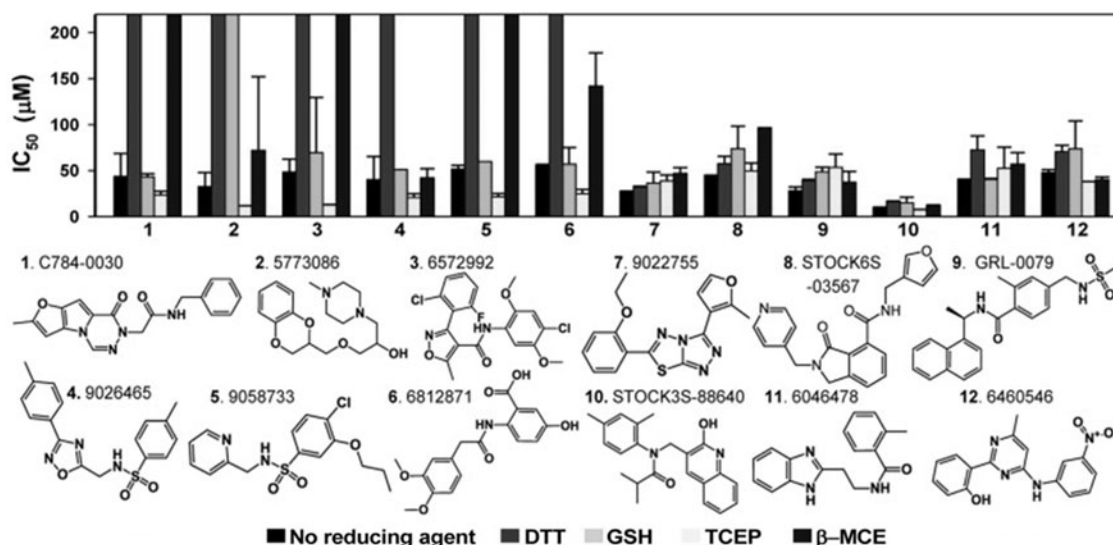


FIG. 3. Comparisons of the IC₅₀ values of active compounds against NS3/4A target protein in the absence or presence of reducing agents. Bars that reach the top of the figure represent IC₅₀ values of more than 200 µM (no inhibitory effect). Reproduced (adapted) with permission from Lee *et al.* (74). Copyright (2013). Elsevier. IC₅₀, half maximal inhibitory concentration; β-MCE, 2-mercaptoethanol.

Mortera *et al.* (86) prepared an MSN-based intracellular cysteine delivery system that could be induced and regulated by cell-produced natural antioxidants (reductants). No cysteine leaching in phosphate-buffered saline (PBS) was seen before a reducing agent was added. However, when a variety of reducing agents were added, vastly different releases were observed: 99%, 90%, 70%, and 60% release was observed 30 min after adding NADH, DTT, DHLA, and GSH, respectively, highlighting that false positives can be obtained if inappropriate reagents are used (86). Lu *et al.* (82) prepared reduction-sensitive poly(urethane-urea)s based on cystine. Greater levels of degradation were observed with DTT than with GSH over the 4 day timeframe investigated, though neither degraded to completion (82). Interestingly, Pan *et al.* (96) prepared redox/pH dual stimuli-responsive biodegradable nanohydrogels, which saw greater drug release in response to GSH than DTT (Fig. 4). Doxorubicin (DOX) was loaded into the hydrogels due to strong electrostatic interactions between the DOX amine group and carboxyl groups present in the nanohydrogel. This possibly counter-intuitive observation [DTT is a stronger reducing agent than GSH (32, 112)], and it was rationalized by considering the synergistic effect of reduction and charge exchange of GSH at low pH. This article also highlights that no studies have discussed the difference in the redox efficiency between DTT and GSH (96). It could also be argued that a material designed for *in vivo* use should be tested for reduction with *in vivo* reducing agents such as GSH.

Manipulating Rates of Disulfide Reduction

The cleavage of a disulfide unit is distinct from that of alternative degradable functionalities such as poly(esters), which can take days, weeks, or even months to fully degrade (36, 95). Compared with an ester, the disulfide bond is generally considered a more labile linkage. In order to achieve desirable release kinetics, a number of studies have been un-

dertaken to fine-tune the rate of disulfide reduction for controlled and predictable cargo release.

Wu *et al.* (136) identified the use of 6-residue peptides containing a cysteine unit as a straightforward platform for studying the impact of disulfide microenvironment on their exchange rates. Exchange kinetics of a number of cysteine-containing peptides measured in a variety of redox buffers representing conditions found in the late endosome/lysosome and cytoplasm illustrated that the electrostatic attraction/repulsion between peptides and reducing agents such as GSH had a pronounced effect on thiol-disulfide exchange (136). The authors also found that the thiol-disulfide exchange kinetics varied depending on the reducing agent (GSH, cysteine or cysteamine) used. A similar observation has been made by Bulaj *et al.* for the exchange of peptide thiols with, for example, cysteine and they noticed that electrostatic attraction/repulsion played a significant role in increasing/decreasing exchange, respectively (16).

Gauthier and co-workers (137) utilized the CXC motif to direct intermolecular and intramolecular pairing of cysteine residues without the need for extensive manipulation of the primary sequence, post-translational modification, or the protection of groups. Here, the authors found that by employing a central arginine residue (cationic), the equilibrium was directed toward the dimer, as the cationic residue promotes thiolate reactivity. Flanking residues were found to not influence thiolate reactivity in the same way as the central residue, while the steric hindrance of the central residue did not significantly influence the equilibrium. Moreover, the charged microenvironment surrounding the CXC motif was found to alter the equilibrium between single and mixed disulfides with negatively charged flanking residues shifting the equilibrium toward the dimeric state and positively charged residues toward the monomeric species (137).

Steiner and co-workers (118) investigated how the therapeutic efficacy of a vascular targeting antibody-drug conjugate is affected by the length of a space between the antibody's

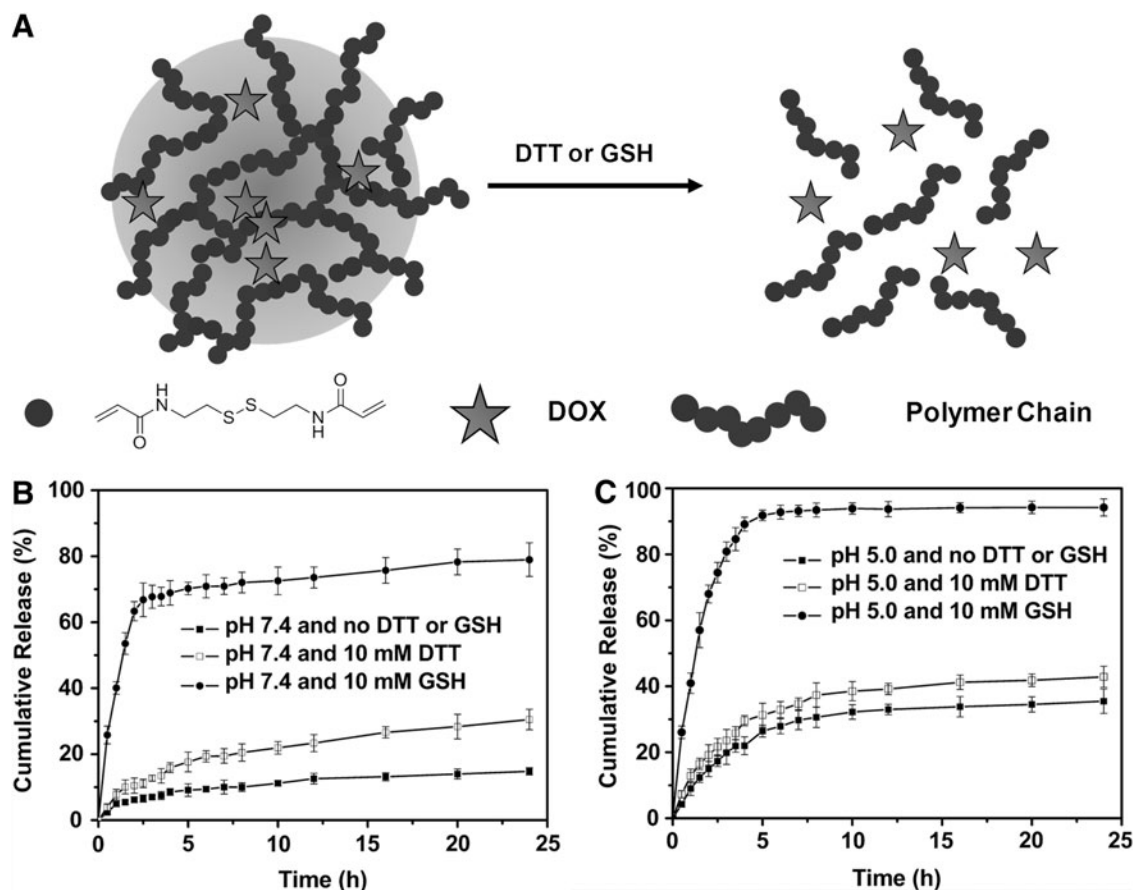


FIG. 4. Redox-triggered drug release. (A) Schematic representation of the release of DOX from nanogels on disulfide-bond reduction with DTT or GSH; pH and dual-responsive DOX profiles from DOX-loaded nanohydrogels with different reducing agents: (B) pH 7.4; (C) pH 5.0. Reproduced (adapted) with permission from Pan *et al.* (96). Copyright (2013) Elsevier. DOX, doxorubicin.

globular fold and the disulfide-linked site of drug attachment. They found that smaller spacer lengths enhanced stability toward disulfide reduction both in plasma and *in vitro*. Ultimately, where the disulfide linkage is less hindered and therefore protrudes from the globular antibody to a greater extent, reduction and, hence, drug release is faster. However, the greater stability toward reduction of the smaller spacers promoted greater therapeutic efficiency, as demonstrated by the authors when the antibody-drug conjugates were tested in an A20 lymphoma model. Moreover, it was speculated that the microenvironment of tumor sites, where dying cells initially release additional GSH/cysteine, locally reinforces drug release and amplifies drug-mediated cell killing, which may provide an addition trigger if the DDS can be tuned to respond to this increased GSH concentration (118).

The ability to trigger structural changes in linear polymer systems on exposure to a reductive environment has been investigated by several groups. For example, Gillies and co-workers (20, 33) prepared a linear polymer backbone based on *N,N'*-dimethylethylenediamine and ME linked by carbamates and thiocarbamates. These polymers were then end-capped with a disulfide that was readily cleaved in a reducing environment utilizing DTT. Cleavage triggered a cascade of cyclization reactions and gave 1,3-oxathiolan-2-one and *N,N'*-dimethylimidazolidinone by-products. Degradation was monitored by ^1H nuclear magnetic resonance spectroscopy, revealing a plateau at $\sim 80\%$ degradation after 10 days (33).

The ability to tune these degradation rates was achieved by incorporating stronger nucleophilic and electrophilic sites to induce faster cyclization reactions, and, hence, complete degradation was observed in a matter of hours (Fig. 5) (20).

Li *et al.* (77) have reported the influence of local mechanical tension on the reduction of a disulfide by DTT. A comb-shaped polymer consisting of a poly(2-hydroxyethyl methacrylate) backbone and poly(*n*-butyl acrylate) side chains with a central disulfide bond was prepared by atom-transfer radical polymerization. The bond tension was generated due to steric repulsion between densely positioned chain-like branches and could be induced spontaneously, without applying any external force. The reduction-induced fracture of the so-called "bottlebrushes" was then monitored by atomic force microscopy (AFM). Increased scission was seen at a DTT concentration of $194\ \mu\text{M}$ DTT compared with $19.4\ \mu\text{M}$ DTT after 4 h. The authors also noted that increasing the disulfide bond tension from 0.85 to 1.26 nN significantly increased the rate of bond cleavage at a DTT concentration of $19.4\ \mu\text{M}$ (Fig. 6) (77). This report is significant, as it shows that mechanical cues can be used to tune a biological response, in addition to chemical methods.

Thiol-disulfide exchange in proteins has also been shown to be dependent on an applied force. Fernandez and co-workers have used force-clamp AFM to probe the reduction rate of the 27th immunoglobulin-like domain of cardiac titin with DTT, observing a 10-fold increase over a 300 pN range (133). The

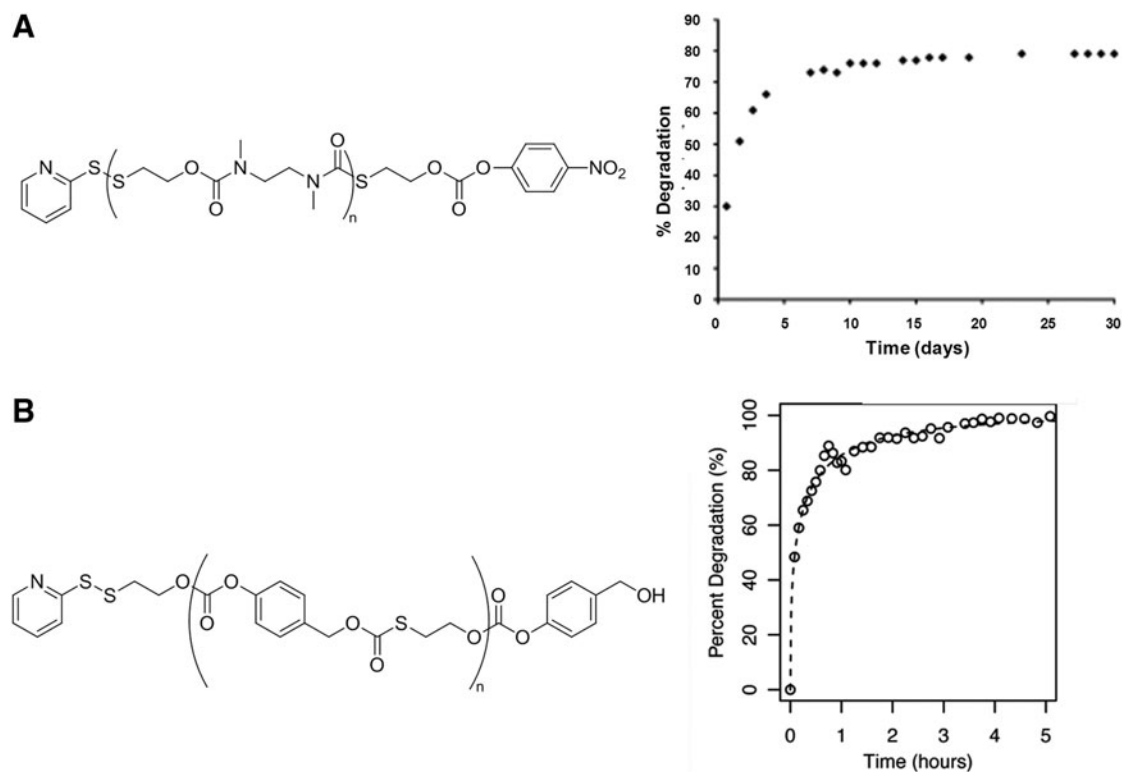


FIG. 5. Linear systems that degrade by a cascade of cyclization reactions on reduction of the disulfide end group. Modification of nucleophilic and electrophilic sites within the polymer backbone results in degradation times of (A) days or (B) hours, triggered by disulfide reduction (20, 33). (A) Reproduced (adapted) with permission from Dewit *et al.* (33). Copyright (2013) Wiley. (B) Reproduced (adapted) with permission from Chen *et al.* (20). Copyright (2013) American Chemical Society.

same group has also demonstrated that a mechanical force can significantly alter the chemistry of the catalytic site in TRX, which is potentially significant in tissues that are exposed to pathological force levels (134). Baldus Ilona and Gräter have used simulations of cysteine as a model system to demonstrate the ability of physiological forces to tune the disulfide redox potential (10).

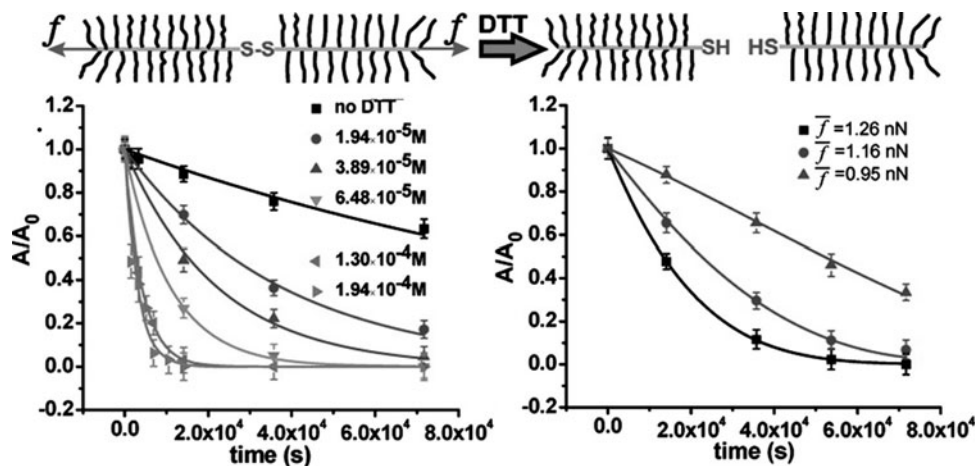
Kellogg *et al.* (66) synthesized a variety of disulfide-linked huC242 (anti-CanAg) antibody maytansinoid conjugates with varying levels of steric hindrance around the disulfide bond to investigate the relationship between stability to reduction of the disulfide linker and antitumor activity of the conjugate

in vivo. When exposed to DTT, the conjugates with more sterically hindered disulfide linkages were shown to be more stable to reductive cleavage. When tested for *in vivo* efficacy, the conjugates with two methyl groups on the maytansinoid side and no methyl groups on the linker side of the disulfide bond displayed the best efficacy (66).

Bioreducible Drug Carriers

The earlier sections clearly demonstrate the inherent complexity of cellular redox environments, with most drug delivery vehicles designed to exploit these gradients focused on GSH-

FIG. 6. Mechanical tension has been used to enhance reduction rate of a disulfide bond. Effect of reducing agent (DTT) concentration (left) and mechanical tension (right, [DTT]=0.194 mM, f =bond tension) on reduction rate. Reprinted (adapted) with permission from Li *et al.* (77). Copyright (2013).



mediated degradation of disulfide bonds (13, 22, 132). This linkage is readily cleaved by reducing agents such as phosphines (100, 124) or, more importantly given a biological context, through thiol-disulfide exchange with other thiol-containing species (88). The versatility of material science enables the inclusion of reducible linkages into a wide range of architectures. This section intends to highlight some of these, including the commonly studied micelle, as well as lesser investigated structures such as gold nanoparticles, silica nanoparticles, and more.

Gold nanoparticles

Gold nanoparticles have been extensively exploited for biotechnological and biomedical applications given that the gold core is essentially inert and non-toxic; they are easy to synthesize in a monodisperse fashion, can be readily functionalized with thiols, and have unique optical properties, thus enabling label-free visualization or electron microscopic contrast (41–43, 45, 94, 116). Ghosh *et al.* (46) prepared gold colloids functionalized with amino acids, including lysine and glycine, to provide a scaffold for effective DNA binding. The transfection efficiency (TE) of a β -galactosidase reporter in monkey kidney cells (Cos-1) revealed the glycine-containing nanoplexes to demonstrate minimal TE, while lysine-functionalized nanoplexes demonstrated a fivefold superior efficiency compared with the polylysine positive control. TE was further improved to 28 times that of polylysine by preparing nanoparticles which were functionalized with first-generation lysine dendrons. GSH was also shown to alter TE, as it can displace the cationic ligands from the gold nanoparticles (Fig. 7a), releasing the DNA. The GSH level was transiently increased by treating cells with glutathione monoester (GSH-OEt), a compound rapidly internalized by cells and processed into GSH by esterases (Fig. 7b), and decreased by treatment with L-butathione-[S,R]-sulfoxamine, an inhibitor of γ -glutamylcysteine synthetase (Fig. 7c). Corre-

spondingly, the TE was seen to increase and decrease, respectively (46).

The displacement of thiol-terminated groups with GSH has also been used by Hong *et al.* (57) to trigger the release of a thiolated Bodipy dye from gold nanoparticle surfaces. The application of 10 mM GSH promoted significant dye release *in vitro*, while a release in pure water and after the addition of a tripeptide with the same structure as GSH but without the thiol group was minimal (Fig. 8A). Dye release was also observed after incubation for 96 h in human liver cells (Hep G2) and in GSH-OEt-treated mouse embryonic fibroblast cells (Fig. 8B) (57).

Zhang and co-workers have used GSH-thiol displacement to release tiopronin *in vitro* and *in vivo* using an acute liver injury model in mice (12), as have Forbes and co-workers (67) released fluorescein isothiocyanate and DOX from gold nanoparticles. The latter showed that nanoparticle surface charge greatly influences the penetration of nanoparticles and the location of cellular uptake and release (67). Positive particles improved the delivery of payloads to the majority of cells in tumors given their extent of uptake into proliferating cells, whereas negative particles were suggested to be better for delivering drugs deep into tissues.

Rotello and co-workers (128) have functionalized a 2 nm gold core with positively charged trimethylammonium-functionalized mixed monolayer-protected clusters of different chain lengths (C_8 and C_{11}). These were used to bind β -galactosidase through complementary electrostatic interactions to give complete enzyme inhibition. The addition of GSH at intracellular GSH concentrations reversed this binding and restored activity in the C_8 case, while no restoration was observed in the C_{11} case, further highlighting methods of tuning material response to GSH (128).

The kinetics of GSH-triggered release from gold nanoparticles has also been monitored. For example, Ock *et al.* directly monitored the GSH-induced *in vitro* and *in vivo*

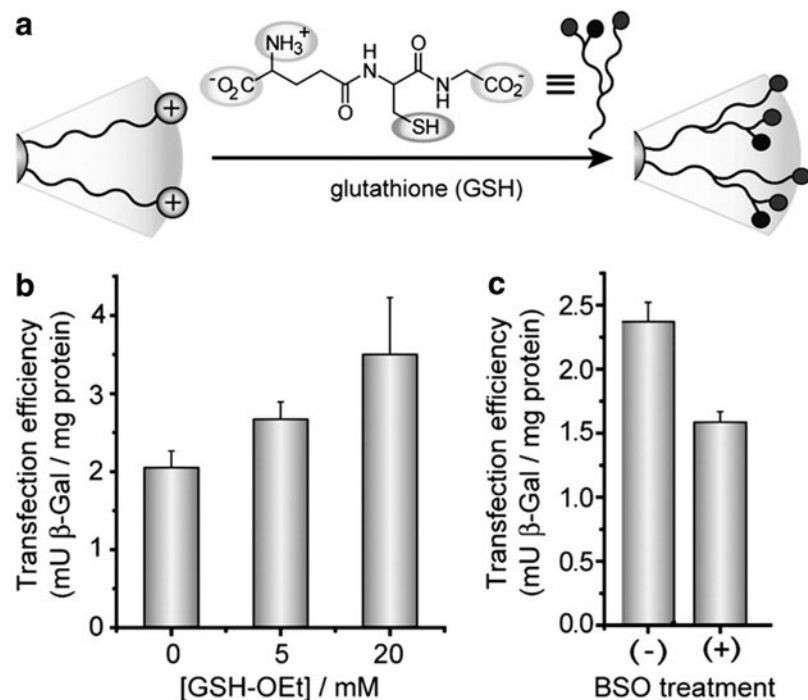


FIG. 7. Drug release from gold nanoparticles. (a) Schematic representation of the ligand displacement that occurs when functionalized gold nanoparticles are incubated with GSH. Effect of (b) GSH monoester concentration and (c) L-butathione-[S,R]-sulfoxamine on transfection efficiency of β -galactosidase reported in Cos-1 cells. Reproduced (adapted) with permission from Ghosh *et al.* (46). Copyright (2013) American Chemical Society.

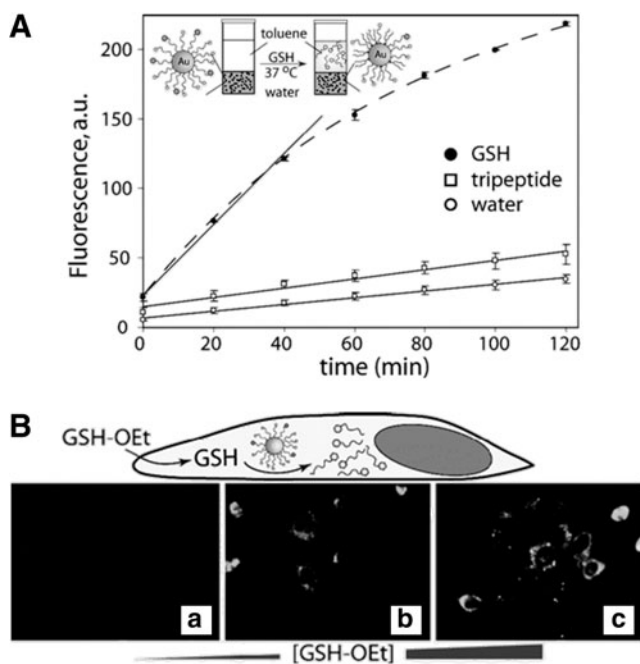
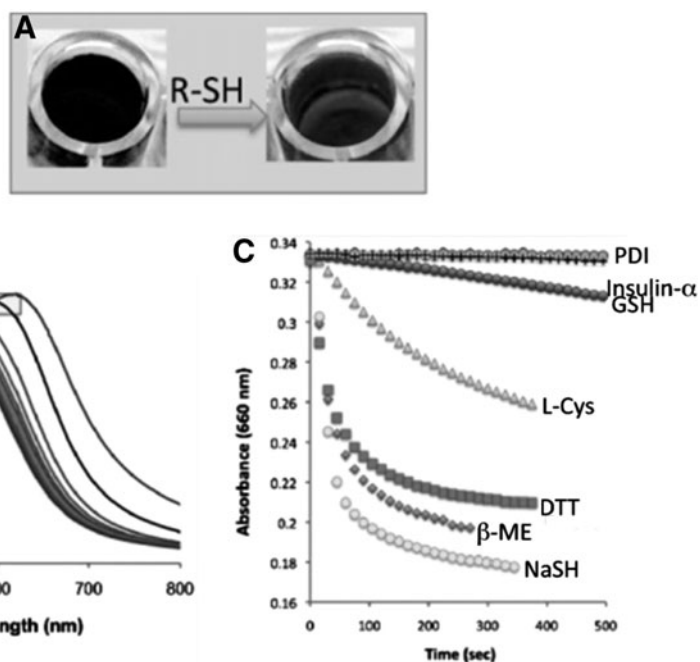


FIG. 8. Dye-release from gold nanoparticles. (A) *In vitro* release of a thiolated dye from gold nanoparticle surfaces (assessed by observed fluorescence at 507 nm in toluene layer of a biphasic system) in pure water, GSH (10 mM) or tripeptide (10 mM) at 37°C. (B) Schematic representation and fluorescence images when using GSH-OEt as an external stimulus to promote dye release from gold nanoparticles in mouse fibroblast cells ([GSH-OEt]=0 (a), 5 (b), 20 (c) mM). Reproduced with permission from Hong *et al.* (57). Copyright (2013) American Chemical Society. GSH-OEt, glutathione monoester.

release of thiopurine anticancer drug from gold nanoparticle surfaces by label-free Raman spectroscopy (93). Kim *et al.* monitored the intracellular GSH-triggered release of topotecan from gold nanoparticles in serum-containing media in real time using a label-free fluorescence live-cell imaging

FIG. 9. Effect of thiols on disulfide-linked gold nanoparticle clusters. (A) Color and (B) localized surface plasmon resonance spectra response after incubation of nanoparticles with thiols. (C) Absorbance change at 610 nm of nanoparticles after reduction by thiols (1 μ M) of different molecular weights: NaSH, sodium hydrosulfide; β -ME, 2-mercaptoethanol; DTT, dithiothreitol; Cys, L-Cysteine; GSH, glutathione; insulin α -chain; PDI, protein disulfide isomerase. Reproduced (adapted) with permission from Durocher *et al.* (35). Copyright (2013) American Chemical Society.



technique (69). Durocher *et al.* (35) exploited the propensity of thiols to exchange on gold nanoparticle surfaces and to create a sensor for low-molecular-weight thiols. A disulfide bridge was placed in a sterically constrained environment, which was accessible only to low-molecular-weight thiols. Reduction of the disulfide-containing gold nanoclusters to monodisperse gold nanoparticles was accompanied by a spectral change (blue to red) that was associated with nanoparticle de-clustering. This system was stable to reduction by thiols for approximately a critical molecular weight of 310 g mol⁻¹, while minimal changes in absorbance were observed on incubation with larger thiols containing compounds such as insulin (Fig. 9) (35).

Silica nanoparticles

MSNs are solid materials containing many empty channels (mesopores) in a honeycomb-like structure. They have been investigated for the controlled release of pharmaceutical compounds for a variety of reasons, including their improved biocompatibility compared with amorphous silica materials, high drug-loading capacity, biodegradability under physiological conditions, and ability to protect internalized cargo (56, 106, 129). MSNs can also be adapted to respond to specific stimuli to release a cargo (114, 125). Lai *et al.* (71) prepared an MCM-41-type mesoporous silica-based controlled-release delivery system in which silica nanospheres were loaded with active ingredients and capped by disulfide-linked, mercaptoacetic acid-derivatized cadmium sulfide nanocrystals. Negligible release of vancomycin and adenosine triphosphate in 10 mM PBS was observed over a 12 h period highlighting a good capping efficiency, while ~80% release was observed within 24 h on end-cap removal by addition of 18.5 mM DTT (71).

Cui *et al.* (29) linked MSNs to a PEG shell via a disulfide linker that was cleaved at tumor relevant GSH levels. This detached the PEG shell and released encapsulated guests in a controlled manner at a rate that was dependent on the GSH concentration used: 20% and 75% release after 22 h was observed with 1 mM and 10 mM GSH, respectively. Confocal

laser scanning microscopy showed that MSNs were internalized in endosome or lysosome of MCF-7 cells with a significantly greater dye release in the presence of elevated GSH concentrations (29).

Kim *et al.* (68) tethered cyclodextrins onto MSNs *via* disulfide stalling to entrap guest molecules in the pores. These were released in response to GSH with the nanocontainers exhibiting efficient GSH-mediated release of DOX in cancer cells. Incubation of A549 cells with MSNs loaded with 1 and 5 μM DOX saw a surviving fraction of 2.0×10^{-3} and 2.7×10^{-1} , respectively, after 24 h (68). Zhang *et al.* (146) also used cyclodextrin as a "gatekeeper" in multifunctional envelope-type MSNs that were designed for tumor-triggered drug delivery. Cyclodextrin was anchored on the surface *via* disulfide bonds for GSH-induced intracellular release. A peptide motif and matrix metalloproteinase substrate peptide was introduced onto the surface *via* host-guest interactions. The nanoparticles were further decorated with poly(aspartic acid) to protect them from uptake into normal cells. At the tumor site, the polyanion protection layer was removed by hydrolysis of the metalloproteinase substrate peptide and the targeting motif was exposed. Once taken into the cell, disulfide cleavage resulted in removal of the cyclodextrin gatekeeper and release of the drug (146).

Bioreducible micelles/self-assembled polymers

The encapsulation of therapeutic agents inside nanoparticles is a popular route for delivery into cells. Micelles are particularly popular and routinely prepared from block copolymers comprising distinct hydrophilic and hydrophobic units. Aqueous dissolution above the critical micelle concentration prompts self-assembly in order to shield the hydrophobic block from the aqueous environment (105). Typically, micelles are used to encapsulate hydrophobic compounds though hydrophilic species can also be sequestered (147). The dynamic nature of these structures can, however, result in poor structural stability and non-specific cargo release. Control over release rates can be imposed by the inclusion of cross-links throughout the structure, including the core, the shell, and between the core and shell domains (Fig. 10) (92). Incorporation of a disulfide unit as the cross-linker can, therefore, introduce redox sensitivity (148).

Core cross-linked micelles have been prepared by Zhang *et al.* (143) by first conjugating the cyclic disulfide lipoic acid to starch-g-PEG copolymers (Fig. 11A) and then adding 10 mol% DTT relative to the lipoic acid residues. The release of se-

questered DOX totalled $\sim 35\%$ at pH 7.4 in the absence of GSH over 59.5 h, while around 70% was released in 12 h and 90% was released in 59.5 h when incubated with 10 mM GSH (143). Although cross-linking minimizes non-specific cargo release, it does not appear to enable a binary "on-off" GSH response such as that observed in the capping of silica nanoparticles, or through the use of gold nanoparticles (*vide supra*). A further example has been presented by Yan *et al.* (139), who prepared a disulfide core cross-linked micelle. The addition of GSH greatly accelerated the release of internalized DOX (65–70% released after 36 h when incubated with 10 or 20 mM GSH), whereas a relatively significant percentage ($\sim 25\%$) was released even without GSH (139).

Micelles that require multiple stimuli to trigger drug release have also been developed. Li *et al.* (76) prepared micelles from a graft copolymer of PEG and keratin in which core cross-links were introduced by oxidation of residual keratin thiol groups. In the presence of 10 mM GSH, only 50% release was observed after 10 h. However, the addition of 0.04 mM trypsin, an enzyme over-expressed in inflamed and cancerous tissues capable of cleaving lysine/arginine residues found in keratin, led to quantitative drug release (76). Similarly, multiply responsive shell cross-linked (SCL) micelles can be used. Hu *et al.* (58) prepared amphiphilic diblock copolymers that were covalently functionalized with aldehyde moieties in the hydrophilic block. These were converted into acylhydrazone cross-links at pH 6.2 using dithiolbis(propanoic dihydrazide) that could be destabilized either by acid-triggered cleavage of acylhydrazone bonds or by thiol-triggered cleavage of disulfide linkages. The cross-linkages provided a drug diffusion barrier in which release of internalized camptothecin was slow at pH 7.4, reaching around 30% after 115 h. Optimum release was observed at 10 mM DTT and pH 5, where 80% release was observed after 115 h (60). Samarajeewa *et al.* (110) prepared disulfide SCL ("knedel-like") structures that demonstrated accelerated paclitaxel (PTX) release (65%) in the presence of 10 mM GSH at both pH 5.5 and pH 7.4 after 8 days. Without GSH, 50% and 35% were released at pH 5.5 and pH 7.4, respectively. After 72 h of incubation against human ovarian adenocarcinoma cells, the nanoparticles exhibited an 11-fold lower IC_{50} value than a Taxol-mimicking formulation (110).

The disulfide bond has also been introduced between the hydrophilic and hydrophobic blocks (21, 122, 123, 138, 145). Sun *et al.* (121) prepared these so-called "shedtable" micelles from PEG-SS-PCL (Fig. 11B). When loaded with DOX and treated in PBS at 37°C with 10 mM DTT, 60% release was observed after 4 h with a near total release seen after 12 h

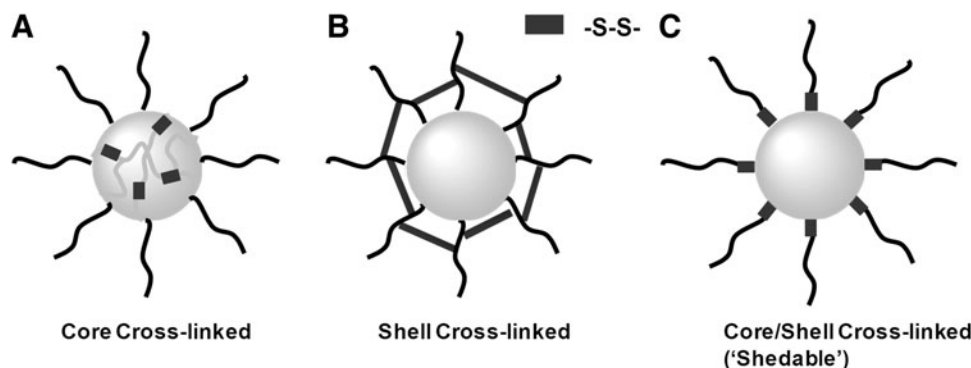


FIG. 10. Schematic representations of sites for reducible cross-link insertion in micelles. (A) Core cross-links. (B) Shell cross-links. (C) Core-shell cross-links.

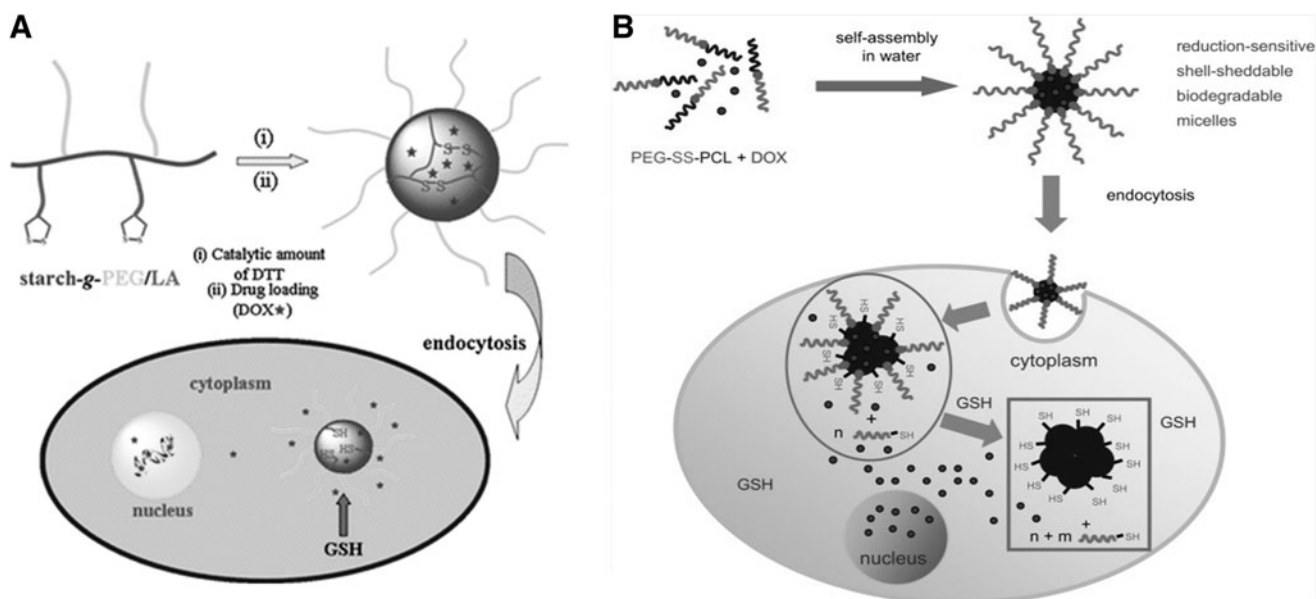


FIG. 11. Bioreducible micelles containing a disulfide cross-linker linker. (A) Reversible disulfide core cross-linked starch-g-PEG micelles, (143) and **(B)** shell-sheddable biodegradable micelles based on PEG-SS-PCL block copolymers, for intracellular GSH-triggered DOX release (121). **(B)** Reproduced (adapted) with permission from Sun *et al.* (121). Copyright (2013) Elsevier. PCL, poly(caprolactam); PEG, poly(ethylene glycol).

compared with less than 20% release after 24 h from the non-disulfide-containing PEG-PCL structures. Moreover, a zero-order release of approximately 60% indicated a mechanism controlled by a combination of diffusion and degradation, but no data for GSH-mediated release were provided (121). Zhang *et al.* (144) demonstrated that the morphology (spheres, vesicles, or rod-like aggregates) of self-assembled structures prepared from PEG-SS-poly(styrene) could be controlled by varying the hydrophilic block length. As the morphology chains from spheres to vesicles to rods, the relative curvature decreases, thus changing the accessibility and tension of the disulfide bond along with the physicochemical properties of the nanoparticles (48). The rate of PEG shedding when incubated with DTT was found to be different depending on the morphology: 56% degradation was observed with spherical structures compared with 25% with vesicles after 4 h (144).

Micelles obtained from more traditional lower-molecular-weight surfactants have also been exploited. Ghosh *et al.* (47) prepared micelles from a surfactant in which the hydrophilic head group was connected to the hydrophobic tail through a disulfide bond. Mixed micelles containing different percentages of the disulfide- and non-disulfide-containing surfactants displayed different disassembly kinetics when exposed to DTT. A mixed micelle containing 25% disulfide-containing surfactant took a little less than 700 min to release the model compound Nile red completely, compared with around 150 min in the 50:50 micelle (47). Liu *et al.* (78) prepared micelles from an amphiphilic homopolymer where noncovalent interactions were the driving force. These micelles exhibited smart redox-responsive properties that could be exploited to deliver DOX into nuclei of tumor cells and enhance inhibition of cell proliferation after GSH reduction (78). A review describing functional block copolymer assemblies that are responsive to tumor and intracellular microenvironments discusses this in detail (44).

Cell penetrating peptides, linear systems, dendrimers, and nanogels

Cationic cell penetrating peptides inspired by the TAT translocation sequence from HIV are of interest in biomedical applications given their ability to transport linked substrates across nearly any bilayer membrane (40). Cell-penetrating poly(disulfides) are, therefore, attractive given their ability to degrade in the cytosol, simultaneously release the cargo, and lower toxicity by decreasing material molecular weight. Bang *et al.* (11) proposed a new approach to cellular uptake using substrate-initiated polymerization of cell-penetrating poly(disulfide)s. Ring-opening disulfide exchange polymerization with units derived from lipoic acid produced polymers with stimuli-responsive transport activity in neutral lipid bilayers (11).

Gibson and co-workers (108) have explored the use of disulfide reduction as a tool toward manipulating the macroscopic solubility properties of polymers. A poly(disulfide) based on the thermally responsive polymer Poly(*N*-isopropylacrylamide) (PNIPAM) was prepared. Incubation of this polymer at a temperature above its lower critical solution temperature (LCST) shifts its solubility (*i.e.*, becomes water insoluble) that can be used to drive cell-membrane insertion or passage (1, 108). The LCST of PNIPAM is molecular-weight dependent, so the addition of 1 mM GSH triggered disulfide reduction and, hence, produced a shorter polymer with a higher LCST while the addition of 1 μ M GSH had no effect (Fig. 12A). The increase in LCST caused by disulfide degradation enabled rapid resolubilization without the need for a change in temperature, a so-called "isothermal" transition (98, 99). The ability to trigger these solubility switches by the incorporation and degradation of a single disulfide bond at the polymer chain end has also been demonstrated (120).

Bae *et al.* (8) prepared reducible heparin nanogels that were cross-linked with disulfide linkages (Fig. 12B). These nanogels

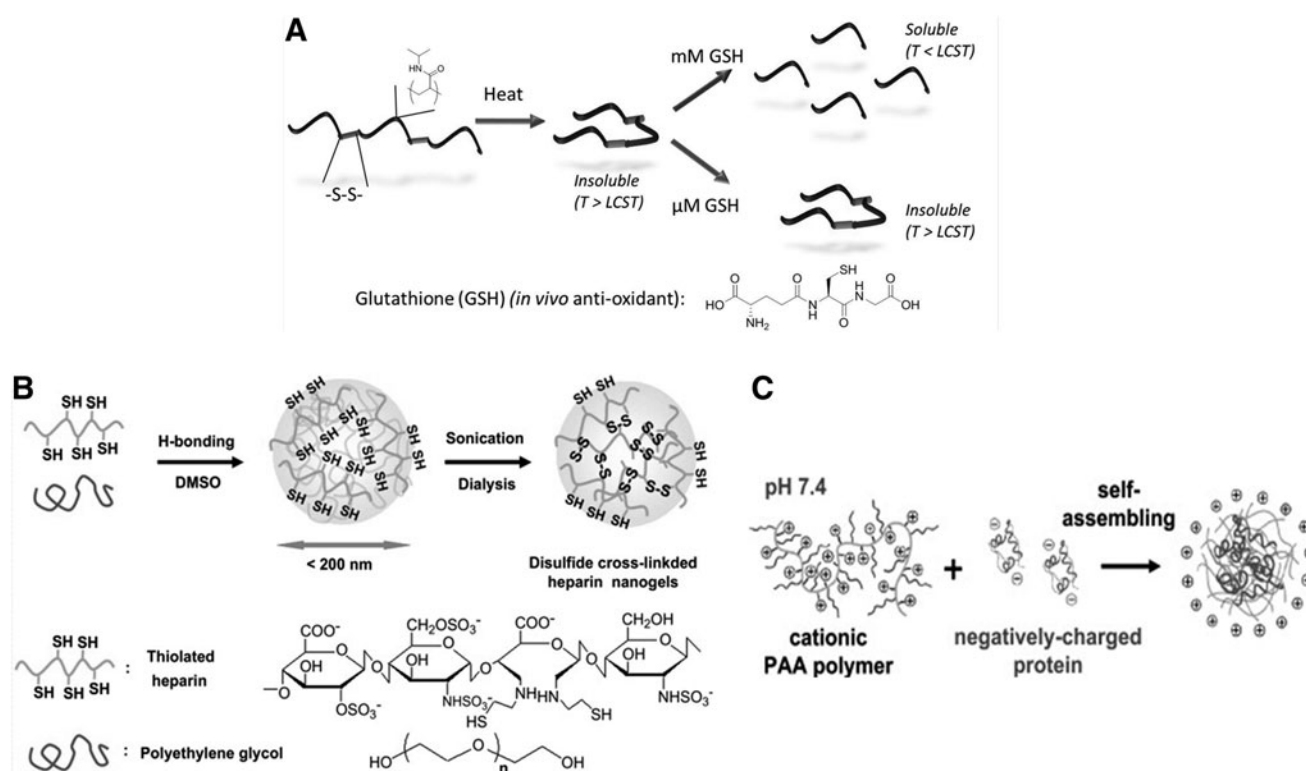


FIG. 12. Reducible polymers. (A) Linear systems designed to trigger changes in solubility without a temperature change (“isothermal” transition) on GSH-mediated disulfide reduction (99). (B) Disulfide cross-linked heparin nanogels which degrade in a reductive intracellular environment to release heparin within cells (8) and (C) disulfide-containing cationic nanocomplexes that are designed to release human serum albumin on intracellular reduction (25). (A) Reproduced with permission from Phillips and Gibson (99). Copyright (2013) Royal Society of Chemistry.

rapidly disintegrated and released free heparin under reductive environments such as those found in the cytosol. The degree of heparin release increased with a GSH concentration with almost 65% released with 5 mM GSH after ~160 h compared with less than 3% in the absence of reducing agent (8). Qiao *et al.* (102) prepared triply responsive nanogels by mini-emulsion radical copolymerization of oligoethylene glycol methacrylate and 2-(5,5-dimethyl-1,3-dioxan-2-yl)oxy ethyl acrylate using bis(2-acryloyloxyethyl) disulfide as a cross-linker. These nanogels were able to encapsulate a variety of hydrophobic compounds, including PTX, which exhibited a concentration-dependent toxicity to MCF-7 cells (102).

Nam *et al.* (89) prepared dendrimer-type bioreducible polymers by incorporating arginine-grafted poly(disulfide amine) into poly(amido amine). Compared with the poly(disulfide amine) alone, the dendrimer exhibited superior condensing ability with plasmid DNA and more controlled release when exposed to a reducing environment (89). Cohen *et al.* (25) prepared cationic nanocomplexes of linear poly(amidoamine)s with oppositely charged proteins such as human serum albumin (Fig. 12C). These complexes showed high mucoadhesive properties and, while stable in extracellular conditions, they rapidly destabilized in a reductive intracellular environment due to disulfide bond cleavage. The transport of human serum albumin to early endosomes, lysosomes, and cytoplasm was determined (25).

Outlook/Conclusions

In vivo redox gradients provide attractive options for selective, targeted intracellular release, particularly given

the vast array of redox-susceptible architectures that are readily accessed using modern macromolecular chemistry. However, this review has sought to highlight that it is also critical to obtain a comprehensive understanding of both the chemical nature of the material and the sub-cellular location being targeted. Evidence has been presented showing very different rates and extents of release for similar materials depending on the “model” reducing agent used. Significant differences are also seen between materials due to their intracellular fate, which itself is directed by the method of cellular uptake. Therefore, in order to enable translation of redox-responsive DDS into real applications it is crucial for the field to address the following outstanding issues:

- What is the actual redox potential inside relevant subcellular locations?
- How do these potentials differ between cell types?
- How can the intracellular reductant for any DDS be determined and correlated to therapeutic outcome?
- What redox gradients existing within tissue will be encountered by the DDS and how will this have an impact on material design?
- What new chemical tools are required to map out the processes described earlier?
- How can the rate of degradation of each linkage be tuned, including effects of local mechanical strain, steric constraints, and electrostatic interactions?
- What is the most appropriate ‘model’ reducing agent that facilitates these studies?

This understanding will not only help with material design, but will also enable the production of more advanced materials with greater dexterity and versatility than simply existing in “on” or “off” states. While beyond the scope of this review, it should also be appreciated that the search for a “perfect” delivery device is further challenged given the natural differences seen from patient to patient. It is known, for example, that while GSH levels are similar in both men and women, the body becomes increasingly oxidized with age (37, 127). Considering the evidence presented earlier, it would seem there is much opportunity for redox-responsive materials to play a role in nanomedicine. In order to fully realize their potential, careful consideration of the actual biological interactions experienced by these delivery systems should be made through a concerted combination of cell biology, biochemistry, pharmacology, and materials science.

Acknowledgments

M.I.G. is a Birmingham Science City Interdisciplinary Research Fellow funded by the Higher Education Funding Council for England (HEFCE). D.J.P. acknowledges UoW for a postgraduate scholarship.

References

1. Abulatefeh SR, Spain SG, Thurecht KJ, Aylott JW, Chan WC, Garnett MC, and Alexander C. Enhanced uptake of nanoparticle drug carriers via a thermoresponsive shell enhances cytotoxicity in a cancer cell line. *Biomater Sci* 1: 434–442, 2013.
2. Alarcon CdLH, Pennadam S, and Alexander C. Stimuli responsive polymers for biomedical applications. *Chem Soc Rev* 34: 276–285, 2005.
3. Allen BL, Johnson JD, and Walker JP. Encapsulation and enzyme-mediated release of molecular cargo in polysulfide nanoparticles. *ACS Nano* 5: 5263–5272, 2011.
4. Allen TM and Cullis PR. Drug delivery systems: entering the mainstream. *Science* 303: 1818–1822, 2004.
5. Anderson ME. Glutathione: an overview of biosynthesis and modulation. *Chem Biol Interact* 111–112: 1–14, 1998.
6. auf dem Keller U, Kumin A, Braun S, and Werner S. Reactive oxygen species and their detoxification in healing skin wounds. *J Investig Dermatol Symp Proc* 11: 106–111, 2006.
7. Austin CD, Wen X, Gazzard L, Nelson C, Scheller RH, and Scales SJ. Oxidizing potential of endosomes and lysosomes limits intracellular cleavage of disulfide-based antibody-drug conjugates. *Proc Natl Acad U S A* 102: 17987–17992, 2005.
8. Bae KH, Mok H, and Park TG. Synthesis, characterization, and intracellular delivery of reducible heparin nanogels for apoptotic cell death. *Biomaterials* 29: 3376–3383, 2008.
9. Bajpai AK, Shukla SK, Bhanu S, and Kankane S. Responsive polymers in controlled drug delivery. *Prog Polym Sci* 33: 1088–1118, 2008.
10. Baldus Ilona B and Gräter F. Mechanical force can fine-tune redox potentials of disulfide bonds. *Biophys J* 102: 622–629, 2012.
11. Bang E-K, Gasparini G, Molinard G, Roux A, Sakai N, and Matile S. Substrate-initiated synthesis of cell-penetrating poly(disulfide)s. *J Am Chem Soc* 135: 2088–2091, 2013.
12. Bao Q-Y, Geng D-D, Xue J-W, Zhou G, Gu S-Y, Ding Y, and Zhang C. Glutathione-mediated drug release from tiopronin-conjugated gold nanoparticles for acute liver injury therapy. *Int J Pharmaceut* 446: 112–118, 2013.
13. Bauhuber S, Hozsa C, Breunig M, and Göpferich A. Delivery of nucleic acids via disulfide-based carrier systems. *Adv Mater* 21: 3286–3306, 2009.
14. Bova MP, Mattson MN, Vasile S, Tam D, Holsinger L, Bremer M, Hui T, McMahon G, Rice A, and Fukuto JM. The oxidative mechanism of action of ortho-quinone inhibitors of protein-tyrosine phosphatase α is mediated by hydrogen peroxide. *Arch Biochem Biophys* 429: 30–41, 2004.
15. Broaders KE, Grandhe S, and Fréchet MJ. A biocompatible oxidation-triggered carrier polymer with potential in therapeutics. *J Am Chem Soc* 133: 756–758, 2010.
16. Bulaj G, Kortemme T, and Goldenberg DP. Ionization—reactivity relationships for cysteine thiols in polypeptides. *Biochemistry* 37: 8965–8972, 1998.
17. Bystrom LM, Guzman ML, and Rivella S. Iron and reactive oxygen species: friends or foes of cancer cells? *Antioxid Redox Signal* 20: 1917–1924, 2014.
18. Carampin P, Lallana E, Laliturai J, Carroccio SC, Puglisi C, and Tirelli N. Oxidant-dependent REDOX responsiveness of polysulfides. *Macromol Chem Phys* 213: 2052–2061, 2012.
19. Cerritelli S, Velluto D, and Hubbell JA. PEG-SS-PPS: reduction-sensitive disulfide block copolymer vesicles for intracellular drug delivery. *Biomacromolecules* 8: 1966–1972, 2007.
20. Chen EKY, McBride RA, and Gillies ER. Self-immolative polymers containing rapidly cyclizing spacers: toward rapid depolymerization rates. *Macromolecules* 45: 7364–7374, 2012.
21. Chen W, Zhong P, Meng F, Cheng R, Deng C, Feijen J, and Zhong Z. Redox and pH-responsive degradable micelles for dually activated intracellular anticancer drug release. *J Control Release* 169: 171–179, 2013.
22. Cheng R, Feng F, Meng F, Deng C, Feijen J, and Zhong Z. Glutathione-responsive nano-vehicles as a promising platform for targeted intracellular drug and gene delivery. *J Control Release* 152: 2–12, 2011.
23. Cho H, Bae J, Garripelli VK, Anderson JM, Jun H-W, and Jo S. Redox-sensitive polymeric nanoparticles for drug delivery. *Chem Commun* 48: 6043–6045, 2012.
24. Coelho J, Ferreira P, Alves P, Cordeiro R, Fonseca A, Góis J, and Gil M. Drug delivery systems: advanced technologies potentially applicable in personalized treatments. *EPMA J* 1: 164–209, 2010.
25. Cohen S, Coué G, Beno D, Korenstein R, and Engbersen JFJ. Bioreducible poly(amidoamine)s as carriers for intracellular protein delivery to intestinal cells. *Biomaterials* 33: 614–623, 2012.
26. Collins DS, Unanue ER, and Harding CV. Reduction of disulfide bonds within lysosomes is a key step in antigen processing. *J Immunol* 147: 4054–4059, 1991.
27. Colson YL and Grinstaff MW. Biologically responsive polymeric nanoparticles for drug delivery. *Adv Mater* 24: 3878–3886, 2012.
28. Crommelin DJA and Florence AT. Towards more effective advanced drug delivery systems. *Int J Pharmaceut* 454: 496–511, 2013.
29. Cui Y, Dong H, Cai X, Wang D, and Li Y. Mesoporous silica nanoparticles capped with disulfide-linked PEG gatekeepers

- for glutathione-mediated controlled release. *ACS Appl Mater Interfaces* 4: 3177–3183, 2012.
30. D'Autreaux B and Toledano MB. ROS as signalling molecules: mechanisms that generate specificity in ROS homeostasis. *Nat Rev Mol Cell Biol* 8: 813–824, 2007.
 31. de Gracia Lux C, Joshi-Barr S, Nguyen T, Mahmoud E, Schopf E, Fomina N, and Almutairi A. Biocompatible polymeric nanoparticles degrade and release cargo in response to biologically relevant levels of hydrogen peroxide. *J Am Chem Soc* 134: 15758–15764, 2012.
 32. Deponte M. Glutathione catalysis and the reaction mechanisms of glutathione-dependent enzymes. *Biochim Biophys Acta* 1830: 3217–3266, 2013.
 33. Dewit MA, Beaton A, and Gillies ER. A reduction sensitive cascade biodegradable linear polymer. *J Polym Sci Part A Polym Chem* 48: 3977–3985, 2010.
 34. Duncan R. Polymer conjugates as anticancer nanomedicines. *Nat Rev Cancer* 6: 688–701, 2006.
 35. Durocher S, Rezaee A, Hamm C, Rangan C, Mittler S, and Mutus B. Disulfide-linked, gold nanoparticle based reagent for detecting small molecular weight thiols. *J Am Chem Soc* 131: 2475–2477, 2009.
 36. Ende AE van der, Kravitz EJ, and Harth E. Approach to formation of multifunctional polyester particles in controlled nanoscopic dimensions. *J Am Chem Soc* 130: 8706–8713, 2008.
 37. Erden-inal M, Sunal E, and Kanbak G. Age-related changes in the glutathione redox system. *Cell Biochem Funct* 20: 61–66, 2002.
 38. Farokhzad OC and Langer R. Impact of nanotechnology on drug delivery. *ACS Nano* 3: 16–20, 2009.
 39. Feener EP, Shen WC, and Ryser HJ. Cleavage of disulfide bonds in endocytosed macromolecules. A processing not associated with lysosomes or endosomes. *J Biol Chem* 265: 18780–18785, 1990.
 40. Fischer R, Fotin-Mleczek M, Hufnagel H, and Brock R. Break on through to the other side—biophysics and cell biology shed light on cell-penetrating peptides. *ChemBioChem* 6: 2126–2142, 2005.
 41. Freese C, Gibson MI, Klok H-A, Unger RE, and Kirkpatrick CJ. Size- and coating-dependent uptake of polymer-coated gold nanoparticles in primary human dermal microvascular endothelial cells. *Biomacromolecules* 13: 1533–1543, 2012.
 42. Freese C, Unger RE, Deller RC, Gibson MI, Brochhausen C, Klok H-A, and Kirkpatrick CJ. Uptake of poly(2-hydroxypropylmethacrylamide)-coated gold nanoparticles in microvascular endothelial cells and transport across the blood-brain barrier. *Biomater Sci* 1: 824–833, 2013.
 43. Freese C, Uboldi C, Gibson MI, Unger RE, Weksler BB, Romero IA, Couraud P-O, and Kirkpatrick CJ. Uptake and cytotoxicity of citrate-coated gold nanospheres: comparative studies on human endothelial and epithelial cells. *Part Fibre Toxicol* 9: 23, 2012.
 44. Ge Z and Liu S. Functional block copolymer assemblies responsive to tumor and intracellular microenvironments for site-specific drug delivery and enhanced imaging performance. *Chem Soc Rev* 42: 7289–7325, 2013.
 45. Ghosh P, Han G, De M, Kim CK, and Rotello VM. Gold nanoparticles in delivery applications. *Adv Drug Deliv Rev* 60: 1307–1315, 2008.
 46. Ghosh PS, Kim C-K, Han G, Forbes NS, and Rotello VM. Efficient gene delivery vectors by tuning the surface charge density of amino acid-functionalized gold nanoparticles. *ACS Nano* 2: 2213–2218, 2008.
 47. Ghosh S, Irvin K, and Thayumanavan S. Tunable disassembly of micelles using a redox trigger. *Langmuir* 23: 7916–7919, 2007.
 48. Gibson MI and O'Reilly RK. To aggregate, or not to aggregate? considerations in the design and application of polymeric thermally-responsive nanoparticles. *Chem Soc Rev* [Epub ahead of print]; DOI: 10.1039/C3CS60035A.
 49. Go Y-M and Jones DP. Redox compartmentalization in eukaryotic cells. *Biochim Biophys Acta* 1780: 1273–1290, 2008.
 50. Graf N and Lippard SJ. Redox activation of metal-based prodrugs as a strategy for drug delivery. *Adv Drug Deliv Rev* 64: 993–1004, 2012.
 51. Guertin KR, Setti L, Qi L, Dunsdon RM, Dymock BW, Jones PS, Overton H, Taylor M, Williams G, Sergi JA, Wang K, Peng Y, Renzetti M, Boyce R, Falcioni F, Garippa R, and Olivier AR. Identification of a novel class of orally active pyrimido[5,4-3][1,2,4]triazine-5,7-diamine-based hypoglycemic agents with protein tyrosine phosphatase inhibitory activity. *Bioorg Med Chem Lett* 13: 2895–2898, 2003.
 52. Halliwell B. Reactive oxygen species in living systems: source, biochemistry, and role in human disease. *Am J Med* 91: S14–S22, 1991.
 53. Hastings KT and Cresswell P. Disulfide reduction in the endocytic pathway: immunological functions of gamma-interferon-inducible lysosomal thiol reductase. *Antioxid Redox Signal* 15: 657–668, 2011.
 54. Holmgren A and Luthman M. Tissue distribution and subcellular localization of bovine thioredoxin determined by radioimmunoassay. *Biochemistry* 17: 4071–4077, 1978.
 55. Holmgren A, Ohlsson I, and Grankvist ML. Thioredoxin from *Escherichia coli*. Radioimmunological and enzymatic determinations in wild type cells and mutants defective in phage T7 DNA replication. *J Biol Chem* 253: 430–436, 1978.
 56. Hom C, Lu J, and Tamanoi F. Silica nanoparticles as a delivery system for nucleic acid-based reagents. *J Mater Chem* 19: 6308–6316, 2009.
 57. Hong R, Han G, Fernández JM, Kim B-j, Forbes NS, and Rotello VM. Glutathione-mediated delivery and release using monolayer protected nanoparticle carriers. *J Am Chem Soc* 128: 1078–1079, 2006.
 58. Hu J, Zhang G, and Liu S. Enzyme-responsive polymeric assemblies, nanoparticles and hydrogels. *Chem Soc Rev* 41: 5933–5949, 2012.
 59. Hu P and Tirelli N. Scavenging ROS: superoxide dismutase/catalase mimetics by the use of an oxidation-sensitive nanocarrier/enzyme conjugate. *Bioconjug Chem* 23: 438–449, 2012.
 60. Hu X, Li H, Luo S, Liu T, Jiang Y, and Liu S. Thiol and pH dual-responsive dynamic covalent shell cross-linked micelles for triggered release of chemotherapeutic drugs. *Polym Chem* 4: 695–706, 2013.
 61. Hwang C, Sinskey AJ, and Lodish HF. Oxidized redox state of glutathione in the endoplasmic reticulum. *Science* 257: 1496–1502, 1992.
 62. Jeong NS, Brebis K, Daniel LE, O'Reilly RK, and Gibson MI. The critical importance of size on thermoresponsive nanoparticle transition temperatures: gold and micelle-based polymer nanoparticles. *Chem Commun* 47: 11627–11629, 2011.
 63. Jones DP, Carlson JL, Mody VC, Jr., Cai J, Lynn MJ, and Sternberg P, Jr. Redox state of glutathione in human plasma. *Free Radic Biol Med* 28: 625–635, 2000.
 64. Jones DP, Carlson JL, Samiec PS, Sternberg P, Jr., Mody VC, Jr., Reed RL, and Brown LAS. Glutathione measurement in

- human plasma: evaluation of sample collection, storage and derivatization conditions for analysis of dansyl derivatives by HPLC. *Clin Chim Acta* 275: 175–184, 1998.
65. Kamaly N, Xiao Z, Valencia PM, Radovic-Moreno AF, and Farokhzad OC. Targeted polymeric therapeutic nanoparticles: design, development and clinical translation. *Chem Soc Rev* 41: 2971–3010, 2012.
 66. Kellogg BA, Garrett L, Kovtun Y, Lai KC, Leece B, Miller M, Payne G, Steeves R, Whiteman KR, Widdison W, Xie H, Singh R, Chari RVJ, Lambert JM, and Lutz RJ. Disulfide-linked antibody – maytansinoid conjugates: optimization of in vivo activity by varying the steric hindrance at carbon atoms adjacent to the disulfide linkage. *Bioconjug Chem* 22: 717–727, 2011.
 67. Kim B, Han G, Toley BJ, Kim C-K, Rotello VM, and Forbes NS. Tuning payload delivery in tumour cylindroids using gold nanoparticles. *Nat Nano* 5: 465–472, 2010.
 68. Kim H, Kim S, Park C, Lee H, Park HJ, and Kim C. Glutathione-induced intracellular release of guests from mesoporous silica nanocontainers with cyclodextrin gatekeepers. *Adv Mater* 22: 4280–4283, 2010.
 69. Kim M, Ock K, Cho K, Joo S-W, and Lee SY. Live-cell monitoring of the glutathione-triggered release of the anticancer drug topotecan on gold nanoparticles in serum-containing media. *Chem Commun* 48: 4205–4207, 2012.
 70. Krauth-Siegel RL, Bauer H, and Schirmer RH. Dithiol proteins as guardians of the intracellular redox milieu in parasites: old and new drug targets in trypanosomes and malaria-causing plasmodia. *Angew Chem Int Ed* 44: 690–715, 2005.
 71. Lai C-Y, Trewyn BG, Jeftinija DM, Jeftinija K, Xu S, Jeftinija S, and Lin VSY. A mesoporous silica nanosphere-based carrier system with chemically removable CdS nanoparticle caps for stimuli-responsive controlled release of neurotransmitters and drug molecules. *J Am Chem Soc* 125: 4451–4459, 2003.
 72. Lallana E and Tirelli N. Oxidation-responsive polymers: which groups to use, how to make them, what to expect from them (biomedical applications). *Macromol Chem Phys* 214: 143–158, 2013.
 73. Langer R and Tirrell DA. Designing materials for biology and medicine. *Nature* 428: 487–492, 2004.
 74. Lee H, Torres J, Truong L, Chaudhuri R, Mittal A, and Johnson ME. Reducing agents affect inhibitory activities of compounds: results from multiple drug targets. *Anal Biochem* 423: 46–53, 2012.
 75. Lee SH, Gupta MK, Bang JB, Bae H, and Sung H-J. Current progress in reactive oxygen species (ros)-responsive materials for biomedical applications. *Adv Healthc Mater* 2: 908–915, 2013.
 76. Li Q, Zhu L, Liu R, Huang D, Jin X, Che N, Li Z, Qu X, Kang H, and Huang Y. Biological stimuli responsive drug carriers based on keratin for triggerable drug delivery. *J Mater Chem* 22: 19964–19973, 2012.
 77. Li Y, Nese A, Lebedeva NV, Davis T, Matyjaszewski K, and Sheiko SS. Molecular tensile machines: intrinsic acceleration of disulfide reduction by dithiothreitol. *J Am Chem Soc* 133: 17479–17484, 2011.
 78. Liu J, Huang W, Pang Y, Huang P, Zhu X, Zhou Y, and Yan D. Molecular self-assembly of a homopolymer: an alternative to fabricate drug-delivery platforms for cancer therapy. *Angew Chem Int Ed* 50: 9162–9166, 2011.
 79. Liu J, Pang Y, Zhu Z, Wang D, Li C, Huang W, Zhu X, and Yan D. Therapeutic nanocarriers with hydrogen peroxide-triggered drug release for cancer treatment. *Biomacromolecules* 14: 1627–1636, 2013.
 80. Lloyd JB. Disulphide reduction in lysosomes. The role of cysteine. *Biochem J* 237: 271–272, 1986.
 81. Lotharius J and Brundin P. Pathogenesis of parkinson's disease: dopamine, vesicles and [alpha]-synuclein. *Nat Rev Neurosci* 3: 932–942, 2002.
 82. Lu H, Sun P, Zheng Z, Yao X, Wang X, and Chang F-C. Reduction-sensitive rapid degradable poly(urethane-urea)s based on cystine. *Polym Degrad Stab* 97: 661–669, 2012.
 83. Ma N, Li Y, Xu H, Wang Z, and Zhang X. Dual redox responsive assemblies formed from diselenide block copolymers. *J Am Chem Soc* 132: 442–443, 2009.
 84. Mahmoud EA, Sankaranarayanan J, Morachis JM, Kim G, and Almutairi A. Inflammation responsive logic gate nanoparticles for the delivery of proteins. *Bioconjug Chem* 22: 1416–1421, 2011.
 85. Matsumura Y and Maeda H. A new concept for macromolecular therapeutics in cancer chemotherapy: mechanism of tumortropic accumulation of proteins and the antitumor agent Smancs. *Cancer Res* 46: 6387–6392, 1986.
 86. Mortera R, Vivero-Escoto J, Slowing II, Garrone E, Onida B, and Lin VSY. Cell-induced intracellular controlled release of membrane impermeable cysteine from a mesoporous silica nanoparticle-based drug delivery system. *Chem Commun* 3219–3221, 2009.
 87. Moses MA, Brem H, and Langer R. Advancing the field of drug delivery: taking aim at cancer. *Cancer Cell* 4: 337–341, 2003.
 88. Nagy P. Kinetics and mechanisms of thiol-disulfide exchange covering direct substitution and thiol oxidation-mediated pathways. *Antioxid Redox Signal* 18: 1623–1641, 2013.
 89. Nam HY, Nam K, Lee M, Kim SW, and Bull DA. Dendrimer type bio-reducible polymer for efficient gene delivery. *J Control Release* 160: 592–600, 2012.
 90. Napoli A, Valentini M, Tirelli N, Muller M, and Hubbell JA. Oxidation-responsive polymeric vesicles. *Nat Mater* 3: 183–189, 2004.
 91. Noiva R. Protein disulfide isomerase: the multifunctional redox chaperone of the endoplasmic reticulum. *Semin Cell Dev Biol* 10: 481–493, 1999.
 92. O'Reilly RK, Hawker CJ, and Wooley KL. Cross-linked block copolymer micelles: functional nanostructures of great potential and versatility. *Chem Soc Rev* 35: 1068–1083, 2006.
 93. Ock K, Jeon WI, Ganbold EO, Kim M, Park J, Seo JH, Cho K, Joo S-W, and Lee SY. Real-time monitoring of glutathione-triggered thiopurine anticancer drug release in live cells investigated by surface-enhanced Raman scattering. *Anal Chem* 84: 2172–2178, 2012.
 94. Pache C, Bocchio NL, Bouwens A, Villiger M, Berclaz C, Gouley J, Gibson MI, Santschi C, and Lasser T. Fast three-dimensional imaging of gold nanoparticles in living cells with photothermal optical lock-in optical coherence microscopy. *Opt Express* 20: 21385–21399, 2012.
 95. Palamoor M and Jablonski MM. Poly(ortho ester) nanoparticle-based targeted intraocular therapy for controlled release of hydrophilic molecules. *Mol Pharmaceut* 10: 701–708, 2012.
 96. Pan Y-J, Chen Y-Y, Wang D-R, Wei C, Guo J, Lu D-R, Chu C-C, and Wang C-C. Redox/pH dual stimuli-responsive biodegradable nanohydrogels with varying responses to

- dithiothreitol and glutathione for controlled drug release. *Biomaterials* 33: 6570–6579, 2012.
97. Perry G, Castellani RJ, Hirai K, and Smith MA. Reactive oxygen species mediate cellular damage in Alzheimer disease. *J Alzheimer's Dis* 1: 45–55, 1998.
 98. Phillips DJ and Gibson MI. Biodegradable poly(disulfide)s derived from RAFT polymerization: monomer scope, glutathione degradation, and tunable thermal responses. *Bio-macromolecules* 13: 3200–3208, 2012.
 99. Phillips DJ and Gibson MI. Degradable thermoresponsive polymers which display redox-responsive LCST behaviour. *Chem Commun* 48: 1054–1056, 2012.
 100. Pinnel P, Mendez-Nelson A, Noh SM, Nam JH, and Oh JK. Rapid and tunable reductive degradation of disulfide-labeled polyesters. *Macromol Chem Phys* 213: 678–685, 2012.
 101. Pisoni RL, Acker TL, Lisowski KM, Lemons RM, and Thoene JG. A cysteine-specific lysosomal transport system provides a major route for the delivery of thiol to human fibroblast lysosomes: possible role in supporting lysosomal proteolysis. *J Cell Biol* 110: 327–335, 1990.
 102. Qiao Z-Y, Zhang R, Du F-S, Liang D-H, and Li Z-C. Multi-responsive nanogels containing motifs of ortho ester, oligo(ethylene glycol) and disulfide linkage as carriers of hydrophobic anti-cancer drugs. *J Control Release* 152: 57–66, 2011.
 103. Reddy ST, Rehor A, Schmoekel HG, Hubbell JA, and Swartz MA. *In vivo* targeting of dendritic cells in lymph nodes with poly(propylene sulfide) nanoparticles. *J Control Release* 112: 26–34, 2006.
 104. Rehor A, Hubbell JA, and Tirelli N. Oxidation-sensitive polymeric nanoparticles. *Langmuir* 21: 411–417, 2004.
 105. Riess G. Micellization of block copolymers. *Prog Polym Sci* 28: 1107–1170, 2003.
 106. Rosenholm J, Sahlgren C, and Linden M. Cancer-cell targeting and cell-specific delivery by mesoporous silica nanoparticles. *J Mater Chem* 20: 2707–2713, 2010.
 107. Ryser HJ, Mandel R, and Ghani F. Cell surface sulfhydryls are required for the cytotoxicity of diphtheria toxin but not of ricin in Chinese hamster ovary cells. *J Biol Chem* 266: 18439–18442, 1991.
 108. Saaka Y, Deller RC, Rodger A, and Gibson MI. Exploiting thermoresponsive polymers to modulate lipophilicity: interactions with model membranes. *Macromol Rapid Commun* 33: 779–784, 2012.
 109. Saito G, Swanson JA, and Lee K-D. Drug delivery strategy utilizing conjugation via reversible disulfide linkages: role and site of cellular reducing activities. *Adv Drug Deliv Rev* 55: 199–215, 2003.
 110. Samarajeewa S, Shrestha R, Elsbahy M, Karwa A, Li A, Zentay RP, Kostelc JG, Dorshow RB, and Wooley KL. In vitro efficacy of paclitaxel-loaded dual-responsive shell cross-linked polymer nanoparticles having orthogonally degradable disulfide cross-linked corona and polyester core domains. *Mol Pharmaceut* 10: 1092–1099, 2013.
 111. Sauer AM, Schlossbauer A, Ruthardt N, Cauda V, Bein T, and Braäuchle C. Role of endosomal escape for disulfide-based drug delivery from colloidal mesoporous silica evaluated by live-cell imaging. *Nano Lett* 10: 3684–3691, 2010.
 112. Schafer FQ and Buettner GR. Redox environment of the cell as viewed through the redox state of the glutathione disulfide/glutathione couple. *Free Radic Biol Med* 30: 1191–1212, 2001.
 113. Sen CK and Roy S. Redox signals in wound healing. *Biochim Biophys Acta* 1780: 1348–1361, 2008.
 114. Slowing II, Trewyn BG, Giri S, and Lin VSY. Mesoporous silica nanoparticles for drug delivery and biosensing applications. *Adv Funct Mater* 17: 1225–1236, 2007.
 115. Song C-C, Ji R, Du F-S, Liang D-H, and Li Z-C. Oxidation-accelerated hydrolysis of the ortho ester-containing acid-labile polymers. *ACS Macro Lett* 2: 273–277, 2013.
 116. Sperling RA, Rivera Gil P, Zhang F, Zanella M, and Parak WJ. Biological applications of gold nanoparticles. *Chem Soc Rev* 37: 1896–1908, 2008.
 117. Staff RH, Gallei M, Mazurowski M, Rehahn M, Berger R, Landfester K, and Crespy D. Patchy nanocapsules of poly(vinylferrocene)-based block copolymers for redox-responsive release. *ACS Nano* 6: 9042–9049, 2012.
 118. Steiner M, Hartmann I, Perrino E, Casi G, Brighton S, Jelesarov I, Bernardes GJL, and Neri D. Spacer length shapes drug release and therapeutic efficacy of traceless disulfide-linked ADCs targeting the tumor neovasculature. *Chem Sci* 4: 297–302, 2013.
 119. Sugamura K and Keaney JFF. Reactive oxygen species in cardiovascular disease. *Free Radic Biol Med* 51: 978–992, 2011.
 120. Summers MJ, Phillips DJ, and Gibson MI. “Isothermal” LCST transitions triggered by bioreduction of single polymer end-groups. *Chem Commun* 49: 4223–4225, 2013.
 121. Sun H, Guo B, Cheng R, Meng F, Liu H, and Zhong Z. Biodegradable micelles with sheddable poly(ethylene glycol) shells for triggered intracellular release of doxorubicin. *Biomaterials* 30: 6358–6366, 2009.
 122. Sun H, Guo B, Li X, Cheng R, Meng F, Liu H, and Zhong Z. Shell-sheddable micelles based on dextran-SS-poly(ϵ -caprolactone) diblock copolymer for efficient intracellular release of doxorubicin. *Biomacromolecules* 11: 848–854, 2010.
 123. Tang L-Y, Wang Y-C, Li Y, Du J-Z, and Wang J. Shell-detachable micelles based on disulfide-linked block copolymer as potential carrier for intracellular drug delivery. *Bioconjug Chem* 20: 1095–1099, 2009.
 124. Tsarevsky NV and Matyjaszewski K. Combining atom transfer radical polymerization and disulfide/thiol redox chemistry: a route to well-defined (bio)degradable polymeric materials. *Macromolecules* 38: 3087–3092, 2005.
 125. Vallet-Regí M, Balas F, and Arcos D. Mesoporous materials for drug delivery. *Angew Chem Int Ed* 46: 7548–7558, 2007.
 126. van der Vlies AJ, Hasegawa U, and Hubbell JA. Reduction-sensitive tioguanine prodrug micelles. *Mol Pharmaceut* 9: 2812–2818, 2012.
 127. van Lieshout EM and Peters WH. Age and gender dependent levels of glutathione and glutathione S-transferases in human lymphocytes. *Carcinogenesis* 19: 1873–1875, 1998.
 128. Verma A, Simard JM, Worrall JWE, and Rotello VM. Tunable reactivation of nanoparticle-inhibited β -galactosidase by glutathione at intracellular concentrations. *J Am Chem Soc* 126: 13987–13991, 2004.
 129. Vivero-Escoto JL, Slowing II, Trewyn BG, and Lin VSY. Mesoporous silica nanoparticles for intracellular controlled drug delivery. *Small* 6: 1952–1967, 2010.
 130. Vo CD, Kilcher G, and Tirelli N. Polymers and sulfur: what are organic polysulfides good for? Preparative strategies and biological applications. *Macromol Rapid Commun* 30: 299–315, 2009.
 131. Waris G and Ahsan H. Reactive oxygen species: role in the development of cancer and various chronic conditions. *J Carcinog* 5: 14–21, 2006.
 132. Wei H, Zhuo R-X, and Zhang X-Z. Design and development of polymeric micelles with cleavable links for in-

- tracellular drug delivery. *Prog Polym Sci* 38: 503–535, 2013.
133. Wiita AP, Ainavarapu SRK, Huang HH, and Fernandez JM. Force-dependent chemical kinetics of disulfide bond reduction observed with single-molecule techniques. *Proc Natl Acad Sci U S A* 103: 7222–7227, 2006.
 134. Wiita AP, Perez-Jimenez R, Walther KA, Grater F, Berne BJ, Holmgren A, Sanchez-Ruiz JM, and Fernandez JM. Probing the chemistry of thioredoxin catalysis with force. *Nature* 450: 124–127, 2007.
 135. Wilson DS, Dalmaso G, Wang L, Sitaraman SV, Merlin D, and Murthy N. Orally delivered thioketal nanoparticles loaded with TNF- α -siRNA target inflammation and inhibit gene expression in the intestines. *Nat Mater* 9: 923–928, 2010.
 136. Wu C, Belenda C, Leroux J-C, and Gauthier MA. Interplay of chemical microenvironment and redox environment on thiol–disulfide exchange kinetics. *Chem A Eur J* 17: 10064–10070, 2011.
 137. Wu C, Leroux J-C, and Gauthier MA. Twin disulfides for orthogonal disulfide pairing and the directed folding of multicyclic peptides. *Nat Chem* 4: 1044–1049, 2012.
 138. Xu Y, Meng F, Cheng R, and Zhong Z. Reduction-sensitive reversibly crosslinked biodegradable micelles for triggered release of doxorubicin. *Macromol Biosci* 9: 1254–1261, 2009.
 139. Yan L, Wu W, Zhao W, Qi R, Cui D, Xie Z, Huang Y, Tong T, and Jing X. Reduction-sensitive core-cross-linked mPEG-poly(ester-carbonate) micelles for glutathione-triggered intracellular drug release. *Polym Chem* 3: 2403–2412, 2012.
 140. Yang J, Chen H, Vlahov IR, Cheng J-X, and Low PS. Evaluation of disulfide reduction during receptor-mediated endocytosis by using FRET imaging. *Proc Natl Acad Sci U S A* 103: 13872–13877, 2006.
 141. Yang J, Chen H, Vlahov IR, Cheng J-X, and Low PS. Characterization of the pH of folate receptor-containing endosomes and the rate of hydrolysis of internalized acid-labile folate-drug conjugates. *J Pharmacol Exp Therapeut* 321: 462–468, 2007.
 142. Yu SS, Koblin RL, Zachman AL, Perrien DS, Hofmeister LH, Giorgio TD, and Sung H-J. Physiologically relevant oxidative degradation of oligo(proline) cross-linked polymeric scaffolds. *Biomacromolecules* 12: 4357–4366, 2011.
 143. Zhang A, Zhang Z, Shi F, Ding J, Xiao C, Zhuang X, He C, Chen L, and Chen X. Disulfide crosslinked PEGylated starch micelles as efficient intracellular drug delivery platforms. *Soft Matter* 9: 2224–2233, 2013.
 144. Zhang J, Liu H-J, Yuan Y, Jiang S, Yao Y, and Chen Y. Thermo-, pH-, and light-responsive supramolecular complexes based on a thermoresponsive hyperbranched polymer. *ACS Macro Lett* 2: 67–71, 2012.
 145. Zhang J, Wu L, Meng F, Wang Z, Deng C, Liu H, and Zhong Z. pH and reduction dual-bioresponsive polymersomes for efficient intracellular protein delivery. *Langmuir* 28: 2056–2065, 2011.
 146. Zhang J, Yuan Z-F, Wang Y, Chen W-H, Luo G-F, Cheng S-X, Zhuo R-X, and Zhang X-Z. Multifunctional envelope-type mesoporous silica nanoparticles for tumor-triggered targeting drug delivery. *J Am Chem Soc* 135: 5068–5073, 2013.
 147. Zhang L, Liu W, Lin L, Chen D, and Stenzel MH. Degradable disulfide core-cross-linked micelles as a drug delivery system prepared from vinyl functionalized nucleosides via the RAFT process. *Biomacromolecules* 9: 3321–3331, 2008.
 148. Zhang Q, Ko NR, and Oh JK. Recent advances in stimuli-responsive degradable block copolymer micelles: synthesis and controlled drug delivery applications. *Chem Commun* 48: 7542–7552, 2012.

Address correspondence to:
 Dr. Matthew I. Gibson
 Department of Chemistry
 University of Warwick
 Coventry CV4 7AL
 United Kingdom

E-mail: m.i.gibson@warwick.ac.uk

Date of first submission to ARS Central, October 30, 2013; date of acceptance, November 12, 2013.

Abbreviations Used

AFM = atomic force microscopy
DDS = drug delivery system
DHLA = dihydrolipoic acid
DOX = doxorubicin
DTT = dithiothreitol
GILT = gamma-interferon-inducible lysosomal thiol reductase
GSH = glutathione
GSH-OEt = glutathione monoester
H ₂ O ₂ = hydrogen peroxide
IC ₅₀ = half maximal inhibitory concentration
LCST = lower critical solution temperature
ME/ β -MCE/ β -ME = 2-mercaptoethanol
MSN = mesoporous silica nanoparticle
NADH = nicotinamide adenine dinucleotide hydride
NADPH = nicotinamide adenine dinucleotide phosphate
NaOCl = sodium hypochlorite
NaSH = sodium hydrosulfide
PBS = phosphate buffered saline
PCL = poly(caprolactam)
PDI = protein disulfide isomerase
PEG = poly(ethylene glycol)
PNIPAM = poly(<i>N</i> -isopropylacrylamide)
PPS = poly(propylene sulfide)
PTX = paclitaxel
ROS = reactive oxygen species
SCL = shell cross-linked
TCEP = tris(2-carboxyethyl) phosphine
TE = transfection efficiency
TRX = thioredoxin